

Get3 in Arabidopsis

Dissertation

zur Erlangung des Doktorgrades

der Naturwissenschaften

vorgelegt beim

Fachbereich Biowissenschaften (FB15)

der Johann Wolfgang Goethe – Universität Frankfurt am Main

von

Uwe Sakamuzi Bodensohn

aus Offenbach am Main

Frankfurt am Main 2021

(D30)

Vom Fachbereich Biowissenschaften der Goethe-Universität als Dissertation angenommen

Dekan: Prof. Dr. Sven Klimpel

Erster Gutachter: Prof. Dr. Enrico Schleiff

Zweiter Gutachter: Prof. Dr. Claudia Büchel

Datum der Disputation:

For my family

TABLE OF CONTENTS

TABLE OF CONTENTS	I
INDEX OF FIGURES.....	V
INDEX OF TABLES.....	VI
Abbreviations	VII
Units	IX
NOMENCLATURE FOR GENES AND PROTEINS	X
ZUSAMMFASSUNG	XI
ABSTRACT	1
1. INTRODUCTION	2
1.1 Signal recognition particle (SRP) pathway.....	3
1.2 SRP independent targeting (SND) pathway.....	4
1.3 Guided entry of tail anchor proteins (GET) pathway	5
1.3.1 Pre-targeting complex in yeast.....	6
1.3.2 Pre-targeting complex in mammals	7
1.3.3 The membrane receptor complex in yeast	8
1.3.4 The membrane receptor complex in mammals	8
1.4 Get3	9
1.4.1 Get3 is a targeting factor.....	9
1.4.2 Get3 in a cellular context	9
1.4.3 Get3 in plants	11
1.5 Photosynthetic membranes	12
1.5.1 cpSRP pathway	12
1.5.2 cpSEC pathway	13
1.5.3 cpTAT pathway	14
1.5.4 Spontaneous pathway.....	14
2 OBJECTIVES.....	15
3. MATERIAL	17
3.1 Chemicals, media and buffers	17
3.2 Enzymes and kits	17
3.3 Bacterial strains and growth	17
3.4 Nucleotides.....	17
3.4 Plasmids.....	19
3.5 Plant lines	21
3.6 Antibodies.....	21

TABLE OF CONTENTS

3.7 Columns and column materials.....	22
4. METHODS	23
4.1 Molecular biological methods.....	23
4.1.1 General molecular biological methods.....	23
4.2 Biochemical methods	23
4.2.1 General biochemical methods.....	23
4.2.2 Protein expression.....	23
4.2.3 Protein purification	24
4.2.4 Recombinant <i>in vivo</i> pull down assay.....	25
4.3 Immunological methods.....	25
4.3.1 Antibody production	25
4.3.2 Affinity purification of antibodies	25
4.3.2 Indirect immunofluorescence	26
4.4 Cell biological methods	26
4.4.1 General cell fractionation.....	26
4.4.2 Organelle isolation	26
4.4.3 BN-PAGE with isolated organelles.....	27
4.4.4 Assays with isolated organelles.....	27
4.4.5 Treatments of isolated organelles.....	28
4.5 Plant methods	29
4.5.1 Plant growth	29
4.5.2 Protoplast isolation and transformation.....	29
4.5.3 Protoplast fractionation and sub fractionation.....	29
4.6 Microscopy	29
4.6.1 Transmission electron microscopy (TEM)	29
4.6.2 Confocal laser scanning microscopy (CLSM)	30
4.7 Holdase assays.....	30
4.7.2 <i>In cellula</i>	30
4.7.3 <i>In vitro</i>	30
4.8 Bioinformatical methods.....	30
4.9 MS/MS analysis	31
5 RESULTS.....	33
5.1 Get3 in Planta	33
5.1.1 Four orthologous groups to Get3 exist in plants.....	33
5.1.2 <i>At</i> Get3c is targeted to mitochondria.....	36
5.1.3 <i>At</i> Get3c resides in the mitochondrial matrix	37

TABLE OF CONTENTS

5.1.4	<i>At</i> Get3c is targeted to mitochondria of <i>Solanum lycopersicum</i> and <i>Allium cepa</i>	39
5.1.5	Medicago Get3 orthologues are present in various organelles	39
5.1.6	<i>Solanum lycopersicum</i> Get3 proteins are targeted to cytosol and chloroplast	42
5.1.7	<i>Physcomitrella patens</i> Get3 orthologues are localized in cytosol and chloroplast.....	42
5.2	<i>At</i> Get3a in <i>Arabidopsis thaliana</i>	43
5.2.1	<i>At</i> GET pathway comprises pre-targeting and receptor components.....	43
5.2.2	Interacting network of <i>At</i> Get3a <i>in vivo</i>	44
5.3	Functional characterization of <i>At</i> Get3a.....	47
5.3.1	Tail anchor translocation (TAT) <i>in cellula</i>	47
5.3.2	Tail anchor translocation (TAT) <i>in vitro</i>	48
5.3.3	<i>At</i> Get3a holdase function <i>in vitro</i> under heat stress.....	49
5.4	<i>At</i> Get3c in mitochondria of <i>Arabidopsis thaliana</i>	51
5.4.1	Homozygous T-DNA insertion line suitable for reverse genetic approach	51
5.4.2	Respiratory chain composition is altered in <i>Atget3c</i>	52
5.5	<i>At</i> Ge3c activity <i>in vitro</i>	53
5.5.1	<i>At</i> Get3c holdase function <i>in vitro</i> under heat stress.....	53
5.6	<i>At</i> Get3b is involved in the assembly of photosystem II (PSII)	54
5.6.1	Two T-DNA insertion lines with opposing attributes	54
5.6.2	Both <i>Atget3b</i> mutants display altered ultrastructural properties.....	55
5.6.3	Abundances of thylakoid membrane complexes effected in both <i>Atget3b</i> mutants	56
5.6.4	<i>Atget3b</i> mutants exhibit opposing effects on early PSII assembly.....	58
5.6.5	<i>At</i> Get3b binds hydrophobic PSII components <i>in vitro</i>	60
5.6.6	Thylakoid tail anchor translocation (τ TAT)	61
5.7	Comparative proteomics of <i>Atget3b</i> mutants.....	62
5.7.1	The effects of the <i>Atget3b-1</i> mutation on the chloroplast proteome	63
5.7.2	The chloroplast proteome of the <i>Atget3b-2</i> mutant line.....	65
5.8	<i>At</i> Get3b under stress.....	69
5.8.1	<i>Atget3b</i> mutants under light stress	69
5.8.2	<i>At</i> Get3b under oxidative stress	71
5.8.3	<i>In vitro At</i> Get3b holdase function under heat stress	72
6	DISCUSSION	74
6.1	Phylogenetic relations	74
6.1.1	GET in planta	74
6.1.2	Get3 in planta	74
6.2	Characterization of <i>At</i> Get3a	75
6.2.1	<i>At</i> Get3a as a targeting factor.....	75

TABLE OF CONTENTS

6.2.2 GET or TRC in <i>Arabidopsis thaliana</i>	76
6.2.3 <i>At</i> Get3a as holdase	76
6.3 Characterization of <i>At</i> Get3c	77
6.4 Characterization of <i>At</i> Get3b	77
6.4.1 Involvement in PS assembly	77
6.4.2 Involvement in Fe-S cluster dependent pathways	79
6.4.3 Involvement in protein transport	80
6.4.4 Involvement in proteostasis	82
6.4.5 Involvement in membrane remodeling	82
7. CONCLUSION	84
8. OUTLOOK	86
8.1 <i>At</i> Get3a	86
8.2 <i>At</i> Get3b	86
8.3 <i>At</i> Get3c	87
9. REFERENCES	88
10. SUPPLEMENTS	114
10.1 Supplemental figures	114
10.2 Supplemental tables	128
ACKNOWLEDGEMENTS	136
PUBLICATIONS	137
Further publications from side projects or method establishment	137
CURRICULUM VITAE	138
Persönliche Daten	138
Ausbildung	138
Vorträge und Posterpräsentationen	138
ERKLÄRUNG	139

INDEX OF FIGURES

Figure 1.1. Described modes of integral membrane protein (IMP) insertion at the endoplasmic reticulum (ER).....	3
Figure 1.2. Molecular steps in signal recognition particle (SRP) mediated targeting.	4
Figure 1.3. Molecular outlining of SRP independent (SND) targeting.	5
Figure 1.4. Molecular ensemble of the guided entry of tail anchored proteins (GET) pathway.	7
Figure 1.5. Auxiliary cellular functions of Get3.....	10
Figure 1.6. Get3 in <i>Arabidopsis thaliana</i>	11
Figure 1.7. Import routes into or across the thylakoid membrane.	13
Figure 5.1. Orthologous relationship of <i>At</i> Get3.	34
Figure 5.2. Selected plant systems to study Get3 proteins.....	36
Figure 5.3. <i>At</i> Get3c in mitochondria of <i>A. thaliana</i>	37
Figure 5.4. Individual Get3 orthologues display particular cellular localization in <i>A. thaliana</i> cells.	38
Figure 5.5. <i>At</i> Get3c targeting fidelity remains unchanged in <i>Solanum lycopersicum</i> and <i>Allium cepa</i>	40
Figure 5.6. The Get3 orthologues of <i>Medicago x varia</i> reside in cytosol, chloroplasts and mitochondria.....	41
Figure 5.7. Get3 orthologues of <i>Solanum lycopersicum</i> and <i>Physcomitrella patens</i> localized in cytoplasm and chloroplast.....	43
Figure 5.8. In <i>A. thaliana</i> Get1 and Get4 locate to ER and cytosol, respectively.....	44
Figure 5.9. Putative components of pre-targeting complex and interaction partners.	46
Figure 5.10. TA model substrate gets glycosylated in cellula.	48
Figure 5.11. Recombinant production of <i>At</i> Get3a - TA model substrate complexes and TAT trial.....	49
Figure 5.12. <i>At</i> Get3a prevents heat induced aggregation of <i>At</i> cpMDH.	50
Figure 5.13. T-DNA insertion line for <i>At</i> GET3C.....	51
Figure 5.14. Organellar ultrastructure is similar to wild-type in <i>Atget3c-1</i>	52
Figure 5.15. Respiratory chain complex composition is distorted in <i>Atget3c</i>	53
Figure 5.16. <i>At</i> Get3c is not capable of preventing heat induced aggregation of <i>At</i> cpMDH.....	54
Figure 5.17. T-DNA insertion lines for <i>At</i> GET3B.	55
Figure 5.18. Both <i>At</i> GET3b T-DNA insertion mutants display altered ultrastructural properties.....	56
Figure 5.19. Both <i>At</i> GET3B mutants exhibit irregular abundances of thylakoid embedded complexes.	57
Figure 5.20. <i>At</i> Get3b is involved in photo system II (PSII) assembly.....	59
Figure 5.21. <i>At</i> PsbW and <i>At</i> Get3b levels altered in respective mutant plant lines and <i>At</i> Get3b binds hydrophobic segments.....	61
Figure 5.22. Thylakoid tail-anchor translocation (τ TAT).....	62
Figure 5.23. Comparative proteomics of the plastid proteomes of <i>Atget3b-1</i> and the wild-type.....	64
Figure 5.24. Label free comparative proteomics reveal photosynthetic components are most affected in <i>Atget3b-2</i>	68
Figure 5.25. <i>Atget3b-2</i> displays hypersensitivity to light stress when grown under low light.....	70
Figure 5.26. <i>At</i> Get3b is recruited to distinct foci which display PMLO characteristics.....	72
Figure 5.27. <i>At</i> Get3b is not capable of preventing heat induced aggregation of <i>At</i> cpMDH.	73
Figure S1. Sequence alignment of representative Get3 plant protein sequences of different orthologous groups.	115
Figure S2. The Phylogenetic relation of PsbW in Viridiplantae.....	115
Figure S3. The Phylogenetic relation of GET3 domain in Viridiplantae.....	116
Figure S4. The Phylogenetic relation of GET3 domain in Viridiplantae.....	117
Figure S5. The Phylogenetic relation of GET3 domain in Viridiplantae.....	118
Figure S6. Get3 antibodies.	119
Figure S7. In vivo distribution of GFP tagged <i>At</i> Get3 proteins.....	119
Figure S8. <i>At</i> Get3a is specifically localized in the cytoplasm, <i>At</i> Get3b in chloroplasts and <i>At</i> Get3c in mitochondria.	120
Figure S9. <i>At</i> Get3c is not localized in chloroplasts in <i>A. cepa</i> epidermal cells.....	121

INDEX OF TABLES

Figure S10. α -AtGet3a co-precipitates candidates.	121
Figure S11. Sequence alignment of Bag6 homologues in Homo sapiens and Arabidopsis thaliana.	122
Figure S12. Optimizing microsomes isolation and recombinant AtGet3 expression.....	123
Figure S13. Examination of heat induced aggregation of model substrate chaperone.....	123
Figure S14. Growth analysis of Atget3 mutants.	124
Figure S15. Topologies of the putative TA proteins in complex II and IV _b	124
Figure S16. Photosynthetic parameters of the wild-type and mutant plants in the first month of development ...	125
Figure S17. Volcano plot of t-test between the proteome wild-type vs Atget3b-1 chloroplasts.	126
Figure S18. Volcano plot of t-test between the proteome of wild-type vs Atget3b-2 chloroplasts.	127
Figure S19. AtGet3b is associated with membranes in stromules and extrusions.	127

INDEX OF TABLES

Table 3.1: cloning of constructs for bacterial protein expression.	18
Table 3.2: Cloning of protoplast expression constructs.	19
Table 3.3 : Generation of deletion constructs.....	19
Table 3.4: Plasmids used in this study.	20
Table 3.5: Plant lines used in this study.....	21
Table 3.6: Antibodies used in this study.....	21
Table S1. Analyzed Get3 sequences.	128
Table S2. Accession numbers of the genes coding for the orthologues of Get1, in the plant species analyzed.	131
Table S3. Accession numbers of the genes coding for the orthologues of Sgt2 in the plant species analyzed.	132
Table S4. Accession numbers of the genes coding for the orthologues of Get4 in the plant species analyzed.	133
Table S5. Distribution of orthologues of Sgt2, Get1, Get3 and Get4 in the plant species analyzed.....	134
Table S6. Positioning of domain architecture HsUbl4A and AtUb-RPL40B.	135

ABBREVIATIONS

Abbreviations

<i>A. cepa</i>	<i>Allium cepa</i>	CURT	curvature thylakoid
<i>A. thaliana</i>	<i>Arabidopsis thaliana</i>	CR	control
AA	amino acid	CRR6	chlororespiratory reduction 6
ARC	accumulation and replication of chloroplasts	Cx(x)	cysteine followed by any amino acid(s)
AGC	automatic gain control	d	days
AKR2A	ankyrin repeat protein 2A	ddH ₂ O	double distilled water
Alb3/Alb4	albino3/4	DDM	n-dodecyl-β-D-maltoside
ArsA	arsenical pump ATPase	DIG	digitonin
ATP	adenosine triphosphate	DiT	dicarboxylate translocator
ATPase	ATP hydrolyzing protein	DNA	desoxyribonucleic acid
BADC	biotin attachment domain containing	dNTP	desoxyribonucleotide
BFA	biogenesis factor required for ATP synthase	DRiP	defective ribosomal products
BiFC	Bimolecular fluorescent complementation	DRT112	plastocyanin
BLAST	basic local alignment search tool	DTT	dithiothreitol
BN-PAGE	blue native PAGE	<i>E. coli</i>	<i>Escherichia coli</i>
bp	basepair	EET	excitation energy transfer
<i>C. reinhardtii</i>	<i>Chlamydomonas reinhardtii</i>	EDTA	ethylenediaminetetraacetic acid
C	cysteine	EGTA	ethylene glycol-bis(β-aminoethyl ether)-N,N,N',N'-tetraacetic acid
CF	chlorophyll fluorescence	ER	endoplasmic reticulum
C-terminus	carboxy terminal	Fd	ferredoxin
CAC	acetyl-coenzyme A carboxylase	Fe-S cluster	iron sulfur cluster
CaCl ₂	calcium chloride	FNR	ferredoxin-NADP ⁺ oxidoreductase
CCS	copper chaperone for superoxide dimutase	gDNA	genomic DNA
cDNA	complementary DNA	GET	guided entry of tail anchors
CDS	coding sequence	(sa)GFP	(self-assembling) green fluorescent protein
CNBr	cyanogen bromide	GTP	guanosine triphosphate
Co-IP	co-immunoprecipitation	GTPase	GTP hydrolyzing protein
		H ₂ O ₂	hydrogen peroxide
		HCF	high chlorophyll fluorescence
		HCl	hydrochloric acid
		His ₆ -tag	hexahistidine tag

ABBREVIATIONS

Hepes	4-(2-hydroxyethyl)-1-piperazineethanesulfonic acid	NaCl	sodium chloride
<i>H. sapiens</i>	<i>Homo sapiens</i>	NADH	nicotinamide adenine dinucleotide
Hsp	heat shock protein	NDH	NADH dehydrogenase like complex
I	isoleucine	Ni-NTA	nickel nitrilotriacetic acid
IE	inner envelope	NL	normal light
IF	immunofluorescence	NLS	nuclear localisation signal
IPTG	isopropyl β -D-1-thiogalactopyranoside	NPQ	non-photochemical quenching
K	lysine	N-terminal	amino terminal
KAS	β -ketoacyl-[acyl carrier] protein synthase	OD	optical density
KCl	potassium chloride	OE	outer envelope
KOH	potassium hydroxide	OEC	oxygen evolving complex
L	leucine	OEP	outer envelope protein
LB	lysogeny broth	OM	outer membrane
LC-MS/MS	liquid-chromatography-tandem mass spectrometry	OMP	outer membrane protein
LHC	light harvesting complex	OPG	opsin glycosylation tag
LL	low light	P.I.C.	proteinase inhibitor cocktail
LS	light stress	<i>P. patens</i>	<i>Physcomitrella patens</i>
LSU	large subunit (ribosome/RuBisCo)	P-loop	phosphate binding loop
<i>M. x varia</i>	<i>Medicago x varia</i>	p-value	probability value
MCS	multiple cloning sites	PAP	plastid lipid associated protein
MES	2-(N-Morpholino) ethanesulfonic acid	PAGE	polyacrylamide gel electrophoresis
(cp)MDH	(chloroplast) malate dehydrogenase	PAM	pulse amplitude modulation
MgCl ₂	magnesium chloride	PBS	phosphate buffered saline
MLP	mislocalized membrane and secretory protein	PCR	polymerase chain reaction
MS	Murashige Skoog	PIPES	piperazine-N-N'-bis(ethanesulfonic acid)
MTS	mitochondrial targeting sequence	PMF	proton motive force
mRNA	messenger RNA	PMSF	phenylmethylsulfonyl fluoride
		PorC	protochlorophyllide oxidoreductase
		Psa	subunit of PSI
		Psb	subunit of PSII

ABBREVIATIONS

PS	photosystem	Tris	tris (hydroxymethyl) amino methan
pSSU	precursor of SSU	TPR	tetratricopeptide repeat
R	arginine	TTE	tris taurine EDTA
RC	recovery	UROS	uroporphyrinogen III synthase
RNA	ribonucleic acid	UTR	untranslated region
RNC	ribosome nascent chain	VDAC	voltage dependent anion channel
Rpl	ribosomal protein from LSU	W	tryptophan
Rps	ribosomal protein from SSU	Y	tyrosine
RT	room temperature		
RT PCR	reverse transcription PCR		
RuBisCo	ribulose-1,5-bisphosphat carboxylase/oxygenase	Units	
<i>S. cerevisiae</i>	<i>Saccharomyces cerevisiae</i>	µg	microgram, 10 ⁻⁶ g
SDS	sodium dodecyl sulphate	µL	microliter, 10 ⁻⁶ L
SIMIBI	SRP, MinD, BioD	µM	micromolar 10 ⁻⁶ M
<i>S. lycopersicum</i>	<i>Solanum lycopersicum</i>	°C	degree Celsius
<i>S. bicolor</i>	<i>Sorghum bicolor</i>	cm	centimeter 10 ⁻³ m
SSU	small subunit (RuBisCo/Ribosome)	cV	column volume
ST	stress	hr	hour
Stic2	suppressor of tic40 2	g	relative centrifugal force
SNARE	N-ethylmaleimide-sensitive-factor attachment receptor	kDa	kilo Dalton, 10 ³ Da
SND	SRP independent	M	molar
SRP	signal recognition particle	mA	milliamper, 10 ⁻³ A
SR	SRP receptor	V	Volt
TAT	twin arginine translocation	mg	milligram 10 ⁻³ g
T.A.T.	tail anchored translocation	min	minute
TGD	trigalactosyldiacylglycerol	mL	milliLiter 10 ⁻³ L
TIC	translocon inner envelope of chloroplast	mM	millimolar 10 ⁻³ M
TMD	transmembrane domain	rpm	rounds per minute
TOC	translocon outer envelope of chloroplasts	sec	seconds
TP	transit peptide	u	unit
		vol.	volume
		v/v	volume per volume
		w/v	weight per volume
		w/w	weight per weight

NOMENCLATURE FOR GENES AND PROTEINS

<i>AtGET3A</i>	wild-type allele (cytosolic orthologue)
<i>AtGET3B</i>	wild-type allele (chloroplastidic orthologue)
<i>AtGET3C</i>	wild-type allele (mitochondrial orthologue)
<i>Atget3b-1</i>	mutant plant (knock-on)
<i>Atget3b-2</i>	mutant plant line (knock-out)
<i>Atget3c-1</i>	mutant plant line (knock-out)
<i>AtGet3a</i>	protein (cytosolic orthologue)
<i>AtGet3b</i>	protein (chloroplastidic orthologue)
<i>AtGet3c</i>	protein (mitochondrial orthologue)
<i>AtPSBW</i>	wild-type allele
<i>AtPsbW</i>	mutant plant (knock-out)

ZUSAMMENFASSUNG

Der *guided entry of tail-anchored proteins* (GET) Biogenese-Weg vermittelt den Transport und die Insertion von *tail-anchor* (TA) Proteinen in die Doppellipidschicht des Endoplasmatischen Retikulums (ER). TA Proteine sind dadurch gekennzeichnet, dass sie eine Transmembran Domäne (TMD) in den letzten 50 Aminosäuren ihrer Sequenz beherbergen. Diese TMD enthält die notwendigen Informationen, mit denen die Proteine an ihren jeweiligen subzellulären Zielort transportiert werden können. TA Proteine erfüllen eine Vielzahl von essentiellen biologischen Prozessen, sie fungieren zum Beispiel als Rezeptoren, sind maßgeblich an der Fusion von Vesikeln beteiligt sowie an der Initiation von Apoptose. Durch ihren modularen Aufbau können TA Proteine nicht mit dem Signalerkennungspartikel interagieren und müssen deshalb posttranslational zum ER geleitet werden. Im Modellorganismus Bäckerhefe (*Saccharomyces cerevisiae*) ist der GET Biogenese-Weg am besten beschrieben und läuft wie folgt ab: Nach der Termination der Translation bindet das Protein SgtA das TA Protein und händigt es über den Adapter-Komplex, bestehend aus Get4 und Get5, an die zytosolische ATPase Get3 aus. Get3 ist der zentrale Zielsteuerungsfaktor des GET Biogenese-Weges. Sobald sich ein Komplex aus Zielsteuerungsfaktor und TA Protein gebildet hat, wird dieses zur Membran des ERs überführt. Dort wird das TA Protein an den Rezeptorkomplex bestehend aus Get1 und Get2 übergeben, welcher anschließend die Insertion des TA Proteins in die Doppellipidschicht des ERs initiiert.

Get3 hat im zellulären Kontext noch eine weitere Funktion. Unter oxidativem Stress oder Energie depletierenden Bedingungen wird Get3 zu spezifischen *Foci* rekrutiert, an denen sich noch weitere durch Stress -induzierbare Proteine, wie z.B. die der Familie der Hitze Stress Proteine (HSPs) versammeln. Analysen haben gezeigt, dass Get3 unter den oben genannten Bedingungen, Konformationsänderungen durchläuft und dann als ATP unabhängige *Holdase* fungiert. Diese kann die exponierten, hydrophoben Anteile von Proteinen binden, um dadurch die Proteostasis aufrechtzuhalten.

Durch die Bedeutsamkeit der TA Proteinen ist die zentrale ATPase Get3 in allen Domänen des Lebens hochgradig konserviert. Phylogenetische Analysen ergaben, dass sich Get3 im Allgemeinen in eine „A“ Gruppe sowie eine „BC“ Gruppe aufspaltet. Im Modellorganismus *Arabidopsis thaliana* (Ackerschmalwand) wurden drei Orthologe zu Get3 identifiziert. Eins davon gehört zu der „A“ Gruppe und befindet sich im Zytoplasma. Die anderen zwei Orthologe befinden sich in den Organellen endosymbiotischen Ursprungs und gehören der „BC“ Gruppe an. Untersuchungen an verschiedenen Deletionsmutanten in *A. thaliana* haben gezeigt, dass die Mutationen einzelner GET Komponenten zu einer signifikanten Verkürzung der Haarwurzeln führen, obwohl der restliche Habitus der Pflanze unverändert bleibt. Diesbezüglich wurde SYP123 als einziges TA Proteine identifiziert, dessen

Abundanz durch die Deletion von GET Komponenten beeinflusst werden kann. Von den anderen beiden Orthologen organellären Ursprungs ist, abgesehen von ihrer Lokalisation nichts weiter bekannt.

Vier Orthologe Gruppen in Pflanzen

Da bislang nicht mehr als zehn Pflanzenarten für phylogenetische Analysen herangezogen wurden, wurden in dieser Arbeit die taxonomischen Beziehungen von Get3 zu einander in 50 Spezies der Viridiplantae auf Basis der Orthologie sowie Homologie untersucht. Dies führte zur Identifizierung einer zytolischen (*At*Get3a), einer plastidären (*At*Get3b), einer mitochondriellen (*At*Get3c) sowie einer Monokotyledone spezifischen Gruppe (*sb*Get3). Die Lokalisation der ersten drei Gruppen wurde in selektierten Pflanzen, sowohl homolog als auch heterolog, der unterschiedlichen Spezies mittels saGFP untersucht, und es konnte gezeigt werden, dass mehrere Get3 Orthologe mit unterschiedlichen subzellulären Lokalisationen eine unter Pflanze häufig auftretende Eigenschaft ist. Das Weiteren konnte gezeigt werden, dass manche Komponenten des Präzielsteuerungskomplexes (SgtA und Get4) sowie des Rezeptorkomplexes (Get1) in fast allen der 50 untersuchten Pflanzenarten vorhanden sind. Dies weist auf eine Konservierung des gesamten GET Biogenese-Weges in Pflanzen hin.

Get3a in *Arabidopsis thaliana*

Da die molekulare Zusammensetzung des Präzielsteuerungskomplexes für *At*Get3a in *A. thaliana* nicht bekannt ist, habe ich Co-Immünpräzipitationen mit Zellextrakten aus weißer Zellkultur und einen von mir selbst aufgereinigten Antikörper gegen *At*Get3a durchgeführt. Nach anschließender Gelelektrophorese und einer Anfärbung mit Coomassie Brilliant Blue ließ sich ein reproduzierbares Muster aus Proteinbanden erkennen, welche ausgeschnitten und mittels LC-MS/MS analysiert wurden. Dadurch wurde ein putativer Kandidat für Get5 identifiziert sowie eine Assoziation mit Chaperonen und proteasomalen Untereinheiten.

Um die Zielsteuerungseffizienz und Topologie von ER-Membranproteinen zu analysieren habe ich (i) die rekombinante Synthese eines Modell-TA Proteins mit glykosylierbarem *opsin bovine glycosylation* Tag (OPG) etabliert sowie (ii) eine Methode etabliert um in isolierten Protoplasten die Richtigkeit der Insertion zu überprüfen. Mit Hilfe dieser Methoden können nun verschiedene Mutanten auf ihre Insertions-Wirksamkeit untersucht werden. Desweiteren können durch Mutationsanalysen die notwendigen physikochemischen Eigenschaften für die Erkennung des Substrates ermittelt werden.

Eine weit verbreitete Methode im GET Feld ist die *tail-anchor translocation* (TAT). Bei dieser Methode werden isolierte mikrosomale Fraktionen des rauen ERs mit rekombinanten Komplexen

bestehend aus Zielsteuerungsfaktor und TA Protein inkubiert. Durch einen rekombinanten OPG, der im Lumen des ERs post-translational modifiziert werden kann, ist die Beobachtung einer zeitabhängigen Kinetik der Glykosylierung möglich. Dieses System wurde bislang nur für Komponenten aus Säugern oder Hefen benutzt, aber noch nie mit einem System auf pflanzlicher Basis. Um dies zu verwirklichen, habe ich die rekombinante Proteinexpression soweit optimiert, dass der Großteil des synthetisierten Proteins sich im löslichen Anteil des Lysats statt in den *Inclusion Bodies* befand. Mittels dieser Optimierung konnte ich die Ko-Expression von Zielsteuerungsfaktor mit TA Protein als löslichen Komplex etablieren. Ergänzend zu den löslichen Komplexen habe ich eine geeignete Methode etabliert um mittels Saccharosegradienten mikrosomale Fraktionen aufzutrennen in denen *AtGet3a* angereichert ist. Leider müssen noch die Parameter der Reaktion optimiert werden, aber die Akquirierung aller nötigen Bestandteile ist etabliert.

AtGet3c ist beteiligt an der Assemblierung und Stabilität von Komplexen der Atmungskette

Da außer der Lokalisation von *AtGet3c* nichts bekannt ist, wurde deren Funktion mit Hilfe von T-DNA Insertionslinien untersucht. In diesen Linien wird ein Gen durch einen flankierten Bereich aus einem modifiziertem *tumor inducing* (TI) Plasmid unterbrochen. Dies kann verschiedene Auswirkungen haben, aber in den meisten Fällen führt es zu einem Verlust des Genproduktes. Homozygote Linien zeigten einen normalen Habitus obwohl kein *AtGet3c* Protein mehr detektierbar war. Im Zuge einer Strukturanalyse mittels Transmission Elektronen Mikroskopie (TEM) konnten auch keine drastischen organellären Unterschiede zum Wildtype detektiert werden. Die elektrophoretische Auftrennung von isolierten solubilisierten mitochondrialen Membrankomplexen zeigte jedoch, dass die *Atget3c* Deletionsmutante weniger Komplex II und IV_b assemblierte als der Wildtype. Diese Beobachtung führte zur Hypothese, dass *AtGet3b* in der Assemblierung und/oder Stabilität von Komplex II und Komplex IV_b involviert ist. Diese muss jedoch noch experimentell bestätigt werden.

AtGet3b ist beteiligt an der Assemblierung von Photo Systemen (PS)

Auch für dieses organelläre Ortholog ist nichts außer seiner plastidären Lokalisation bekannt. Um die Funktionalität von *AtGet3b* zu untersuchen, wurden wieder T-DNA Insertionslinien eingesetzt. Diesmal wurden zwei Linien zur Analyse verwendet. Eine Doppel-Insertion in der 5' UTR Region des Gens, die zu einer Überexpression des Genproduktes geführt hat (*Atget3b-1*) und eine Insertion im vierten Intron, die zu einem Verlust des Genproduktes geführt hat. Beide Mutanten waren vital, haben die selbe Entwicklung wie der Wildtyp durchlaufen und sich phänotypisch kaum von diesem unterschieden. Um ein besseres Bild der plastidären Struktur der Mutanten zu erhalten habe ich diese mittels TEM

untersucht und festgestellt, dass beiden Mutanten signifikant mehr Thylakoid-Lamellen innerhalb ihrer Granathylakoide enthalten als der Wildtyp. Dies deutete auf eine verschiedenartige Zusammensetzung der Thylakoide hin. Um Einblicke in dessen Aufbau zu erhalten, habe ich aus den verschiedenen Insertionslinien Thylakoide isoliert, solubilisiert und die membran-gebunden Komplexes mittels Blau Native (BN) PAGE elektrophoretisch aufgetrennt. Dabei bestätigte sich, dass die Proteinzusammensetzung der Thylakoide beider Mutanten unterschiedlich zum Wildtyp war. Um eine potentielle Beteiligung an der Biogenese von Photosystemen zu untersuchen, habe ich etiierte Keimlinge belichtet und den Grad der Assemblierung mit Hilfe von PAM Messungen evaluiert. Dabei konnte ich zeigen, dass die Linie ohne Genprodukt signifikant „gedrosselt“ im Aufbau der Photosysteme war, während die Linie mit verstärkter Genexpression dagegen etwas schneller war als der Wildtyp. Dies war nicht nur während der *de novo* Assemblierung der Fall, sondern auch im Gleichgewichtszustand der frühen Phasen der generellen Assemblierung. Weitere PAM Messungen in späteren Entwicklungsstadien sowie der gemessene Chlorophyllgehalt der verschiedenen Insertionslinien bestätigten eine potentielle Beteiligung des *AtGET3B* Genproduktes an der Biogenese des photosynthetischen Apparates.

Nachdem ich beobachtet habe, dass die Protein Niveaus von PsbW, das Teil des photosynthetischen Apparates ist, in den Insertionslinien unterschiedlich zum Wildtyp waren, habe ich diesen Zusammenhang weiter untersucht. Dabei konnte ich mit einem etabliertem *in vitro* Assay, in dem ein Zielsteuerungsfaktor zusammen mit potentielltem Substrat ko-exprimiert wird, zeigen, dass *AtGet3b* das TA Protein PsbW binden kann. Mit Hilfe einer PsbW-Deletions-Variante konnte ich zeigen, dass diese Interaktion abhängig von der Anwesenheit einer TMD ist. Um das volle Substrat-Spektrum näher zu untersuchen, wurde mit demselben System *AtGet3b* zusammen mit *LHCB2* ko-exprimiert. *LHCB2* ist eine Lichtsammelantenne aus dem Lichtsammelkomplex und besitzt im Gegensatz zu PsbW drei statt einer TMD. Mit dem *in vitro* Assay konnte ich zeigen, dass *AtGet3b* in der Lage ist *LHCB2* zu binden und damit anscheinend ein erweitertes Substrat Spektrum hat als das zytosolische Ortholog in anderen Systemen.

Vergleich der Plastidären Proteome

Um die Auswirkungen der beiden Mutationen auf proteomischer Ebene besser zu verstehen und Einblicke in die potentielle Beteiligung an zellulären Prozessen zu gewinnen, habe ich isolierte Chloroplasten aus genetischen modifizierten *Arabidopsis thaliana* sowie aus Wildtyp mit LC-MS/MS analysiert, die Proteome quantitative verglichen und statistisch ausgewertet. Dabei konnte gezeigt werden, dass viele Faktoren, die an der Assemblierung oder Instandhaltung sowie wichtige Teile des photosynthetischen Apparates negativ betroffen waren in der Mutante mit verminderter

Genexpression. Verschiedene Komponenten, die an der Regelung sowie der Ausführung des zyklischen Elektronentransports beteiligt sind, waren signifikant abgereichert. Da der Zyklische Elektronen Transport hilft das NADPH/ATP Verhältnis zu regeln für die Dunkelreaktion der Photosynthese, wurden auch viele Komponenten aus der Dunkelreaktion reduziert. Eventuell um diesen Missstand zu kompensieren wurden die Metabolit Translokatoren sowie fast all Lichtsammelkomplexe hochreguliert. Um den Transport dieser zu gewährleisten, wurden die entsprechenden Translokationssysteme auch signifikant Angereichert. Dies könnte den beobachteten strukturellen Phänotyp der Mutante mit fehlender Genexpression erklären. Interessanterweise benutzten viele der betroffenen photosynthetischen Komponenten Ferredoxin als Ko-Faktor. Ferredoxin selbst war in der Mutante mit verstärkter Genexpression zugleich der das am stärksten angereicherte Protein. Desweiteren waren alle Bestandteile der Haupt *Fe-S Cluster* Assemblierungsmaschinerie in beiden Insertionsmutanten affektiert. Dies legt nahe, dass *AtGet3b* nicht nur an der Biogenese von Ferredoxin beteiligt ist, sondern darüber hinaus eventuell mit der Eisen-Schwefel *Cluster* Maschinerie interagiert. Entgegen aller Annahmen wurden in der Mutante mit fehlender Genexpression keine TA Proteine runterreguliert, sondern eher lösliche Proteine aus dem Lumen der Thylakoide herunter-reguliert. Dies wurde dadurch untermauert, dass auch die korrespondierenden stromalen Zielsteuerungsfaktoren betroffen waren. Interessanterweise waren in beiden Mutanten auch verschiedene Teile des plastidären Translokationsapparates signifikant betroffen. Zusammengenommen deutet dies auf eine Beteiligung der analysierten Gene an stromalen Transportprozessen hin. Überraschenderweise waren in beiden Mutanten viele der für die Membranmodellierung zuständigen Faktoren in ihrer Abundanz beeinträchtigt. Dies deutet darauf hin, dass *AtGet3b* eventuell an solchen Prozessen beteiligt ist.

Get3 Chaperone Aktivität

Die Chaperone Aktivität aller Get3 Orthologe aus *A. thaliana* wurde auch *in vitro* analysiert. Dabei konnte gezeigt werden, dass *AtGet3a* als einziges Ortholog dazu fähig war, die hitzeinduzierte Aggregation von einem Modell-Substrat zu verhindern. Die anderen Orthologe konnten das Substrat nicht löslich halten und sind zusammen mit diesem aggregiert. Es müsste noch evaluiert werden ob diese Ko-Aggregation eventuell eine Form des Schutzes darstellt, wie es schon in anderen Systemen beschrieben wurde. Um die *in vitro* Analyse zu ergänzen, konnte ich in isolierten Protoplasten zeigen, dass unter oxidativen Stress *AtGet3b* zu spezifischen *Foci* relokalisiert wird. Diese verhalten sich wie *proteinaceous membrane less organelles* (PMLOs) und bleiben resistent gegenüber Detergenz-Behandlungen.

ZUSAMMENFASSUNG

Zusammenfassend kann man sagen, dass die Methoden, die von mir zur Erforschung von *AtGet3a* in dieser Arbeit etabliert wurden, künftig in der Forschung von GET in Pflanzen eingesetzt werden können, um verschiedene evtl. pflanzenspezifische Parameter zu ermitteln. In Bezug auf die organellären Orthologe konnte ich bereits die ersten Belege für eine eventuelle Beteiligung an der Assemblierung von membrangebunden Komplexen experimentell generieren. Speziell die mannigfaltigen Beteiligungen von *AtGet3b* in der Biogenese von Thylakoiden liefert neue Ansätze für weitere Forschungen.

ABSTRACT

The guided entry of tail-anchored proteins (GET) pathway mediates the targeting and insertion of tail-anchored proteins into the lipid bilayer of the endoplasmic reticulum (ER). A highly regulated protein triage hands over the TA protein from a pre-targeting complex composed of Sgt2 and Get4/5 to the receptor complex comprised of Get1/2 in a Get3 dependent manner. Previous studies have identified that, Get3 the central ATPase of the pathway, has three orthologues in *Arabidopsis thaliana*. These belong to two different conserved clades, namely an “a” clade and a “bc” clade localized to the cytosol and endosymbiotic-originated organelles, respectively. Here, the taxonomic relationship of Get3 in planta was re-evaluated and identified groups orthologous to the cytosolic (*At*Get3a), plastidic (*At*Get3b) and mitochondrial (*At*Get3c) as well as a fourth Poales specific orthologous group (*sB*Get3). The localizations of the former three groups were evaluated in selected homologous as well as heterologous systems and displayed that several Get3 orthologues with divergent localizations is communal in plants. However, knowledge of the function of these proteins is still limited. For this, I could identify putative elements of the pre-targeting complex and establish two systems to functionally characterize *At*Get3a. One to (i) monitor the membrane insertion and subsequent glycosylation of recombinant model substrates *in cellula* and (ii) co-express and purify targeting-factor/substrate complexes of all *At*Get3 orthologues that can be used for *in vitro* analyses. In a reverse genetic approach, I could show that the function of *At*Get3c seems to be involved in the assembly and stability of components of the respiratory chain in mitochondria. And, that *At*Get3b is involved in *de novo* photosystem (PS) assembly and repair in thylakoids. Further, I could also show that *At*Get3b binds photosynthetic membrane proteins in transmembrane domain (TMD) dependent manner and under oxidative stress it shares features of proteinaceous membrane less organelles (PMLOs). Additionally, the comparison of the wild-type chloroplast proteome to mutant chloroplasts lacking and overexpressing *At*Get3b revealed a possible involvement in protein transport, Fe-S cluster biogenesis and membrane remodeling. This study characterizes the yet undescribed organellar Get3 orthologues of *Arabidopsis thaliana* and paves a way for subsequent scientific interrogations. Further, the methods established for the cytosolic Get3 orthologues can help propel the biochemical *in vitro* analysis of plant derived GET constituents.

1. INTRODUCTION

A hallmark of eukaryotic cells is the establishment of compartmentalized biochemical reaction spaces enclosed in lipid bilayers (Watson, 2015). In order to maintain and fine-tune this compartmentalization, cells have evolved dedicated molecular machineries to correctly identify, target and translocate newly synthesized proteins to the proper organelle (Bohnsack and Schleiff, 2010). Coherently, proteins are equipped with so-called topogenic signals which aid their inclusion in the sorting processes (Blobel, 1980). During or after translation the topogenic signals are recognized by factors that transport them to their destination. Once arrived at the membrane of an organelle, other molecular apparatuses arbitrate their translocation across or into a bordering membrane.

The communication with as well as passage through a membranous enclosure like an organelle is typically facilitated by integral membrane proteins (IMPs). These constitute roughly 20 % to 30 % of all protein coding open reading frames (ORFs) (Wallin and Von Heijne, 1998; Krogh et al., 2001; reviewed in Elofsson and Von Heijne, 2007). IMPs fulfill a multitude of functions ranging from the translocation of proteins (Pfeffer et al., 2015; reviewed in Park and Rapoport, 2012) over organelle biogenesis (Sommer et al., 2013; reviewed Schleiff and Becker, 2011) to signal receptors (Hilger et al., 2018; reviewed in Perez, 2005). IMPs are ascribed to encompassing transmembrane domains (TMDs). These are highly hydrophobic and can fold into a single α -helix as well as α -helical bundles or β -barrel structures within a membrane (Mariappan et al., 2011; Pleiner et al., 2020; Ni et al., 2014). This biophysical property poses a challenge to cellular proteostasis as (i) hydrophobic segments exposed to the bulk cytosol are prone to aggregation (Mahler et al., 2012) and (ii) these are energetically most stable in a folded state within a lipid environment (White and Von Heijne, 2008). Thus, the transfer of IMPs from their cytosolic synthesis into a lipid bilayer presents a crucial stage in their biogenesis. This procedure requires selective TMD recognition, protection from hydrophilic exposure, targeting to the membrane bound translocation system followed by TMD integration into the lipid bilayer with the correct topology. These obstacles have to be overcome by all IMP insertion pathways and cognate quality control systems. This is typically done by utilizing dedicated molecular machineries in the cytosol and designated membrane. Membrane proteins synthesized on cytosolic ribosomes can be post-translationally targeted to chloroplasts (reviewed in Nakai, 2018), mitochondria (reviewed in Wiedemann and Pfanner, 2017), peroxisomes (Walter and Erdmann, 2019), nuclei (Hicks and Raikhel, 1995) and endoplasmic reticulum (ER) (Luirink and Sinning, 2004). The common route of membrane protein targeting to the ER is co-translational translocation (Rapoport, 1992). By encompassing both nuclear membranes as well as the entire endomembrane system the ER accommodates the largest amounts of IMPs (Palade et al., 1975). Depending on the position of a TMD on an emerging polypeptide chain, different pathways interact and facilitate its insertion into the lipid bilayer of the ER (Figure 1.1)

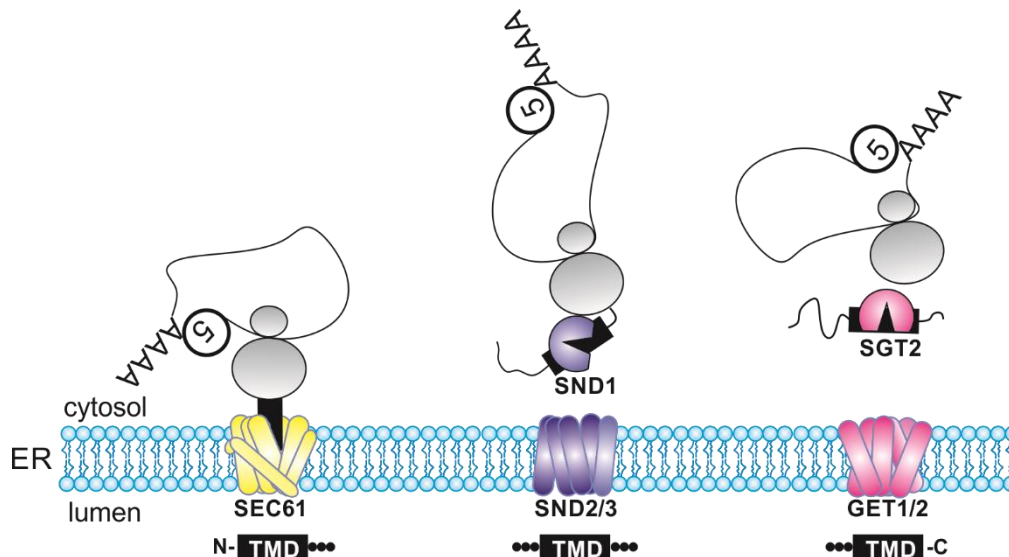


Figure 1.1. Described modes of integral membrane protein (IMP) insertion at the endoplasmic reticulum (ER). The positioning of the hydrophobic signal determines the targeting pathway. Topogenic signals within hydrophobic segments positioned at the extreme N-terminus utilize the co-translational signal recognition particle (SRP) pathway (yellow). Hydrophobic topogenic signals positioned further downstream of the polypeptide stretch use the SRP independent (SND) pathway (blue). Signals within TMDs positioned at the extreme C-terminus of a protein employ the guided entry of tail anchored (GET) proteins pathway (magenta).

1.1 Signal recognition particle (SRP) pathway

If the topogenic signal of an ER-destined protein is located in the N-terminal region of a polypeptide stretch it is targeted by the SRP pathway. It is highly conserved in all three major branches of the phylogenetic tree and of ancient evolutionary origin (Althoff et al., 1994). The pathway is triggered by the interaction of the topogenic signal of an ER-destined protein and the SRP (Blobel, 1980). These topogenic signals are termed signal peptides or signal anchors. Signal peptides are typically cleavable and used by soluble secretory proteins while signal anchors are classically embedded within the first TMD of an IMP and forms part of the mature protein (reviewed in Rutz et al., 2015). Both share modular features like a hydrophobic core flanked by polar residues on the one side and helix breaking residues on the other (Martoglio and Dobberstein, 1998; Hegde and Bernstein, 2006). The SRP is a heterodimeric ribonucleoprotein complex (Walter and Blobel, 1982) that interacts with the ribosome (Powers and Walter, 1996). The methionine-rich domain (M-domain) of SRP54 subunit interacts with the hydrophobic core of the emerging topogenic signal (High et al., 1993; Zopf et al., 1990). In order to shield this entity from the bulk cytosol, the SRP attaches in vicinity to the ribosomal exit tunnel (Halic et al., 2004). This initial interaction transiently slows down translation (Lipp et al., 1987; Walter et al., 1981), which in turn expands the kinetic window to recruit the complex to the SRP receptor (SR) (Lakkaraju et al., 2008). Thereafter the ribosome nascent chain complex (RNC) dissociates from the SRP (Gilmore et al., 1982; Meyer et al., 1982) to relocate to the protein conducting channel, SEC61 (Simon and Blobel, 1991; Görlich et al., 1992). The ribosome stays bound to the SEC61 translocon and

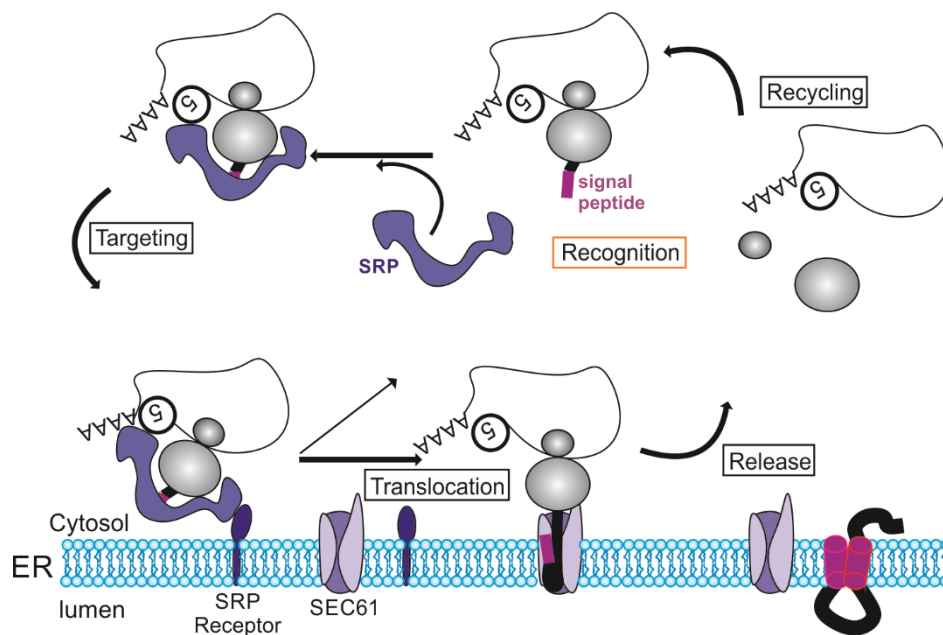


Figure 1.2. Molecular steps in signal recognition particle (SRP) mediated targeting.

The signal recognition particle (SRP; blue) recognizes the emerging signal sequence of the nascent chain (purple). The ribosome-nascent chain-SRP complex is recruited to the ER membrane by an interaction with the SRP receptor (SR). The signal peptide is then released from the SRP, docks at the SEC61 translocon and co-translational integral membrane protein (IMP) insertion is initiated. The (re)initial step of the pathway is highlighted in orange.

completes synthesis of the membrane protein. In a co-translational manner, the SEC61 translocon facilitates the lateral insertion of the emerging TMDs into the lipid bilayer of the ER (Junne et al., 2010; Gogala et al., 2014). After dissociating from the RNC, the SRP can undergo repeated cycles of topogenic signal recognition and shielding followed by cargo handover (Figure 1.2).

1.2 SRP independent targeting (SND) pathway

Recently, a novel mode of post-translational targeting to the ER was discovered. When the signal anchor of an ER-destined IMP is located further downstream of the polypeptide stretch it is transported by the SRP independent targeting (SND) pathway (Aviram et al., 2016). In yeast, three key players have been identified to date: the cytosolic, ribosome associated protein Snd1 (Huh et al., 2003; Fleischer et al., 2006), the polytopic IMP Snd2 and the single pass IMP Snd3 (Aviram et al., 2016). The two IMPs were shown to localize at the ER, associated with SEC61 (Fleischer et al., 2006; Huh et al., 2003; Aviram and Schuldiner, 2014; Aviram et al., 2016). The mammalian homologue, hSnd2 is part of a protein targeting network that includes components of the TRC and SRP pathway (Haßdenteufel et al., 2017). The mechanistic outline of the pathway includes client identification and capture by Snd1 at the ribosome followed by a recruitment to the translocation machinery, at which client hand over

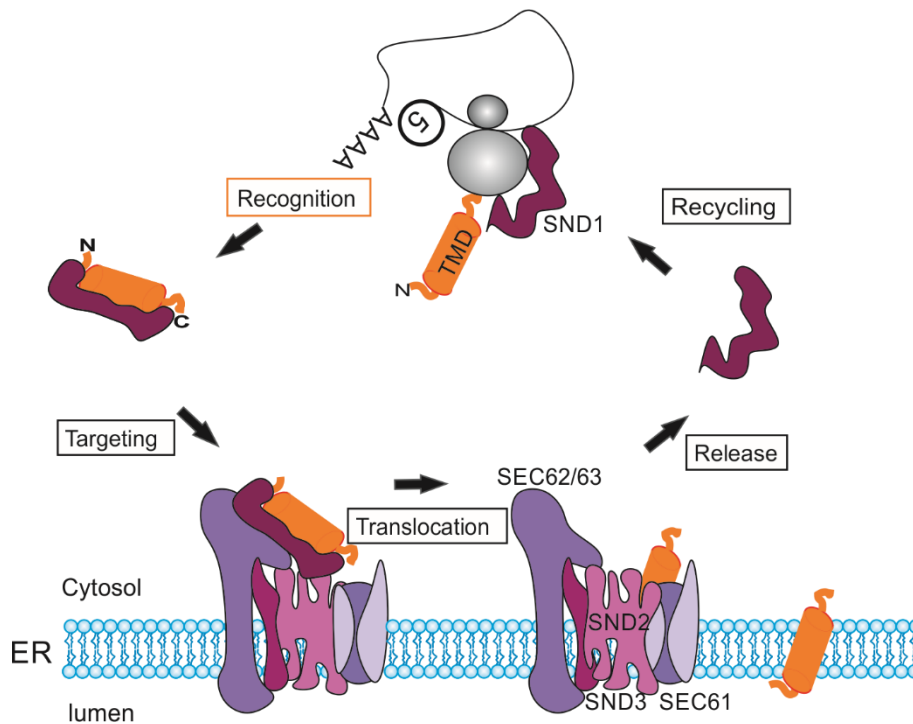


Figure 1.3. Molecular outlining of SRP independent (SND) targeting.

The ribosome associated SND1 recognizes and binds the downstream TMD of clients. This complex is then recruited to the translocon composed of SND2, SND3, SEC61 as well as SEC62/63 where post translational translocation takes place. The (re)initial step of the pathway is highlighted in orange.

takes place till membrane insertion is mediated (Figure 1.3) (Aviram et al., 2016). It seems that the TRC/GET and SND pathways are backup systems for one another involved in the guidance of IMPs further downstream of the polypeptide stretch. If the one fails to capture client or is absent, the other can still fulfill the function of hydrophobic motif identification and targeting (Aviram et al., 2016; Haßdenteufel et al., 2017).

1.3 Guided entry of tail anchor proteins (GET) pathway

Next to the co-translational mode of IMP insertion that has been intensively studied over the past 40 years (Blobel and Dobberstein, 1975; Walter et al., 1981; Powers and Walter, 1996; Junne et al., 2010; McGilvray et al., 2020), novel pathways that facilitate IMP insertion in a post-translational manner have been described in the past decade (Stefanovic and Hegde, 2007; Aviram et al., 2016). Tail-anchored (TA) proteins share a modular topological feature of a transmembrane domain (TMD) within the last 50 amino acids (AAs) of their polypeptide stretch and make up 3-5 % of all eukaryotic IMPs (Kalbfleisch et al., 2007). TA proteins fulfill a multitude of essential biological functions like apoptosis (Jiang et al., 2014), vesicle transport (van Berkel et al., 2020) and organelle biogenesis (Sommer et al., 2013). The ribosome exit tunnel can accommodate 30 AAs of an elongated peptide chain or 60 AAs in

a α -helical conformation (Voss et al., 2006; Picking et al., 1992; Malkin and Rich, 1967). Due to these constraints TA proteins cannot interact with the SRP as their signal anchor would still be buried in the exit tunnel till translation is terminated, thereby necessitating a new set of factors to mediate post translational TA protein targeting (Rachubinski et al., 1980; Okada et al., 1982; Kutay et al., 1993, 1995). A major breakthrough in understanding TA protein biogenesis was the identification of the transmembrane recognition complex of 40 kDa (Trc40) in mammals (Stefanovic and Hegde, 2007; Favalaro et al., 2009). Due to a high degree of conservation the yeast homologue golgi ER transport3 (Get3), the protein formally known as Arr4 was readily identified (Shen et al., 2003). Synthetic genetic and physical interaction studies soon led to the identification of the key players of the GET pathway in *Saccharomyces cerevisiae* (Copic et al., 2009; Ho et al., 2002; Jonikas et al., 2009; Schuldiner et al., 2005). Coherently, homology based queries and biochemical studies led to the identification of the major players of the TRC pathway in mammals (Mariappan et al., 2010; Leznicki et al., 2010, 2011; Vilardi et al., 2011; Yamamoto and Sakisaka, 2015). Both TRC and GET utilize the same mechanistic paradigm of capturing and shielding the TA protein with the pre-targeting complex, followed by a highly regulated substrate handover to the respective targeting factor. This is proceeded by the recruitment to the membrane bound receptor and ends with the insertion of the TA protein into the lipid bilayer of the ER followed by targeting factor recycling to the cytosol (Figure 1.4) (Reviewed in Hegde and Keenan, 2011; Denic et al., 2013; Borgese et al., 2019).

1.3.1 Pre-targeting complex in yeast

Since Trc40 does not associate with ribosomes in mammals (Stefanovic and Hegde, 2007), the factors involved in post-translational delivery to Get3 were explored in *Saccharomyces cerevisiae*. Structural, functional, mutational and biochemical studies led to the identification of the pre-targeting complex (Jonikas et al., 2009; Wang et al., 2010; Chang et al., 2010; Chartron et al., 2012). It is composed of the small glutamine rich tetratricopeptide repeat (TPR) containing protein2 (Sgt2), Get4, Get5 and TA client (Wang et al., 2010). Get4 is an elongated α -helical solenoid (Chang et al., 2010) that arranges to an obligate heterodimer with Get5 (Chartron et al., 2012). This is enforced by the hydrophobic interactions of the C-terminus of Get4 with the N-terminus of Get5 (Chartron et al., 2010). The N-terminus of Get5 is preceded by an ubiquitin-like (UBL) domain and a C-terminal homo-dimerization domain (Tung et al., 2013; Chartron et al., 2012). Sgt2 is highly conserved across eukaryotes (Kordes et al., 1998). It comprises a N-terminal homo-dimerization domain that binds the Ubl domain of Get5 (Liou et al., 2007; Tung et al., 2013), three tetratricopeptide repeat (TPR) domains that can interact with an ensemble of different chaperones (Liou et al., 2007) and a C-terminal methionine-rich domain that can selectively recognize hydrophobic signal anchors (Wang et al., 2010). The mechanistic outline

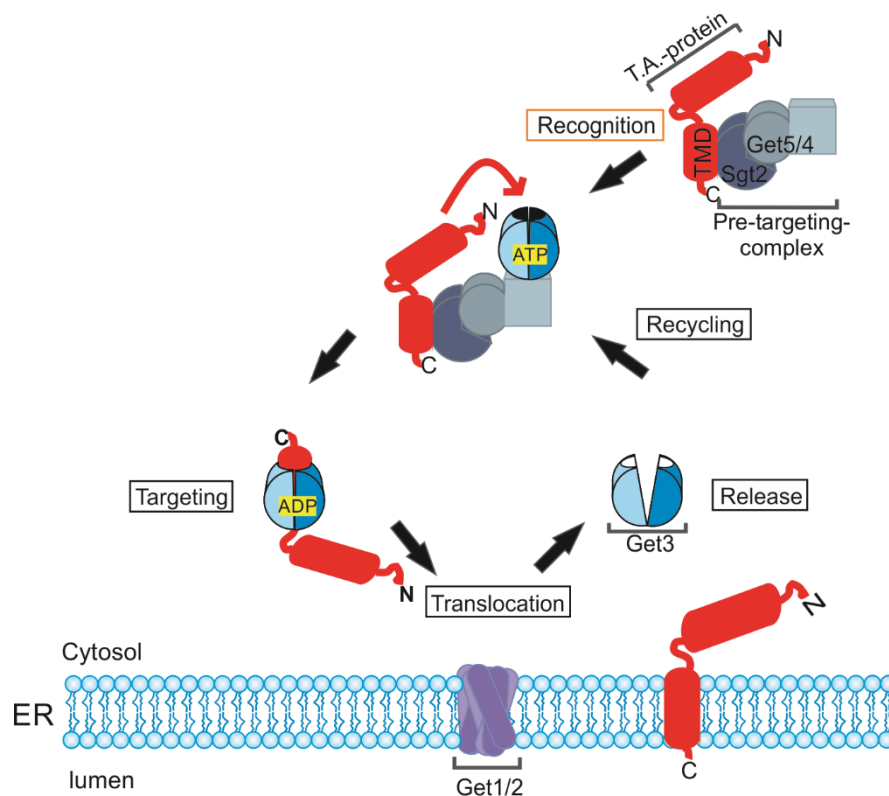


Figure 1.4. Molecular ensemble of the guided entry of tail anchored proteins (GET) pathway.

After translation termination Sgt2 associated with the C-terminal TMD of TA proteins and hands these over to Get3 in a Get4/5 dependent manner. The Get3-TA protein complex is then recruited to translocon at the ER membrane that then facilitates its post-translational membrane insertion. The (re)initial step of the pathway is highlighted in orange.

is as follows: Sgt2 binds to freshly synthesized TA client most probably in a chaperone dependent manner via its C-terminus and TPR domains, respectively (Wang et al., 2010; Cho and Shan, 2018). The N-terminus interacts with the Ubl domain of Get5 (Chartron et al., 2010) which is tethered to Get4 (Chang et al., 2010) whose N-terminus interacts with Get3 and restrains its ATPase activity (Gristick et al., 2014). Therefore, Get4/5 is an adapter complex that aids the transfer of client from Sgt2 to Get3 and modulates Get3 activity.

1.3.2 Pre-targeting complex in mammals

One key aspect that differs between the fungal GET and mammalian TRC pathways is the composition of the pre-targeting complex. Instead of a Get4/5 heterodimer, the mammalian counterpart utilizes a trimeric complex, termed BAG6 composed of Bag6, TRC35 (Get4) and Ubl4a (Get5) (Leznicki et al., 2010; Mariappan et al., 2010). Upstream of BAG6, the mammalian homologue to Sgt2, SGTA, is required (Chartron et al., 2012; Leznicki et al., 2011; Mock et al., 2015). SGTA does not only arbitrate the initial capture of the signal anchor but is also able to shield specific TMDs in complex IMPs during their biogenesis (Leznicki and High, 2020). Bag6 is equipped with a N-terminal Ubl domain to which

Trc35 binds and a C-terminal bag domain which mediates the interaction with Ubl4A. Latter interaction masks the NLS of Bag6 thereby facilitating cytosolic retention (Mock et al., 2015). SGTA binds the BAG6 complex by recognizing the Ubl domain of Ubl4a (Xu et al., 2012; Chartron et al., 2012). Analogous to the fungal counterpart, SGTA and the BAG6 complex mediate TA client handover from SGTA to Trc40 (Casson et al., 2017; Shao et al., 2017). Bag6 also participates in protein quality control by interacting with the E3 ligase RNF126 via its Ubl domain (Rodrigo-Brenni et al., 2014). This interaction is thought to facilitate the ubiquitination and proteasomal degradation of defective ribosomal products (DRiPs) (Minami et al., 2010) as well as mislocalised membrane and secretory proteins (MLPs) (Rodrigo-Brenni et al., 2014; Leznicki and High, 2012). Interestingly, SGTA is capable of antagonizing Bag6/RNF126 arbitrated ubiquitination of MLPs as well as stimulating the deubiquitination of these (Leznicki and High, 2012; Wunderley et al., 2014).

1.3.3 The membrane receptor complex in yeast

The yeast counterpart was identified by a large-scale based genetic interaction map of the secretory pathway, which was then further characterized in proceeding studies (Schuldiner et al., 2005; Auld and Silver, 2006; Jonikas et al., 2009). It consists of a heterodimer of Get1 and Get2 (Wang et al., 2014; McDowell et al., 2020). Each subunit is embedded within the lipid bilayer of the ER by three TMDs (McDowell et al., 2020). Get3 recognition is mediated by the cytosolic domains of Get2 which in turn hands it over to Get1 (Wang et al., 2013; Stefer et al., 2013; McDowell et al., 2020). The complex acts as a *bona fide* insertase, facilitating the insertion of TA proteins into the lipid bilayer of the ER (Wang et al., 2014).

1.3.4 The membrane receptor complex in mammals

Get1 homologues can be identified by sequence similarity in distantly related phyla (Vilardi et al., 2011; Srivastava et al., 2017; Xing et al., 2017; Bodensohn et al., 2019; Borgese, 2020). Biochemical studies led to the identification of the mammalian Get1 counterpart, tryptophan-rich basic protein (WRB) (Vilardi et al., 2011). Get1/WRB is a member of the evolutionary conserved Oxa1/Alb3/YidC protein family mediating membrane protein biogenesis (Anghel et al., 2017). Generally, this protein family supplies a three helix bundle in membrane that cooperates with another bundle from an interacting protein to mediate IMP insertion (McDowell et al., 2020). However, these are not identifiable based on sequence similarity (Borgese, 2020). Albeit, the mammalian homologue was detected biochemically (Yamamoto and Sakisaka, 2012). The mammalian counterparts mutually regulate themselves and the

mechanistic hierarchy of handover is analogous to the yeast counterpart (Vilardi et al., 2014; Colombo et al., 2016; Yamamoto and Sakisaka, 2015).

1.4 Get3

1.4.1 Get3 is a targeting factor

The central player of the GET pathway, Get3 has 27 % homology to bacterial ATPase (AraA) (Stefanovic and Hegde, 2007). In terms of evolutionary classification, it belongs to an ancient subfamily of nucleotide-binding proteins, the signal recognition particle, MinD and BioD (SIMBI) (Leipe et al., 2002). SIMBI proteins assemble into homo- or hetero-dimers to complement the catalytic machinery of one protomer with the active site of another (Gasper et al., 2009). Like all phosphate-binding (P-loop) proteins, Get3 comprises the Walker A motif with switch I, switch II as well as P-loop and A-loop motifs to bind α -, β -phosphate, respectively as well as the magnesium ion (Saraste et al., 1990; reviewed in Wittinghofer and Vetter, 2011). Switch motifs undergo conformational conversions under nucleotide hydrolysis, thereby acting as molecular switches that transition between a NTP-bound “on” state and NDP- bound “off” state (Bourne, 1995; reviewed in Wittinghofer and Vetter, 2011). Conserved CxxC motifs in Get3 coordinate a zinc ion forming a symmetric homodimer equipped with a static ATPase domain and a flexible α -helical domain which is sensitive to nucleotide binding (Mateja et al., 2009; Bozkurt et al., 2009). In the ADP-bound open state the helical subdomain of each monomer is wide apart and hydrophobic residues are buried within the fold. However, in an ATP-bound state the helical subdomain structurally rearranges to form a deep hydrophobic groove that can bind TMDs (Bozkurt et al., 2009; Mateja et al., 2015). Once client protein is bound a dynamic α -helix functions as a lid, preventing off pathway interactions (Chio et al., 2017, 2019).

1.4.2 Get3 in a cellular context

GET3 appears to play an important role in cellular integrity as its lack leads to embryo lethality in mice (Mukhopadhyay et al., 2006). In yeast however, its loss is only conditionally lethal (Shen et al., 2003; Jonikas et al., 2009). By recognizing, shielding and shuttling hydrophobic segments through the bulk cytosol and thereby preventing their aggregation, Get3 contributes considerably to cellular proteostasis (Jonikas et al., 2009). However, a novel involvement in proteostasis has been described for Get3. Under energy limiting conditions Get3 relocates to distinct cytosolic foci together with other chaperones thereby acting as an ATP-independent holdase, by binding the exposed hydrophobic patches of disrupted proteins. This recruitment is reversible when the system is replenished with a

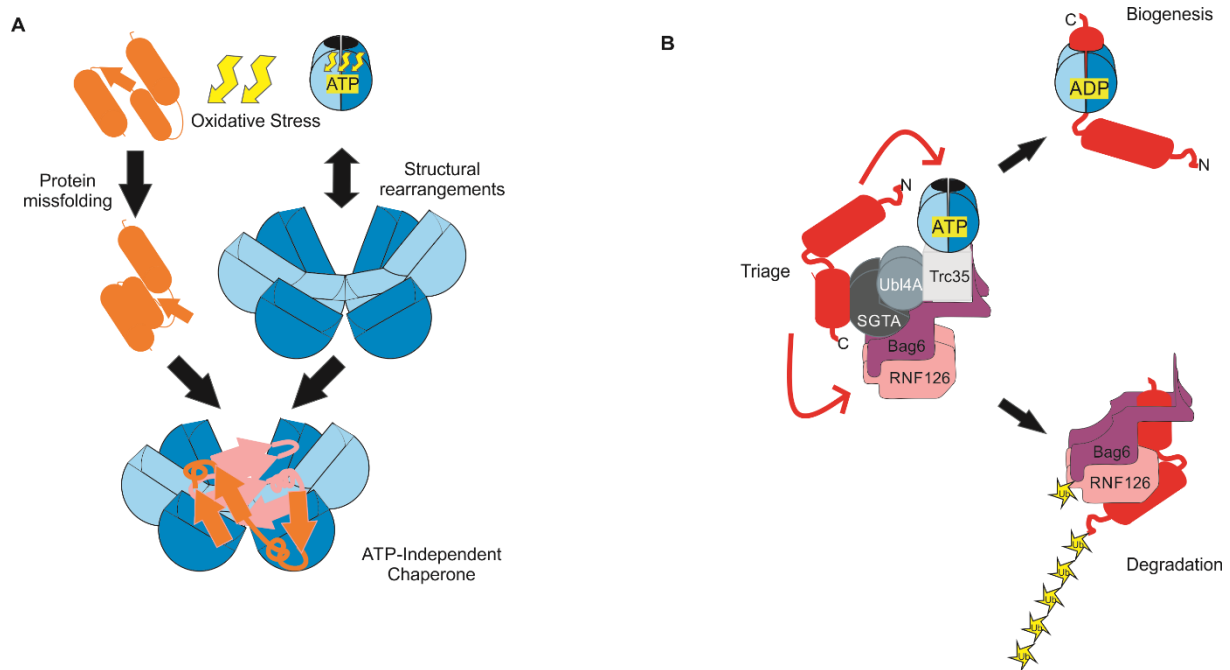


Figure 1.5. Auxiliary cellular functions of Get3.

A. Under oxidative stress or energy limiting conditions, Get3 (blue) undergoes structural rearrangements and acts as an ATP-independent chaperone. This holdase function is mediated by binding the exposed hydrophobic patches of denaturing proteins. **B.** Bag6 (purple), a constituent of the BAG6 complex (gray scale and purple) is able to interact with the E3 ligase RNF126 (pink) to facilitate the ubiquitination (yellow) of client proteins (red) that cannot properly engage with the TRC pathway. Note, that SGTA is capable of antagonizing Bag6 as well as deubiquitination to relay clients back to the TRC pathway. Ubiquitin molecules are depicted as yellow star-like structures.

carbon source (Powis et al., 2013). A further study, revealed that under highly oxidative conditions, Get3 undergoes structural rearrangements involving the formation of disulfide bonds in the conserved CxxC motif with concomitant release of the coordinated zinc ion. This resulting oligomeric structure is capable of acting as a holdase (Voth et al., 2014). This mode of action is very reminiscent of Hsp33, a redox regulated, oxidation sensitive, zinc binding and ATP independent chaperone in bacteria (Jakob et al., 1999). Apart from the secondary holdase function, the pre-targeting complex of the TRC pathway displays an involvement in proteostatic events. Through the interaction of Bag6 with the E3 ligase RNF126 (Wang et al., 2010; Rodrigo-Brenni et al., 2014; Payapilly and High, 2014; Wunderley et al., 2014). In conjunction with the deubiquitination capacity of SGTA, the resulting molecular triage mediated by GET constituents reflects the molecular verdict between biogenetic and degradative pathways (Figure 1.5) (Leznicki and High, 2012; Wunderley et al., 2014).

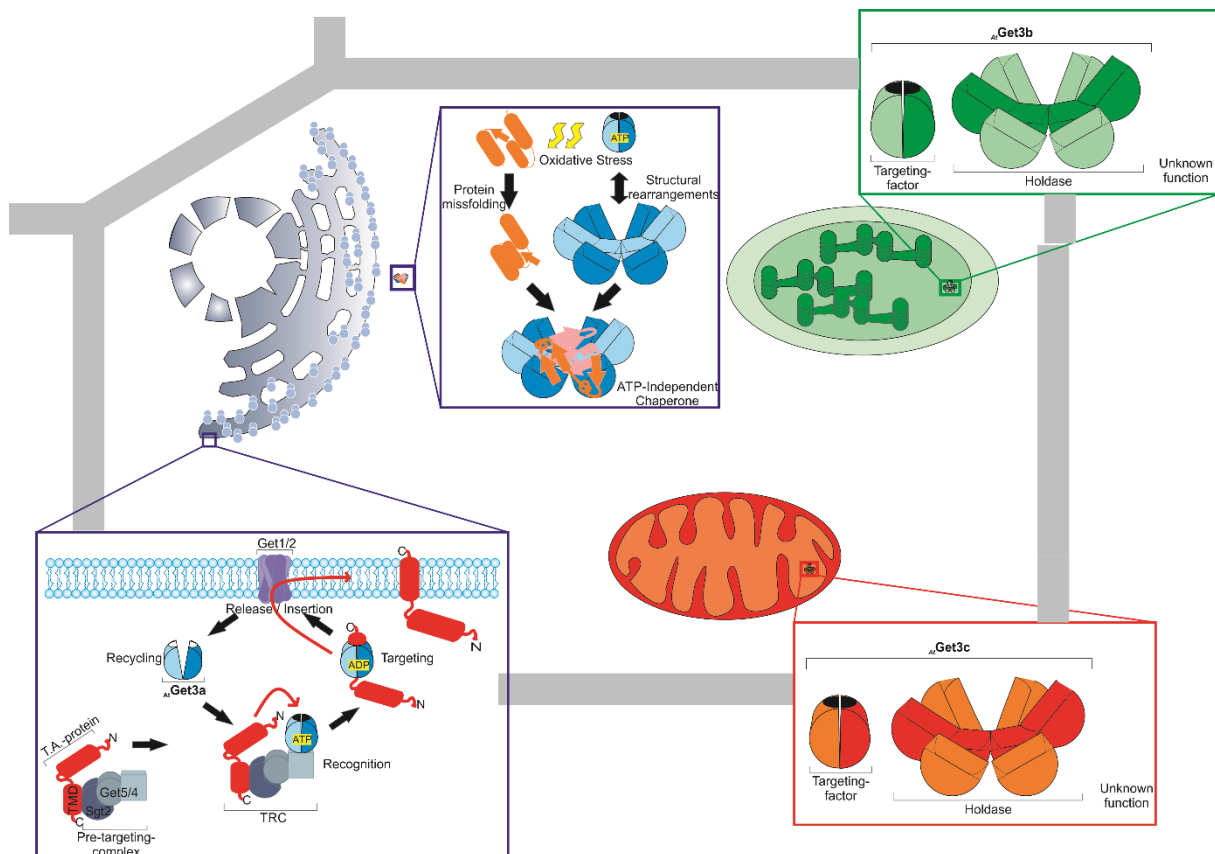


Figure 1.6. Get3 in *Arabidopsis thaliana*.

Depicted are the three Get3 orthologues and their potential functional role in *A. thaliana*. The cytosolic localized $AtGet3a$ (blue), the stromal localized chloroplastidic $AtGet3b$ (green) and the matrix localized mitochondrial $AtGet3c$ (orange). These orthologues could either fulfill the targeting or holdase functions as previously reported from other systems or a novel unknown function, generally in plants or specifically in *A. thaliana*.

1.4.3 Get3 in plants

Due to the high degree of conservation Get3 it is also present in planta (Srivastava et al., 2017; Paul et al., 2013; Duncan et al., 2013; Xing et al., 2017; Bodensohn et al., 2019). Contrasting non-plant metazoans, plants have multiple Get3 orthologues. Phylogenetic analysis of the whole tree of life revealed that Get3 diversified into two clades, namely clade “a” and clade “bc” (Xing et al., 2017). *Arabidopsis thaliana* has three Get3 orthologues, namely $AtGet3a$ (At1g01910), $AtGet3b$ (At3g10350) and $AtGet3c$ (At5g60730) localized to cytosol, chloroplasts and mitochondria, respectively (Figure 1.6) (Duncan et al., 2013; Xing et al., 2017; Bodensohn et al., 2019). Furthermore, Get1 and Get4 could also be identified and their localization assigned to ER and cytosol, respectively (Duncan et al., 2013; Xing et al., 2017; Bodensohn et al., 2019). The loss of function of any one of these did not display any severe growth defects in *A. thaliana*. However, $AtGet3a$, $AtGet4$ and $AtGet1$ deficiency led to reduced root hair with concomitant reduction of protein levels of the soluble N-ethylmaleimide-sensitive-factor attachment receptor (SNARE) protein Syp123 (Xing et al., 2017). In *Chlamydomonas reinhardtii* a total of three Get3 orthologues exist (Bodensohn et al., 2019). Two of these, namely ArsA1 and ArsA2 are

predicted to reside in the cytosol of *C. reinhardtii* and bind hydrophobic motifs destined for endosymbiotic organelles or ER, respectively (Maestre-Reyna et al., 2017; Lin et al., 2019). Interestingly, ArsA1 displays a monomeric assembly, more similar to the bacterial ArsA than the metazoan dimeric architecture (Lin et al., 2019). ArsA1 deficiency leads to defects in chloroplastidic biogenesis (Formighieri et al., 2013).

1.5 Photosynthetic membranes

The membrane of the chloroplast thylakoid is the most abundant bilayer system in nature, mediating crucial processes like light capture, electron transport and photophosphorylation. The light reaction of photosynthesis is mediated by four large intrinsic multimeric pigment-protein complexes embedded in the thylakoid membrane. High resolution structures have aided our understanding of the overall processes arbitrated by the individual components of the electron transport chain, namely photosystem II (PSII) (Van Bezouwen et al., 2017; Wei et al., 2016), cytochrome b_6/f (Kurusu et al., 2003; Stroebel et al., 2003), photosystem I (PSI) (Pan et al., 2018), ATP synthase (Hahn et al., 2018) and LHCII (Wang and Kühlbrandt, 1991; Liu et al., 2004; Wei et al., 2016). Despite our comprehension of the overall composition of the system and functional mechanistic, our understanding of how it is assembled is extremely scarce. For assembly, stability and repair of PSII alone, more than 60 auxiliary factors have been proposed (Nixon et al., 2010; reviewed in Nickelsen and Rengstl; reviewed in 2013; Järvi et al., 2015). To further complicate the matter, the majority of the proteins necessitated during biogenesis have to be post-translationally imported and circumstantially interact with plastid encoded proteins (Bauer et al., 2000; Albus et al., 2010). Hence a high degree of regulation as well as anterograde and retrograde signaling has to take place to efficiently facilitate this crucial process. The topogenic signal for plastid import is the transit peptide (TP) (Smeekens et al., 1986; Bruce, 2001). For thylakoid translocation it is bipartite with an N-terminal stromal targeting domain (STD) and C-terminal luminal targeting domain (LTD) (von Heijne et al., 1989; de Boer et al., 1991). Stromal translocation is mediated by the translocon on the outer/inner envelope of chloroplasts (TOC/TIC) machinery (Schleiff and Soll, 2000). After processing the STD, four different pathways facilitate the transport to, into or across the thylakoid membrane (Figure 1.7) (Cline et al., 1993; reviewed in Mori and Cline, 2001; reviewed in Aldridge et al., 2009).

1.5.1 cpSRP pathway

In higher-plant chloroplasts, a unique SRP pathway has been identified that targets proteins into the thylakoid membrane without requirement of RNA (Li et al., 1995). The post-translational cpSRP

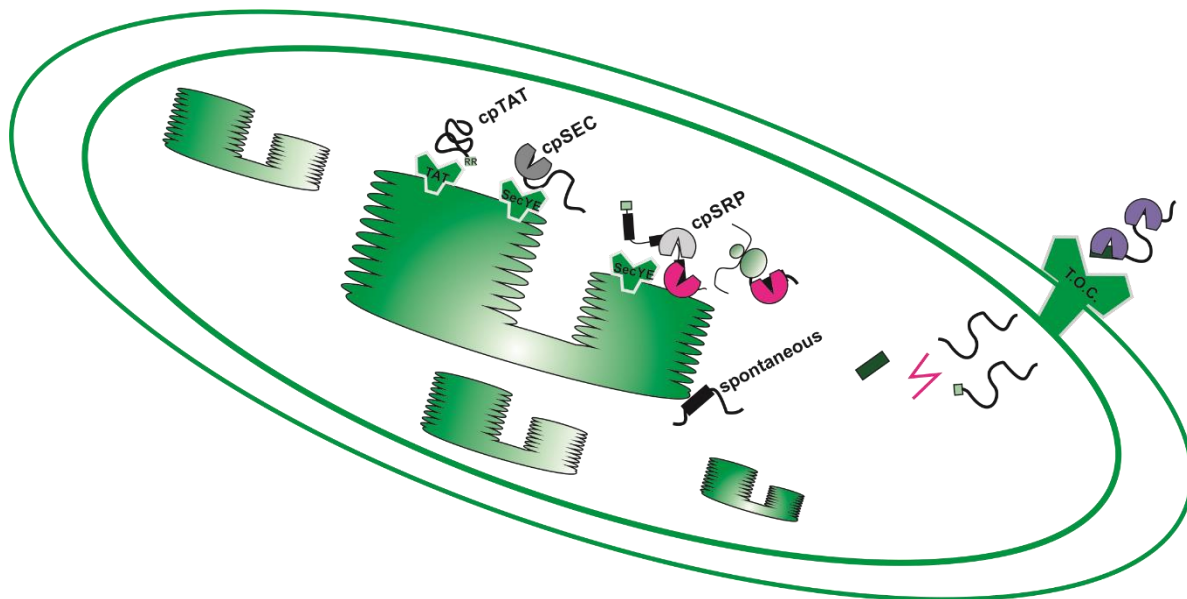


Figure 1.7. Import routes into or across the thylakoid membrane.

After canonical transport by cytosolic factors (purple) followed by import via the translocon in the outer/inner envelopes of chloroplasts (TOC/TIC) the stromal targeting domain (STD; dark green) is cleaved off by the stromal processing peptidase (SPP; magenta lines). Recognition is either facilitated by luminal targeting domains (LTD; light green) or hydrophobic segments (black). Integral membrane proteins (IMPs) can either interact co-translationally with cpSRP component cpSRP54 (magenta) or post-translationally in cooperation with cpSRP54 and cpSRP43 (light grey and magenta, respectively). Luminal proteins can either be transported in an unfolded conformation by the cpSEC pathway with the help of SecA (dark grey). As well as in a folded conformation by the cpTAT pathway. Topologically simple proteins with a single TMD in a polypeptide stretch are thought to insert unassisted, spontaneously without the need of proteinaceous factors, nucleotide or $\Delta\mu\text{H}$.

pathway generally targets the members of light harvesting chlorophyll a/b binding proteins (LHCPs) family (Klimmek et al., 2006). The key players of this pathway are cpSRP54 and cpSRP43. Former shares homology to the prokaryotic as well as eukaryotic homologues and latter is plant specific (Li et al., 1995; Franklin and Hoffman, 1993). cpSRP54 and cpSRP43 bind TMD3 and a loop between TMD2 and TMD3, respectively thereby forming the transit complex (High et al., 1997; Schuenemann et al., 1998; Tu et al., 2000). It is assumed that cpFtsY associates with the transit complex, targets it to the thylakoid membrane and thylakoid membrane insertion is facilitated by Alb3 and cpSecY. (Kogata et al., 1999; Moore et al., 2000, 2003). cpSRP54 is also capable of co-translational IMP insertion like its cytosolic counterpart (Nilsson and van Wijk, 2002; Zhang and Aro, 2002).

1.5.2 cpSEC pathway

The bacterial counterpart is composed of the membrane bound translocon comprised of SecY, SecE, SecG, the chaperone SecB and ATPase SecA (reviewed in Tsirigotaki et al., 2017). The plant cpSEC pathway is most probably comprised of a cpSecAYE translocase (Nakai et al., 1994; Yuan et al., 1994; Laidler et al., 1995; Roy and Barkan, 1998; Schuenemann et al., 1999). The cpSecAYE translocon is typically utilized to translocate unfolded proteins into the lumen of the thylakoids and probably

involved in co-translational IMP insertion (High et al., 1997; Yuan et al., 1994; Walter et al., 2015). The post-translational mode of translocation is probably mediated by cpSecA binding to the LTD of a client, recruiting it to SecYE and arbitrating its translocation (Yuan et al., 1994). In the role of co-translational IMP insertion, ribosomes interact with the translocon and Alb3 probably aids the insertion process (Walter et al., 2015).

1.5.3 cpTAT pathway

If a pre-protein carries two consequent arginine residues in the N-terminal region of its LTD, it will engage with the twin-arginine translocation (TAT) pathway (Reviewed in Mori and Cline, 2001; reviewed in Aldridge et al., 2009). The TAT pathway is energized by the trans-thylakoidal proton gradient and is capable of translocating fully folded proteins into the thylakoid lumen (Berghöfer and Klösgen, 1999; Mould and Robinson, 1991; Klösgen et al., 1992; Creighton et al., 1995; Marques et al., 2004). The TAT pathway in chloroplasts consists of three integral membrane proteins. These constituents constitute two membrane complexes. Tha4 (TatA) organizes into oligomers that vary in size (Dabney-Smith et al., 2006; Leake et al., 2008; Dabney-Smith and Cline, 2009), Hcf106 (TatB) and cpTatC form a large (~ 700 kDa) complex (Cline and Mori, 2001). The topogenic signal interacts with receptor complex constituted by cpTatC-Hcf106 (Gérard and Cline, 2006, 2007). Precursor binding stimulates TatA oligomerization and recruitment to the receptor complex to assemble the translocon (Dabney-Smith et al., 2006; Gohlke et al., 2005). Thereafter the folded protein is translocated into the thylakoid lumen and TatA dissociates from the receptor complex (Reviewed in Mori and Cline, 2001).

1.5.4 Spontaneous pathway

A subset of IMPs does not require any nucleotide, stromal factor or membrane bound insertion machinery for translocation (Aldridge et al., 2009). Initially, it was proposed that only single pass IMPs with one TMD share such properties (Michl et al., 1994; Lorkovic et al., 1995; Kim et al., 1998; Thompson et al., 1998). However, spontaneous insertion has also been attributed to topologically complex proteins (Zygodlo et al., 2006; Mant et al., 2001; Thompson et al., 1999; Kim et al., 1999). Especially the subunits of some translocons are supposed to insert spontaneously into membranes (Reviewed in Schünemann, 2007).

2 OBJECTIVES

The phylogenetic relationship of Get3 has been analyzed in five plant species and the tree of life including ten plant species (Duncan et al., 2013; Xing et al., 2017). However, it was never analyzed in Viridiplantae. This would be of special interest since plants generally have two orthologues and at least *Arabidopsis thaliana* seems to have three. Consequently, the first objective was to reanalyze the phylogenetic relationship of Get3 in planta. Since the localization of *At*Get3c was under debate (Duncan et al., 2013; Xing et al., 2017), the localizations of the different species-specific Get3 orthologues should be verified in homologous if not heterologous systems. This should give insight into the degree of functional conservation in different species.

The understanding of the GET/TRC system in plants is very limited. Even though components of the pathway and its general mode of action seem to be conserved in metazoans, in plants the entire pre-targeting and receptor complex have not been fully identified. In general, two different pre-targeting complexes exist in yeast and mammals: the one of the GET pathway does not include Bag6 (see 1.3.1) whereas the mammalian TRC pathway utilizes Bag6 to form the BAG6 complex (see 1.3.2). Hence, the second objective was to examine the molecular architecture of the pre-targeting complex in *A. thaliana* and find possible candidates to fulfill this function. With this information it should be possible to clarify the composition of the pre-targeting complex and see if the incorporation of Bag6 is a general metazoan feature. Furthermore, orthogonal systems can be established to gain a deeper understanding of the client handover reactions *in vitro*.

An *in vitro* method frequently used in the field is tail-anchor translocation (TAT). In brief, recombinant Get3/TA complexes are incubated with isolated microsomes and time-dependent glycosylation can be observed due to an engineered N-glycosylation tag. This method aids biochemical characterizations of targeting fidelity, determinants as well as upstream handover reactions *in vitro* (Cho et al., 2018). Thus, another objective was the characterization of *At*Get3a by the establishment of TAT. The fabrication of the method necessitates a functional plant derived N-glycosylation of the recombinant opsine bovine glycosylation (OPG) tag. This should be tested in isolated protoplasts providing a system in which the translocation fidelity of mutant lines disrupted in GET pathway components can be inspected. Further, the expression and purification of a Get3/TA complexes as well as an appropriate microsome isolation method should be established. The establishment of these methods will help elucidating the process of TA protein insertion at the ER *in vitro*.

The only knowledge present about the organellar Get3 orthologues in *A. thaliana* is their occurrence and localization (Duncan et al., 2013; Xing et al., 2017). Hence, another objective was to characterize the two orthologues *At*Get3b and *At*Get3c in *A. thaliana*. In a previous report, commercially available

OBJECTIVES

mutant lines of the two organellar orthologues were analyzed and displayed no severe growth defects in comparison to the wild-type (Xing et al., 2017). A similar reverse genetic approach should be chosen, thereby examining the endosymbiotic organelles, not only the habitus of the plant. This requires an appropriate method to isolate the single organelles in an adequate quality. Once this is established, the organelles should be studied on an ultrastructural level. Further, the composition of their energizing membranes should also be analyzed. In the energizing membranes of the endosymbiotic organelles, IMP insertion machineries exist that belong to the same protein family as Get1 (Anghel et al., 2017), namely Alb3 and Oxa1 in chloroplast and mitochondria, respectively. Assuming that both organellar proteins fulfill a similar function as their cytosolic counterpart, these could also utilize their respective homologous insertase to facilitate the post-translational insertion of IMPs. Thereby facilitating a convergent function within endosymbiotic derived organelles.

To interrogate if these *At*Get3 orthologues are capable of binding hydrophobic segments of proteins an *in vitro* assay had to be established. Hence, a further objective was the establishment of such an assay. This assay should be robust and not too time consuming. With the help of such an assay it would be possible to not just screen for putative clients but also assess different motifs or physicochemical properties within clients that affect the interaction with the targeting factor.

3. MATERIAL

3.1 Chemicals, media and buffers

All chemicals used in this study were purchased in analytical grade from VWR (Darmstadt, Germany), Merck (Darmstadt, Germany), Roche (Mannheim, Germany) or Roth (Karlsruhe, Germany). N-decyl-maltosid, n-dodecyl-maltosid and digitonin were supplied by Roth (Karlsruhe, Germany). Media to work with plants were ordered from Duchefa Biochemie (Haarlem, Netherland). Plants were grown on soil (Hawita fruhstorfer Erde) or *in vitro* on Murashige Skoog (MS) (Murashige and Skoog, 1962) (0.44 % (v/w) MS salts, 0.3 % (v/w) gelrite and 20 mM 2-(N-Morpholino)ethanesulfonic acid(MES)/KOH pH 5.7). Standard media and buffers were prepared according to (Sambrook and Russel, 2001) and autoclaved, if necessary.

3.2 Enzymes and kits

All enzymes utilized for cut and paste molecular cloning strategies like restriction endonucleases, T4-DNA-ligases were purchased from Thermo Fisher Scientific (Frankfurt, Germany). Enzymes for plant work were ordered from Duchefa Biochemie (Haarlem, Netherland). Trypsin and thermolysin were purchased from Sigma Aldrich (München, Germany). The polynucleotidekinase kit as well as RevertAid kit for Reverse transcription were acquired from Thermo Fischer Scientific (Frankfurt, Germany). The DNeazy Kit for DNA recovery from agarose gels as well as the RNeazy Kit for RNA isolation from plant tissue were supplied by VWR (Darmstadt, Germany).

3.3 Bacterial strains and growth

Cloning and propagation of plasmids was accomplished with *Escherichia coli* DH5 α (Invitrogen). Overexpression of proteins was performed in *E. coli* BL21 (DE3) star pRosetta (Invitrogen) which harbors the λ DE3 lysogen (DE3) a mutation in RNase E (star) and a plasmid for the expression of rare tRNAs (pRosetta). And, *E. coli* Lemo21 (DE3) (New England Biolabs) comprising a plasmid with a titratable promotor (arabinose; araBp) encoding the T7-lysozyme to modulate the degree of overexpression. Bacteria were grown in LB (1 % (w/v) tryptone, 0.5 % (w/v) yeast extract, 0.5 % (w/v) NaCl) supplemented with antibiotics as described (Sambrook and Russel, 2001).

3.4 Nucleotides

All nucleotides used in this study were ordered from Sigma Aldrich (München, Germany) and stored in 100 μ M stock solutions.

Table 3.4: Plasmids used in this study. Proteins that were co-expressed are noted in bold.

	name	ID ¹	accession number	tag	
pET21	Ex-Get3	395	At1g01910	cHis ₆	Bacterial protein expression
	Ex-mtGet3	396	At3g10350	cHis ₆	
	Ex_cpGet3	397	At5g60730	cHis ₆	
	pET21d_cpMDH	882	At3g47520	cHis ₆	
pETDuet	pDuet_AtCGet3	725	At1g01910	nHis ₆	Bacterial co-expression
	pDuet_AtCpGet3	726	At3g10350	nHis ₆	
	pDuet_AtmtGet3	881	At5g60730	nHis ₆	
	pDuet_AtCGet3+ Sec61β-Flag-OPG-6His	798	At1g01910, At2g45070	Flag+OPG ² +cHis ₆	
	pDuet_AtCpGet3+ PsbW-Flag-6His	799	At3g10350, At2g30570	Flag+cHis ₆	
	pDuet_AtCpGet3+ PsbW-ΔTMD-Flag-6His	800	At3g10350, At2g30570	Flag+cHis ₆	
	pDuet_AtCpGet3+ PsbX-Flag-6His	801	At3g10350, At2g06520	Flag+cHis ₆	
pDuet_cpGet3+ Lhcb3-Flag-6His	802	At3g10350, At2g06520	Flag+cHis ₆		
pML	pMLGet3cGFP	359	At3g10350	cGFP	Protoplast expression
	pMLmtGet3cGFP	360	At5g50730	cGFP	
	pMLcpGet3cGFP	361	At3g10350	cGFP	
	pML pMGD1-S1-10	204	At4g31780	cGFP _{S1-10}	
	pAVAGet3-sa11c	362	At3g10350	cGFP _{S11}	
	pAVAmtGet3-sa11c	363	At5g60730	cGFP _{S11}	
	pAVAcPGet3-sa11c	364	At3g10350	cGFP _{S11}	
	pAVA S1-10 cytosolic	202		GFP _{S1-10}	
	pAVA pF1-S1-10	274		cGFP _{S1-10}	
	pAVA pSSU-S1-10	264		cGFP _{S1-10}	
pAVA	pAVA_Get1_S11	727	At4g16444	cGFP _{S11}	
	pAVA_S11_Get4	729	At5g63220	nGFP _{S11}	
	pAVA_Sec61 β -Flag-OPG-6His _c		At2g45070	Flag+OPG ² +cHis ₆	
	pAVA_Sec61 β -Flag-6His _c		At2g45070	Flag+cHis ₆	

¹The ID refers to the plasmid number in the genetic records of the Toc lab (S06).

²OPG: opsine bovine tag including NKT tripeptide for glycosylation

GFP (saGFP) fragments and whole GFP fusions, respectively were employed for transient protoplast transfection and expression. All open reading frames cloned into pET21 or pETDuet plasmids were devoid of their topogenic signals.

3.5 Plant lines

All T-DNA insertion lines were acquired from the Nottingham Arabidopsis Stock Centre (NASC). The zygosity and position of the insertions was verified by PCR.

Table 3.5: Plant lines used in this study

name	AGI number	Stock centre ID	T-DNA position ¹	reference
<i>Atget3b-1</i>	At3g10350	SALK 112297	1	This study
<i>Atget3b-2</i>	At3g10350	SALK 017702	1021	This study
<i>Atget3c</i>	At5g60730	SALK 091152	1457	This study
<i>AtPsbW</i>	At2g30570	SALK 054191		García-Cerdán et al., 2011

¹Number of bases in the genetic locus starting with the first base of the 5' UTR

3.6 Antibodies

Antibodies were raised in Guinea pigs by Dr. Pineda Antibody Service (Berlin, Germany) against recombinant protein and purified as described in methods (see 3.3.1) or purchased from Sigma Aldrich (München, Germany), Santa Cruz (Heidelberg, Germany) or Agrisera (Sweden, Vännäs).

Table 3.6: Antibodies used in this study. Antibodies shown in bold were purified in this study.

name	source	raised in	dilution	reference
α -GFP	Roche	mouse	1:5000	
α -GFP _{S11}	Purchased ¹	guinea pig	1:5000	Klinger et al., 2019
α -Flag	Sigma	mouse	1:5000	
α -His _{HRP}	Sigma	rabbit	1:2000	
α -Dna K	Santa Cruz	mouse	1:5000	
α-<i>At</i>Get3a	purified	guinea pig	1:1000	Bodensohn et al., 2019
α-<i>At</i>cpGet3b	purified	guinea pig	1:1000	Bodensohn et al., 2019
α-<i>At</i>mtGet3c	purified	guinea pig	1:1000	Bodensohn et al., 2019
α -Calnexin	Agrisera	rabbit	1:5000	Bodensohn et al., 2019
α -BiP	Agrisera	rabbit	1:5000	Bodensohn et al., 2019

α -VDAC	Agrisera	rabbit	1:5000	Bodensohn et al., 2019
α -ICDH	Agrisera	rabbit	1:5000	Bodensohn et al., 2019
α -Tic110	purified	rabbit	1:5000	Bodensohn et al., 2019
α -LHCB2	Agrisera	rabbit	1:5000	Mao et al., 2018
α -PsbA	Agrisera	rabbit	1:5000	Chen et al., 2017

¹Purchased from Peptide Specialities Laboratories GmbH.

²The respective serum were kind gifts from Prof. Dr. Danja Schünemann

3.7 Columns and column materials

Gel filtration and Ion exchange as well as Ni-NTA columns were purchased from GE Healthcare (München, Germany). Ni-NTA agarose slurry for column based gravity flow immobilized metal affinity chromatography (IMAC) was obtained from Qiagen (Düsseldorf, Germany). Ni-NTA magnetic beads were obtained from Cube biotech (Monheim, Germany). Amicon centrifugal filter units were obtained from Millipore (München, Germany).

4. METHODS

4.1 Molecular biological methods

4.1.1 General molecular biological methods

Polymerase chain reactions (PCR) were completed in a Mastercycler EppigradientS (Eppendorf) according to (White et al., 1989). RNA was reverse transcribed with the M-MuLV reverse transcriptase according to the manufacturers recommendations (RT, Thermo Scientific). Analytical and preparative DNA restriction reactions, precipitations, ligations, bacterial transformation and growth were conducted as described (Sambrook and Russel, 2001). Plasmid DNA was isolated by alkaline lysis (Birnboim and Doly, 1979). Nucleic acids were separated by agarose gel electrophoresis using Tris Taurin EDTA (TTE) buffer (90 mM Tris, 30 mM Taurin, 1 mM EDTA) with 30 V/cm (Mühlhardt, 2013) together with GeneRuler DNA ladder mix (Thermo Fisher Scientific) as length marker. If necessary DNA fragments were extracted with the E.Z.N.A. Gel extraction Kit (VWR) according to the manufacturers recommendations. Competent cells were established with rubidium chloride (Roychoudhury et al., 2009).

4.2 Biochemical methods

4.2.1 General biochemical methods

Protein concentrations were determined using the Biorad reagent (München, Germany) or the amido black method (Popov et al., 1975). Proteins were precipitated by chloroform methanol (Fic et al., 2010). Polyacrylamid gel electrophoresis (PAGE) of denatured and native proteins was conducted according to (Schägger, 2006) and (Wittig et al., 2006), respectively. Gels were stained with Coomassie Brilliant blue (Sambrook and Russel, 2001) or silver nitrate (Nesterenko et al., 1994). Separated proteins were transferred to nitrocellulose or PVDF membranes utilizing the semi-dry method (Towbin et al., 1992). Transferred protein and marker bands were visualized with Direct Blue 71 (DB71) staining (Hong et al., 2000).

4.2.2 Protein expression

All recombinant proteins were either expressed in BL21 (DE3) star pRosetta cells (Invitrogen) or Lemo21 cells (Invitrogen). A single colony was picked and inoculated into 50 mL of LB (1 % (w/v) trypton, 0.5 % (w/v) yeast extract, 0.5 % (w/v) NaCl) supplemented with the respective antibiotic and incubated overnight at 37 °C. Normal expression cultures were inoculated 1:40 from overnight cultures

into fresh LB, grown till an OD_{600} of 0.6 and expression was induced with 0.25 mM IPTG for 2.5 - 3.5 hrs. Cell pellets were either snap frozen in liquid nitrogen or directly lysed.

4.2.3 Protein purification

4.2.3.1 Immobilized metal affinity chromatography (IMAC)

Cell pellets were resuspended in lysis buffer (50 mM Tris pH 8.0, 150 mM NaCl, 0.5 mM EDTA, DNaseI (Roche), 10 mM Imidazol), vortexed to homogeneity and lysed via French Press (Thermo Electron Corporation, 8.27 MPa). Lysates were cleared at (48,000 x g for 20 min, 4 °C) for 20 min. One column volume (cV) of Ni-NTA agarose resin (Qiagen) was equilibrated with 10 cV of lysis buffer and incubated by rotation with the cleared lysate for 30 min at room temperature. The matrix was washed with at least three times 10 cVs of lysis buffer containing 40 mM Imidazol including at least one wash step with high salt (1M NaCl) to remove electrostatically bound impurities. Bound proteins were eluted with lysis buffer containing 400 mM Imidazol. Elution fractions were pooled, concentrated with Amicon columns and if needed buffer exchange was also performed with these. Proteins were snap frozen in liquid nitrogen and stored at -80 °C in the presence of 10 % glycerol.

For insoluble proteins, inclusion bodies were pelleted (6,000 x g, 15 min, 4°C), washed and recovered successively with (i) 50 mM Tris, 150mM NaCl, 1 mM EDTA, pH 8; (ii) 50 mM Tris, 2M Urea, 10 mM $MgSO_4$, pH 8 and (iii) with 50 mM Tris, 0,5% Triton-X 100, 10 mM EDTA, pH 8. Inclusion bodies were either washed with H_2O and stored at -20 °C or solubilized in solubilization buffer (50 mM Tris, 50 mM NaCl, 10 mM Imidazole, 8 M Urea, pH 8), centrifuged (25,000 x g, 10 min, 18°C) and the supernatant passed 3x over a Ni-NTA column (Qiagen, Germany). The column was washed with 10 column volumes (cV) (i) 50 mM Tris HCl pH 8, 1 M NaCl, 15 mM Imidazol, 8 M Urea; 10 cV (ii) 50 mM Tris HCl pH 8, 15 mM NaCl, 15 mM Imidazol, 0,2% Triton-X 100, 8 M Urea and 10 cV (iii) 50 mM Tris HCl pH 8, 50 mM NaCl, 10 mM Imidazol, 8 M Urea. Protein was eluted in 5 x 1 cV 50 mM Tris HCl pH 8, 50 mM NaCl, 400 mM Imidazol, 8 M Urea.

4.2.3.2 Size exclusion chromatography (SEC)

All buffers for SEC were filtered through a 0.24 μ M filter and degassed by sonication prior to using the ÄKTA for gel filtration. The respective column was washed with 1.5 cV H_2O , equilibrated with 1.5 cV of the running buffer and the input had 1-4 % cV. Flow rates were set to the manufacturers recommendations and peak fractions were collected by fractionation. Collected fractions were either precipitated or concentrated with Amicon columns and then analyzed by SDS-PAGE.

4.2.4 Recombinant *in vivo* pull down assay

This assay was developed to probe the interaction of an untagged targeting factor that is recombinantly co-expressed with a potential tagged substrate. The aim was to establish a quick and robust assay to screen multiple putative substrates in a single run. For this a single colony was inoculated into 7 mL of LB (1 % (w/v) trypton, 0.5 % (w/v) yeast extract, 0.5 % (w/v) NaCl) supplemented with the respective antibiotic and incubated overnight at 37 °C. The entire overnight culture was inoculated into 50 mL of fresh LB supplemented with the respective antibiotic and expression was induced when an OD₆₀₀ 0.6 was reached (roughly an hour). After 60 min of expression, cultures were harvested (14.000 x g, 2 min, 4 °C), snap frozen in liquid nitrogen, thawed, resuspended in 2 mL lysis buffer (50 mM Tris pH 8.0, 150 mM NaCl, 20 mM Imidazol) containing DNaseI (Roche) and 1 mg/mL lysozyme and incubated at room temperature. After 30 min cultures were sonicated on ice 3 times for 20 seconds with a pulse of 75 % and cleared (25,000, 2 min, 4 °C). Cleared lysates were incubated with equilibrated Ni-NTA magbeads (Cube Biotech) for 30 min at room temperature and washed with 500 µL of (i) Lysis buffer (ii) 50 mM Tris pH 8, 1 M NaCl, 0.1 % (w/w) glycerol, 0.1 % (w/v) Triton-X 100, 25 mM Imidazol; (iii) 50 mM Tris pH 8, 1 M NaCl, 0.1 % (w/w) glycerol, 0.1 % (w/v) Triton-X 100, 50 mM Imidazol and (iv) with 50 mM Tris pH 8, 0.3 M NaCl, 0.1 % (w/w) glycerol, 100 mM Imidazol by gently vortexing. Tagged proteins were eluted by sequentially adding 3x 25 µL of elution buffer (50 mM Tris pH 8, 150 mM NaCl, 500 mM Imidazol) to the beads and vortexing.

4.3 Immunological methods

4.3.1 Antibody production

The expression of the C-terminal hexahistidin (*cHis*₆) tagged epitopes of *At*Get3a (At1g01910), *At*Get3b (At3g10350) and *At*Get3c (At5g60730) and their purification as solubilized inclusion bodies was executed as described (3.2.2 and 3.2.3.1). Each protein for paratope production was send in buffer (25 mM Tris HCl pH 7.5, 100 mM NaCl, 8 M Urea) for the immunization of two guinea pigs for three months each.

4.3.2 Affinity purification of antibodies

Specific antibodies were purified from sera by antigen affinity columns. Recombinantly expressed proteins were coupled to CNBr-Sepharose (Amersham Biosciences, Freiburg, Germany) in 0.1 M NaHCO₃, 0.5 M NaCl. Free activated sites were blocked with 0.1 M Tris-HCl (pH 8.0) for 2 hours at room temperature. Serum was cleared (20,000 x g, 20 min, 4 °C) and incubated with the antigen – sepharose overnight at 4 °C. Unspecific interactions as well as unbound proteins were washed away with 1x

phosphate buffered saline (PBS) with 500 mM NaCl. Antibodies were eluted with 0.2 M Glycine (pH 2.2) proceeded by direct neutralization with 1/7 volume 2 M Tris (pH 8.8). Proteins were precipitated by saturated $(\text{NH}_4)_2\text{SO}_4$ overnight at 4 °C and tested against recombinant protein as well as leaf extracts.

4.3.2 Indirect immunofluorescence

Indirect immunofluorescence was conducted as previously described (Lyck et al., 1997) with slight modifications. *A. thaliana* protoplast suspensions were mixed with one volume of W5 washing buffer (125 mM CaCl_2 , 154 mM NaCl, 5.3 mM KCl, 0,1 % glucose, 0.5 mM MES), recollected (80 x g, 5 min, 4 °C) and fixed in one volume fixing solution (100 mM PIPES pH 6.9, 1 mM MgCl_2 , 2 mM EGTA, 3.7 % Paraformaldehyde) for an hour at RT. Collected protoplasts were washed for 5 min in MtSB (microtubule stabilizing buffer, 100 mM PIPES pH 6.9, 1 mM MgSO_4 , 2 mM EGTA) and permeabilized in 0.5 % triton X-100 in MtSB for 30 min at RT. Thereafter protoplasts were carefully immobilized on poly-L-lysine coated cover slips. These were washed twice with PBS for 5 min followed by blocking of residual aldehyde groups for 15 min with 100 mM glycine in PBS. Thereafter protoplasts were blocked with 1 % BSA in PBS for 30 min at RT and incubated with the primary antibody in an appropriate dilution in 1 % BSA in PBS over night at 4 °C. The next day slips were washed twice and incubated with the secondary fluorophore labeled antibody for 1.5 h at RT. Slips were washed and mounted with anti-fading agent.

4.4 Cell biological methods

4.4.1 General cell fractionation

In general cell fractionation was performed by differential centrifugation of cell extract. Depending on the plant species, cell extract was obtained by homogenization by blender or ultrathorax, followed by filtering through several layers of miracloth (pore diameter 80 – 120 μm , VWR). After collecting nuclei and chloroplasts (1,500 x g, 3 min, 4 °C) the mitochondrial fraction was pelleted (16,000 x g, 20 min, 4 °C) followed by the microsomal fraction (120,000 x g, 1 h, 4 °C).

4.4.2 Organelle isolation

Chloroplasts, mitochondria and microsomes from green tissue of *Arabidopsis thaliana* were isolated according to a published protocol (Bodensohn et al., 2020) and cytosol enriched fractions were obtained as described (Bodensohn et al., 2019).

4.4.3 BN-PAGE with isolated organelles

When thylakoids were isolated for BN PAGE 14- to 21-day old *Arabidopsis thaliana* seedlings were submerged in MCP (500 mM Sorbit, 1 mM CaCl₂, 29 mM MES pH 5.7) supplemented with 0.1 % (w/v) BSA, 1 % Cellulase, 0.5 % Macerozyme and placed in an orbital shaker (120 RPM, 25 °C). After 3 h the cell extract was filtered through one layer of miracloth and the nuclei and chloroplasts enriched fraction was acquired (2,450 x g, 1 min, 4 °C) and layered on a 2 step Percoll gradient (42 % layered on 82 % Percoll in 330 mM Sorbit, 50 mM Hepes KOH pH 7.6, 2 mM MgCl₂). Thylakoids were recovered at the 42 % interphase and washed once with SRM (330mM Sorbit, 50 mM Hepes pH 7.6, 2 mM MgCl₂) followed by one wash step with Thylakoid wash buffer (330 mM Sorbit, 50 mM Bis-Tris pH 7). Roughly 200 µg of chlorophyll were collected (3,341x g, 3 min, 4 °C), carefully resuspended in 175 µL 25_BTH_20G (25 mM Bis-Tris pH 7, 20 % (w/v) glycerol, 10 mM NaF, 4 % (w/v) P.I.C. (Sigma)) and mixed with 200 µL of 25_BTH_20G_3D (25 mM Bis-Tris pH 7, 20 % (w/v) glycerol, 3 % Digitonin, 5 % (w/v) P.I.C. (Sigma)). After ten minutes on ice in the dark solubilized membrane protein complexes were cleared (9,972x g, 1 min, 4 °C) and then snap frozen in liquid nitrogen or mixed with 1/10 vol. BN loading dye (100 mM Bis-Tris pH 7, 0,5 M amioncaproic acid, 5 % (w/v) Serva Blue G, 30 % (w/v) sucrose) and separated as described (3.2.1).

4.4.4 Assays with isolated organelles

4.4.4.1 Stroma isolation

Isolated chloroplasts (see 3.4.2) were washed twice with wash buffer (20 mM Hepes KOH pH 7.8, 330 mM Sorbit, 10 mM KCl, 5 mM MgCl₂) and collected by centrifugation (1,100x g, 2 min, 4 °C). The resulting pellet was resuspended in osmotic shock buffer (10 mM Na-pyrophosphate NaOH, pH 7.8) to a final chlorophyll concentration 0.2 µg/µL, allowed to rest on ice for 5 min, transferred to a douncer and mechanically lysed with 15 strokes. After another 5 min on ice, thylakoids were pelleted (7,500 x g, 3 min, 4 °C) and envelopes were removed from the supernatant (300,000 x g, 15 min, 4 °C). Stromal concentration was increased by Amicon columns with a molecular weight (MW) cutoff of 3 kDa.

4.4.4.2 Thylakoid tail anchor translocation (τ TAT)

Isolated thylakoids (see 3.4.4.1) were washed with thylakoid wash buffer (30 mM NaH₂PO₄ NaOH pH 7.8, 5 mM MgCl₂, 50 mM NaCl, 100 mM sucrose, 1 mM EDTA) and recovered (7,500 x g, 3 min, 4 °C). 150 µg of these were resuspended and mixed with 15 µg of purified *At*Get3b/*At*PsbW-Flag-His complexes in translocation buffer (50 mM Hepes KOH pH 7.6, 330 mM Sorbit, 50 mM Na-ascorbate, 10

mM MgCl₂, 2 mM ATP) in a final volume of 150 µL. Periodically, 30 µL of sample were taken, split into three equal portions and either left untreated, treated with thermolysin or Na₂CO₃ (see 3.4.5). After washing the samples three times, they were snap frozen in liquid nitrogen.

4.4.4.3 Tail anchor translocation (TAT)

TAT assays were performed as described (Cho et al., 2018) with slight modifications. The preliminary screens were performed as follows: Final reaction volumes were 100 µL consisting of 20 %, 30 % or 40 % (V/V) of isolated microsomes (see 3.4.2; concentration: 3.9 µg/µL) and 9 µg of *At*Get3a/*At*Sec61β-OPG-Flag-His in translocation buffer T (50 mM Hepes LiOH pH 7.6, 150 mM KoAc, 50 mM MgoAc, 1 mM Dithiothreitol (DTT), 10 % glycerol, 2 mM ATP). Periodically 12 µL of sample were taken and snap frozen in liquid nitrogen.

4.4.5 Treatments of isolated organelles

4.4.5.1 Thylakoids

Proteolytic treatments of thylakoids were employed by diluting a 5 mg/mL stock solution 1:25 in thermolysin buffer (50 mM Hepes KOH pH 7.6, 330 mM Sorbit, 4 mM CaCl₂, 10 mM MgCl₂) and resuspending recovered thylakoids in 25 µL of these. After 30 min on ice reactions were stopped by adding 25 µL of 100 mM EDTA. Thylakoids were further washed with thermolysin wash buffer (50 mM Hepes KOH pH 7.6, 330 mM Sorbit, 5 mM EDTA).

The extraction of proteins that were peripherally associated with membranes was performed by alkaline treatment. Thylakoids were washed, recovered (7,500 x g, 3 min, 4°C) and resuspended in 0.1 N NaOH, kept on ice for 5 min and washed repeatedly.

4.4.5.2 Microsomes

Proteolytic treatments of microsomes were performed by diluting an 18 mg/mL stock solution of proteinase K 1:3 in subfractionation buffer (50 mM Hepes pH 7.6, 1 mM EDTA, 1 mM DTT, 2 mM MgCl₂, 1 mM CaCl₂, 15% (w/v) sucrose, 1% P.I.C. (Sigma, G)). Microsomes were isolated from *A. thaliana* protoplasts as described in 3.5.3 and the resulting microsomal pellet was resuspended in 5 µL (~12.5 µg proteinase K) of the above mentioned solution by releasing the pellet from the reaction tube with a 2.5 µL pipette tip. Samples were kept on ice for 15 min and reactions were quenched by the addition of 0.5 µL of 330 mM Phenylmethylsulfonylfluorid (PMSF). Samples were directly subjected to SDS-PAGE followed by immunological analysis.

4.5 Plant methods

4.5.1 Plant growth

Wild-type and T-DNA insertion lines utilized in this study were *Arabidopsis thaliana* ecotype Col. 0. Plants used for gDNA, RNA, protoplast and organelle isolation for BN-PAGES were grown under short day conditions (8 h light with $120 \mu\text{mol m}^{-2}\text{s}^{-1}$ and $22 \text{ }^\circ\text{C}$; 16 h dark at $18 \text{ }^\circ\text{C}$). When cultivated *in vitro* on Murashige Skoog medium (Murashige and Skoog, 1962) plants were grown under long day conditions (14 h light with $120 \mu\text{mol m}^{-2}\text{s}^{-1}$ and $22 \text{ }^\circ\text{C}$; 10 h dark at $18 \text{ }^\circ\text{C}$). Seeds disseminated on plates were surface sterilized subsequently with 9 % (w/w) sodium hypochlorite and 70 % (w/w) Ethanol followed by repeated wash steps with freshly autoclaved ddH₂O. Germination was synchronized by keeping the plates upside down at $4 \text{ }^\circ\text{C}$ in the dark for 72 h.

4.5.2 Protoplast isolation and transformation

Protoplasts from *Arabidopsis thaliana* were isolated and transformed as previously described (Sommer et al., 2013) and protoplasts from *Solanum lycopersicum* according to (Mishra et al., 2002). For transfections 10 μg of midi DNA were used for 10^5 protoplasts and analyzed after 6 h or over-night expression under constant light at RT.

4.5.3 Protoplast fractionation and sub fractionation

2×10^6 transfected protoplasts were lysed in 80 μl of subfractionation buffer (50 mM Hepes pH 7.6, 1 mM EDTA, 1 mM DTT, 2 mM MgCl₂, 1 mM CaCl₂, 15% (w/v) sucrose, 1% P.I.C. (Sigma, G)). After preclearing (600 x g, 3 min), the supernatant was fractionated into cytosolic and microsomal fraction by centrifugation (80,000 rpm in an AT4-830 rotor, 10 min, 4°C). The cytosolic fraction was precipitated by chloroform/methanol (Fic et al., 2010) and the resulting pellets of both fractions were resuspended in Schagger buffer (Schagger, 2006).

4.6 Microscopy

4.6.1 Transmission electron microscopy (TEM)

Samples for transmission electron microscopy (TEM) were prepared as described in (Burnat et al., 2014) with the modification that leaf tissue of plants at different developmental stages was utilized instead of *Anabaena* cultures.

4.6.2 Confocal laser scanning microscopy (CLSM)

GFP and mCherry fluorescence as well as MitoTracker emission was examined with a Zeiss LSM 780 with a Plan Apochromat 63x/1.2. Fluorescence was excited and detected as follows: GFP 488/ 505 – 525 nm; YFP 510/ 520 – 550; mCherry 615/ 650 – 750 nm; MitoTracker DeepRed FM 633/ 640 – 680 nm.

4.7 Holdase assays

4.7.2 *In cellula*

Protoplasts isolated from *A. thaliana* were incubated in K3 (20 mM MES KOH pH 5.6-6, 400 mM Sorbit, 1 mM CaCl₂, 1x MS-salts including vitamins) supplemented with 4 mM H₂O₂ for an hour at 30 °C. Thereafter protoplasts were recovered (600 x g, 22 °C, 1 min) and directly lysed by solubilization with increasing amounts of N-Dodecyl-beta-Maltoside (β-DM). Proteinaceous membrane less organelles (PMLOs) were pelleted (6,000 x g, 4 °C, 5 min) and the supernatant was precipitated by chloroform/methanol (Fic et al., 2010). Samples were directly subjected to SDS-PAGE followed by immunodecoration.

4.7.3 *In vitro*

Recombinant *At*Get3 orthologues and *At*cpMDH were either mixed in stoichiometric molar ratios or individually exposed to heat stress in 60 μL reaction volumes for an hour. Aggregates were retrieved by centrifugation (25,000 x g, 4 °C, 20 min) and the supernatant was precipitated by chloroform/methanol (Fic et al., 2010). Samples were separated by SDS-PAGE and gels were stained by coomassie brilliant blue (CBB).

4.8 Bioinformatical methods

The Get3 orthologue analyses was performed according to Bodensohn et al. (2019). For the maximum likelihood tree construction protein sequences from 52 species were selected for the phylogeny, representing most of the plant groups and yeast as outgroup: *Arabidopsis thaliana*, *Arabidopsis lyrata*, *Capsella rubella*, *Brassica rapa*, *Carica papaya*, *Cucumis sativus*, *Manihot esculenta*, *Linum usitatissimum*, *Populus trichocarpa*, *Theobroma cacao*, *Eucalyptus grandis*, *Prunus persica*, *Fragaria vesca*, *Citrus clementina*, *Citrus sinensis*, *Medicago truncatula*, *Phaseolus vulgaris*, *Glycine max*, *Vitis vinifera*, *Solanum lycopersicum*, *Solanum tuberosum*, *Coffea canephora*, *Mimulus guttatus*, *Daucus carota*, *Aquilegia coerulea*, *Zea mays*, *Sorghum bicolor*, *Setaria italica*, *Panicum virgatum*,

Brachypodium distachyon, *Oryza sativa*, *Spirodela polyrhiza*, *Amborella trichopoda*, *Ginkgo biloba*, *Picea abies*, *Selaginella moellendorffii*, *Anthoceros agrestis*, *Marchantia polymorpha*, *Sphagnum fallax*, *Physcomitrella patens*, *Spirogyra pratensis*, *Klebsormidium nitens*, *Chara braunii*, *Nitella mirabilis*, *Chlamydomonas reinhardtii*, *Volvox carteri*, *Klebsormidium nitens*, *Coccomyxa subellipsoidea C-169*, *Galdieria sulphuraria*, *Ostreococcus lucimarinus*, *Micromonas pusilla*, *Saccharomyces cerevisiae*.

Using the *Arabidopsis thaliana* genes as reference, homologous proteins for these species were found using BLASTp (Camacho et al., 2009) and filtered to contain the GET3 domain (Pf02374) or respective domains for the receptors, substrates and other proteins related to GET3 in Pfam (Finn et al., 2014). MAFFT (Kato et al., 2002) with the options linsi and 1000 maximum iterations was used for sequence multiple alignment, and JalView (Clamp et al., 2004) for manual trimming of the multiple alignment. IQtree (Nguyen et al., 2015) was used to generate maximum likelihood trees, using best-fit substitution model prediction, SH-aLRT test and ultrafast bootstrap with 10000 replicates. Figtree was used (<https://github.com/rambaut/figtree>) to format the phylogenetic trees.

4.9 MS/MS analysis

For in-solution mass spectrometry proteins were digested (León et al., 2013; ISD:SDC; AP&PT) and peptides were purified by C18 STAGE-TIPS (Rappsilber et al., 2007). Peptides were analyzed using an ultra-HPLC Proxeon EASY-nLC 1000 system coupled online to Q Exactive Plus mass spectrometer (Thermo Fisher Scientific). Reversed-phase separation was performed using a 30 cm analytical column (100 µm diameter; DNU-MS (Novak) packed in-house with Reprosil-Pur 120 C18-AQ, 2.4 µm). Mobile-phase solvent A consisted of 0.1% formic acid and 4% acetonitrile in water, and mobile-phase solvent B consisted of 0.1% formic acid in 80 % acetonitrile. The flow rate of the gradient was set to 200 nl/min. A 70-min gradient was used (0–40% solvent B within 40 min, 40–100% solvent B within 10 min, 100% solvent B for 10 min, 100–0% solvent B within 5 min and 0% solvent B for 5 min).

Data acquisition was performed with the ddMS2 method with the following configuration: For the MS scans, the scan range was set to 250–2,000 m/z at a resolution of 70,000, and the automatic gain control (AGC) target was set to 1×10^6 . For the MS/MS scans, Top 13 ions were chosen, the resolution was set to 35,000, the AGC target was set to 1×10^5 , the precursor isolation width was 2 Da and the maximum injection time was set to 80 ms. The HCD normalized collision energy was 27%. MaxQuant was used to analyze the LC-MS/MS data (ver 1.5.5.; Cox and Mann, 2008) which allowed qualitative and quantitative analysis. The Uniprot reference *Arabidopsis* database (UP000006548) was used for the identification of proteins. Default settings for fixed modifications were used, Dynamic modifications were set: Oxidation for M and Deamidation for NQ. Contaminants were included for peptide detection of a minimum length of 6 amino acids. FDR threshold was set to 0.01. Perseus was

used to transform the quantitative data and perform a statistical analysis (Tyanova and Cox, 2018). The default settings for a students' t-test were utilized for the analysis.

5 RESULTS

5.1 Get3 in Planta

5.1.1 Four orthologous groups to Get3 exist in plants

Two previous studies analyzed the phylogenetic relationship of Get3, one focused on eight plant taxa (Duncan et al., 2013) and the other examined the whole tree of life including ten plant species (Xing et al., 2017). To corroborate the conservation and localization of Get3 in planta this investigation was revised by extracting fifty Viridiplantae proteomes and compiling an orthologue originated “pan-genome” (conducted by Stefan Simm and Katharina Kramer). The aforementioned analysis (Xing et al., 2017) was able to distinguish between a cytosolic Get3a and organellar Get3bc clade whereas our analysis revealed a cytosolic Get3a, plastidic Get3b, mitochondrial Get3c group orthologous to the *A. thaliana* proteins *AtGet3a*, *AtGet3b* and *AtGet3c*, respectively (Figure 5.1 A). Furthermore, a fourth orthologous group solely composed of sequences from the order Poales termed *SBGet3* (SB = *Sorghum bicolor*) was identified (Figure 5.1 A). Get3a and Get3b were present in all analyzed taxa. The only exceptions were the proteomes of *Ostreococcus lucimarinus*, *Micromonas commode* and *Micromonas pusilla* in which no orthologous Get3a sequence could be detected. Interestingly, the Get3c comprising sequences were only identified in Brassicaceae (Figure 5.1 A). An Assessment of the AA sequences of the orthologous groups (exemplified in Figure S1) displayed that *AtGet3b*, *AtGet3c* and *SBGet3* shared group specific AAs in the area between Helix $\alpha 4$ and $\alpha 10$ (Figure 5.1 B). This section encompasses subdomains forming the “composite hydrophobic groove” (Mateja et al., 2009) responsible for substrate binding (Mateja et al., 2015) and Get1/2 interaction sites (Stefer et al., 2013). Additionally, a C-terminal segment equipped with AAs specific for *AtGet3a* was identified, whereas the other orthologous groups shared mutual residues (Figure 5.1 B). Overall only a few AAs varied in the motifs of the conserved ArsA-ATPase domain (Mateja et al., 2009) of the yeast homologue in comparison to the four orthologous plant groups (Figure 5.1 C). The 4 conserved cysteine residues of the yeast homologue composed of a CxC motif preceded by a CxxC motif appeared to be dissected in planta. The *AtGet3a* orthologous group contained the CxC motif and the other groups the CxxC motif (Figure 5.1 C). The predicted localizations of the Get3 orthologues (Table S1) proposed a cytosolic localization for the group orthologous to *AtGet3a* as well as a mitochondrial localization for the *AtGet3c* group due to the detection of a mitochondrial targeting signal (Figure 5.1 D). Even though topogenic signals for both endosymbiotic derived organelles as well as proteins devoid of these were identified in the *SBGet3* and *AtGet3b* groups, the majority encompassed mitochondrial (67 %) and plastid (52 %) topogenic signals, respectively (Figure 5.1 D).

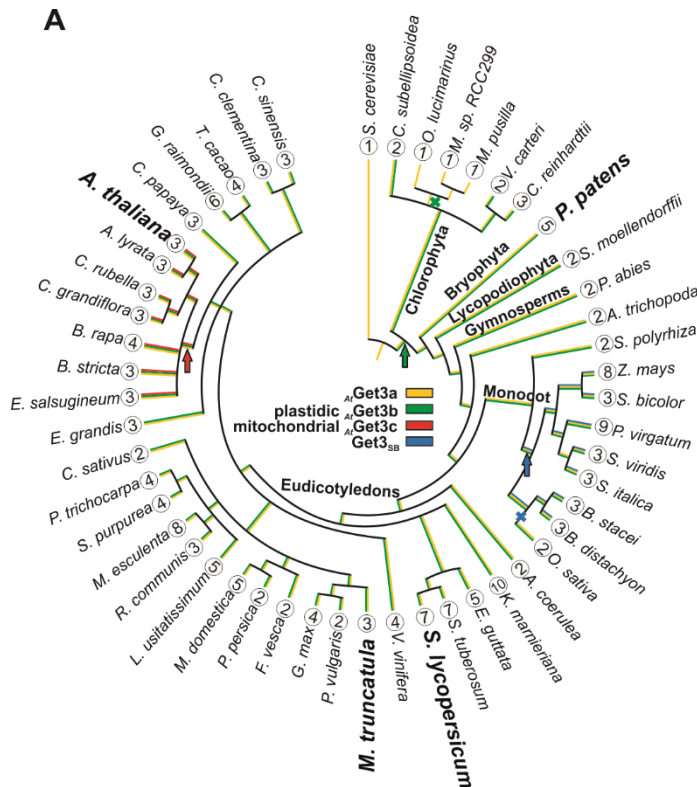
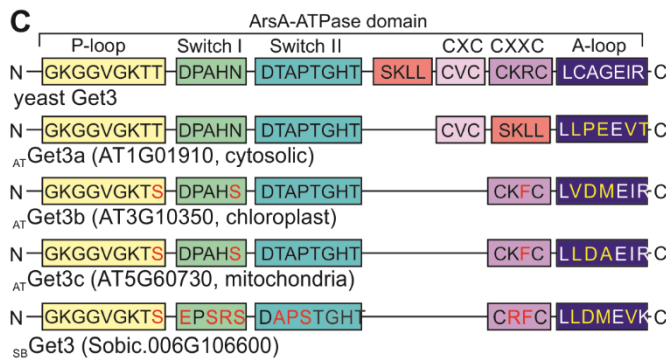
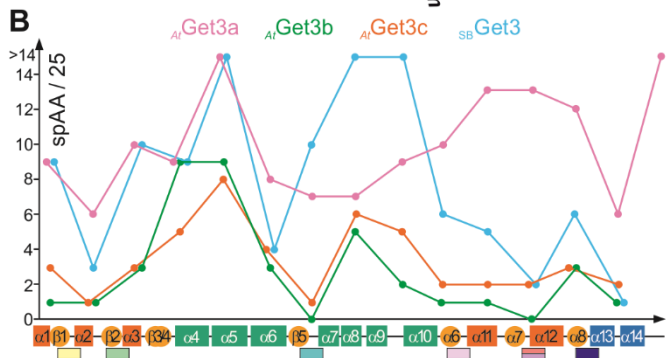


Figure 5.1. Orthologous relationship of *AtGet3*.

A. Depicted the taxonomic relationship of Viridiplantae analyzing the existence *AtGet3* orthologues utilizing *S. cerevisiae* as outgroup. The identification of *AtGet3a* (yellow lines), *AtGet3b* (green lines), *AtGet3c* (red lines) and *SBGet3* (blue lines). The number of identified homologues by BLAST queries or orthologue analysis is shown (Table S1). The Colored arrows and crosses illustrate the emergence and loss of the corresponding orthologous group, respectively. **B.** In a 25 amino acid window the incidence of specific amino acids (spAA) was examined in multiple sequence alignments (Figure S1) of the four orthologous groups (color code on top). The x-axis depicts the secondary structure arrangement of Get3 (orange helices: ATPase domain; green helices: substrate binding and hetero-complex formation). The position of the conserved motifs in (C) are illustrated as small boxes underneath. **C.** Correlating motifs identified both in yeast and plant Get3 proteins. The conserved motifs (P-loop, Switch I, Switch II, CxC, CxxC, A-loop) are shown as one-letter consensus. Red/yellow: Differing AA between yeast and plant motifs. **D.** Targeting signals predicted for all Get3 proteins in the orthologous groups or identified by BLAST (Table S1). The percentages of sequences devoid of signal (CYT), equipped with mitochondrial (MIT) or chloroplast signal (CHL) or a signal not clearly classifiable (M/L) are shown. The total number sequences are listed in the last column. Modified from Bodensohn et al. (2019)



D

	CYT	CHL	MIT	M/C	n.d.	total
<i>AtGet3a</i>	100 %	—	—	—	—	66
<i>AtGet3b</i>	15 %	52 %	32 %	1 %	—	75
<i>AtGet3c</i>	—	—	100 %	—	—	7
<i>SBGet3</i>	25 %	8 %	67 %	—	—	12
BLAST	70 %	5 %	5 %	5 %	15 %	20

In order to corroborate the previous orthologue search, a phylogenetic tree based on maximum likelihood was compiled (in cooperation with Stefan Rensing, executed by Noe Fernandez-Pozo). The resulting tree displayed the branching of the Get3 sequences into two major clades as previously reported (Xing et al., 2017). However, more details became evident in regards to sequence variation. Since more details became apparent the clade a was termed Get3a. Bryophytes nested in the most basal nested clade followed by ferns, gymnosperms and *Amborella trichopoda*. The angiosperm clade branched into the nested clades of eudicotyledons and monocots (Figure S3 B). Interestingly, the basal lineages in the sister known as clade bc (Xing et al., 2017) contained sequences that shared higher sequence similarity to clade a than to blade bc. This nested clade was present in the lineages of Chlorophyta, Rodophyta and Bryophyta and it was termed Get3ab (Figure S4 A; blue rectangle). This could explain why we did not detect an *At*Get3a orthologue in some Chlorophyta in our previous analyses (Figure 5.1). Remarkably, the Get3 homologue of *Saccharomyces cerevisiae* was also present in the Get3ab clade. In Chlorophyta, Rodophyta, Bryophyta, ferns and gymnosperms another nested clade became evident. This basal clade did not exhibit a clear distinction between the clades to which *At*Get3b or *At*Get3c nested in and was termed Get3bc (Figure S4 A; magenta rectangle). In the angiosperm clade, two major nested clades became apparent (Figure S5). *At*Get3b was present in one clade and *At*Get3c in the other. Hence the clades were termed Get3b and Get3c. Interestingly, the sequences of the *Sb*Get3 orthologous group were also present in a nested clade in the *At*Get3c clade (Figure S5; orange). Moreover, the homologue of *S. lycopersicum* was present in the *At*Get3c clade and the *M. x varia* homologues were present in *At*Get3b as well as *At*Get3c clades, respectively (Figure S5; blue and magenta asterisks, respectively).

The preceding bioinformatic query provided a general classification as well as an overview of the Get3 orthologues in planta, however the occurrence and localizations of the putatively organellar targeted orthologues had to be corroborated. In order to address this, homologous and heterologous systems were chosen to verify the organelle targeting of one Bryophyte and three Eudicotyledon species (Figure 5.2). *A. thaliana* was analyzed as the localization of *At*Get3c was under debate due to contradicting reports (Duncan et al., 2013; Xing et al., 2017). Since one Get3a and two Get3b proteins with differing organellar localizations were predicted, *Medicago x varia* was examined (Figure 5.2). A detailed inspection of the seven sequences (Table S1) of *Solanum lycopersicum* revealed that only four of these actually contain all necessary motifs for a fully functioning Get3 protein. So these four proteins with predicted cytosolic and plastidic localization were inspected (Figure 5.2). Last *Physcomitrella patens* was chosen as an elementary system to analyze the intracellular distribution of Get3 orthologues. As in the case of *S. lycopersicum* only four of the five predictions were proteins capable of Get3 function with putative cytosolic and plastidic localizations (Figure 5.2).

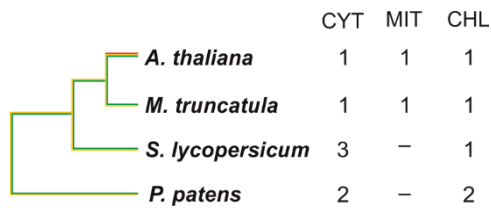


Figure 5.2. Selected plant systems to study Get3 proteins.

The phylogenetic relation of Get3 orthologues in the four analyzed plant species is depicted (left). The number of orthologues with predicted cytosolic (CYT, yellow), mitochondrial (MIT, red) and chloroplastic (CHL, green) localization are illustrated (right). Adapted from Bodensohn et al. (2019)

5.1.2 *At*Get3c is targeted to mitochondria

In order to substantiate the localization of the endogenous proteins, antibodies against the three *A. thaliana* proteins were raised, purified (Figure S6) and used for Western blot analysis. Furthermore, *A. thaliana* seedlings were homogenized (Figure 5.3 A, T) and the homogenate was partitioned into a soluble (S), a chloroplast enriched (Ch), mitochondria enriched (Mt) and microsomal enriched (Mc) fractions. The purity of the different fractions was verified by specific antibodies. Even though Tic110 was enriched in the chloroplast enriched fraction it was also present in all other fractions (Figure 5.3 A; fourth panel). This could be due the homogenization procedure in which bulky, highly abundant organelles, like plastids get ruptured and their debris contaminate other organelles. The mitochondrial outer membrane protein (OEP) VDAC was mainly enriched in the mitochondrial fraction (Figure 5.3 A; fifth panel). The antibody for the isocitrate dehydrogenase (ICDH) recognized both the mitochondrial and peroxisomal counterparts as judged from the organelle specific migration behavior, (Letierrier et al., 2016) but was still enhanced in the mitochondrial enriched fraction (Figure 5.3 A; eighth panel). Both the luminal binding protein BiP and the ER membrane protein calnexin (CNX) (Figure 5.3 A; sixth and seven panel, respectively) were mainly present in the microsomal enriched fractions. *At*Get3a was detected in all fractions, but highly enriched in the microsomal fraction (Figure 5.3 A; first panel). The former observation could be due to the additional holdase function of *At*Get3a which leads to changes in sedimentation characteristics (see 4.8). The latter is in line with previous observations that Get3 co-migrates with microsomes (Schuldiner et al., 2008). *At*Get3c was most abundant in the mitochondrial fraction (Figure 5.3 A, third panel). Surprisingly, *At*Get3b was mostly represented in the chloroplast fraction (Figure 5.3 A; second panel), even though the control protein was distributed in all fractions. In order to assist the previous results a cell-free *in organello* dual import assay was employed (Rödiger et al., 2010; Rudhe et al., 2002). *In vitro* translated radiolabeled precursor proteins of *At*Get3b and *At*Get3c were incubated with mixtures of both endosymbiotic organelles isolated from *Pisum sativum* (pea) seedlings. Subsequently after re-isolation of chloroplasts (Figure 5.3 B, cp) and mitochondria (mt), organelles (-) were treated with thermolysin (TH) or Triton X-100 (TX) to remove surface bound proteins and discriminate between membrane inserted or aggregated protein, respectively. Both precursors (p) were surface bound and removed after protease conduct (TH). *At*Get3b was imported

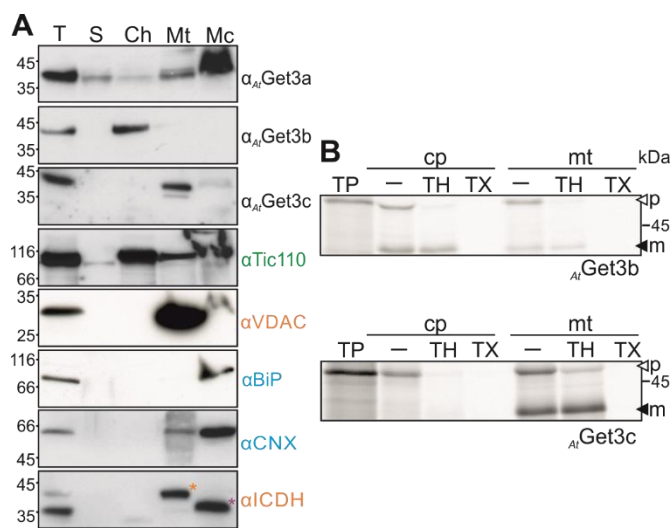


Figure 5.3. $AtGet3c$ in mitochondria of *A. thaliana*.

A. 14-day old *A. thaliana* seedlings were fractionated into soluble (S), chloroplastic (Ch), mitochondrial (Mt) and microsomal (Mc) enriched fractions. These as well as total protein extract (T) were separated by SDS-PAGE and immunologically analyzed with the indicated antibodies (Figure S6). Organelle purity was also immunologically confirmed: α -Tic110 (green: Ch); α -VDAC and α -ICDH (orange: Mt); α -BiP and α -CNX (blue: Mc). **B.** Dual import experiments with *in vitro* translated ^{35}S -Get3 orthologues and isolated chloroplasts (cp) and mitochondria (mt). Isolated organelles (-) were treated with thermolysin (TH) or Triton X-100 (TX). Processed precursor (p) to the mature form (m) verified the import reaction. 10 % of translation product (TP) were added as control. Modified from Bodensohn et al., (2019).

into both organelles, but with a much higher efficiency into chloroplasts. This was assessed by protease shielding and Triton X-100 sensitivity of the mature protein (m). Such minimal mitochondrial import of plastidic precursors has also reported, while using the same system (Rudhe et al., 2002). Nevertheless, it could be concluded that $AtGet3b$ was imported into chloroplasts and $AtGet3c$ exclusively into mitochondria (Figure 5.3 B; m). This was coherent with the results from the fractionation (Figure 5.3 A; second and third panel).

5.1.3 $AtGet3c$ resides in the mitochondrial matrix

Even though $AtGet3c$ was present in and targeted to mitochondria (Figure 5.3) its sub-organelle localization still had to be delineated. Due to the opposing reports of the localization of $AtGet3c$ -GFP fusion protein residing either at the mitochondrial outer membrane (OM) or within the organelle (Duncan et al., 2013; Xing et al., 2017) coupled to my observations of punctuate structures while utilizing the same system (Figure S7; third panel), a different approach was chosen. For this, the self-assembly GFP (saGFP) system (Cabantous et al., 2005) was used. Having the advantage that (i) a small tag is fused to a protein of interest and (ii) by the choice of the right reporter fused to the remaining GFP moiety, the subcellular localization can be outlined. Due to the high affinity of the 11th β -strand of GFP to the first 10 β -strands, both entities only have to inhabit the same subcellular compartment to auto-catalytically self-assemble to a functional fluorescent protein (Cabantous et al., 2005).

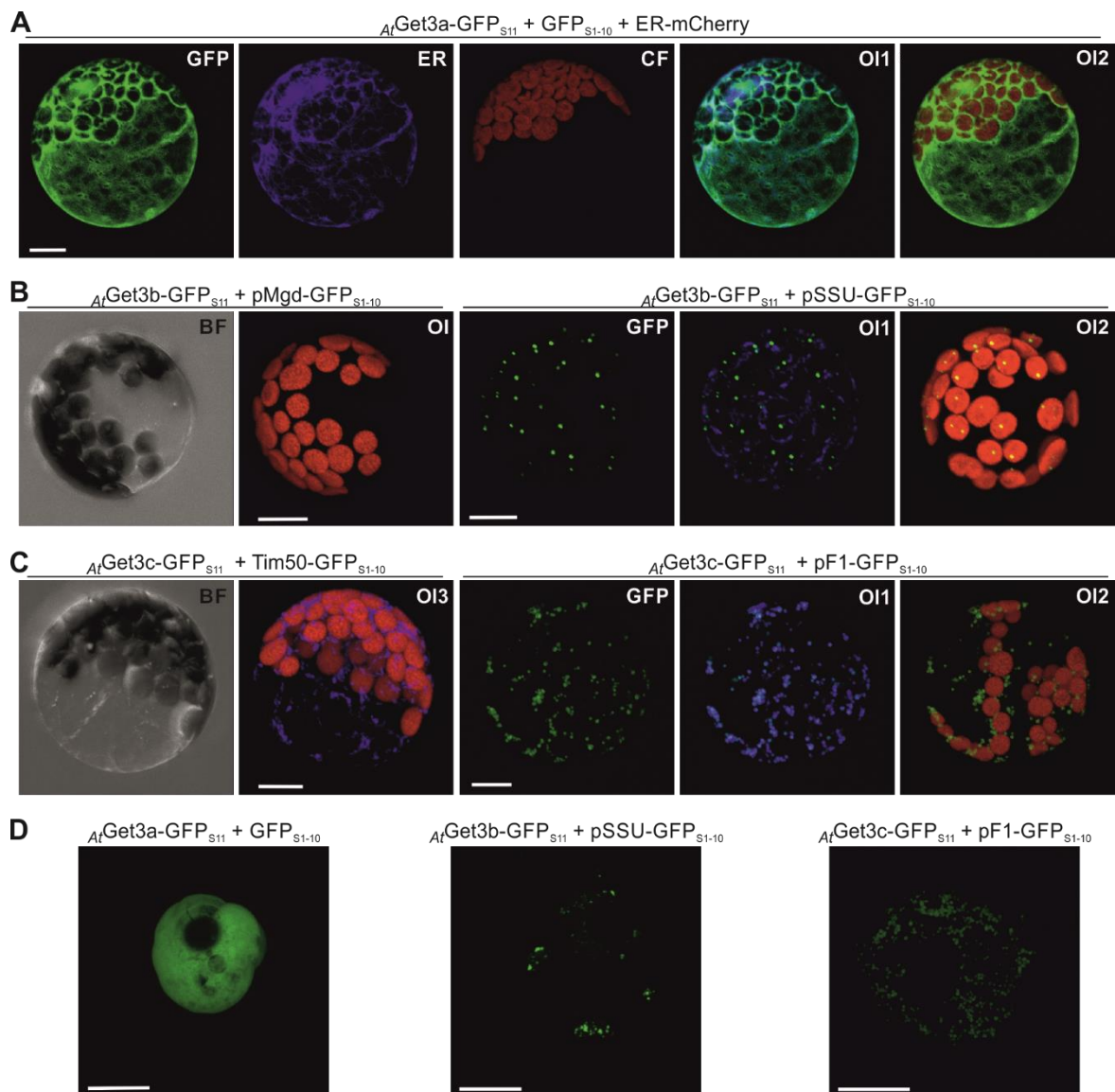


Figure 5.4. Individual Get3 orthologues display particular cellular localization in *A. thaliana* cells.

A. *AtGet3a*-GFP_{S11}, GFP_{S1-10} and ER-mCherry were transiently co-transfected in *A. thaliana* protoplasts and analyzed by confocal laser scanning microscopy (CLSM). GFP fluorescence (GFP), mCherry fluorescence (ER), chlorophyll fluorescence (CF) and GFP-/mCherry-signal (OI1) as well as GFP-signal/CF (OI2) are depicted. **B, C.** *A. thaliana* mesophyll protoplasts transiently co-expressed *AtGet3b*-GFP_{S11} and pSSU-GFP_{S1-10} or MGD-GFP_{S1-10} (B) or *AtGet3c*-GFP_{S11} and pF1-GFP_{S1-10} or Tim50-GFP_{S1-10} (C). Cells were stained with MitoTracker (MT). Bright field (BF), GFP- (GFP), GFP-/CF (OI), GFP-/MT (OI1), GFP-/CF (OI2) and GFP-/CF/MT (OI3) are illustrated. **D.** Protoplasts isolated from *A. thaliana* white cell culture were co-transfected with *AtGet3*-GFP_{S11} constructs with denoted reporter construct and GFP fluorescence was recorded by CLSM after 18 hrs of co-expression. Figures (A-D) are representative images, scale bars indicate 10 μm.

To verify the localization of the *AtGet3* orthologues they were transiently co-expressed as GFP_{S11}-fusions together with organellar GFP_{S1-10} fusion reporters in *Arabidopsis thaliana* protoplasts. *AtGet3a*-GFP_{S11} only evoked a fluorescent signal when co-expressed with the cytosolic GFP_{S1-10} reporter (Figure 5.4 A) and did not fluoresce with the other organellar reporters (Figure S8 A). Substantial amounts were proximal to the ER as judged by the fluorescent signal of the co-expressed ER-mCherry, (Figure 5.4 A; OI1) which has been observed before (Xing et al., 2017). *AtGet3b*-GFP_{S11} was clearly

localized in the stroma of plastids, because the co-expression with the stromal reporter pSSU-GFP_{S1-10} and not the intermembrane space reporter pMDG-GFP_{S1-10} or other reporters (Figure S8 C) resulted in fluorescence (Figure 5.4 B; left). The signal was clearly within the margins of chlorophyll fluorescence and not co-localizing with MitoTracker, (Figure 5.4 B; right) coherent with previous observations (Xing et al., 2017). Fluorescence coinciding with the MitoTracker signal was only obtained when *At*Get3c-GFP_{S11} was co-expressed together with the matrix reporter pF1-GFP_{S1-10} (Figure 5.4 C; right) and not with the intermembrane space reporter Tim50-GFP_{S1-10} (Figure 5.4 C, left) or other reporters (Figure 5.8 B). The observations of mitochondrial OM localization (Duncan et al., 2013) could be due to the GFP moiety similar to my preceding analysis (Figure S7; third panel). However, the GFP_{S11}-fusion led to a matrix localization like already established (Xing et al., 2017). The transient co-expression of the same constructs in *A. thaliana* root-derived white cell culture reproduced the results of the mesophyll protoplasts, showing that the targeting fidelity is not tissue specific (Figure 5.4 D).

5.1.4 *At*Get3c is targeted to mitochondria of *Solanum lycopersicum* and *Allium cepa*

In order to assess if the targeting fidelity of *At*Get3c is globally conserved, its intracellular distribution was examined in *A. cepa* (onion, monocotyledon) epidermal cells (Figure 5.5 A, C) and *S. lycopersicum* (tomato, eudicotyledon) protoplasts (Figure 5.5 B, D). The co-expression of *At*Get3c-GFP_{S11} with pF1-GFP_{S1-10} and additionally pSSU-mCherry (to visualize plastids in *A. cepa* cells; (Jores et al., 2016)) resulted in punctuate structures dissimilar from plastids, overlapping with the MitoTracker stain (Figure 5.5 A, B; Figure S9; note: crosstalk between mCherry and MitoTracker). When *At*Get3c-GFP_{S11} was co-expressed with the intermembrane space reporter Tim21-GFP_{S1-10}, epidermal cells displayed a partial overlap with MitoTracker (Figure S9) while *S. lycopersicum* protoplasts did not (not shown). Hence *At*Get3c targeting fidelity remains unchanged in both *A. cepa* and *S. lycopersicum* cells.

The intracellular divisions of *At*Get3a and *At*Get3b were also explored in these two heterologous plant systems. *At*Get3b clearly localized in stroma of plastids in *A. cepa* and *S. lycopersicum* cells (Figure 5.5 C) upper panels and D upper panel) whereas *At*Get3a is present in the cytosol of *A. cepa* and *S. lycopersicum* cells (Figure 5.5 C, D; lower panel). Consequently, all *A. thaliana* orthologues were accurately directed to the correct organelle, irrespective of the heterologous plant system.

5.1.5 *Medicago* Get3 orthologues are present in various organelles

In order to illustrate the intracellular partitioning of Get3 proteins in Fabidae, *Medicago x varia* (crossing of *Medicago sativa* and *Medicago falcata*) was analyzed. Due to the collinearity of their genomes (Choi et al., 2004) we used the closely related *Medicago truncatula* as a genetic scaffold for the lacking sequenced genome of *Medicago x varia*. This led to the identification of *M_S*Get3a

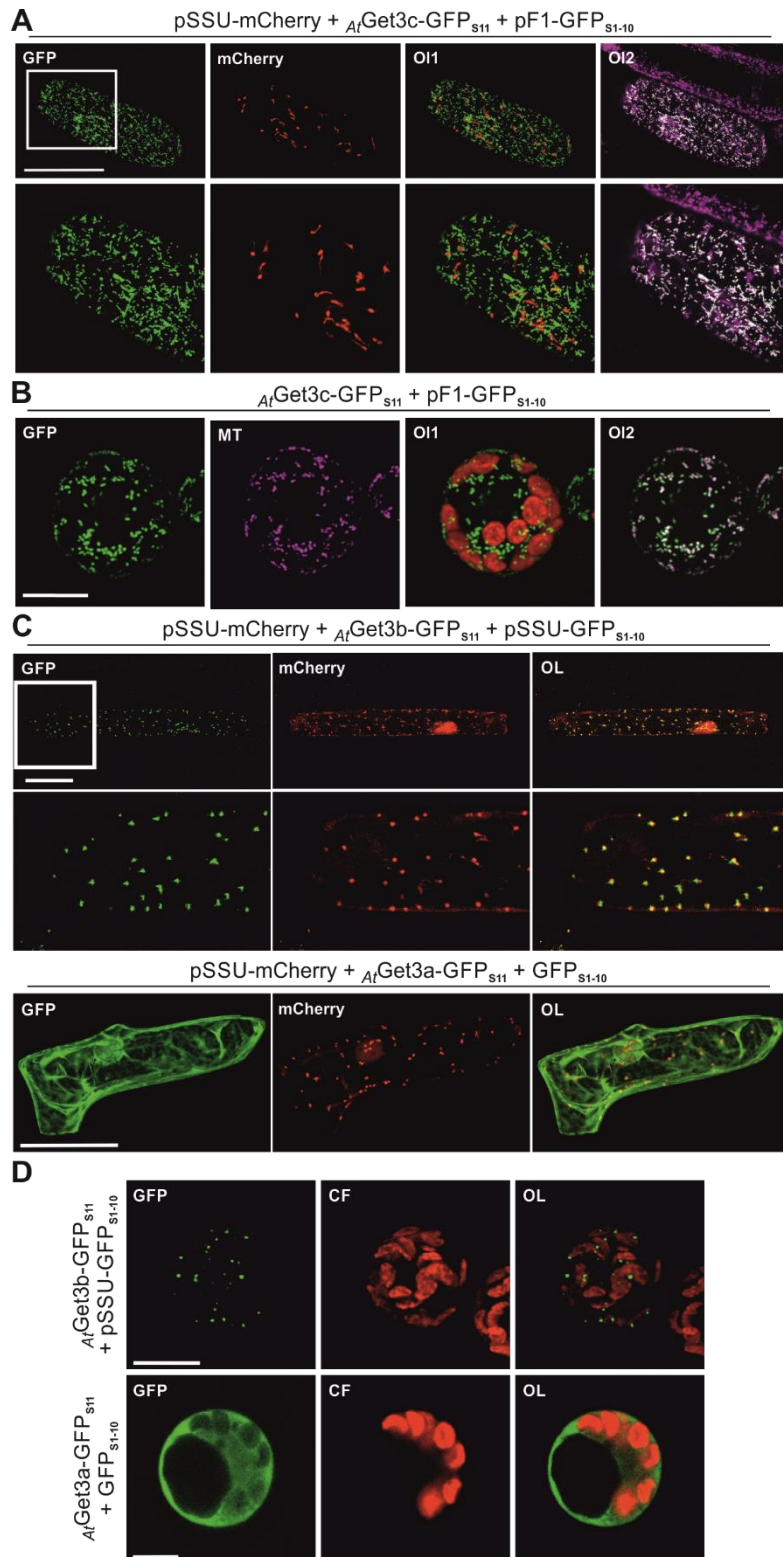


Figure 5.5. *At*Get3c targeting fidelity remains unchanged in *Solanum lycopersicum* and *Allium cepa*.

A. Epidermal *Allium cepa* cells were co-transfected with *At*Get3c-GFP_{S11}, pSSU-mCherry and pF1-GFP_{S1-10}. After 16 hrs of co-expression, cells were stained with MitoTracker (MT) and analyzed by CLSM. GFP, mCherry-fluorescence, GFP/mCherry (OI1) and GFP/MitoTracker (OI2) are displayed. **B.** Protoplasts isolated from *Solanum lycopersicum* transiently co-expressed *At*Get3c-GFP_{S11} together with pF1-GFP_{S1-10} and MT staining. GFP, MitoTracker (MT), GFP/CF (OI1) and GFP/MT (OI2) are shown. **C.** *At*Get3b-GFP_{S11}, pSSU-GFP_{S1-10} and pSSU-mCherry (top) as well as *At*Get3a-GFP_{S11}, GFP_{S1-10} and pSSU-mCherry were co-transfected into *Allium cepa* cells. GFP, mCherry and their overlay (OI) are depicted. **D.** Same constructs as (C) without pSSU-mCherry transiently transfected into *Solanum lycopersicum* protoplasts. GFP, chlorophyll fluorescence (CF) and overlay (OI) of both are shown. Scale bar 10 μ m, adapted from Bodensohn et al. (2019).

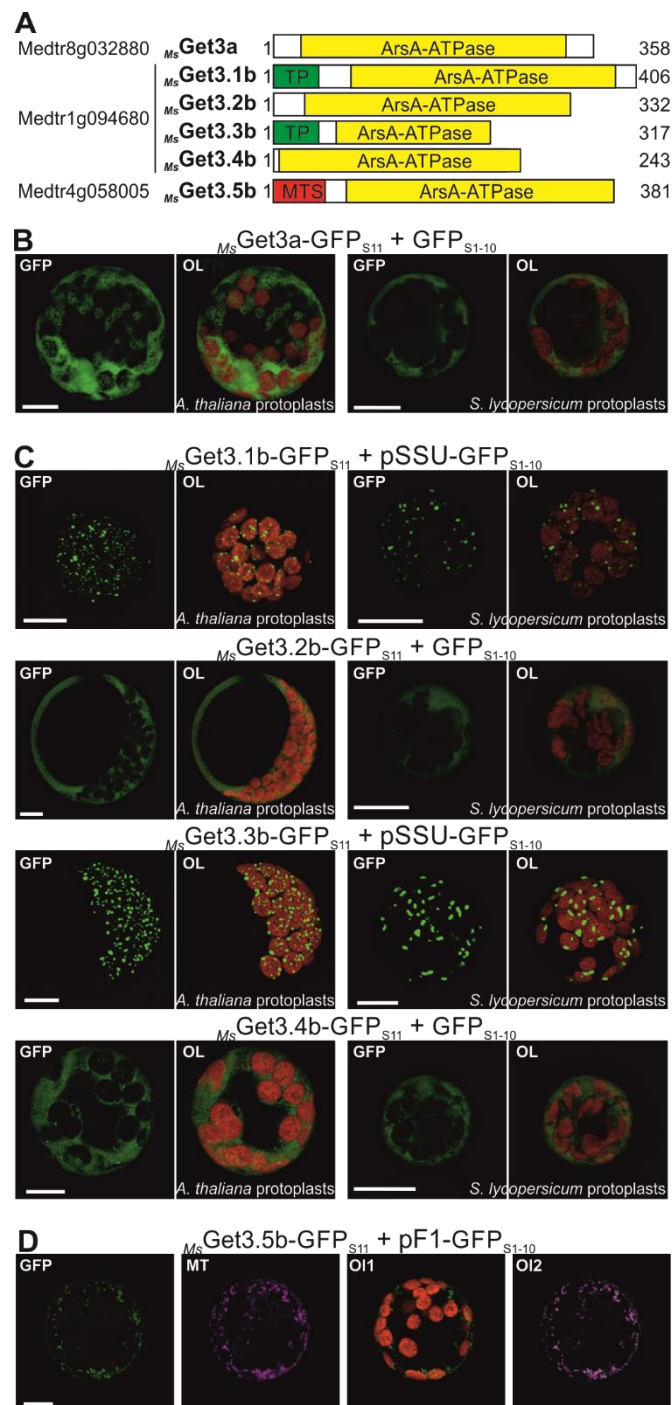


Figure 5.6. The Get3 orthologues of *Medicago x varia* reside in cytosol, chloroplasts and mitochondria.

A. Schematic representation of the domain architecture within the AA sequence of *M_s*Get3a, the isoforms of *M_s*Get3.1b and *M_s*Get3.5b. TP: transit peptide; MTS mitochondrial targeting signal. Note that *M_s*Get3.3b and *M_s*Get3.4b have truncated ArsA domains. B, C. Protoplasts isolated from *A. thaliana* and *S. lycopersicum* were co-transfected with the *M_s*Get3a (B) or isoforms of *M_s*Get3b1 (C) as GFP_{S11} fusion proteins together with the indicated organellar GFP_{S1-10} reporter proteins and analyzed by CLSM. GFP and GFP/CF (OI) are shown. D. After *A. thaliana* protoplasts co-expressed *M_s*Get3.5b-GFP_{S11} with pF1-GFP_{S1-10} for 16 hrs they were stained with MT and examined by CLSM. Fluorescent channels of GFP, MT, GFP/CF (OI1) and GFP/MT (OI2). Scale bar 10 μm, modified from Bodensohn et al. (2019).

(Medtr8g032880), and *M_s*Get3.5b (Medtr4g058005) *M_s*Get3b (Medtr1g094680). For latter, four different splice variants were suggested (*M_s*Get3.1b, *M_s*Get3.2b, *M_s*Get3.3b, *M_s*Get3.4b; Figure 5.6 A)

including two isoforms devoid of topogenic signals (M_s Get3.1b, M_s Get3.3b) and two with truncated ArsA domains (M_s Get3.2b, M_s Get3.4b). Transient heterologous co-expression of M_s Get3a-GFP_{S11}, M_s Get3.4b-GFP_{S11} together with cytosolic GFP_{S1-10} in protoplasts derived from *A. thaliana* or *S. lycopersicum* displayed a cytosolic localization (Figure 5.6 B, C). The analysis of M_s Get3.1b-GFP_{S11} and M_s Get3.3b-GFP_{S11} revealed a stromal localization in both protoplast systems (Figure 5.6 C) and as predicted M_s get3.5b-GFP_{S11} was targeted to the mitochondrial matrix in *A. thaliana* protoplasts (Figure 5.6 D). Hence *Medicago x varia* possess two genes that code for organelle particular Get3 proteins one is targeted to mitochondria and the other has two cytosolic isoforms.

5.1.6 *Solanum lycopersicum* Get3 proteins are targeted to cytosol and chloroplast

The analysis identified s Get3.1a (Solyc01g091880), s Get3.2a (Solyc05g050490), s Get3.3a (Solyc10g017810) and a plastid predicted s Get3b (Solyc11g069830). Transient co-expression of s Get3.1a-GFP_{S11}, s Get3.2a-GFP_{S11} and s Get3.3a-GFP_{S11} revealed a cytosolic localization whereas s Get3b-GFP_{S11} was targeted to the stroma of plastids in *S. lycopersicum* protoplasts (Figure 5.7 A). This clearly illustrates an example of an Eudicotyledon devoid of a mitochondrial Get3 orthologue.

5.1.7 *Physcomitrella patens* Get3 orthologues are localized in cytosol and chloroplast

In order to exemplify the intracellular distribution of Get3 proteins in Bryophyta we examined *Physcomitrella patens*. Two *At*Get3a orthologues p_p Get3.1a (Pp3c19_12470), p_p Get3.2a (Pp3c14_22160) and two *At*Get3b orthologues p_p Get3.1b (Pp3c22_13860), p_p Get3.2b (Pp3c17_16460) were discovered. Even though no topogenic signal was identified for the *At*Get3b orthologues (Table S1) both p_p Get3.1b-GFP_{S11} as well as p_p Get3.2b-GFP_{S11} were targeted to the stroma of plastids and p_p Get3.1a-GFP_{S11} and p_p Get3.2a-GFP_{S11} to the cytosol in *P. patens* protoplasts (Figure 5.7 C, D, respectively). Thereby demonstrating an example of a primordial moss lacking a mitochondrial targeted Get3 orthologue but still equipped with a *At*Get3b orthologue devoid of a predictable transit peptide.

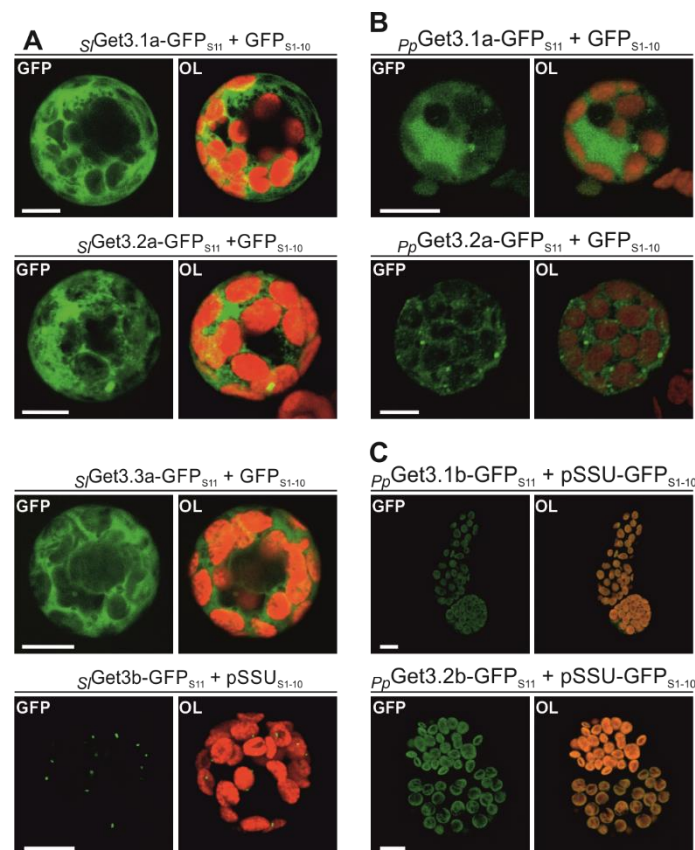


Figure 5.7. Get3 orthologues of *Solanum lycopersicum* and *Physcomitrella patens* localized in cytoplasm and chloroplast.
A. *S. lycopersicum* protoplasts were co-transfected with the indicated S_j Get3 orthologues and corresponding organellar reporter. Channels of GFP and GFP/CF (OL) are shown. **B, C.** *P. patens* protoplasts were co-transfected with the shown constructs orthologous to A_t Get3a (B) and A_t Get3b (C). Scale bar 10 μ m, adapted from Bodensohn et al., (2019).

5.2 A_t Get3a in *Arabidopsis thaliana*

5.2.1 A_t GET pathway comprises pre-targeting and receptor components

It has been reported that in *A. thaliana* one homologue of Get1 and one Get4 homologue are present (Srivastava et al., 2017; Xing et al., 2017). The aforementioned analysis (4.1.1) was employed and at least one Get1 and Get4 homologue were identified in the majority of the analyzed plants (Figure 5.8 A). The co-expression of A_t Get1-GFP $_{S11}$ and GFP $_{S11-A_t}$ Get4 with GFP $_{S1-10}$ revealed that the latter was cytosolic and the polytopic membrane protein Get1 co-localizes with ER-mCherry with a $N_{out}-C_{in}$ topology (Figure 5.8 B). To validate this distribution, protoplasts (T) expressing A_t Get1-GFP $_{S11}$ and GFP $_{S11-A_t}$ Get4 were fractionated into cytosolic (Cy) and microsomal (Mc) enriched fractions (Figure 5.8 C). Immunodecoration of the fractions showed that BiP and A_t Get3a were distributed in all fractions but were mostly enriched in the microsomal ones (Figure 5.8 C; T, Cy, **Mc**). A_t Get1-GFP $_{S11}$ was present in the total as well as microsomal fractions (Figure 5.8 C; T & Mc) and GFP $_{S11-A_t}$ Get4 in the total and cytosolic subdivisions (Figure 5.8 C; T & Cy). By verifying the occurrence of a component of the pre-targeting complex (A_t Get4), the receptor complex (A_t Get1) and the cytosolic ATPase (A_t Get3) a

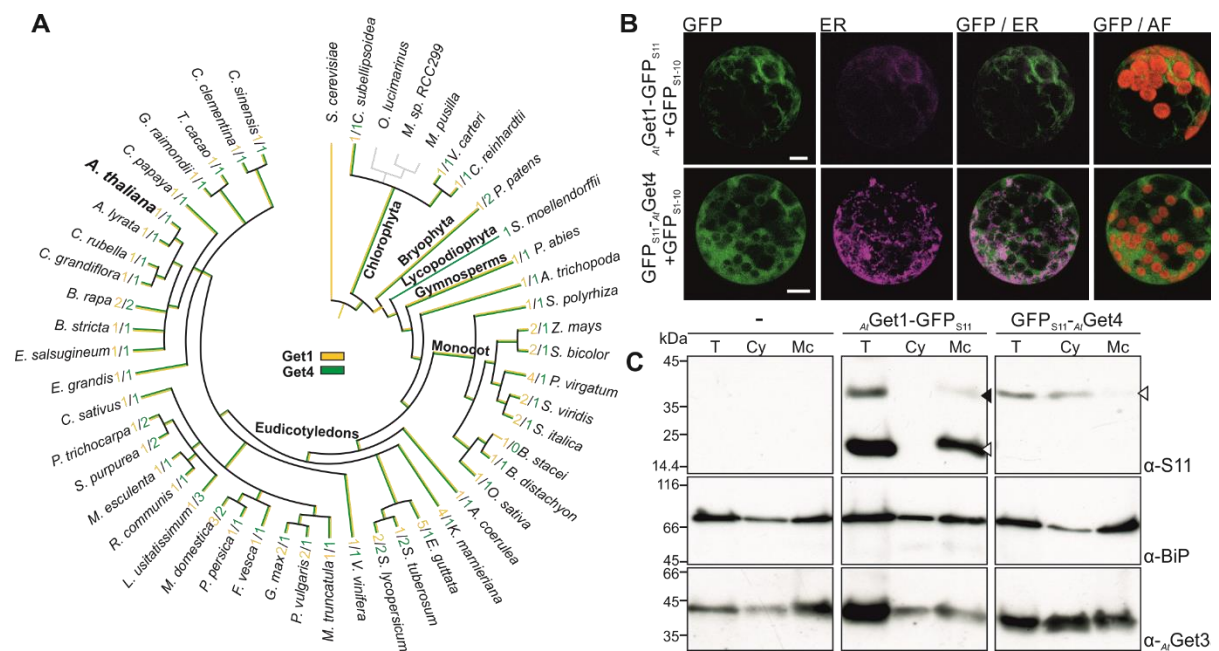


Figure 5.8. In *A. thaliana* Get1 and Get4 locate to ER and cytosol, respectively.

A. Taxonomic relationship of Viridiplantae analyzing the existence Get1 and Get4 using *S. cerevisiae* as outgroup. The identified orthologues of Get1 (yellow) and Get4 (green) as well as the number of orthologues with respective color code (Table S2, Table S4). **B.** Protoplasts from *A. thaliana* were co-transfected with GFP $_{S11}$ together with A_t Get1-GFP $_{S11}$ (top) and GFP $_{S11}$ - A_t Get4 (bottom). Signals from GFP, ER-mCherry (ER), overlay of GFP/ER and GFP/CF are shown. Scale bar 10 μ m. **C.** Protoplasts (-) isolated from *A. thaliana* were transfected with A_t Get1-GFP $_{S11}$ and GFP $_{S11}$ - A_t Get4 and fractionated. Total cell lysate (T), cytosolic (Cy) and microsomal (Mc) fractions were separated by SDS-PAGE and analyzed by immunodecoration. White arrowheads indicate monomeric migration and the black arrowhead the dimeric Get1 as previously reported (Srivastava et al., 2017; Xing et al., 2017). Modified from Bodensohn et al., (2019).

further implication of a degree of conservation of the GET pathway in *A. thaliana* was retrieved, substantiating previous observations (Srivastava et al., 2017; Xing et al., 2017).

5.2.2 Interacting network of A_t Get3a *in vivo*

To date the main focus has been laid on A_t Get3a with respect to its function, molecular interactions and impact on plant development (Srivastava et al., 2017; Xing et al., 2017). In order to further address the molecular composition of complexes formed by A_t Get3a, I utilized white cell culture derived from root tissue of *Arabidopsis thaliana* for immune-precipitations. This form of cultivation has the advantage that: (i) cultures reach the exponential phase after three to five days to ensure proficient biomass production and (ii) they are devoid of chloroplasts, which can lead to massive contaminations (see 4.1.1). With the aim of approximating cellular abundances to estimate the right amount of biomass as well as the appropriate lysis method, cells were fractionated into soluble and membranous portions as well as directly solubilized in 1 % Triton X-100 and compared to recombinant A_t Get3a

(Figure S1 A). After precipitation in detergent solubilized cell extract a reproducible profile of eight coomassie stainable proteinaceous bands was observed (Figure S10 B). These were excised from the PAGE and subjected to LC MS/MS analysis. In a previous analysis (Lim et al., 2003) a minimal sequence coverage of 10 % was chosen as criteria for inclusion, however while using the same cutoff many mitochondrial proteins including ribosomal proteins were identified. With the intention to narrow down the hits to ease the identification of putative interacting proteins a cut off of 20 % sequence coverage was chosen. To gain a better overview, the identified hits were manually grouped according to their annotated cellular activity (Figure 5.9). Depending on their role, proteins acting in mitochondria, metabolic, vacuolar, nuclear or signaling pathways were regarded as contaminations due to their sheer abundance. Seven of eight identified hits from three excised bands contained proteins which were classified as the aforementioned contaminations (Figure 5.9 B1, B2, B4, grey). Interestingly the other bands displayed a form of partitioning in regards to the co-immune-precipitated proteins. One band was distinguished by containing mainly different cytosolic Hsp70s (*At*Hsp70.1-4; Figure 5.9 B3; purple) and one mitochondrial Hsp60 which was regarded as contamination (Figure 5.9 B3; grey). Since a direct involvement of Hsp70 in the GET pathway has been observed in yeast (Cho and Shan, 2018) this was not surprising. Additionally, in the same band one ribosomal protein was identified which had a rather low sequence coverage but the highest overall protein enrichment (Figure 5.9 B3; black rectangle). Remarkably, the protein Ub-RPL40B (*At*3g52590) exhibits a very similar domain architecture to Ub41A from the mammalian TRC pathway (Table S6). Two further excised band contained only ribosomal proteins as putative candidates (Figure 5.9 B5, B6) and two other bands included ribosomal and proteasomal proteins (Figure 5.9 B7, B8). This also parallels the observation of the ribosomal association of TRC components in mammals (Leznicki and High, 2020) and an involvement of TRC40 in proteasomal degradation (Itakura et al., 2016). Some putative interacting proteins as well as contaminations were identified twice in two different excised bands (Figure 5.9; connected by red dotted line) and interestingly one protein reoccurred in 5 different excised bands with the highest overall sequence recovery (Figure 5.9 B4–8, connected by red dotted line). The protein of unknown function (*At*2g25280) contains a memo-like domain and is not comparable to any component of the yet described GET or TRC pathway. Unfortunately, no suitable candidate for Get2, Get5 or Bag6 could be identified by immune-precipitations coupled to MS/MS. However, an inspection of the genomes of *Homo sapiens* and *Arabidopsis thaliana* revealed that six and eight BAG proteins were present, respectively (Figure S11; inlet). The Bag6 proteins of both organisms were more than double as big as the biggest BAG protein of the respective organism and sequence alignment of the BAG domains displayed multiple insertions within the BAG domains of the two Bag6 proteins as well as a c-terminal extension of *At*Bag6 (Figure S11). This insertion in *Hs*Bag6 could explain the mock BAG domain of *Hs*Bag6 (Mock et al., 2015). Furthermore, no TA protein candidates could be identified.

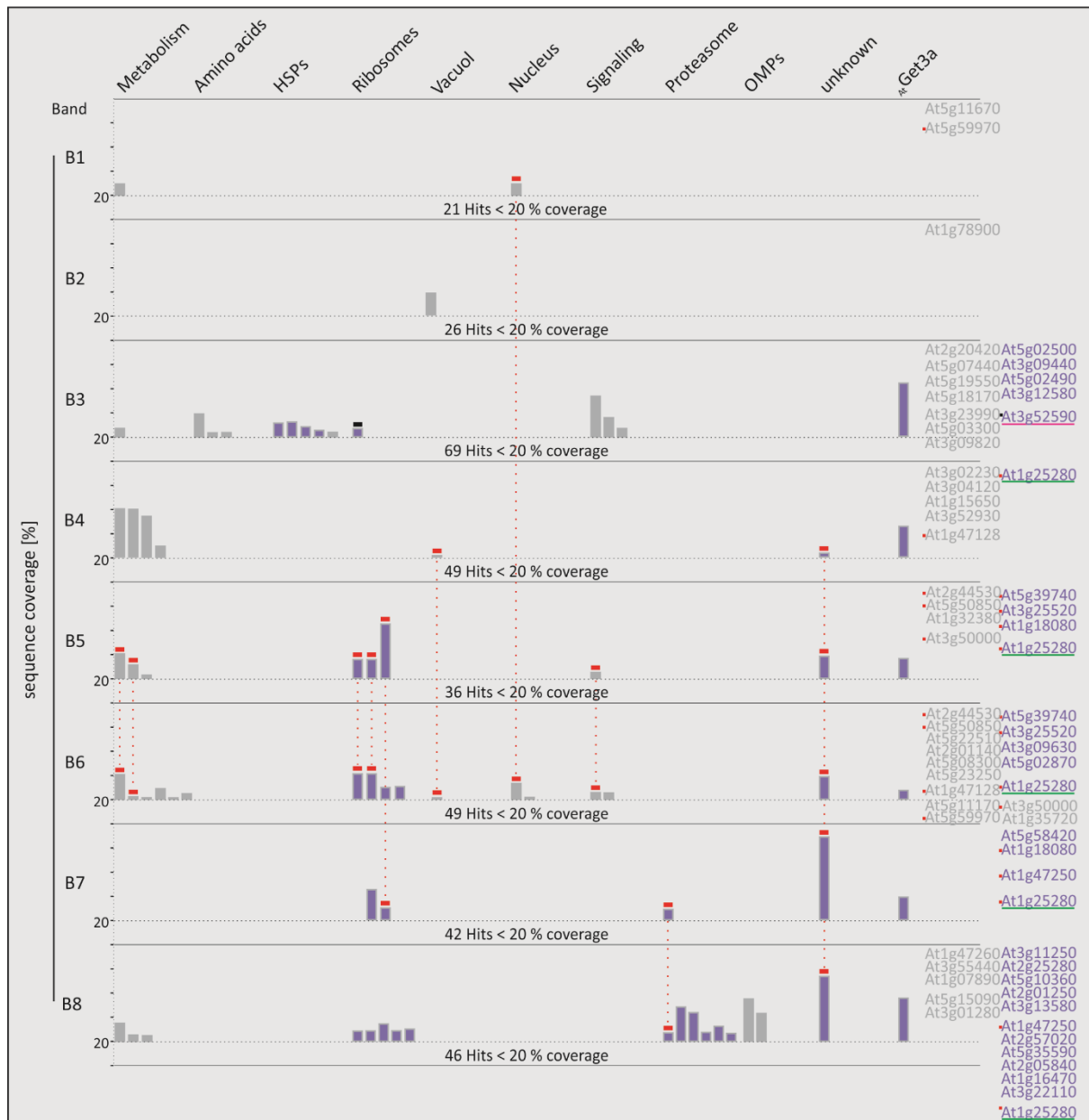


Figure 5.9. Putative components of pre-targeting complex and interaction partners.

Eight reproducible bands from a coomassie stained gel from CoIP experiments were excised and subjected to LC-MS/MS analysis. The retrieved proteinaceous hits were manually classified into different cellular occupations (top; 10 groups). The percentage of sequence coverage of the identified proteins from the excised bands (B1-8) is displayed. Due to too many organellar contaminations, a cut-off of 20% sequence coverage (dotted horizontal lines) was chosen. Hits that were regarded as contaminations are shown in grey and cytosolic hits in purple. Hits that were found in more than one band are marked with a red rectangle and connected by red dots. The AGIs of the different hits are listed on the right in the respective color and order. The number of hits that were disregarded per band are illustrated under the dotted lines. The AGIs of the putative Ubl4A counterpart (black rectangle) is underlined in magenta and the repeatedly co-precipitating protein is underlined in green. The gel from which the bands were excised is shown in Figure S10.

Summarizing, a putative Ubl4A (Get5) candidate, a protein of unknown function and Hsp70-, ribosomal- as well as proteasomal- associations were identified by immune-precipitations. Additionally, a putative Bag6 candidate was identified by bioinformatic means.

5.3 Functional characterization of *At*Get3a

5.3.1 Tail anchor translocation (TAT) *in cellula*

Trc40 was initially identified as a targeting factor involved in the post-translational delivery of tail-anchored proteins to the ER (Stefanovic and Hegde, 2007). This is mediated by binding to hydrophobic segments of client TMDs and releasing these at the receptor complex in a nucleotide dependent manner (Mateja et al., 2009; Wang et al., 2014; Rome et al., 2013). A well-established method in the field is TAT in which a recombinantly expressed complex of Targeting factor and TA protein are incubated with isolated rough microsomes. Due to an engineered OPG tag (Kutay et al., 1995) preceding the TMD of client TA proteins, N-glycosylation by the oligosaccharyltransferase (OST) complex can take place in the lumen of the ER. The resulting difference in migration of the glycosylated substrate can be visualized on a SDS PAGE (Cho et al., 2018). So far, only one *At*Syntaxin protein (SYP72, At3g45280) from *A. thaliana* was used as a plant originated model TA protein, however in concert with yeast rough microsomes and *sc*Get3 (Srivastava et al., 2017). Still, a fully plant reconstituted system has not been established. So I sought out to establish a TAT assay with microsomes derived from *A. thaliana* together with recombinant complexes of *At*Get3a and substrate synthesized in *E. coli*. Since the plant OST complex was only recently isolated for the first time (Jeong et al., 2018) our general knowledge of glycosylation in *A. thaliana* is scarce. Furthermore, the recombinant OPG tag has never been used in plants before, leading to no verification of its functionality in plants. To gain insights into the TA targeting fidelity and glycosylation efficiency of *A. thaliana* I expressed a model TA comprised of *At*Sec61 β (At2g45070) with a flag tag preceded by the OPG tag as well as a hexahistidine tag (*At*Sec61 β -Flag-OPG_{His}) in protoplasts (Figure 5.10 A). Expressing protoplasts were split in two, fractionated into cytosolic (Cy) and microsomal (Mi) enriched divisions and either left untreated (-) or subjected to proteinase K (PK) treatment (Figure 5.10 B). In contrast to the model TA proteins without an OPG tag, (Figure 5.10; lane 6 and 12) the equipped ones were glycosylated (Figure 5.10; lane 4 and 10). The highest migrating form of glycosylation (Figure 5.10; Lane 4) could be due to unfinished processing (reviewed in Pattison and Amtmann, 2009). The residual amounts of *At*Sec61 β -Flag-OPG_{His} present in the cytosolic fraction, were diminished after proteinase K treatment indicating that these were not properly inserted (Figure 5.10; lane 3 vs 9). The occurrence of the protected fragment of the unglycosylated (PF) and glycosylated (gPF) model TA protein verified the proper membrane translocation and topology (Figure 5.10; lane 10 and 12). In summary, for the first time in plants a recombinant OPG tag was translocated across the ER membrane with a N_{in}-C_{out} orientation and glycosylated in the lumen as judged by its protease protection.

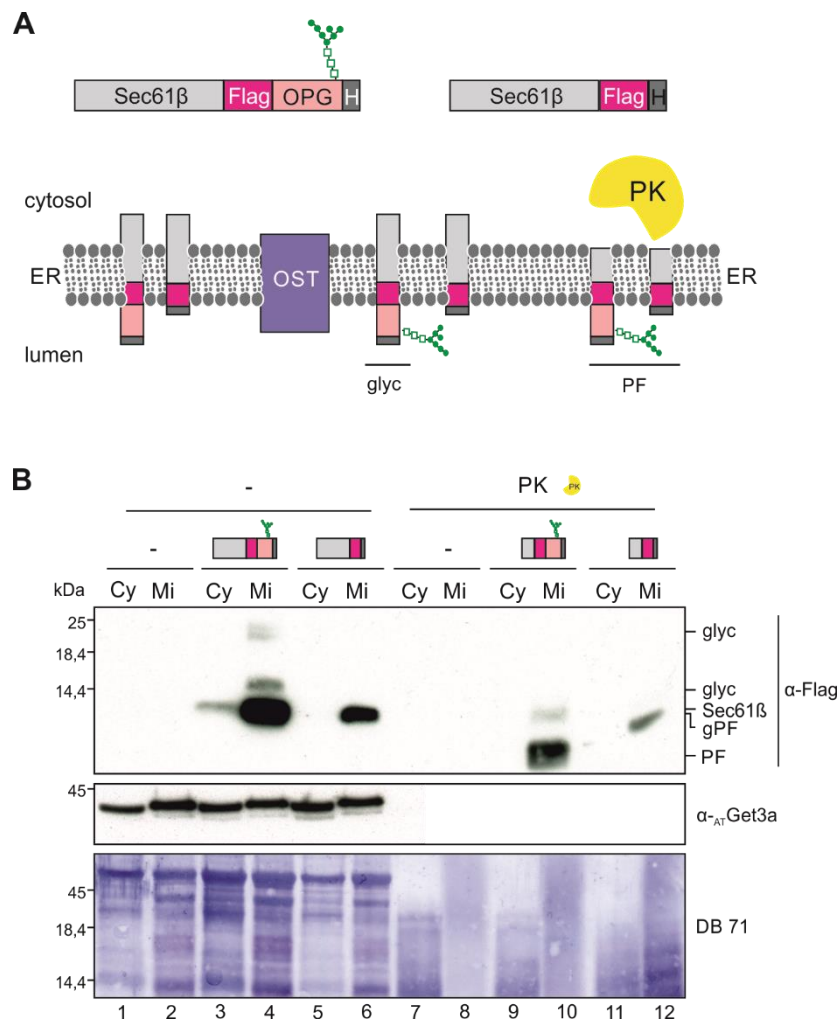


Figure 5.10. TA model substrate gets glycosylated *in cellula*.

A. Top, schematic representation of the expressed TA model substrate of Sec61 β (light grey) followed by flag tag (magenta), without (top right) or with OPG tag (top left - pink) preceded by a hexahistidine tag (dark grey). After translocation into ER-membranes the oligosaccharyltransferase (OST) complex (blue) glycosylates (glyc) an oligosaccharide (green) to the OPG tag (pink) of the model substrate (top). The addition of proteinase K (PK, yellow) initiates the digestion of cytosolic exposed elements leading to protected fragments (PF) (bottom). **B.** Either empty plasmid (-) or the constructs containing Sec61 β with or without OPG tag (pink) were transfected into *A. thaliana* protoplasts. After 8 hours of expression, cells were partitioned into cytosolic (Cy) and microsomal (Mi) fractions. Untreated (-) and proteinase K treated (PK) samples were subjected to SDS-PAGE followed by immunodecoration with α -Flag or α -*At*Get3a antibodies. The migrations of Sec61 β or glycosylated (glic) Sec61 β as well as PF and glycosylated version gPF after protease treatment are indicated.

5.3.2 Tail anchor translocation (TAT) *in vitro*

After having verified that *A. thaliana* is capable of TAT, a suitable method was devised to attain an appropriate microsomal fraction. The comparison of two different linear sucrose gradients displayed that *At*Get3a coincides with the luminal binding protein BiP in a range from 20 % to 40 % sucrose (Figure S12 A, B). In order to enrich *At*Get3a the latter range with 10 % increments formed a three step gradient in which *At*Get3a was enriched in both the 20/30 % interface as well as the 30/40 % interface, however the latter displayed a higher enrichment (Figure S12 C). When recombinantly expressed in *E. coli* the

produced $AtGet3a_{His}$ protein was insoluble (data not shown). By exchanging the position of the hexahistidine tag from the C- to the N-terminus a major population of the synthesized His_AtGet3 protein remained soluble and was not sequestered as inclusion bodies (Figure S12 D; IB vs E1-4). Intrigued by this observation and in order to establish a targeting factor-substrate complex, I co-expressed untagged $AtGet3a$ with $AtSec61\beta$ -Flag-OPG_{His} as polycistronic transcript in *E. coli*. After Ni-NTA purification $AtGet3a$ was present in the elution fractions of $AtSec61\beta$ -Flag-OPG_{His} in semi stoichiometric ratios as assessed by immune-detection (Figure 5.11 A). These purified complexes were incubated with isolated microsomes in differing ratios and samples were taken at periodic time points. Unfortunately, in the time frame of 45 minutes no glycosylation could be observed under the utilized conditions (Figure 5.11 B). All in all, an appropriate microsomal isolation method was devised and the recombinantly expressed construct was modified to yield more soluble protein. This was then utilized to co-express an untagged targeting factor with a tagged membrane protein and purify a soluble complex containing both proteins in semi stoichiometric ratios. Unfortunately, the experimental conditions for TAT have to be modified, but the acquirement of the most vital constituents was established.

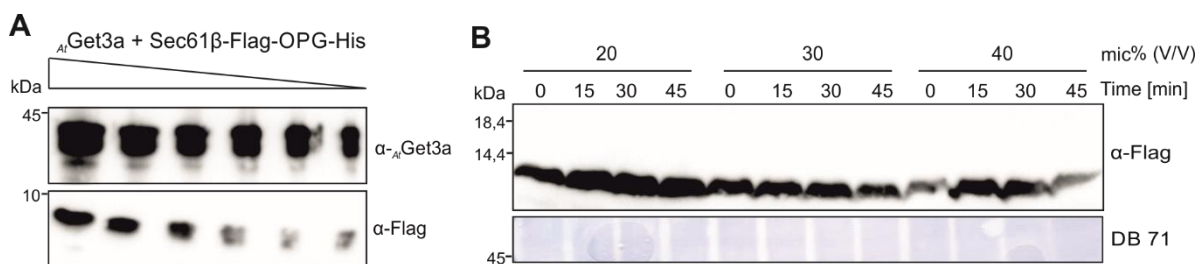


Figure 5.11. Recombinant production of $AtGet3a$ - TA model substrate complexes and TAT trial.

A. The tag-less variant of $AtGet3a$ was co-expressed with the Sec61-Flag-OPG-His model substrate (Figure 5.10) and co-purified. Decreasing amounts of an elution fraction of $AtGet3a$ /TA-substrate complex produced were analyzed by immune decoration with the indicated antibodies. **B.** Complexes from A) were mixed with isolated microsomal fractions in the shown ratios (% (V/V)) and samples were taken at the given time points. Reaction mixes were set up according to (Cho et al., 2018).

5.3.3 $AtGet3a$ holdase function *in vitro* under heat stress

Even though the susceptibility of *get1* and *get3* mutants to the ER stress agent dithiothreitol (DTT) has been tested (Srivastava et al., 2017), to date the holdase function of the $AtGet3a$ has never been addressed. In previous trials *in vitro* grown plants on MS (Murashige Skoog) medium were stressed with H_2O_2 but thereafter plants were either flooded or the medium starting dissolving (data not shown). For this the holdase function of $AtGet3a$ was assessed *in vitro*. In order to pursue, both luciferase and the mature domain (without transit peptide) of the plastidic malate dehydrogenase tested for heat sensitivity (Figure S13). Both proteins have been used as *in vitro* ATP independent

chaperone substrate (Graumann et al., 2001; Basha et al., 2004; Xu et al., 2010). After heat stress at increasing temperatures we observed that only the malate dehydrogenase was fully aggregated at 65 °C and present in the pellet fraction after centrifugation (Figure S13). As a control recombinant *At*Get3a and malate dehydrogenase (from here on *At*cpMDH) were individually kept at room temperature (C), followed by a 65 °C heat stress (S) and brought back to RT (R) for the same time and periodically samples were taken to assess aggregation (Figure 5.12 A). Surprisingly minute amounts of *At*CpMDH already started to aggregate under control conditions but in the heat and recovery phase the majority of protein aggregated in the pellet fraction (Figure 5.12 A; upper panel). In contrast, a substantial population *At*Get3a protein was always present in the pellet, irrespective of the treatment (Figure 5.12 A; lower panel). To assess its holdase capability, *At*Get3a it was incubated with *At*cpMDH in differing molar ratios and subjected to heat stress at 65 °C and after centrifugation the aggregated pellet was analyzed (Figure 5.12 B). Even though *At*Get3a was proportionally present in the pellet it was able to keep *At*cpMDH out of this fraction when it was added to the reaction in equimolar or two-fold molar excess (Figure 5.12 B; 1:1, 2:1). In contrast, when *At*cpMDH was included in molar excess, the majority was recovered as aggregates in the pellet fraction (Figure 5.12 B; 1:4). These data imply that *At*Get3a can act as a heat inducible holdase that prevents the aggregation of the heat sensitive chaperone substrate *At*cpMDH. Even though the holdase itself is prone to aggregation, substrate protection is mediated at equimolar or molar excess of *At*Get3a.

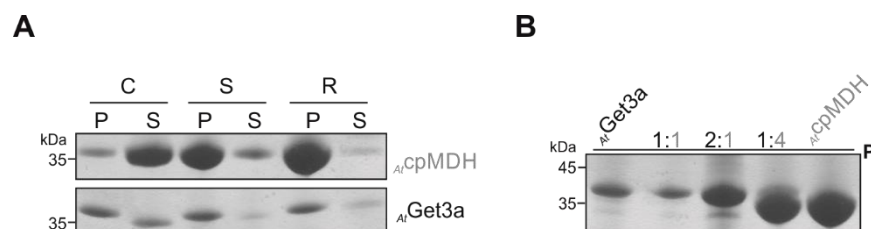


Figure 5.12. *At*Get3a prevents heat induced aggregation of *At*cpMDH.

A. *At*CpMDH (top) and *At*Get3a (bottom) were fractionated into insoluble (P) and soluble (S) fractions at room temperature (C), 65 °C heat stress (S) and the following recovery (R) at RT. Samples were separated by SDS-PAGE and stained by coomassie
B. *At*Get3a (black) and *At*cpMDH (grey) were either separately or in the indicated ratios subjected to a 65 °C heat stress and insoluble material was recovered by centrifugation. Samples were run on SDS-PAGE and stained with coomassie. P in bold denotes that only pellet fractions were loaded. Adapted from MSc thesis of Victoria Gosch under my supervision.

5.4 *At*Get3c in mitochondria of *Arabidopsis thaliana*

5.4.1 Homozygous T-DNA insertion line suitable for reverse genetic approach

To date solely the localization of *At*Get3c was analyzed leading to contradicting observations (Duncan et al., 2013; Xing et al., 2017). This issue was also addressed in this thesis and we were able to show a targeting into the mitochondrial matrix irrespective of the analyzed tissue of *A. thaliana* or heterologous expression system (see 4.1.2 to 4.1.4). In order to analyze the *in vivo* function of *At*Get3c a reverse genetic approach was employed. For this T-DNA insertion lines were utilized, in which a fragment of a modified tumor inducing (TI) plasmid is randomly recombined into the genomic DNA of *Arabidopsis thaliana*. Due to little intergenic material, a size of about 5 kb is sufficient to disrupt gene functionality (Krysan et al., 1999). One T-DNA insertion line could be obtained, bearing a single intronic insertion at position 1457 in the *At*GET3C locus (Figure 5.13 A). This line could be segregated to a homozygous state judged by the absence of the wild type allele (Figure 5.13 B). RT-PCR with primers flanking the insertion detected an expressed transcript (Figure 5.13 C). Notably, western blot analysis utilizing the generated *At*Get3c antibody displayed a lack of the matching *At*Get3c protein (Figure 5.13 D). These results showed that the *Atget3c* line is appropriate for a reverse genetic approach to study *At*Get3c deficiency in *A. thaliana*.

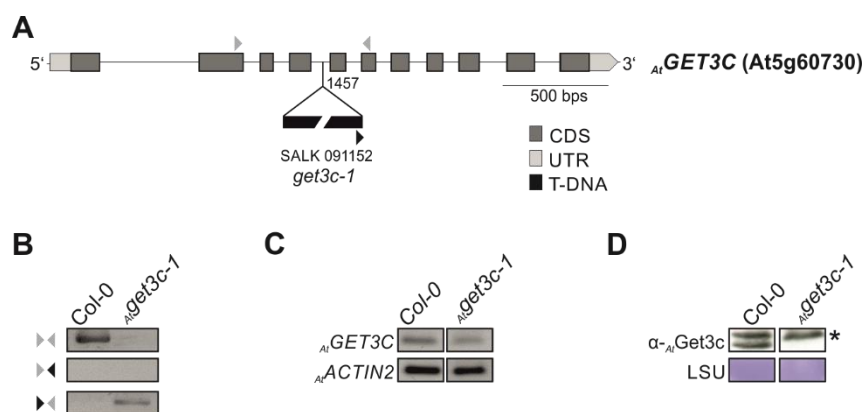


Figure 5.13. T-DNA insertion line for *At*GET3C.

A. Diagram showing the gene structure with location and orientation of the T-DNA insertion. Coding sequences (CDS) are represented by dark grey boxes and untranslated regions (UTRs) in light grey. Arrowheads indicate primer sites for PCRs on gDNA (**B**). T-DNA left border primer (black arrowhead) was used in PCR reactions with primers for the *GET3C* alleles (grey arrowheads) and gDNA isolated from the indicated plant lines. **C.** RT-PCR with specific exon junction primers were used for RT-PCRs with reverse transcribed cDNA from isolated RNA from the denoted plant lines. **D.** Total protein isolated from leaf tissue was used for western blot analysis with the *At*Get3c antibody. Asterisk illustrates an unspecific cross reactivity. Gel slices in (**C**) and (**D**) stem from the same agarose and SDS gel, respectively.

5.4.2 Respiratory chain composition is altered in *Atget3c*

Cultivated *Atget3c* plants did not show any differences to the wild-type in terms of leaf shape (not shown) or plant size (Figure S14 A). Plants were also subjected to transmission electron microscopy (TEM) analysis and no severe ultrastructural modifications were detected in mitochondria or other organelles (Figure 5.14).

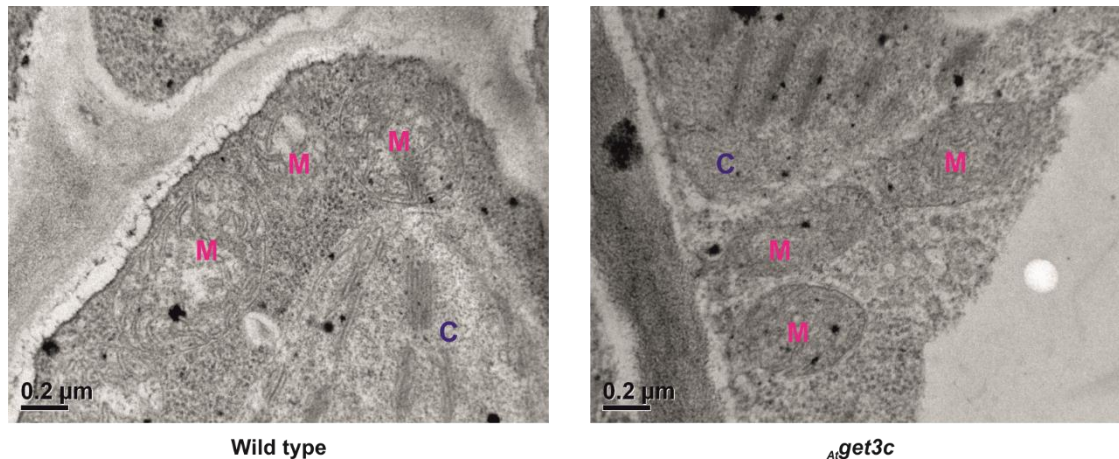


Figure 5.14. Organellar ultrastructure is similar to wild-type in *Atget3c-1*.

Leaf tissue of seven-day old *A. thaliana* wild-type (left) and *Atget3c* (right) seedlings were subjected to by transmission electron microscopy (TEM) analysis. Scale bar is indicated. Mitochondria (M) and chloroplasts (C) are labeled in magenta and blue, respectively.

In order to acquire mitochondria in high purity from *A. thaliana* the isolation method had to be optimized. Instead of a three step Percoll gradient (Rödiger et al., 2010) an optimized linear PVP gradient was utilized (Whelan et al., 2015) which led to better separation of mitochondria from chloroplastidic debris (Figure 5.15 A). I isolated mitochondria, solubilized these with digitonin, as it was shown to be suitable for mitochondrial research in plants (Eubel et al., 2003) and separated the resulting complexes by blue native (BN)-PAGE (Figure 5.15 B). I was able to observe minute but distinct differential abundances of respiratory chain complexes. In numerous plant species complex IV (cytochrome c oxidase) migrates in two forms in a native gel (Eubel et al., 2003). Surprisingly complex IV_b was reduced in *Atget3b-1* in comparison to the wild type (Figure 5.15 B). Even though it known that complex II (succinate dehydrogenase) tends to dissociate under detergent treatment, (Eubel et al., 2003) it was detectable in the wild type but not in *Atget3b-1* sample (Figure 5.15 B). Interestingly, three out of nine as well as four out of ten proteins constituting complex IV_b and II, respectively share a TA topology (Figure 5.15 B; inlets Figure S15; Figure S14). Taken together, *Atget3c* hardly displayed any developmental phenotypic traits, but showed perturbed respiratory chain complex abundances. The affected complexes comprised several TA proteins, which could present putative substrates.

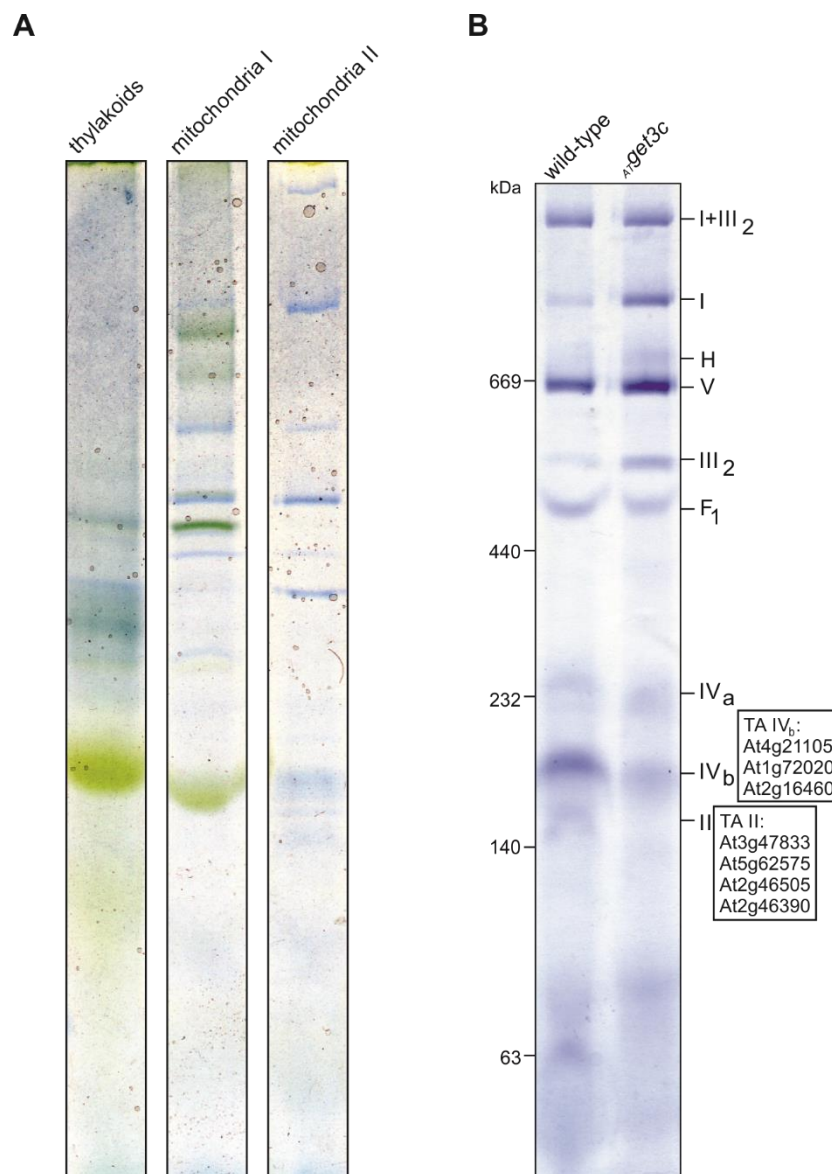


Figure 5.15. Respiratory chain complex composition is distorted in *Atget3c*.

A. Solubilized mitochondria isolated from 14-day old *A. thaliana* plants with the previous method (mitochondria I) and the newly devised method (mitochondria II) were compared to solubilized isolated thylakoids. Gel slices are from the same gel. **B.** Mitochondria isolated from *A. thaliana* wild-type (left) and *Atget3c-1* (right) plants were isolated with the optimized method (A), solubilized and separated by BN-PAGE. The AGIs of the IMPs in complex II and complex IV_b with a TA topology are listed in the respective boxes.

5.5 *AtGe3c* activity *in vitro*

5.5.1 *AtGet3c* holdase function *in vitro* under heat stress

To elucidate if *AtGet3c* is also capable of heat induced holdase activity it was analyzed *in vitro* with recombinant holdase and heat sensitive substrate produced in *E. coli*. The preliminary test (see 4.3.3) revealed that the majority of the putative holdase and substrate aggregated after heat stress at 65 °C and stayed insoluble after the recovery phase (Figure 5.16 A). When mixed together in altering molar

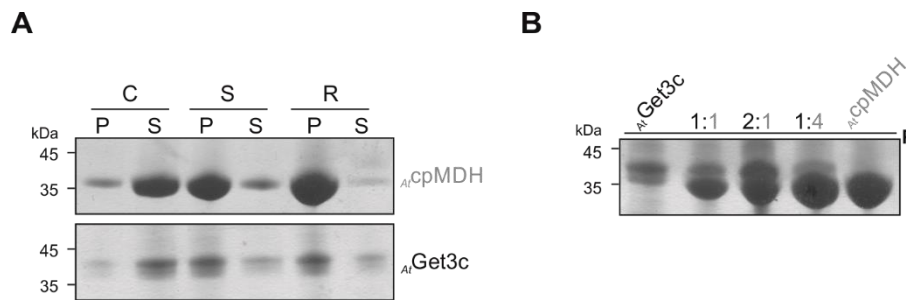


Figure 5.16. *AtGet3c* is not capable of preventing heat induced aggregation of *AtcpMDH*.

A. *AtcpMDH* (top) and *AtGet3c* (bottom) were fractionated into insoluble (P) and soluble (S) fractions at room temperature (C), 65 °C heat stress (S) and the following recovery (R) at 25 °C. Samples were separated by SDS-PAGE and stained by coomassie
B. *AtGet3c* (black) and *AtcpMDH* (grey) were either separately or in the indicated ratios subjected to a 65 °C heat stress and insoluble material was recovered by centrifugation. Samples were run on SDS-PAGE and stained with coomassie. P in bold denotes that only pellet fractions were loaded. Adapted from MSc thesis of Victoria Gosch under my supervision.

ratios, *AtGet3c* aggregated together with MDH and was unable to prevent the its aggregation irrespective of the ratios of the constituents (Figure 5.16 B). This displayed that *AtGet3c* could not act as a heat inducible holdase. At least not with the utilized substrate in this assay.

5.6 *AtGet3b* is involved in the assembly of photosystem II (PSII)

5.6.1 Two T-DNA insertion lines with opposing attributes

To date nothing is known about the cellular role of the plastid localized *AtGet3b*. As for *AtGet3c*, I chose a reverse genetic approach to gain insights into its function. Two T-DNA insertion lines with insertions in the *AtGET3B* locus were obtained (Figure 5.17). Both lines were homozygous, with *Atget3b-1* comprising a back-to-back insertion at position 1 in the 5' UTR of the genomic DNA (Figure 5.17 A, B) and *Atget3b-2* with a single intronic insertion at position 1021 (Figure 5.17 A, C). RT-PCR amplified slightly less transcript in *Atget3b-1* than in the wild type. While no transcript was detected in *Atget3b-2* (Figure 5.17 D). Most relevantly, immune detection with the generated *AtGet3b* antibody revealed an increased signal intensity for *Atget3b-1* and none for *Atget3b-2*. These results show that the insertion *Atget3b-1* leads to a so called knock-on mutation with increased expression and *Atget3b-2* is a knock-out mutation (Krysan et al., 1999). Both lines were suitable to study *AtGet3b* overproduction and deficiency in *A. thaliana*, respectively.

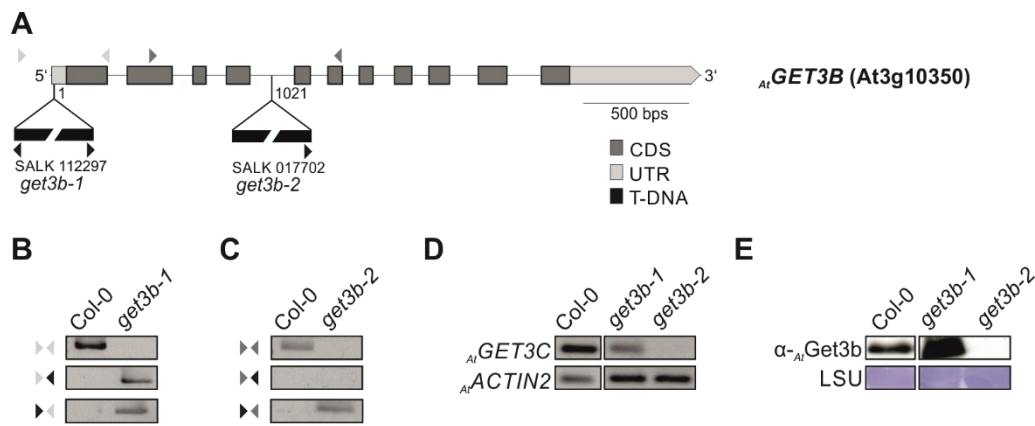


Figure 5.17. T-DNA insertion lines for *AtGET3B*.

A. Representation of the gene structure with location and direction of T-DNA insertion(s). Coding sequences (CDS) are represented by dark grey boxes and untranslated regions (UTRs) in light grey. Arrowheads indicate primer sites for PCRs on gDNA (**B**). T-DNA left border primer (black arrowhead) was used in PCR reactions with primers for the *GET3B* alleles (arrowheads in grey scale) with gDNA isolated from the indicated plant lines. **C.** RT-PCR with specific exon junction primers were used for RT-PCRs with reverse transcribed cDNA from isolated RNA from the denoted plant lines. **D.** Total protein isolated from leaf tissue was used for western blot analysis with the *AtGet3b* antibody. Gel slices in (**D**) and (**E**) stem from the same agarose and SDS gel, respectively.

5.6.2 Both *Atget3b* mutants display altered ultrastructural properties

Plants were cultivated on soil and growth stages were assessed according to Boyes et al. (2001). *Atget3b* mutants did not display any developmental effects on a general morphological scale (Figure S14 B). To gain insights on photosynthetic performance, plants were subjected to pulse amplitude modulation (PAM) measurements (Bradbury and Baker, 1981) during the first four weeks of development (Figure S16). In the role of four weeks, maximum quantum efficiency was not significantly effected in the mutant plants (data not shown). However, the electron transport kinetics were significantly altered throughout the second to fourth week in these (Figure S16; top panel). Furthermore, the non-photochemical-quenching (NPQ) parameters were also significantly dissimilar to wild-type levels in the second and third week of development (Figure S16 bottom panel). In order to gain some insights on these photosynthetic fluctuations, chloroplasts were inspected in further detail. Leaf material of plants grown for one to four weeks was examined by TEM (Figure 5.18 A). No severe differences were observed on an overall plastidic ultrastructural level. However, a detailed assessment of the thylakoid fine structure displayed that both *Atget3b* mutants assembled more appressed grana stacks per granum than the wild-type. This phenotype was only apparent in the second and third week of development but was absent in the fourth (Figure 5.18 B). Strikingly, the average height of a granum of both mutants was significantly smaller than the wild-type in this growth period (Figure 5.18 C). This observed thylakoid arrangement is reminiscent of the luminal assembly factor mutant, *Atcyp38-2*, in which a higher thylakoid content than the wild-type was described. In contrast to this analysis, the mean height of a granum was more than the wild-type (Vojta et al., 2019).

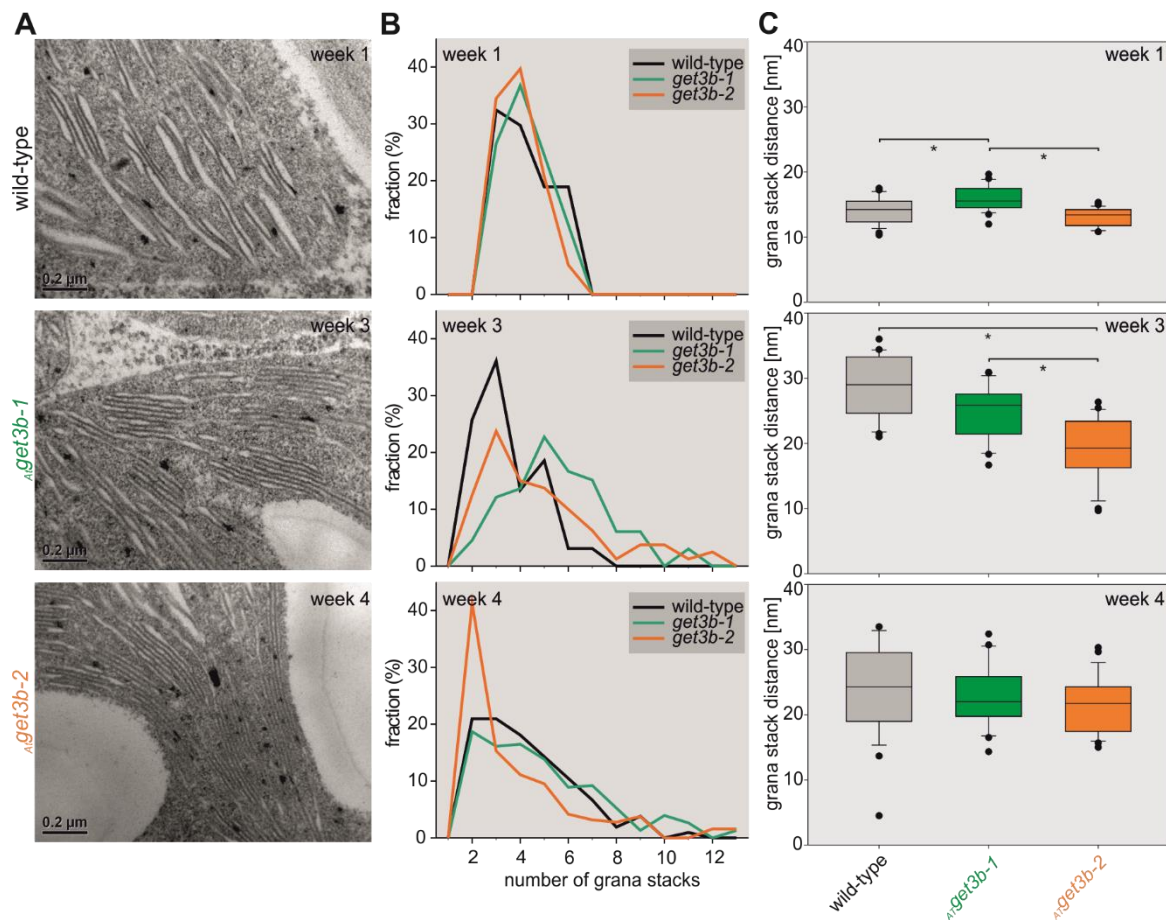


Figure 5.18. Both *AtGET3b* T-DNA insertion mutants display altered ultrastructural properties.

A. wild-type, *Atget3b-1* and *Atget3b-2* plants were subjected to transmission electron microscopy (TEM) analysis. As example, sections of plastids from 2 week old plants are shown. The scale bar is indicated. **B.** The number of stack per granum was quantified and the fraction of grana with a defined number of stacks is shown for plants grown for 1 week, 3 weeks or 4 weeks. **C.** The average height of a granum was quantified for the different growth stages. Statistical analyses was performed with ANOVA for three independent experiments with 8 images analyzed per experiment for each line.

These results showed the *Atget3b* mutants were morphologically indistinguishable from the wild-type. However, photosynthetic parameters as well thylakoid fine structural properties were altered in comparison to the wild-type. Nevertheless, except for the electron transport efficiency, all observed alterations acclimatized to wild-type levels in the fourth week of development.

5.6.3 Abundances of thylakoid membrane complexes effected in both *Atget3b* mutants

In order to assess if the *Atget3b* mutations have an effect on the molecular architecture of the photosynthetic apparatus, its composition was analyzed. The previous PAM and TEM analyses revealed that the respective effects of the mutations were most apparent between the second the third week of development (Figure 5.18). For this, I isolated thylakoids from 14-day old seedlings, solubilized these with digitonin and separated the resulting complexes via BN-PAGE (Figure 5.19 A). As a control, I

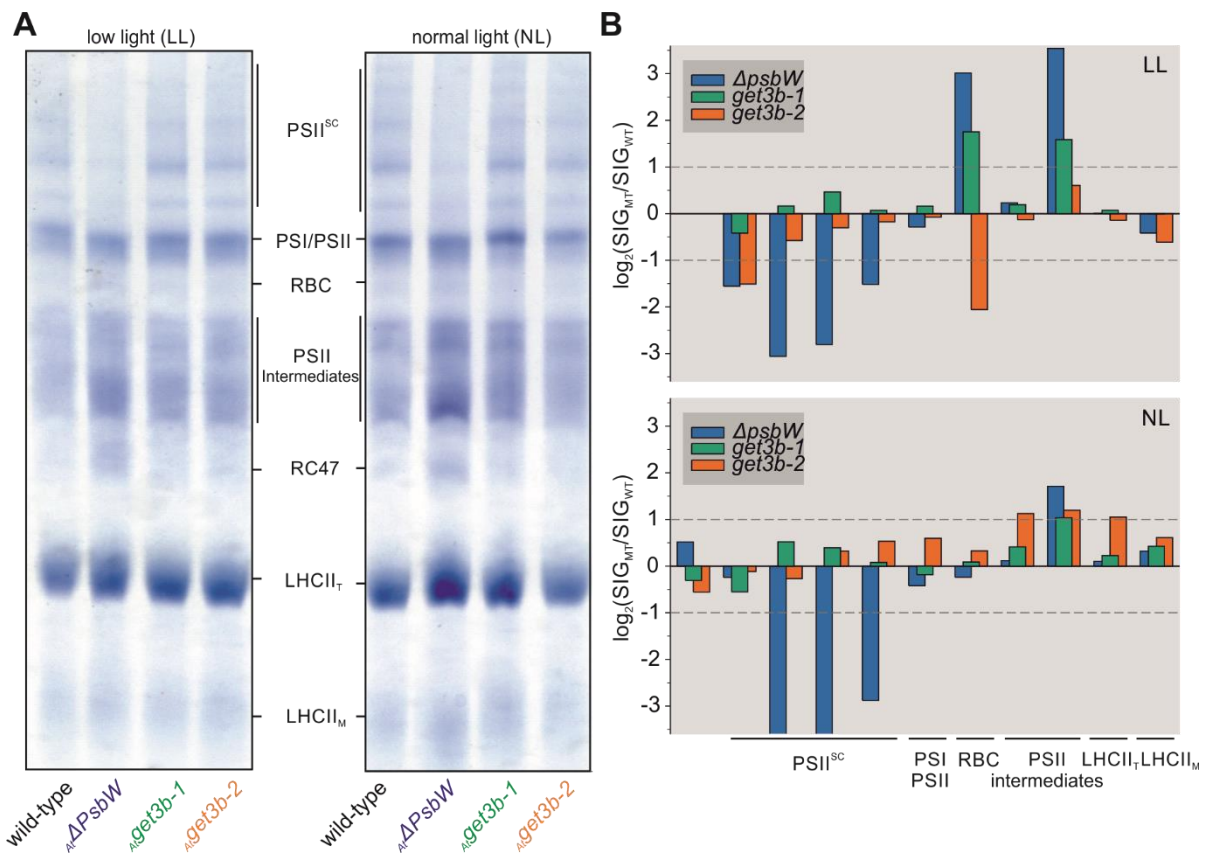


Figure 5.19. Both *AtGET3B* mutants exhibit irregular abundances of thylakoid embedded complexes.

A. Thylakoids of the denoted lines (bottom) were isolated from plants grown under low light (LL) or normal light conditions (NL). Thylakoids were solubilized and separated by BN-PAGE. **B.** Quantification of the bands in (A) is shown as \log_2 relative to wild-type (WT) intensities after normalization to the entire protein density. $\Delta PsbW$ mutant was analyzed as a control, because in this mutant super-complexes are not assembled. PS=photosystem, ^{SC}=super-complexes, RBC=rubisco, RC47=initial formation of PSII, LHCII=light harvesting complex II, _τ=trimeric, _M=monomeric

utilized the $\Delta_{At}PsbW$ mutant that is described to hardly assemble any super-complexes under low light (LL) conditions (García-Cerdán et al., 2011). Interestingly, a reduction of super-complex assemblies was observed for this mutant with a concomitant increase of PSII intermediates and RC47, irrespective of the light exposure (Figure 5.19 A, $\Delta_{At}PsbW$). Signal intensities of the individual complexes were quantified. Revealing that under low light (LL $\sim 70 \mu\text{mol m}^{-2} \text{s}^{-1}$) conditions $Atget3b-1$ assembled overall more super-complexes, Ribulose-1,5-bisphosphate carboxylase/oxygenase (RuBisCo) and PSII intermediates relative to the wild-type. $Atget3b-2$ on the other hand displayed a general reduction of the aforementioned complexes in comparison to the wild-type (Figure 5.19 B, top). Under normal light (NL $\sim 120 \mu\text{mol m}^{-2} \text{s}^{-1}$) conditions the degree of super-complex reduction was not as pronounced in $Atget3b-2$. Instead the line displayed an enhanced abundance of PSII intermediates as well as LHC moieties (Figure 5.19 B, bottom). Taken together, this data show that the $Atget3b$ mutations both lead to alterations in the abundances of individual complexes of the photosynthetic apparatus. These differences also returned back to wild-type levels in the fourth week of development (data not shown).

5.6.4 *Atget3b* mutants exhibit opposing effects on early PSII assembly

Due to the accumulation of PSII intermediates (Figure 5.19) paired with the similarity to a mutant impaired in PSII assembly (Figure 5.18) I raised the question if *AtGet3b* is involved in PSII assembly. To address this issue, I employed pulse amplitude modulation (PAM) measurements during de-etiolation to assess the degree of involvement in *de novo* PSII assembly. For this, plants were grown *in vitro* on Murashige Skoog (MS) medium for 5 days in the dark and subsequently normally illuminated. The process of de-etiolation and concomitant *de novo* PS biogenesis was tracked by PAM measurements which took place after 1, 7 and 24 hours after initial illumination (Figure 5.20 A, B). After 24 hours of de-etiolation without carbon source, *Atget3b-1* was significantly more efficient in PSII assembly than the wild-type which was verified by a better maximum quantum yield. Inversely, *Atget3b-2* was significantly obstructed in PSII assembly, irrespective of the presence of sucrose (Figure 5.20 A).

As a control, the same plates were cultivated for five days under normal illumination to then examine them fluorometrically. When grown autotrophically (absence of sucrose), *Atget3b-1* exhibited a higher and *Atget3b-2* a significantly lower maximum quantum yield (Figure 5.20 B). Displaying that not only the *de novo* assembly is hindered in *Atget3b-2* but also steady state levels in later stages in early thylakoidal biogenesis. Since these photosynthetic deficiencies were not apparent after seven days (Figure S16), but evident from *de novo* synthesis to five days, I examined four day old normally grown seedlings. The PAM measurements mirrored the previous assessment with a significantly hampered *Atget3b-2* (Figure 5.20 C). Coherently chlorophyll extraction revealed a slightly higher chlorophyll content for *Atget3b-1* and a significant reduction in *Atget3b-2* in comparison to the wild-type (Figure 5.20 D). The obtained data displayed that the lack of *AtGet3b* led to impediments in *de novo* as well as steady state levels of later stages of PSII assembly. The overexpression led to a more effective assembly relative to the wild-type. Not only the maximum quantum yield of the *Atget3b* mutants was effected but also the chlorophyll content was increased in *Atget3b-1* and conversely reduced in *Atget3b-2*, supporting further its involvement in photosynthetic processes.

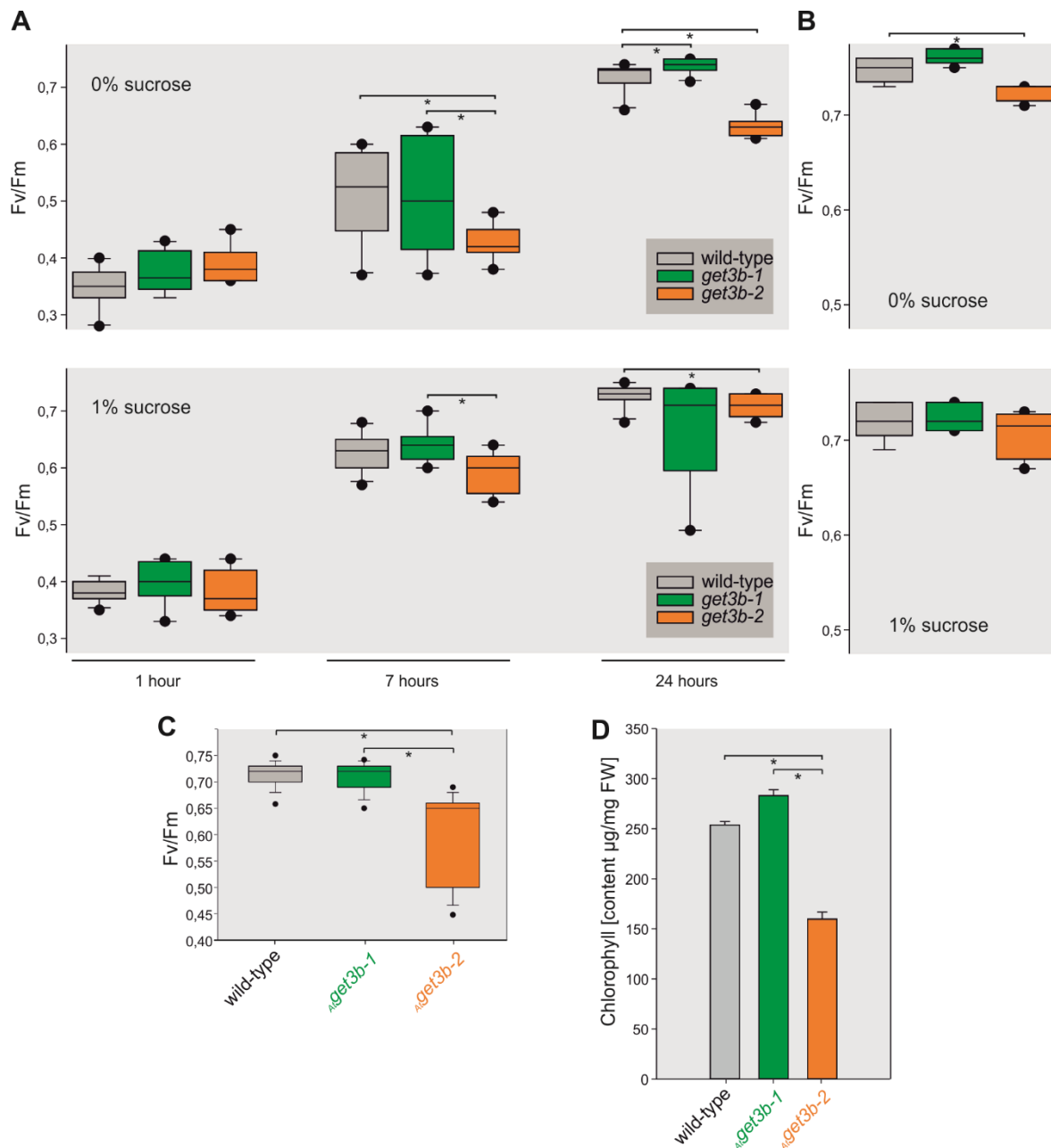


Figure 5.20. *AtGet3b* is involved in photo system II (PSII) assembly.

A. After growth of the lines depicted (dark grey box) on 0 % sucrose (top) or 1 % sucrose (bottom) for 5 days under etiolating conditions, plants were illuminated and pulse amplitude modulation (PAM) measurements were conducted. The Fv/Fm ratio (maximum quantum yield) was determined after 1, 7 and 24 hours to monitor PSII assembly. **B.** Seedlings of the depicted lines were grown under normal light conditions on 0 % sucrose (top) and 1 % sucrose (bottom). After five days, plants were subjected to PAM measurements. **C.** Normally grown 4-days old seedlings were used for PAM measurements as described above or **D.** utilized to determine the chlorophyll per milligram (mg) fresh weight (FW) concentration. Statistical analyses for (A) and (B) were performed using the students t-test, for three independent experiments with 40 seedlings per experiment. Statistical analyses for (C) were performed with ANOVA for 15 independent experiments with 40 seedlings per experiment as well as (D) for 3 experiments with 120 seedlings per experiment.

5.6.5 *At*Get3b binds hydrophobic PSII components *in vitro*

While working with the $\Delta_{At}PsbW$ mutant I noticed an enhanced level of *At*Get3b protein in this line (Figure 5.21 A). Interestingly, *At*PsbW protein levels were slightly enhanced in *Atget3b-2*. This observation was strongly increased in *Atget3b-1* (Figure 5.21 B). In order to clarify if the enhanced levels of protein are actually inserted into the thylakoids or aggregate in the stroma, I fractionated 14 day old *Arabidopsis thaliana* seedlings (T) of the four lines into chloroplast (Ch) and thylakoid (Th) partitions (Figure 5.21 C). *At*PsbW was imported into chloroplasts and incorporated into thylakoids as judged by immune-detection with the PsbW antibody. Yet, *Atget3b-1* displayed the highest degree of thylakoid incorporation (Figure 5.21 C; lane 9 vs 3, 6, 12). This raised the question if this could represent a putative targeting-factor, substrate interaction between *At*Get3b and *At*PsbW. As established for *At*Get3a, the relocation of the hexahistidine tag to the N-terminus increased the soluble population of *mAt*Get3b (mature domain devoid of topogenic signal) after recombinant expression in *E. coli* (see chapter 4.3.2). I employed the same strategy as for *At*Get3a and *At*Sec61 β and co-expressed an untagged *mAt*Get3b together with a tagged variant of *mAt*PsbW followed by a flag and a hexahistidine-tag (*mAt*PsbW-Flag-His). When co-expressed with the full length *mAt*PsbW-Flag-His, I was able to co-purify *mAt*Get3b (Figure 5.21 D; lane 4-6). In absence of substrate, *mAt*Get3b did bind to the affinity matrix (Figure 5.21 D; lane 1-3). To assess if this interaction is dependent on the transmembrane domain (TMD) of *At*PsbW, the assay was repeated with a variant of *At*PsbW without a TMD (*mAt*PsbW $_{\Delta TMD}$). When co-expressed with *mAt*PsbW $_{\Delta TMD}$, the levels of co-purified *mAt*Get3b were drastically reduced (Figure 5.21 D; lane 7-9). Additionally, the capability of *mAt*Get3b to bind a polytopic membrane protein was tested. For this, a LHC3 variant including a Flag and His tag (*mAt*LHC3-Flag-His) was utilized with the same strategy. Interestingly, I was able to co-purify *mAt*Get3b when co-expressed with the three TMD bearing *mAt*LHC3-Flag-His (Figure 5.21 D; lane 10-12). Taken together this data set clearly pointed towards an interaction between *At*Get3b and *At*PsbW. This interaction was dependent on the presence of the TMD of *At*PsbW. The co-purification of *At*LHC3 either points towards an extension of the putative substrate beyond solely TA proteins or a general high chaperone capability of *At*Get3b. Moreover, the recombinant expression could have primed artificial complex formations.

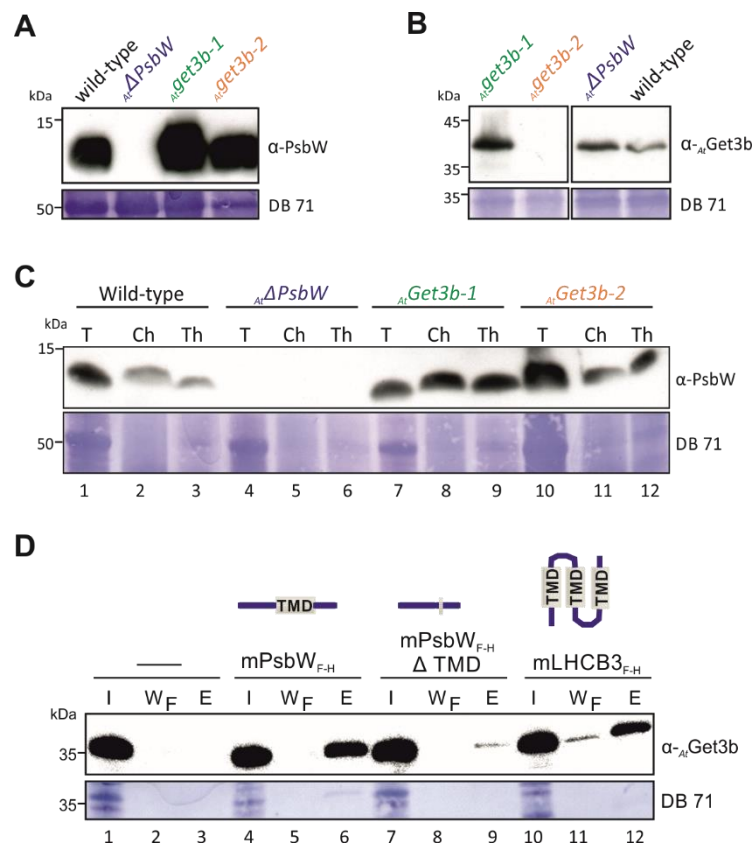


Figure 5.21. *AtPsbW* and *AtGet3b* levels altered in respective mutant plant lines and *AtGet3b* binds hydrophobic segments. **A, B.** Equal amounts of protein extract from 14-day old plants of the indicated lines were separated by SDS-PAGE and immunodecorated with antibodies against *AtPsbW* (A) and *AtGet3b* (B). **C.** 14 day-old *A. thaliana* seedlings (T) of the indicated plant lines were fractionated into chloroplast (Ch) and thylakoid (Th) portions. Equal amounts of protein of each fraction were subjected to SDS-PAGE followed by immunoblot analysis. **D.** The tag free mature domain of *AtGet3b* was expressed (left) or co-expressed with the indicated Flag-6xHIS (F-H) tagged proteins in *E. coli*. Co-purification of *AtGet3b* by itself (-), with *mAtPsbW*-Flag-His, *mAtPsbW*_{TMD}-Flag-His and *AtLHCB3*-Flag-His was performed as established for *AtGet3a*. “m” denotes the mature protein without transit peptide. A schematic representation of the protein (blue) with TMD (light gray) is shown. I=input, W_F=final wash, E=elution

5.6.6 Thylakoid tail anchor translocation (τ TAT)

After having established a soluble targeting-factor-substrate complex, I sought out to assess if these were capable of τ TAT. In a preliminary trial, thylakoids were isolated from 14-day old *A. thaliana* seedlings, incubated with purified recombinant *mAtGet3b*/*mAtPsbW*-Flag-His complexes and samples were acquired periodically. These were washed and split into three. Kept untreated, subjected to proteolytic digestion or treated with 0.1 M NaOH to remove peripheral associated proteins (Figure 5.229. The latter treatment did not work as *mAtGet3b* was still recovered with the thylakoids as judged by immune-detection (Figure 5.22; lane 2, 5, 8, 11). The untreated sample showed an increase in signal intensity over time. This could either be *bona fide* membrane insertion or the unspecific association to the membrane (Figure 5.22; Lane 1, 4, 7, 10). Interestingly, the protease treated sample seemed to

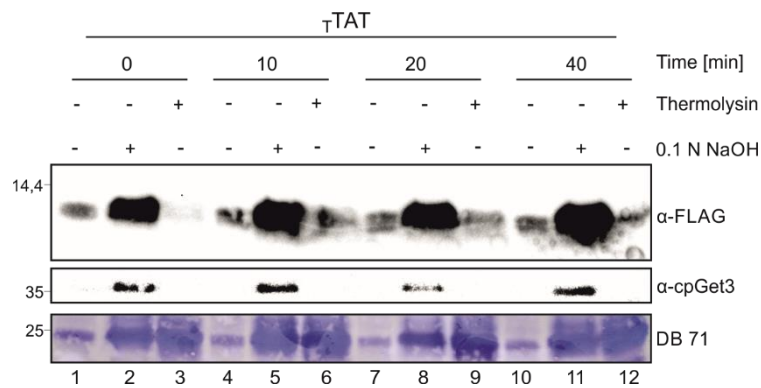


Figure 5.22. Thylakoid tail-anchor translocation (τ TAT).

Thylakoids isolated from *A. thaliana* were incubated with recombinant *At*Get3b/*At*PsbW complexes synthesized in *E. coli*. After the indicated time points aliquots were taken, and split into three. These were either kept untreated (lane 1, 4, 7, 10), treated with 0.1 N NaOH to remove peripheral membrane association (lane 2, 5, 8, 11) or with thermolysin to remove aggregates as well as peripheral associations (lane 3, 6, 9, 12). Samples were analyzed by immuno-detection with the indicated antibodies.

display a time dependent increase in intensity even though this was slightly overshadowed by the signal of the 0.1 M NaOH sample (Figure 5.22; Lane 3, 6, 9, 12). This could be indicative for true membrane translocation. Nevertheless, this preliminary experiment displayed that TAT with these purified complexes could work in isolated thylakoids.

5.7 Comparative proteomics of *Atget3b* mutants

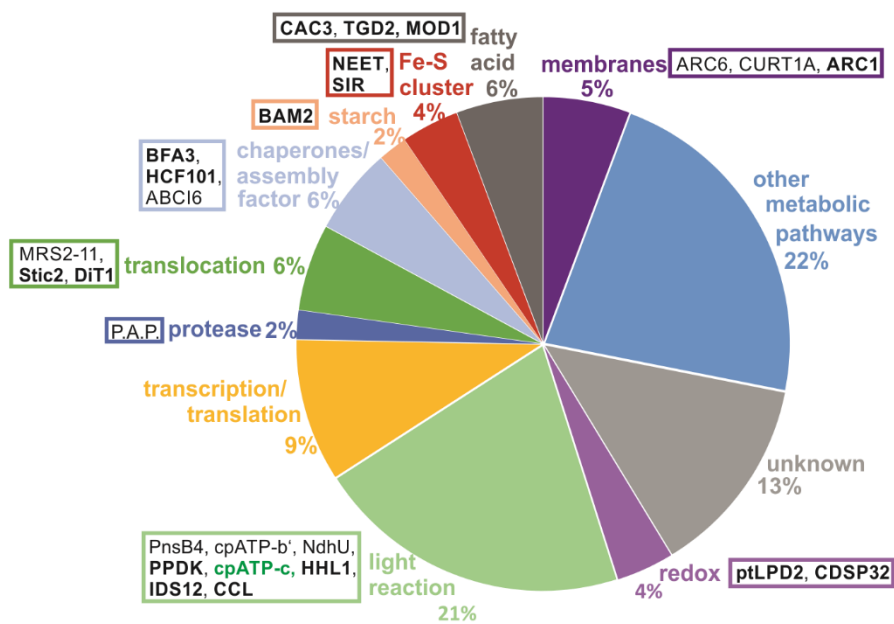
The scope of the different *Atget3b* mutations was additionally examined on a proteomic level. The rationale behind the analysis was to (i) assess the effects of the two mutations on the total proteome of chloroplasts and (ii) identifying proteins that are affected in both mutants could imply putative mutual pathways. By utilizing either one of the *Atget3b* mutants in conjunction with wild-type plants, a label-free procedure could be employed in a quantitative manner as previously established (Vermeulen et al., 2008). Since the effects of the mutations were most evident in the second and third week of development, I isolated chloroplasts from 14 day-old wild-type and mutant *A. thaliana* seedlings. Triplicates of each line individually containing 80 μ g of protein were subjected to LC-MS/MS. Peptides were fractionated by discontinuous gradient displacement from strong cation exchange (SCX) and pooled for the measurement. Label-free quantification was facilitated by MaxQuant (Cox and Mann, 2008) and data was normalized, trimmed and statistically evaluated with Perseus (Tyanova and Cox, 2018).

5.7.1 The effects of the *Atget3b-1* mutation on the chloroplast proteome

The comparative analysis identified a total of 1,173 shared proteinaceous hits. 56 of these were significantly reduced and 16 were significantly increased in *Atget3b-1* (Figure S17). The identified hits covered a wide range of molecular functions and biological processes. I manually reviewed the significantly differing hits to exclude organellar contaminations and categorize them according to their cellular association. 53 of the 56 significantly reduced hits represented plastid localized proteins. The majority of the proteins (22 %) were categorized into other metabolic pathways. These mainly consisted of elements involved in the synthesis of amino acid and secondary metabolites (Figure 5.23 A; blue). Nearly as many proteins (21 %) were involved in the light reaction of photosynthesis (Figure 5.23 A, light green). These included subunits of the chloroplast NDH complex, PnsB4 and NdhU of subcomplex EDB and subcomplex B, respectively (reviewed in Shikanai, 2016), an alpha and gamma subunit of the ATP synthase as well as regulatory elements. Interestingly all regulatory components as well as one ATP synthase subunit that were encoded by the plastid and these were reduced in *Atget3b-2* as well (Figure 5.23 A; light green box, bold). Proteins regulating transcription and translation (9 %) together with proteins of unknown function (13 %) shared approximately the same proportion as the two previous categories (Figure 5.23 A; dark yellow and light grey, respectively). Translocation, chaperones/assembly factors and fatty acid synthesis were categories of equal size (6 %). Within the classification linked to translocation, the Mg transporter essential for chloroplast development and photosynthesis, MRS2-11 (Sun et al., 2017) was negatively affected. Interestingly, Stic2 a protein involved in protein trafficking (Bédard et al., 2017) and 2-oxoglutarate/malate translocator DiT1 (Schneidereit et al., 2006) were also significantly reduced in *Atget3b-2* (Figure 5.23 A, dark green). The identified chaperones/assembly factors were part of the major Fe-S cluster assembly machinery itself e.g. ABCI6 (Xu and Møller, 2004) and assembly factors for the ATP synthase or Fe-S clusters like BFA3 (Zhang et al., 2016) and HCF101 (Schwenkert et al., 2009), respectively. The latter two were also reduced in *Atget3b-2* (Figure 5.23 A, light blue). Surprisingly, all proteins associated with fatty acid synthesis (6 %) were reduced in *Atget3b-2* as well (Figure 5.23 A; dark grey). Namely the Acetyl-coenzyme A carboxylase3 (CAC3) (Roesler et al., 1994), TGD2 involved in ER to plastid lipid trafficking (Roston et al., 2012) and a subunit of the fatty acid synthase II MOD1 (Serrano et al., 2007). In the category of membrane remodeling and mechanics (5 %) the essential ARC1 (Kadirjan-Kalbach et al., 2012) was also reduced in both *Atget3b* mutants. Also the plastid division machinery coordinating ARC6 (Glynn et al., 2008) and membrane modulating CURT1A (Luque and Ochoa de Alda, 2014) (Figure 5.23 A; dark purple). Factors involved in redox regulation as well as Fe-S cluster dependent reactions were represented to the same proportion (4 %) with all hits being reduced in *Atget3b-2* too (Figure 5.23 A; light purple and red, respectively). One protease (2 %) was significantly reduced in *Atget3b-1* (Figure 5.23 A; light blue). One component associated with starch synthesis (2 %) was reduced in both

A

53 hits in total



B

16 hits in total

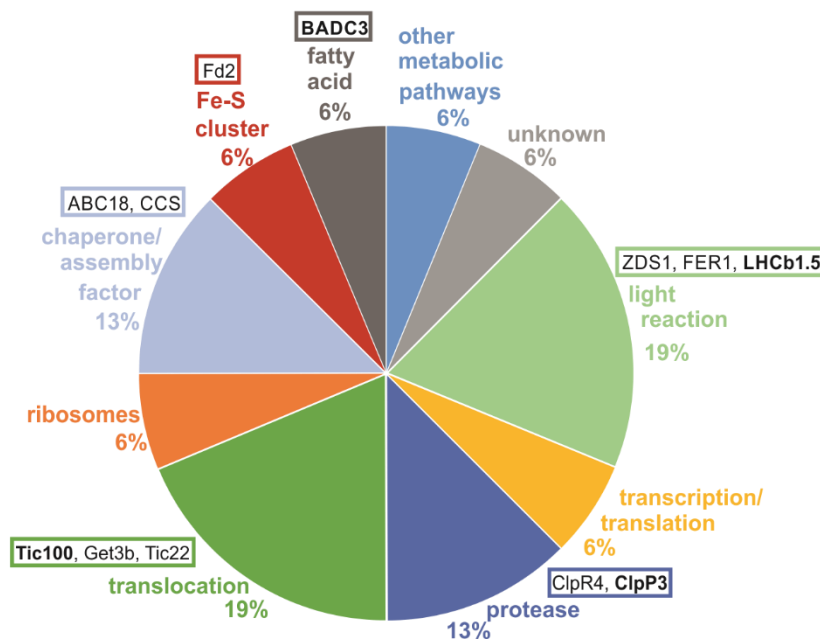


Figure 5.23. Comparative proteomics of the plastid proteomes of *Atget3b-1* and the wild-type.

Chloroplasts were isolated from 14-day old wild-type and *Atget3b-1* plants, subjected to LC-MS/MS analysis followed by label free quantification. Significantly differing proteins were categorized according to their participation in cellular processes. These are represented as percentages. **A.** Shows proteins that are significantly enriched in comparison to the wild-type. **B.** Displays proteinaceous hits that were significantly depleted in comparison to the wild-type. Proteins that were reduced or enriched in both mutant lines are denoted in bold.

Atget3b mutants (Figure 5.23 A; light pink).

The identified proteinaceous hits with significantly increased abundance in *Atget3b-1* did not include any contaminations from other organelles (Figure 5.23 B). The majority of these was categorized into photosynthetic light reaction and translocation (19 %). These included proteins

dedicated to iron homeostasis like ferritin (PETIT et al., 2001), carotenoid synthesis, ZNS1 (Flores-Ortiz et al., 2020) as well as Lhcb1.5 that was increased in both *Atget3b* mutants (Figure 5.23 B; light green). The other group contained two translocation associates residing in the intermembrane space (IMS). Namely the IMS chaperone Tic22 (Rudolf et al., 2013) and Tic 100 (Kikuchi et al., 2013), which was also increased in *Atget3b-2* (Figure 5.23 B; dark green). Proteases and chaperones/assembly factors were represented to the same degree (13 %). The protease ClpP3 also displayed an increased abundance in *Atget3b-2* (Figure 5.23 B; dark blue). The copper chaperone CCS (Abdel-Ghany, 2009) as well as a member of the main Fe-S cluster assembly machinery ABC18 (Xu and Møller, 2004) was increased in the other group (Figure 5.23 B; light blue). The groups of other metabolic pathways, proteins with unknown function, ribosomes, transcription/translation, fatty acid synthesis and Fe-S cluster biogenesis were equally embodied (6 %). Acetyl-CoA carboxylase BADC3 (Ye et al., 2020) in fatty acid synthesis was increased in both *Atget3b* mutants (Figure 5.23 B, dark grey). Interestingly, ferredoxin2 was the proteinaceous hit with the most significant enrichment *Atget3b-1* (Figure 5.23 B; red). The proteomic comparison to the overrepresentation of *AtGet3b* displayed that apart from other metabolic pathways, photosynthetic components and constituents of translocation, chaperones as well as proteases are most effected.

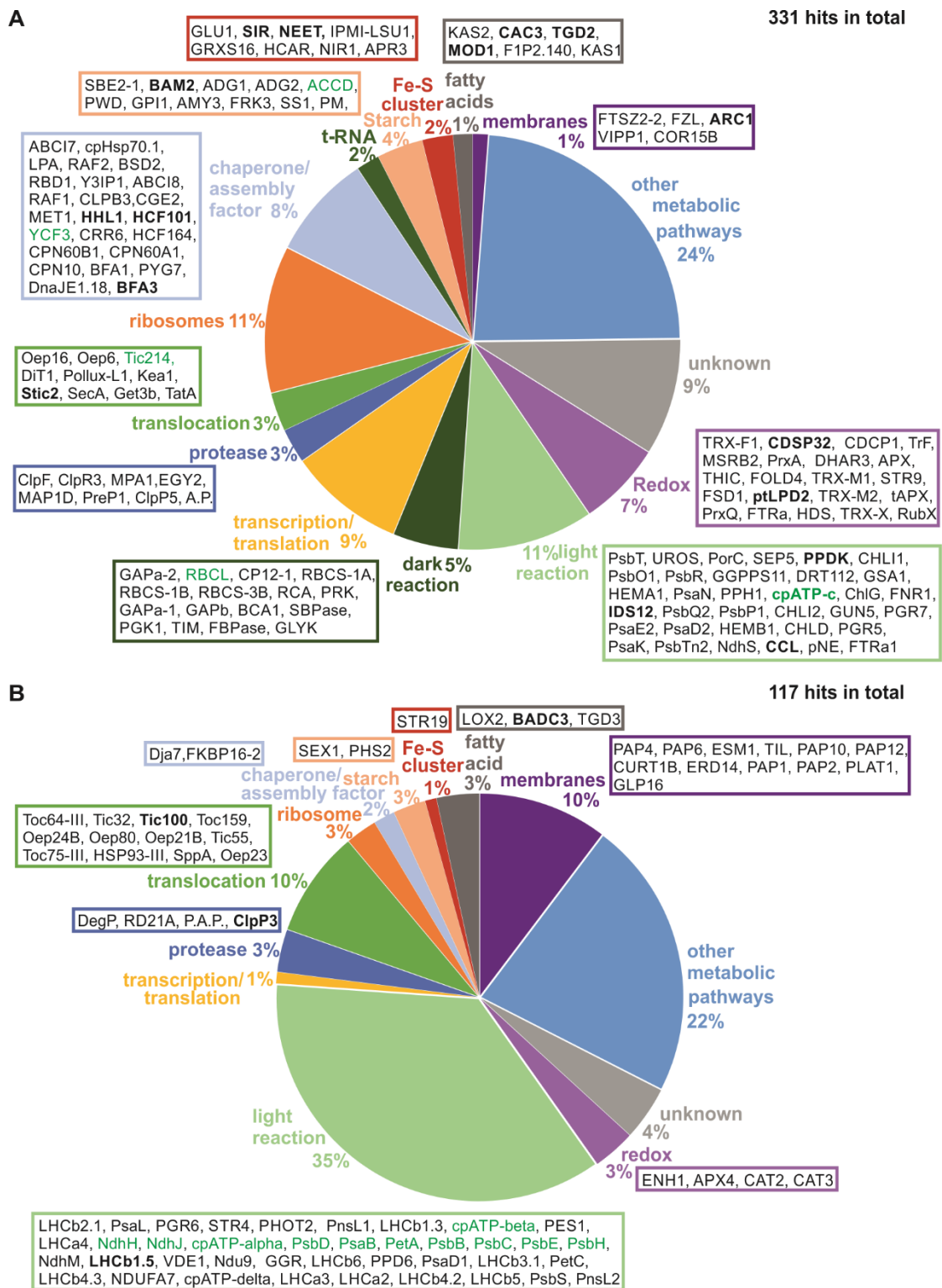
5.7.2 The chloroplast proteome of the *Atget3b-2* mutant line

After corroborating the consequences of overrepresentation of *AtGet3b* on a proteomic level, the outcome of a knockout of the same protein was analyzed. The examination revealed a total of 999 mutual proteinaceous hits. 338 were considered depleted and 214 enriched with p-values < 0.05 (Figure S18). After manual curation, 9 of the 338 enriched proteins were classified as organellar contaminations. The majority of the remaining plastidic hits (24 %) were categorized as belonging to other metabolic pathways (Figure 5.24 A; blue). The next two biggest groups were involved in the light reaction of photosynthesis and ribosomes (11 %). The proteins belonging to the light reaction of photosynthesis were entangled in different processes ranging from the biogenesis of chlorophyll, like UROS (Tan et al., 2008), PorC (Masuda et al., 2003) to extrinsic components of the electron transport chain and even one subunit of the reaction center of PSI as well as regulatory photosynthetic factors (Figure 5.24 A; lightest green). The most crucial depletory effect on components of the electron transport chain was the depletion of PsaD2 that has an impact on PSI stability and regulates the expression of nuclear genes (Ihnatowicz et al., 2004) and DRT112 (plastocyanin), which is indispensable for photosynthetic electron flow (Weigel et al., 2003). PsaN, the TAT dependent only membrane extrinsic subunit on the luminal side of PSI (Nielsen et al., 1994) which connects Lhca2 to PsaA for efficient excitation energy transfer (EET) (Pan et al., 2018). As well PsaE2, another module on the luminal side of PSI that is not essential for linear electron flow (Ihnatowicz et al., 2007), but involved

in O₂ reduction at PSI (Krieger-Liszkay et al., 2020) and can bind ferredoxin (Fd) (Sétif et al., 2002). PsaK is the only subunit exposed to the stromal side of PSI which is involved in alternative EET from Lhcb1 (Pan et al., 2018). Ferredoxin-NADP⁺ oxidoreductase2 (FNR2) which is involved in cyclic electron flow (CET) was also reduced (Lintala et al., 2009). The subunit of the chloroplast NDH, NdhS is predicted to fold into a structure similar to PsaE implying the formation of a Fd binding site within the chloroplast NDH was also affected (Strand et al., 2017). In terms of PSII, one entire set of nuclear encoded genes of the oxygen evolving complex (PsbO1, PsbR, PsbQ2, PsbP1), that are also important for the supramolecular organization of PSII (Allahverdiyeva et al., 2013) were affected. Furthermore, PsbT that impacts photodamage, repair and biogenesis of PSII in cyanobacteria (Fagerlund et al., 2020) was minimized. Another luminal subunit situated in proximity to PsbE of cytochrome 559 was PsbTn (Chen et al., 2019). Proteins grouped to ribosomes were mainly plastid encoded subunits of the chloroplast ribosome (Figure 5.24 A; orange). Factors involved in transcription/translation (9 %) as well as proteins of unknown function (9 %) were categories of equal size (Figure 5.24 A; dark yellow and light grey, respectively). Chaperones/assembly factors were represented by eight percent (Figure 5.24 A; light blue). One member of the cpHsp70 family as well as CPN60A1, CPN60B1 and CPN 10 were affected (reviewed in Zhao and Liu, 2018). Assembly factors involved in PSII assembly, like LPA (Ma et al., 2007), RBD1 (García-Cerdán et al., 2019), MET1 (Bhuiyan et al., 2015) or RuBisCo assembly like RAF1 (Whitney et al., 2015), RAF2 (Fristedt et al., 2018), BSD2 (Aigner et al., 2017). The cooperating PSI assembly factors Y3IP1 and YCF3 (Albus et al., 2010) as well as Pyg7 (Yang et al., 2017). Additionally, assembly elements of cytochrome b₆f, like HCF164 (Lennartz et al., 2001) as well as ATP synthase, i.e. BFA1 (Zhang et al., 2018) and BFA3 (Zhang et al., 2016). Further, Hsp100/Clp protein levels were reduced, like ClpB3 (Parcerisa et al., 2020) as well as factors participating in photodamage repair like HHL (Jin et al., 2014). Also elements facilitating chloroplast NDH assembly as CRR6 (Peng et al., 2010) and proteins involved in Fe-S cluster assembly were depleted i.e. HCF101 (Schwenkert et al., 2009) as well as components of the major Fe-S cluster assembly machinery, ABI7 and ABCI8 (Xu and Møller, 2004). Constituents maintaining redox homeostasis were also negatively affected (7 %). These were mainly thioredoxins and a few peroxiredoxins (Figure 5.24 A; light purple). Elements of the dark reaction were also reduced in abundance (5 %). These were primarily RuBisCo subunits or factors involved its biogenesis or regulation (Figure 5.24 A, darkest green). Constituents of starch metabolism were reduced (4 %) with one member of this group being encoded by the plastid (Figure 5.24 A; light pink). Proteases and translocation associates embodied around three percent of the depleted group. The former encompassing non multimeric complex forming proteases as well as different subunits of Clp-type proteases (Figure 5.24 A, dark blue). The group of translocation associates contained solute and ion translocases like the translocase of pPorA, Oep16 (Reinbothe et al., 2004), the 2-oxoglutarate/malate translocator DiT1 (Schneidereit et al., 2006) and Pollux-L1 (Trentmann et al.,

2020) in the outer envelope (OE). Interestingly, Tic 214 (Kikuchi et al., 2013) as well as the potassium transporter Kea1 (Bölter et al., 2020) were significantly reduced in the inner envelope (IE). Remarkably, stromal targeting factors, like the cpSRP associated Stic2 (Bédard et al., 2017), cpSecA (Liu et al., 2010) and cpTatA (Pettersson et al., 2021) were affected (Figure 5.24 A; light green). Fe-S cluster dependent reactions (2 %) and t-RNA synthesis (2 %) were represented in equal amounts (Figure 5.24 A; dark green and red, respectively). In the Fe-S cluster dependent group, two proteins were depleted in both *Atget3b* mutants, the sulfite reductase SiR participating in the assimilatory sulfate reduction pathway (Khan et al., 2010) and NEET, playing an “ancient role in Fe metabolism” (Nechushtai et al., 2012). Fatty acid synthesis and membrane remodeling and mechanics were embodied to the same extent (1 %) (Figure 5.24 A; dark grey and dark purple, respectively). Fatty acid synthesis contained acetyl-coenzyme A carboxylase (Roesler et al., 1994), TGD2 involved in ER to plastid lipid trafficking (Roston et al., 2012), a subunit of the fatty acid synthase II MOD1 (Serrano et al., 2007) as well as β -ketoacyl-acyl carrier protein synthase I and II (KASI, KASII) (Wu and Xue, 2010; Carlsson et al., 2002). Interestingly, the membrane remodeling included the chloroplast morphology and internal organization module FtsZ2-2 (Karamoko et al., 2011), the GTPase that regulates thylakoid organization FZL (Gao et al., 2006), vesicle-inducing protein in plastids 1 (VIPP) (Kroll et al., 2001), the monogalactosyldiacylglycerol (MGDG) binding and intrinsically disordered protein COR15B (Thalhammer et al., 2010) and the essential ARC1 (Kadirjan-Kalbach et al., 2012) was depleted in *Atget3b-1* as well.

97 Of the 214 significantly enriched proteins were cogitated as organellar contaminations. The majority of the remainder (35 %) were categorized to the light reaction of photosynthesis. Nearly all the LHC proteins of PSII and a few of PSI were affected as well as crucial subunits of the electron transport chain. Interestingly, plastid encoded subunits of the reaction center of PSII i.e. PsbB, PsbC, PsbD, PsbE, PsbH as well as nuclear encoded PsbS (Van Bezouwen et al., 2017) were amplified. Further plastid encoded alpha and beta subunits as well as nuclear encoded delta subunit of the ATP synthase were affected. Plastid encoded PetA of the cytochrome b_6f complex (Dinkins et al., 1994) and two subunits of subcomplex A of the chloroplast NDH complex were also increased. Another subunit subcomplex A, NdhM was affected (Reviewed in Shikanai, 2016) as well as luminal subunits of the chloroplast NDH complex, PnsL1 and PnsL2 (Ishihara et al., 2007; Suorsa et al., 2010). PsaD1, PsaL and PetC (Dekker and Boekema, 2005) were enriched too (Figure 5.24 B; light green). Other metabolic pathways made up 22 % of the total hits (Figure 5.24 B; blue). The group of membrane remodeling and mechanics and translocation were represented to the same extend (10 %). The bulk of the first group included numerous plastid lipid associated proteins (PAP) (Leitner-Dagan et al., 2006), the membrane



curvature inducing CURT1A (Armbruster et al., 2013) and other lipid binding factors (Figure 5.24 B; dark purple). The translocation group encompassed components of the TOC_{CORE} complex, Toc159 and Toc 75-III (Schleiff et al., 2003) as well as TOC_{HOLE} complex, Toc 64-III (Sommer et al., 2013) and the β -barrel insertase Toc75-V (Groß et al., 2021; submitted and accepted). Additional enriched OE translocases were the bidirectional rectifying channel Oep21B (Bölter et al., 1999), the solute exchange channels Oep23 (Goetze et al., 2015) and Oep24 (Bölter et al., 1999). Tic32, Tic55 and Tic100 (Reviewed in Nakai, 2015) were enriched in the IE. Stromal factors were the Hsp100 (cpHsp93) putatively involved translocation (Kovacheva et al., 2007) and the protease SppA (Richter et al., 2005), which is supposed to be associated with thylakoids (Figure 5.24 B; darker green). Proteins of unknown function made up four percent of the hits (Figure 5.24 B; light grey). Categories of redox homeostasis, proteases, ribosomes and the synthesis of fatty acids as well as starch were equally embodied (3 %). Surprisingly, two of three catalase proteins (Frugoli et al., 1996) were enriched in the redox homeostasis group (Figure 5.24 B; light purple) and only one protease with catalytic activity was enriched in the respective category (Figure 5.24 B; dark blue). An acetyl-CoA carboxylase BADC3 (Ye et al., 2020) was enriched in both *Atget3b* mutants in the fatty acid synthesis group (Figure 5.24 B; dark grey). Components involved in transcription/translation and Fe-S cluster dependent reactions were represented to the same extend (1 %) (Figure 5.24 B; dark yellow and red, respectively).

The quantitative proteomic approach did not just corroborate the previous observation of an involvement in photosynthetic pathways. It also shed light on identity of the affected components of the electron transport chain. Additionally, elements of the translocation machinery were identified with significant enrichment. Furthermore, components involved in membrane remodeling were affected as well as fatty acid and starch synthesis. These were also accompanied with fluctuations in chaperone abundances and the downregulation of plastidic ribosomes, t-RNA synthesis as well as amino acid synthesis. Taken together these data reflect the numerous pathways in which *AtGet3b* might be involved in as well as how far reaching the effects of its absence are on a molecular level.

5.8 *AtGet3b* under stress

5.8.1 *Atget3b* mutants under light stress

The fungal Get3 homologue in *S. cerevisiae* has a secondary holdase function under oxidative stress (Voth et al., 2014) as well as energy limiting conditions (Powis et al., 2013). The response to stress was probed in the *Atget3b* mutant plants. The previous results point toward an involvement in photosynthetic assembly pathways. Thus, plants were subjected to light stress to assess the protective to as well responsive attributes of the mutant lines. The majority of the previously observed varying parameters reached wild-type levels in the fourth week of development. For this *A. thaliana* seedlings

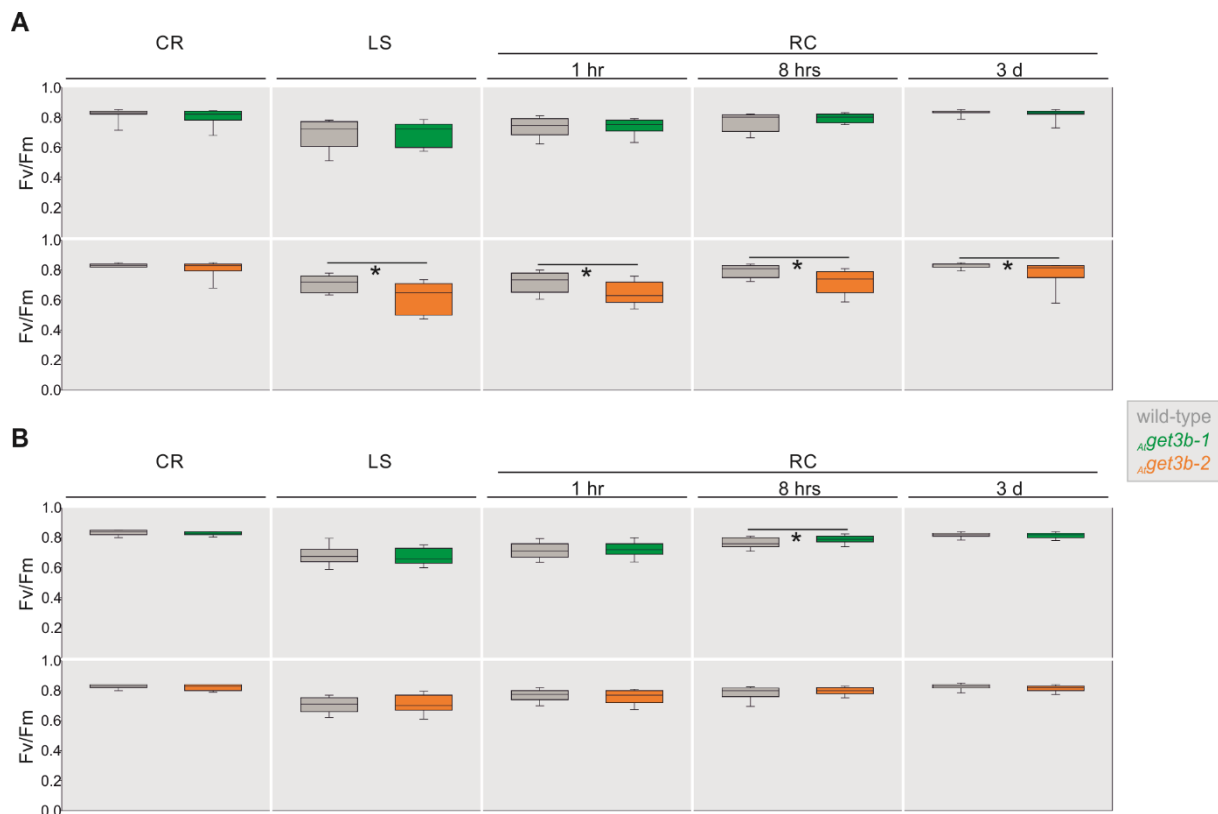


Figure 5.25. *Atget3b-2* displays hypersensitivity to light stress when grown under low light.

A. Plants were cultivated under low light (LL) and the maximum quantum yield (Fv/Fm) of the indicated plant lines was assessed by pulse amplitude modulation (PAM) measurements during normal growth (CR), light stress (LS) as well as 1 hr, 8 hrs and three days (3d) of recovery (RC). **B.** Plants were grown under normal light (NL) and subjected to the same procedure as in (A).

were either grown under low-light (LL $\sim 70 \mu\text{mol m}^{-2} \text{s}^{-1}$) or normal (NL $\sim 120 \mu\text{mol m}^{-2} \text{s}^{-1}$) for four weeks, subjected to a 14-hour light stress (LS $\sim 1,400 \mu\text{mol m}^{-2} \text{s}^{-1}$) period and placed back to the respective previous condition. With the use of LED based illumination, the possibility of a concomitant heat stress was ruled out. Pulse amplitude modulation (PAM) measurements were used to query photosynthetic parameters during control (CR), light stress (LS), one hour (1 hr; early), eight hours (8 hrs; intermediate) as well as three days (3d; late) stages of recovery (RC) (Figure 5.25). When cultivated under LL conditions, the photosynthetic performance of *Atget3b-1* did not differ from the wild-type during the time course of the experiment. On the contrary, *Atget3b-2* was significantly hampered in its maximum quantum efficiency during light stress and stayed significantly hindered throughout the recovery phases (Figure 5.25 A). When grown under NL however, *Atget3b-2* did not display these traits during stress. Also *Atget3b-1* exhibited wild-type characteristics, except after 8 hours of recovery where the line showed a higher maximum quantum efficiency (Figure 5.25 B). In order to assess the adaptation to light stress, non-photochemical quenching parameters were obtained. Non-photochemical quenching (NPQ) is a mechanism employed by higher plants to maintain photosynthetic integrity during high light intensity (Goss and Lepetit, 2015). When cultivated under LL, *Atget3b-1* had a

significantly lower NPQ than the wild-type in control conditions. During stress both showed approximately the same value. During the early and intermediate phases of recovery *Atget3b-1* had a higher NPQ which dropped below wild-type levels in the late phase of recovery. In contrast, *Atget3b-2* displayed a slightly lower NPQ than the wild-type which was reduced significantly after 8 hours of recovery (Figure 5.25 C). Growth under NL led to a significant increase in NPQ during light stress in *Atget3b-1*. Remarkably, the NPQ levels were significantly decreased after 1 hour of recovery, but increased to a significant level after eight hours of recovery. *Atget3b-2* showed the overall same trend in the time course with a reduction after an hour of recovery that was not significant (Figure 5.25 D). The light stress evaluation displayed that the cultivation under LL conditions lead to an obstructed protection as well as repair in *Atget3b-2*. When grown under NL conditions, *AtGet3b-1* was able to recover faster than the wild-type after 8 hours of recovery. Furthermore, both mutant lines acclimatize better to the stress than the wild-type, except after an hour of recovery.

5.8.2 *AtGet3b* under oxidative stress

After observing that the *Atget3b-2* was hypersensitive to light stress when grown under LL conditions, I sought out to examine the effect of oxidative stress on *AtGet3b*. I isolated protoplasts from 5-week old *A. thaliana* seedlings and administered the localization of *AtGet3b* by immuno-fluorescence (IF) utilizing the generated *AtGet3b* specific antibody. When left untreated the immuno-detected signal was well dispersed in the stroma of plastids (Figure 5.26 A; UT). After the addition of 4 mM H₂O₂ the scattered signal was recruited to distinct foci (Figure 5.26 A; H₂O₂). This recruitment to apparent focus points is very similar to the *Get3* induced protein deposition sites reported in *S. cerevisiae* under energy limiting conditions (Powis et al., 2013). Detailed inspection of the resulting punctuate structures revealed that these clearly co-localize with puncta emitting auto-fluorescence in vicinity of thylakoids (Figure 5.26 A, insets). This structure is reminiscent of stress granules identified in the chloroplast of *Chlamydomonas reinhardtii* (Uniacke and Zerges, 2008). To corroborate if these structures were bona fide stress granules I exposed wild-type protoplasts to oxidative stress and partitioned these. This was done by the addition of 4 mM H₂O₂ followed by the fractionation into soluble and insoluble portions. After the oxidative treatment *AtGet3b* was mainly recovered in the insoluble fraction. Even when cells were lysed with 0.5 % n- dodecyl- β -d- maltosid (β -DM). This detergent concentration was sufficient to solubilize LHCB2 out of the membrane (Figure 5.26 B). This phase-phase separation characteristic, paired with the resistance to detergent treatment displayed that *AtGet3b* shares at least one trait of so called proteinaceous membrane less organelles (PMLOs).

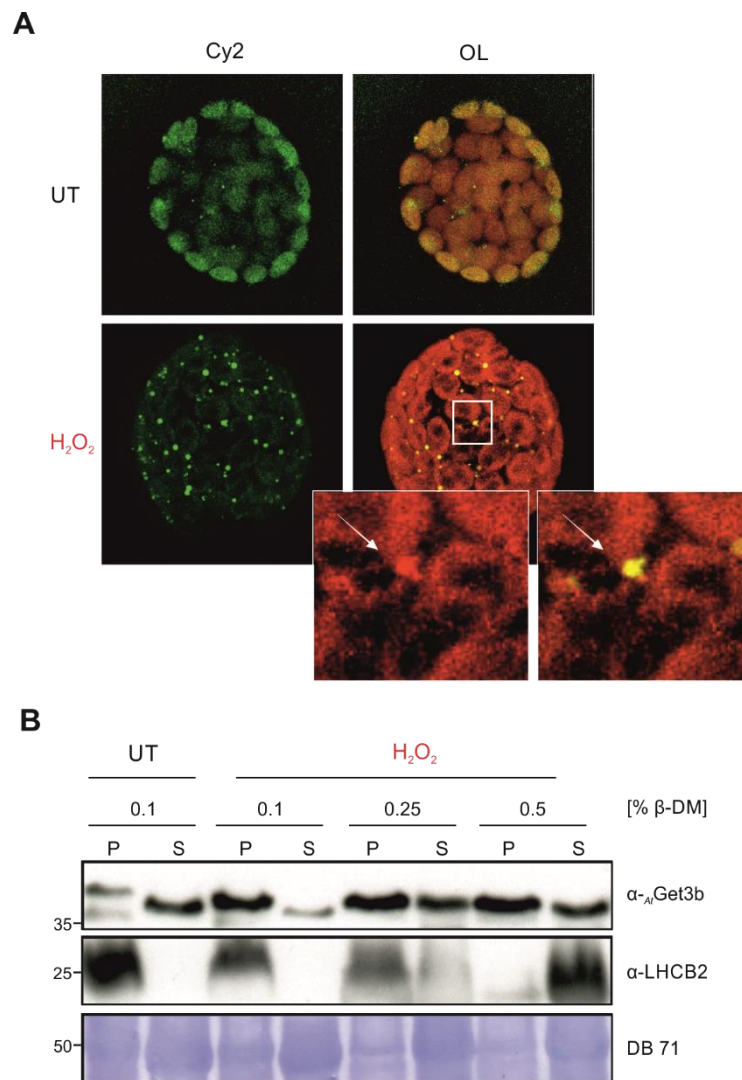


Figure 5.26. *At*Get3b is recruited to distinct foci which display PMLO characteristics.

A. Protoplasts isolated from *A. thaliana* were left untreated (UT, top panels) or stressed by addition of 4 mM H₂O₂ (H₂O₂, bottom panels) followed by immunofluorescence (IF) with antibodies against *At*Get3b. Left, the CY2 signal and right the overlay between CY2 signal and chlorophyll auto-fluorescence is shown. Inlets depict enlargements of selected white square. **B.** Protoplasts were either untreated (UT) or stressed with 4 mM H₂O₂ (H₂O₂), lysed with the indicated detergent concentrations (% β-DM) and fractionated into soluble (S) and insoluble (P) fractions. The fractions were subjected to Western blot analysis with the indicated antibodies.

5.8.3 *In vitro* *At*Get3b holdase function under heat stress

As for *At*Get3a and *At*Get3c the capability to protect substrate from heat induced denaturing was probed *in vitro*. First the recombinant heat sensitive substrate and *At*Get3b were kept separate and denatured (Figure 5.27 A). The former was slightly present in pellet fraction under control conditions (CR), but was mainly present in this fraction after stress (ST) and recovery (RC). The majority of *At*Get3b stayed in the pellet fraction irrespective of the treatment (Figure 5.27 A). When mixed in differing molar ratios, *At*Get3b was recovered with MDH in the pellet fraction. Indicating an inability to prevent aggregation irrespective of the ratios of the constituents (Figure 5.27 B). This displayed that *At*Get3b could not act as a heat inducible holdase.

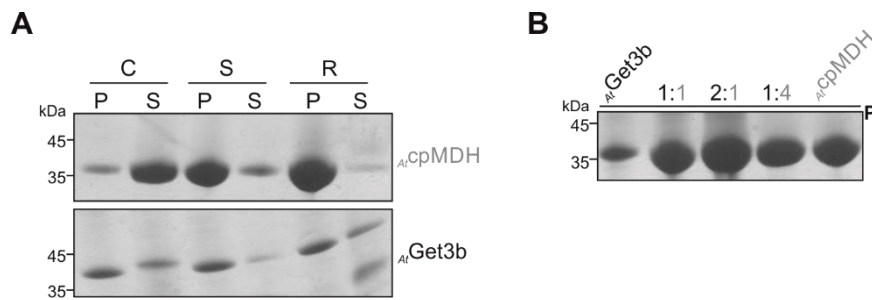


Figure 5.27. *At*Get3b is not capable of preventing heat induced aggregation of *At*cpMDH.

A. *At*cpMDH (top) and *At*Get3b (bottom) were fractionated into insoluble (P) and soluble (S) fractions at room temperature (C), 65 °C heat stress (S) and the following recovery (R) at 25 °C. Samples were separated by SDS-PAGE and stained by coomassie **B.** *At*Get3b (black) and *At*cpMDH (grey) were either separately or in the indicated ratios subjected to a 65 °C heat stress and insoluble material was recovered by centrifugation. Samples were run on SDS-PAGE and stained with coomassie. P in bold denotes that only pellet fractions were loaded. Adapted from MSc thesis of Victoria Gosch under my supervision.

6 DISCUSSION

6.1 Phylogenetic relations

6.1.1 GET in planta

By the occurrence of pre-targeting and receptor components (Figure 5.8) as well as the respective targeting factor (Figure 5.1) it becomes evident that the GET pathway is not only conserved in *Arabidopsis thaliana* but also in the majority of the analyzed viridiplantae species. The only exception is in *Mamiellophyceae* (*Prasinophytes*) in which a member of the Get3ab clade is present (Figure 5.1). This lineage underwent multiple genetic alterations since diverging from the ancestral green flagellate (Leliaert et al., 2012). Still it remains to be uncovered in which processes this protein is involved in since no orthologues of Get1, Get4 or Sgt2 were detected (Figure 5.8 A, Table S3). In Chlorophyta, Streptophyta and landplants however, it seems that there are always two homologues present. Either a Get3ab homologue together with a “bc” clade member or an Get3a clade paired with a “bc” clade member (Figure 5.1, Figure S4). In regards to the receptor complex, WRB/Get1 belongs to the highly conserved Oxa1 superfamily of membrane biogenesis factors (Anghel et al., 2017). This superfamily forms a three helix bundle in the membrane that interacts with another such bundle from its dimerizing partner (McDowell et al., 2020). These interacting entities seem to have evolved differently depending on their respective molecular purposes, resulting in mere functional homology. Thereby troubling bioinformatic queries based on sequence similarity. A very recent study utilized Position-Specific Iterated (PSI)-BLAST search and was able to detect around 20 putative Get2 homologues in plants. This was only possible when using the N-terminal region and not the TMD bearing C-terminal section of CAML (Borgese, 2020). Indicating that TMD sequences have diverged differently in planta. Nevertheless, the identification of Sgt2, Get1 and Get4 orthologues in most analyzed plants further points towards a global conservation of the GET pathway in planta (Table S2, Table S4).

6.1.2 Get3 in planta

The ancient p-loop ATPase ArsA emerged at the diversification of archaea and bacteria (Leipe et al., 2002). The bacterial ArsA has a monomeric architecture with two tandem ATPase motifs in one polypeptide stretch which form a catalytic dimer and lack the conserved cysteine motif (Borgese and Righi, 2010). To date, all examined archaeal ArsA homologues display a dimeric architecture. Some do not require a CxxC motif for dimerization or TA binding while others do (Suloway et al., 2012). The majority of the plants that we analyzed display a dimeric arrangement and encompassed the conserved CxxC motif. The only exceptions were members of Chlorophyta which nested in the Get3ab clade as well as the Get3 homologues of *C. reinhardtii*. Latter includes one orthologue belonging to the

Get3ab clade and two to the Get3bc clade (Figure S4). Most interestingly, the two homologues in the Get3bc clade are the only analyzed plant sequences that display a tandem ArsA domain similar to the bacterial counterpart. This forms a “composite hook-like motif” that mediates the discrimination between client TA proteins. The Get3ab homologue resides in the cytoplasm and binds ER destined TA proteins. At least one of the Get3bc homologues specifically binds organellar TA proteins in the cytoplasm (Lin et al., 2019). Perhaps that is the reason why *C. reinhardtii* has two Get4 orthologues (Figure 5.8 A) to sort TA proteins to different subcellular localizations. Such a mode of Get3 dependent targeting to organelles is highly unlikely in *A. thaliana*. Since (i) several studies have suggested that AKR2A (ankyrin repeat containing protein 2A) is involved in the targeting of outer membrane proteins (OMPs) (Bae et al., 2008; Shen et al., 2010). And, (ii) Two Get3 homologues are not simultaneously present in the same compartment as in *C. reinhardtii* (Figure 5.1-Figure 5.8, Xing et al., 2017). Even though it was shown that AKR2A already interacts with the ribosome nascent chain (RNC) during the translation of clients (Kim et al., 2015), the exact hierarchy of triage, its molecular composition as well as spatiotemporal attributes remain fairly elusive. Thereby not fully excluding a possible involvement of a Get3 orthologue in this process.

6.2 Characterization of *At*Get3a

6.2.1 *At*Get3a as a targeting factor

The usage of a recombinant OPG tag for luminal glycosylation was shown to be applicable *in cellula* and should also work in planta (Figure 5.10). This method can be a useful tool to study the insertion capacity of mutants disrupted in GET components. Furthermore, targeting as well as topological determinants encoded within the AA sequence can be delineated by mutational studies. However, the application of TAT *in vitro* remains questionable. It is still a matter of clarification, if *At*Get3a acts as the dedicated TA protein targeting factor for the ER. Co-IP MS experiments identified 22 TA proteins that co-precipitated with *At*Get3a-GFP. One was an ER resident TA protein, the others localized to other organelles (Xing et al., 2017). Also in this study rather organellar proteins than ER resident IMPs were identified (Figure 5.9. Putative components of pre-targeting complex and interaction partners.). Indicating that *At*Get3a might rather be involved in organellar targeting routes than ER transport. Perhaps the vicinity of the GET/TRC/SND components makes it difficult to identify client proteins without a previous stabilization e.g. by crosslinking. Since mRNA and Get3 have been shown to associate with microsomes and the free ribosomes are also close to the ER (Pyhtila et al., 2008; Schuldiner et al., 2008). The client handover reactions to the membrane receptor can be fast and very short lived due to a restriction in space. This could be the reason why interactions with a wider client spectrum were reported with the rBiFC system (Xing et al., 2017) in which no dissociation of interaction

partners takes place thereby stabilizing the interaction. In this study *At*Get3a co-purified with Sec61 β -Flag-OPG-His. Unfortunately, the TMD dependence of this interaction was not evaluated, however the interaction itself might have been stabilized because no specific receptor is present in *E. coli*. Thereby the hand over reaction could not be terminated and arrested at *At*Get3a or it was an artefact of recombinant overexpression. In regards to the organellar TA proteins interacting with *At*Get3a, perhaps an association with these clients is possible. And, maybe due to a longer distance to transport the client to an organelle the interaction is of longer duration and can be identified by CoIP-MS. Or these interactions should rather be attributed to a Get3 holdase function than a Get3 targeting function. Also in this study no TA proteins were precipitated, pointing towards either the afore mentioned transient interactions or a complete different, undescribed function of *At*Get3a. However, it was still possible to identify some possible candidates as putative interaction partners (Figure 5.9. Putative components of pre-targeting complex and interaction partners.). As addressed Ub-RPL40b could represent Ubl4A. The protein of unknown function (At2g25280) could represent Ybr137wp, a yeast protein that associates with the GET constituents, possibly also involved in the pathway (Yeh et al., 2014). Furthermore, the partitioning of the co-immunoprecipitated proteins does imply that *At*Get3a is associated with chaperones, ribosomes and proteasomal subunits (Figure 5.9. Putative components of pre-targeting complex and interaction partners.) which was also reported in other systems (Cho and Shan, 2018; Leznicki and High, 2020; Itakura et al., 2016).

6.2.2 GET or TRC in *Arabidopsis thaliana*

In terms of delineating if the TA biogenesis pathway in planta is more related to the GET pathway in *S. cerevisiae* or the TRC pathway in *H. sapiens* one can only speculate. The difference in both pathways is the occurrence of the BAG6 complex, composed of Bag6, TRC35 and Ubl4A acting upstream of Trc40. In contrast to the GET pathway in which Get4 and Get5 form an obligate heterodimer due to hydrophobic interactions of the C-terminal domain (CTD) of Get4 with Get5 N-terminus (Chartron et al., 2010). In the mammalian counterpart Bag6 separately binds these factors (Mock et al., 2015; Mariappan et al., 2010). Since neither Get4 nor Bag6 co-precipitated with *At*Get3a or were recovered in the Ub-RPL40b containing fraction one can only speculate that the complex dissociated in the role of the experiment or a pre-targeting complex with another architecture exists in *A. thaliana*.

6.2.3 *At*Get3a as holdase

In regards to a potential holdase function, *At*Get3a was the only orthologue that was capable of preventing the aggregation of the heat sensitive substrate *At*MDH (Figure 5.12). Even though a small population of *At*Get3a precipitated under control conditions. This mode of preventing aggregation and

keeping substrate soluble is very similar to the chaperones like Hsp70. This function was mediated despite the absence of the CxxC motif in this orthologue (Figure 5.1). However, the CxC motif present in *At*Get3a is attributed to redox sensitivity in Hsp33 (Ilbert et al., 2007). It was hypothesized that the CxxC motif is necessary for the structural rearrangements for the holdase function of Get3 (Voth et al., 2014). Interestingly this motif is present in the organellar orthologues, which were not able to prevent heat induced aggregation of substrates *in vitro* (Figure 5.16, Figure 5.27). However, it should be mentioned that different sHSPs (small HSPs) also display a holdase function with substrate specificity. The authors of the study concluded that the N-terminal region preceding the α -crystallin domain conveys this specificity (Basha et al., 2004). Perhaps the different Get3 orthologues in *A. thaliana* also exhibit such specificity towards substrate.

6.3 Characterization of *At*Get3c

Even though there were no severe differences to the wild-type in terms of morphological developmental traits (Figure S14) and organellar ultrastructural attributes (Figure 5.14), the *Atget3c* mutant line displayed differences in respiratory chain complex abundances (Figure 5.15). Signifying that the *At*Get3c function could be involved in the assembly of these complexes. Interestingly, several IMPs in these complexes share a TA-protein topology (Figure 5.15), making it tempting to speculate that *At*Get3c function can be attributed to TA protein targeting. Apart from transporting TA proteins, *At*Get3c could also be involved in the assembly of Fe-S clusters (see below). Interestingly complex II comprises a subunit that encompasses three Fe-S clusters (Sun et al., 2005) and the assembly factor for this subunit is absent in higher plants (Mistry et al., 2013). Yet it is unlikely that *At*Get3c function complements the absence of this assembly factor as *At*Get3c only occurs in the family of Brassicaceae (Figure 5.1). Albeit, the acquired data allow to establish a hypothesis that the function of *At*Get3c is involved in the assembly and stabilization of complex II and complex IV. If this is arbitrated by targeting TA proteins, aiding the biogenesis of Fe-S cluster or an unknown function needs to be further examined.

6.4 Characterization of *At*Get3b

6.4.1 Involvement in PS assembly

The combination of a reverse genetic approach coupled to ultrastructural (Figure 5.18), biochemical (Figure 5.19) and fluorometric (Figure 5.20) analyses strongly suggests an involvement of *At*Get3b in PS assembly. This became most evident in the early stages of PS assembly during de-etiolating when not only the assembly kinetics but also the steady state assembly were affected by the function of *At*Get3b

(Figure 5.20 A, B, C). Furthermore, in a later 4-day old autotrophic grown stage a significant reduction of chlorophyll was observed in *Atget3b-2* and an increase in *Atget3b-1* (Figure 5.20 D), mirroring the fluorometric results of photosynthetic performance (Figure 5.20). Initially it was puzzling why the two *Atget3b* mutants displayed similar ultrastructural properties in the second and third week of development but opposing traits when analyzed biochemically. The LC MS/MS analysis was able to shed some light on this issue. It appears that absence of *AtGet3b* led to a reduction of several components of the electron transport chain as well as their cognate assembly factors and targeting factors (Figure 5.24 A) which led to impairments in electron transport (Figure S16). As a response nearly all LHCs were increased as well as electron transport elements that could compensate for the former described reduction (Figure 5.24 B). For instance, the reduction of PsaD2 was balanced by an increase of the highly homologous PsaD1. This functional redundancy is coherent with previous reports (Ihnatowicz et al., 2004). This response in photosynthetic component enrichment could explain the similar ultrastructural attributes in the second week of development (Figure 5.18 B). In order to import all the nuclear encoded photosynthetic constituents to mediate this molecular compensation, the plastid import machinery for these elements was increased to meet the necessary demands (Bauer et al., 2000). Maybe thereby explaining the amplification of TOC/TIC subunits. Regarding the surprising reduction of RuBisCo, substantial evidence exists that cyclic electron flow (CEF) plays a crucial role in balancing the ATP/NADPH energy budget for downstream reactions (Kramer and Evans, 2011). This can be maintained in thylakoids by: (i) proton pumping via the chloroplast NDH complex (Efremov et al., 2010), (ii) the PGR5 and PGRL1 dependent Fd-PQ oxidoreductase (FQR) pathway (DalCorso et al., 2008), (iii) the Cytochrome b_6/f Complex and Fd NADP reductase (Iwai et al., 2010) and (iv) alterations of ATP synthase subunits to reduce the number of c-subunits to utilize less H^+ for the production of ATP (Stock et al., 2000). The lack of *AtGet3b* led to the reduction of several components of some of the aforementioned CEF pathways (Figure 5.24 A). Which in turn could have led to imbalances in the ATP/NADPH ratios and therefore caused defects in the Calvin-Benson cycle. This could be mirrored by the reduction of RuBisCo as well as elements contributing to starch synthesis. This on the other hand could have triggered the enhancement of Oep21B to compensate for reduced levels of 3-phosphoglycerate by importing it from the cytosol (Bölter et al., 1999). The reduction of protein synthesis governed by ribosomes, t-RNAs and its regulatory elements could be partly compensated by importing cytosolic amino acids via transporters like Oep24B, which could explain its enrichment in the OE (Pohlmeyer et al., 1998). The insertion of these β -barrel OEPs into their respective membrane, necessitates the action of the newly identified β -barrel insertase, Toc 75-V (Groß et al., 2021). This could reason the observed enrichment in our analysis. The overall effects on PS biogenesis and the resulting molecular responses to compensate for these aberrations in photosynthetic activity strongly

suggest an involvement in PS assembly. Allowing the formulation of such a hypothesis. However, the exact mode of molecular action remains to be determined.

6.4.2 Involvement in Fe-S cluster dependent pathways

Solely the comparative proteomic data gave implications that *At*Get3b could be involved Fe-S cluster dependent pathways (Figure 5.23, Figure 5.24). Remarkably, the major ferredoxin in *A. thaliana* Fd2 (Wang et al., 2018) displayed the highest significant enrichment in *Atget3b-1* (Figure 5.23). The iron storage protein ferritin Fer1 which was shown to be transcriptionally upregulated during or after Fe overload (Petit et al., 2001) was also significantly enriched in *Atget3b-1* (Figure 5.23 B). This observation however, can also be attributed to defects in protein import (Kikuchi et al., 2009). Even though Fd was not significantly reduced in an *Atget3b-2* background, interacting factors e.g. PsaE2 (Sétif et al., 2002), FNR2 (Lintala et al., 2009) and the NdhS subunit of the chloroplast NDH complex (Strand et al., 2017) were significantly negatively affected in *Atget3b-2* (Figure 5.24 A). Indicating that *At*Get3b function could be involved in ferredoxin dependent processes. However, it was not only Fd but also other Fe-S cluster dependent processes that were affected (Figure S17). The Fd dependent enzyme sulfite reductase SiR (Krueger and Siegel, 1982) as well as the Fe-S cluster insertion module NEET (Zandalinas et al., 2020) had accumulated to lesser extend in both mutant plants (Figure 5.23 A Figure 5.24 B Interestingly, other factors that carry Fe-S clusters were not as negatively affected as Fd associated proteins. Instead, these displayed an enrichment in *Atget3b-2*. For instance, PsaC, PetC and PetA, whereas other Fe-S proteins like PsaA and PsaB were not even statistically significant in the analysis. Suggesting a higher degree of participation in Fd dependent processes than general [2Fe-2S] cluster dependent procedures. Most strikingly, key components of the Fe-S cluster assembly machinery, namely the non-integral ABC proteins of the SufBCD complex (Hu et al., 2017) were differently affected in both *Atget3b* mutants (Figure 5.23 B, Figure 5.24 A. Suf-mediated Fe-S assembly is initiated by a cysteine desulfurase SufS together with its activase SufE. The major assembly scaffold SufBCD manufactures the reduced S into Fe-S clusters. Carrier proteins insert them into apo recipients to make them halo Fe-S proteins (Reviewed in Balk and Pilon, 2011). Strikingly, SufB levels were more or less proportional to *At*Get3b levels with an increase in *Atget3b-1* and reduction *Atget3b-2* (Figure 5.23 B, Figure 5.24 A) Implying an interaction or functional interdependence. This module was the only one of the three to regulate SufBCD complex abundance by its own abundance (Hu et al., 2017). This possible interaction is reminiscent of the co-chaperone HSC20 (Uhrigshardt et al., 2010) that binds the mammalian SufB counterpart and its cognate chaperone HSPA9 (Maio et al., 2014) thereby facilitating cluster transfer to intermediate carriers or final acceptor apoproteins (Bonomi et al., 2011). HSC20 forms a functional dimer and encompasses a CxxC motif which coordinates a zinc ion *in vitro* (Bitto et al., 2008), very

similar to Trc40/Get3. Another similarity in these two systems is the use of tripeptides. In mammals the consensus sequence (L-Y-R) was identified as molecular signature in Fe-S cluster assembly (Maio et al., 2017). The tripeptide (I-W-K) exists at the extreme C-terminus of all “bc” clade proteins (exemplified in Figure S1). There can be variations in the flanking amino acids leading to similar physicochemical properties, but a bulky hydrophobic residue is followed by an invariant tryptophan residue then by a positively charged one. The only exceptions devoid of this motif were the sequences of *Micromonas pusilla* and *Coccomyxa subellipsoidea*. The sequences of *Amborella trichopoda* and *Picea abies* were the only ones that utilized (V-W-Q) motif in their extreme C-terminus. Maybe this highly conserved tripeptide is involved in co-factor recognition like in mammals (Maio et al., 2014). Not only the major assembly scaffold SufBCD was perturbed, but also the [4Fe-4S] scaffold protein HCF101 was negatively affected in both mutants (Schwenker et al., 2010). Implying that (i) overall *At*Get3b abundance influences the steady state levels of HCF101 and (ii) a link to [4Fe-4S] cluster assembly not just [2Fe-2S]. However, even though HCF101 was reduced, components in PSI including [4Fe-4S] clusters were not. Indicating that the significant reduction did not affect the action HCF101 or another factor compensated for its minimization. Even though it is often used as substrate in import experiments, ferredoxin biogenesis itself has been studied to some extent (Li et al., 1990; Pilon et al., 1992; Yabe et al., 2004) but detailed knowledge of the involvement of co-factors, their assembly as well as proteins triage remains obscure. Even though NEET can transfer Fe-S clusters to Fd *in vitro* (Nechushtai et al., 2012) and purified cpSufA is sufficient to establish a Fe-S cluster in Fd with only cysteine and ferrous iron salt present. Latter enzymatic activity is elevated 50 – 80 fold in presence of stromal extract in which components oligomerize with cpSufA to form a higher molecular complex putatively embodying SufBCD (Ye et al., 2005). The observed effects on Fd dependent processes as well as on the major Fe-S cluster assembly machinery makes it tempting to speculate that *At*Get3b function might participate in this these. Placing its mode of molecular action spatio-temporally similar to HSC20 by interacting with SufBCD and facilitating the protection and concomitant handover of labile Fe-S clusters to carrier proteins like HCF101 or NEET to that then insert these into apoproteins like ferredoxin (see conclusion).

6.4.3 Involvement in protein transport

Initially I hypothesized that *At*Get3b might be a targeting factor involved in thylakoidal membrane protein targeting. Coined by the idea of a functional convergence to the cytosolic GET pathway. This notion was supported by the abundance of Alb3 and Alb4 in thylakoids, being members of the “Oxa1 superfamily” to which also Get1/WRB belongs (Anghel et al., 2017). The observations of fluctuating PsbW protein levels in the *At*get3b mutants (Figure 5.21 A-C) led to the hypothesis that *At*Get3b might

be a specific targeting factor for *AtPsbW*. Coherent to *AtGet3a* and *AtSyp123* (Xing et al., 2017). Similar to the transition from cyanobacteria to plants, novel targeting factors were necessitated for the newly evolved LHC proteins. This probably led to a reprogramming of cpSRP54 and establishment of cpSRP43. Particularly, some higher plants contain three PSII subunits that cyanobacteria do not, namely *PsbW*, *PsbT_n* and *PsbR* (Shi and Schröder, 2004). Latter two are soluble luminal proteins. Hence the membrane protein *AtPsbW* was postulated as substrate of *AtGet3b* and *in vitro* that proved to be true. Furthermore, this interaction was dependent on the TMD and was extendable to LHCb3 (Figure 5.21 D). Indicating that *AtGet3b* is capable of recruiting membrane proteins and may participate in the cpSRP pathway, however the results of the preliminary γ TAT were not conclusive (Figure 5.22). Most crucially, the comparative proteomic data revealed that neither *PsbW*, cpSRP54, cpSRp43, Alb3 or Alb4 were significantly altered in the *Atget3b-2* background (Figure S18). If *AtGet3b* would participate in the cpSRP pathway, one could assume that one of the aforementioned factors would also be significantly affected. Furthermore, phylogenetic analysis displayed that even though the “bc” clade was present in all analyzed plants, (Figure 5.1) *PsbW* was not (Figure S2). Thus, leading to the obliteration of my hypothesis.

Interestingly, two of the three proteins present in PSII of eukaryotes and not cyanobacteria, namely *PsbR* and *PsbT_n* were reduced in *Atget3b-2*. Not only these but also other luminal proteins like the subunits of the OEC and PPD6 were negatively affected in this mutant (Figure 5.23. Comparative proteomics of the plastid proteomes of *Atget3b-1* and the wild-type. Furthermore, stromal targeting factors of luminal proteins like cpSecA and cpTatA were also reduced. Suggesting that *AtGet3b* function could rather be linked to trafficking soluble luminal proteins than IMPs. Tic100 was increased and Stic2 was decreased in both mutant lines (Figure 5.23, Figure 5.24). Implying that the steady state levels of *AtGet3b* have an effect on the steady state levels of the former two proteins. If Stic2 is involved in the cpSRP pathway as proposed (Bédard et al., 2017) it is the only component of this pathway that was affected in this analysis. Most interestingly, Tic214 was the only component involved in protein translocation that was reduced in abundance in *Atget3b-2*. Implying a potential interaction or even interdependence between Tic214 and *AtGet3b*. Tic214 is a newly identified component of the TIC complex (Kikuchi et al., 2013) exhibiting one of only few examples of a plastid gene gain (Wicke et al., 2011). That was probably introduced into the plastid genome of the common ancestor of Chloroplastida but then again lost in the Monocot order Poales (de Vries et al., 2015). Remarkably, the fourth orthologous group *sbGet3* also encompasses sequences of Poales (Figure 5.1. Orthologous relationship of *AtGet3*. A). Another component that linked *AtGet3b* function to protein translocation was the significant accumulation of Tic22 in *Atget3b-1* (Figure 5.23 B). Interestingly, phylogenetic analysis of the stromal constituent of the translocation machinery revealed that both paralogues diversified differently in members of Poales (Kasmati et al., 2013). Implying that also other factors

involved in pre-protein transport underwent differing changes in this order, perhaps due to a divergent translocation machinery. Another factor that linked *At*Get3b function to translocation was negative effect in both mutants on a subunit of the FtsH1 AAA ATPase, ARC1. This machinery is hypothesized to energetically drive chloroplast protein import (Kikuchi et al., 2018). These observations allowed me to formulate a new hypothesis in which *At*Get3b might be involved in the trafficking of soluble proteins. Spatiotemporally interacting directly with pre-proteins after their stromal arrival, potentially via an interaction with Tic214 or ARC1. An involvement in Fd biogenesis as well as an eventual molecular contribution to targeting upstream of cpSecA and cpTatA, perhaps by transiently arresting or aiding the maturation of pre-proteins, respectively.

6.4.4 Involvement in proteostasis

The *in vivo* fluorometric analysis revealed a hypersensitivity to high light exposure in *Atget3b-2*. This was not apparent under NL conditions (Figure 5.25). Suggesting that rather the acclimatization to LL in conjunction with the lack of *At*Get3b than solely the lack of latter lead to hypersensitivity. Furthermore, perturbations throughout the examined three-day course of recovery imply a higher degree of involvement in repair rather than protection. In order to understand the engagement of *At*Get3b in these processes the subcellular relocation in response to oxidative stress was analyzed *in situ* as well as the proteinaceous membrane-less organelle (PMLO) characteristics of these (Figure 5.26). Indeed, *At*Get3b sequence does include intrinsically disordered portions (data not shown) and partially behaved as phase-separated droplets (Reviewed in Uversky, 2017), but these seemingly liquid-liquid phase transitions were not reversible (data not shown). One trait of *At*Get3b is the propensity to “precipitate” without any preceding treatments *in cellula* or *in vitro* (Figure 5.26. *At*Get3b is recruited to distinct foci which display PMLO characteristics. Figure 5.27 A, respectively). These features are also attributable to sHsp holdases that orchestrate organized protein aggregation (Kaganovich et al., 2008). Even though *At*Get3b was unable to protect MDH from aggregation (Figure 5.27) it was still able to bind photosynthetic membrane proteins in a TMD dependent manner (Figure 5.21 D). Implying that maybe a certain form of client specificity is present like in other holdase systems (Basha et al., 2004) and thus not ruling out an involvement in proteostatic events.

6.4.5 Involvement in membrane remodeling

Once again the comparative proteomic data revealed a potential involvement in membrane modification. Membrane associated factors critical for thylakoid biogenesis and envelope maintenance like FZL, FtsZ2-2, ARC1 and VIPP1 (Liang et al., 2018; Kadirjan-Kalbach et al., 2012; Zhang et al., 2012) accumulated to a lesser extent in *Atget3b-2* (Figure 5.24 A). Furthermore, multiple factors interacting

with lipids were significantly accumulated in the same line (Figure 5.24 B). Signifying a possible form of compensation. On the other hand, none of these factors were increased in *Atget3b-1*. Suggesting that *AtGet3b* function could be linked to these processes. Even though many of the increased factors were reported to be associated with plastoglobuli (Kessler et al., 1999) an effect on their abundance was not observable on an ultrastructural level (Figure 5.18). Both *AtGET3b* T-DNA insertion mutants display altered ultrastructural properties. Additionally, in the role of a BiFC experiment I observed that stromules and extrusions were formed in protoplasts. Interestingly, the fluorescent trail of *AtGet3b*-YFP_N + *AtGet3b*-YFP_C was highly associated with the peripheral outlines of the membranes of these structures (Figure 5.19). This was the only time that I observed stromule formation by the overexpressing fluorescently tagged *AtGet3b*. Perhaps the additional co-expression of pSSU-mCherry might have influenced the emergence of these structures. However, it is tempting to speculate that *AtGet3b* might participate in membrane remodeling processes.

7. CONCLUSION

The GET pathway seems to be conserved in planta, however its exact role in targeting TA proteins to the ER as well as the molecular architecture has to be delineated. The conservation of Bag6 among metazoans as well as the resemblances between *Hs*Bag6 and *At*Bag6 make it tempting to speculate that *A. thaliana* might utilize a system similar to TRC. *At*Get3a was found associated with ribosomal and proteasomal subunits as well as chaperones. All in line with previous reports, however no indication of an interaction with a TA protein, except when enforced recombinantly. *At*Get3a was the only orthologue capable of preventing the heat induced aggregation of MDH *in vitro*. Signifying that client protection is mediated in a similar fashion as Hsp70. Further implying that *At*Get3a might rather be involved in other processes i.e. proteostasis than the transport of TA proteins to the ER. Perhaps an auxiliary factor facilitates this dedicated function and *At*Get3a participates in other protein triage reactions, potentially to other organelles.

The function of *At*Get3b plays an important role in the early stages of PS assembly and has effects on the general stoichiometry of components of the photosynthetic apparatus. Unfortunately, fluorometric analyses were deduced solely from PSII. However, these still displayed that *At*Get3b function effects electron transport. Components arbitrating CEF were also affected, indicating a possible involvement. When stressed, the lack of *At*Get3b became most evident in the recovery cycle. When recombinantly co-expressed *At*Get3b interacted with hydrophobic segments of clients, similar to chaperones, but displayed no holdase capacity *in vitro*. Implying that *At*Get3 function might rather be attributed to protein handover than proteostasis. When proteostatic involvement is required, the mode of action could be more similar to sHsps than to Hsp70. Thereby undergoing controlled aggregation together with clients. The molecular contribution to PS assembly could range from Fe-S cluster assembly and Fd biogenesis over triage of maturing pre proteins to membrane modulation (Figure 6.1). Even though *At*Get3b function seems to participate in a multitude of cellular pursuits of which some are crucial, its knockout does not seem to affect overall plant fitness. Implying that either other factors compensate for its absence or a minute amount of gene product is still present since it was identified in the LC-MS/MS analysis.

Unfortunately, data does not allow too many conclusions about *At*Get3c. Its function could also be linked to the Fe-S biogenesis or protein transport which in turn would lead to the observed perturbations in respiratory chain complexes.

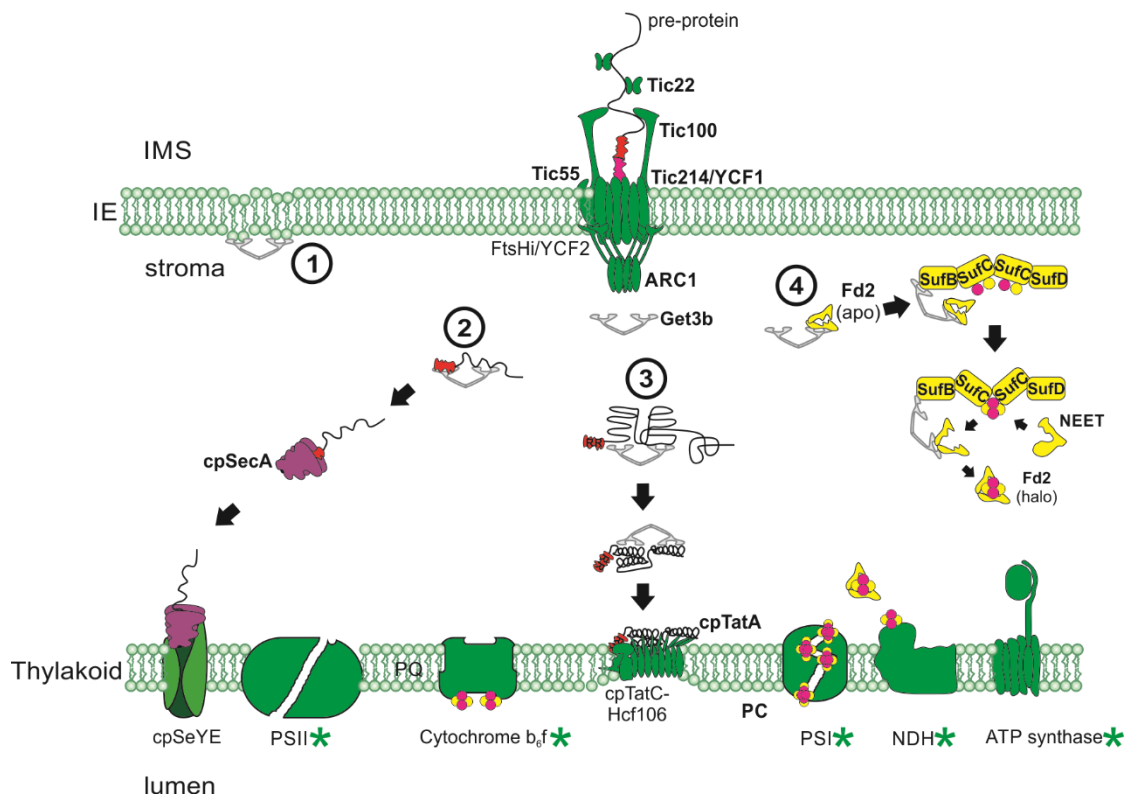


Figure 6.1. Putative function of *AtGet3b* in the stroma of chloroplasts.

Summarizing the findings of this study to delineate the stromal function of *AtGet3b*. (1) Latter could be involved in lipid interactions or general membrane remodeling processes. In terms of an involvement in protein targeting (2) *AtGet3b* could either keep precursors in an unfolded conformation to hand over to cpSecA for cpSecYE dependent translocation or (3) aid the maturation of precursors to then subject these to TAT dependent luminal translocation. Further, (4) an involvement in Fe-S cluster biogenesis could be envisioned. This could be a general association with the SufBCD complex or a specialized participation in ferredoxin2 (Fd2) biogenesis. Molecules that were shown to be affected in the comparative proteomics are depicted in bold and complexes whose sub units were affected are indicated with a green asterisk. Elements involved in Fe-S cluster assembly are represented in yellow and Fe-S clusters as magenta/yellow circles.

8. OUTLOOK

8.1 *At*Get3a

In regards to *At*Get3a the preliminary work is established to fine tune the experimental settings for TAT. Since it is still not known if this assay is possible with a fully reconstituted plant system and to what degree *At*Get3a is involved in TA protein handover at the ER membrane. The *in cellula* assay is ready to use. To verify if the proteins identified in this study are part of the *At*GET/TRC pathway one could first check their transcript levels in the *Atget3a-1* or *Atget3a-2* (not shown in this study, but ready to use) mutant background. If these display perturbations, molecular interactions can be tested *in vitro* and *in vivo* i.e. pulldown, BiFC, ectopic expression of tagged variants followed by purification. In order to address the molecular architecture of the GET/TRC pathway in *A. thaliana* IP experiments coupled to MS/MS should be repeated with leaf and root tissue of normally cultivated plants. Generally, a negative control should be included to ease the proceeding evaluation of these. Additionally, pull down experiments with recombinant *At*Get3a and cytosolic extracts of the *Atget3a-1* or *Atget3a-2* should aid the detection of interacting parties. To verify if *At*Get3a actually represents the dedicated TA protein targeting factor, pull down experiments with recombinantly expressed TA proteins like Syp123 or Sec61 β with cell lysates stemming from wheat germ or tobacco cell culture could be performed. If necessary, cross-link reagents can be used to stabilize the potentially short lived interactions.

8.2 *At*Get3b

The τ -TAT should be repeated to verify if it possible to release client proteins at the thylakoid membrane. The devised co-expression system could be used to screen possible substrates. In conjunction with a mutational approach, single AAs could be substituted to inspect their role in molecular interactions. Most importantly to verify if *At*Get3b is capable of binding soluble proteins of the cpSEC and cpTAT pathways. The fluorometric analyses in the *Atget3b* mutants should be extended to examine the primary charge separation in PSI as well as cyclic and linear electron flows. Furthermore, oxygen evolution and CO₂ consumption should be measured to corroborate the proteomic data *in vivo*. To assess an involvement in iron homeostasis, mutant plant could be grown *in vitro* on MS media, supplemented with increasing amounts of excess iron, copper, zinc and manganese. To test if *At*Get3b is involved in the translocation of Fd2 it can either be *in vitro* imported into chloroplasts or overexpressed in protoplasts isolated from *Atget3b-1* as well as *Atget3b-2* and compared to wild-type kinetics. Additionally, the interaction can be examined *in vitro* by incubating *Flag-At*Get3b with the soluble C-terminal domain of Tic214_{HA}, with or without the addition of pFd2_{His} and Fd2_{His}. To address the Fe-S cluster assembly participation, the interaction of *At*Get3b and *At*SufB could be tested

in vivo and *in vitro*. If this proves promising, denatured recombinant pFd2_{His} could be incubated with stromal extract of *Atget3b-2* with and without Flag-*AtGet3b* and time dependent Fd maturation can be monitored spectroscopically or by non-reducing SDS-PAGE. The verification of a genetic linkage is tedious job since Tic214, ARC1, cpTatA, cpSecA as well as SufBCD are all essential. Only Stic2, Tic22 and Tic100 are left as possible candidates for genetic examinations. However, in order to address if *AtGet3b* is involved in a protein trafficking pathway together with Tic22, Tic100 and Stic2, TatA and SecA a maximum likelihood tree could be established with theses. If the branching patterns are similar this could hint toward a mutual pathway. To retrieve some preliminary data on lipid interactions, different plastidic lipids can be spotted on nitro-cellulose for dot blots with *AtGet3b*.

8.3 *AtGet3c*

As an initial overview the BN PAGES should be repeated weekly in the first four weeks of development to identify a developmental stage at which differences are most pronounced. These solubilized extracts from *Atget3c-1* and wild-type mitochondria should also be DIGE-labeled and employed in two-dimensional difference gel electrophoresis (2D-DIGE) experiments. Further, a label-free comparative proteomic approach could be used for isolated mitochondria from wild-type and *Atget3c-1* plants. The subunits of complex I and complex IV with a TA topology should be tested in the co-expression system together with *AtGet3c*.

9. REFERENCES

- Abdel-Ghany, S.E.** (2009). Contribution of plastocyanin isoforms to photosynthesis and copper homeostasis in *Arabidopsis thaliana* grown at different copper regimes. *Planta* **229**: 767–779.
- Aigner, H., Wilson, R.H., Bracher, A., Calisse, L., Bhat, J.Y., Hartl, F.U., and Hayer-Hartl, M.** (2017). Plant RuBisCo assembly in *E. coli* with five chloroplast chaperones including BSD2. *Science* (80-.). **358**: 1272–1278.
- Albus, C.A., Ruf, S., Schöttler, M.A., Lein, W., Kehr, J., and Bock, R.** (2010). Y3IP1, a nucleus-encoded thylakoid protein, cooperates with the plastid-encoded Ycf3 protein in photosystem I assembly of tobacco and *Arabidopsis*. *Plant Cell* **22**: 2838–2855.
- Aldridge, C., Cain, P., and Robinson, C.** (2009). Protein transport in organelles: Protein transport into and across the thylakoid membrane. *FEBS J.* **276**: 1177–1186.
- Allahverdiyeva, Y. et al.** (2013). *Arabidopsis* plants lacking PsbQ and PsbR subunits of the oxygen-evolving complex show altered PSII super-complex organization and short-term adaptive mechanisms. *Plant J.* **75**: 671–684.
- Althoff, S., Selinger, D., and Wise, J.A.** (1994). Molecular evolution of SRP cycle components: Functional implications. *Nucleic Acids Res.* **22**: 1933–1947.
- Anghel, S.A., McGilvray, P.T., Hegde, R.S., and Keenan, R.J.** (2017). Identification of Oxa1 Homologs Operating in the Eukaryotic Endoplasmic Reticulum. *Cell Rep.* **21**: 3708–3716.
- Armbruster, U. et al.** (2013). *Arabidopsis* CURVATURE THYLAKOID1 proteins modify thylakoid architecture by inducing membrane curvature. *Plant Cell* **25**: 2661–2678.
- Auld, K.L. and Silver, P.A.** (2006). Transcriptional regulation by the proteasome as a mechanism for cellular protein homeostasis. *Cell Cycle* **5**: 1503–1505.
- Aviram, N. et al.** (2016). The SND proteins constitute an alternative targeting route to the endoplasmic reticulum. *Nature* **540**: 134–138.
- Aviram, N. and Schuldiner, M.** (2014). Embracing the void—how much do we really know about targeting and translocation to the endoplasmic reticulum? *Curr. Opin. Cell Biol.* **29**: 8–17.
- Bae, W., Lee, Y.J., Kim, D.H., Lee, J., Kim, S., Sohn, E.J., and Hwang, I.** (2008). AKR2A-mediated import of chloroplast outer membrane proteins is essential for chloroplast biogenesis. *Nat. Cell Biol.* **10**: 220–227.
- Balk, J. and Pilon, M.** (2011). Ancient and essential: The assembly of iron-sulfur clusters in plants. *Trends Plant Sci.* **16**: 218–226.
- Basha, E., Lee, G.J., Demeler, B., and Vierling, E.** (2004). Chaperone activity of cytosolic small heat shock proteins from wheat. *Eur. J. Biochem.* **271**: 1426–1436.

REFERENCES

- Bauer, J., Chen, K., Hiltbunner, A., Wehrli, E., Eugster, M., Schnell, D., and Kessler, F. (2000). The major protein import receptor of plastids is essential for chloroplast biogenesis. *Nature* **403**: 203–207.
- Bédard, J., Trösch, R., Wu, F., Ling, Q., Flores-Pérez, Ú., Töpel, M., Nawaz, F., and Jarvis, P. (2017). Suppressors of the chloroplast protein import mutant *tic40* reveal a genetic link between protein import and thylakoid biogenesis. *Plant Cell* **29**: 1726–1747.
- Berghöfer, J. and Klösgen, R.B. (1999). Two distinct translocation intermediates can be distinguished during protein transport by the TAT (Δ ph) pathway across the thylakoid membrane. *FEBS Lett.* **460**: 328–332.
- van Berkel, A.A., Santos, T.C., Shaweis, H., van Weering, J.R.T., Toonen, R.F., and Verhage, M. (2020). Loss of MUNC18-1 leads to retrograde transport defects in neurons. *J. Neurochem.*
- Van Bezouwen, L.S., Caffarri, S., Kale, R., Kouřil, R., Thunnissen, A.M.W.H., Oostergetel, G.T., and Boekema, E.J. (2017). Subunit and chlorophyll organization of the plant photosystem II supercomplex. *Nat. Plants* **3**: 1–11.
- Bhuiyan, N.H., Friso, G., Poliakov, A., Ponnala, L., and Van Wijk, K.J. (2015). MET1 is a thylakoid-associated TPR protein involved in photosystem II supercomplex formation and repair in *Arabidopsis*. *Plant Cell* **27**: 262–285.
- Birnboim, H.C. and Doly, J. (1979). A rapid alkaline extraction procedure for screening recombinant plasmid DNA. *Nucleic Acids Res.* **7**: 1513–1523.
- Bitto, E., Bingman, C.A., Bittova, L., Kondrashov, D.A., Bannen, R.M., Fox, B.G., Markley, J.L., and Phillips, G.N. (2008). Structure of human J-type co-chaperone HscB reveals a tetracysteine metal-binding domain. *J. Biol. Chem.* **283**: 30184–30192.
- Blobel, G. (1980). Intracellular protein topogenesis. *Proc. Natl. Acad. Sci. U. S. A.* **77**: 1496–1500.
- Blobel, G. and Dobberstein, B. (1975). Transfer of Proteins across Membranes II. Reconstitution of Functional Rough Microsomes from Heterologous Components. *J. Cell Biol.* **67**: 852–862.
- Blum, T., Briesemeister, S., and Kohlbacher, O. (2009). MultiLoc2: integrating phylogeny and Gene Ontology terms improves subcellular protein localization prediction. *BMC Bioinformatics* **10**: 274.
- Bodensohn, U., Ruland, C., Ladig, R., and Schleiff, E. (2020). Membrane Extracts from Plant Tissues.
- Bodensohn, U.S., Simm, S., Fischer, K., Jäschke, M., Groß, L.E., Kramer, K., Ehmann, C., Rensing, S.A., Ladig, R., and Schleiff, E. (2019). The intracellular distribution of the components of the GET system in vascular plants. *Biochim. Biophys. Acta - Mol. Cell Res.* **1866**: 1650–1662.
- de Boer, D., Bakker, H., Lever, A., Bouma, T., Salentijn, E., and Weisbeek, P. (1991). Protein targeting towards the thylakoid lumen of chloroplasts: proper localization of fusion proteins is only observed in vivo. *EMBO J.* **10**: 2765–2772.
- Bohnsack, M.T. and Schleiff, E. (2010). The evolution of protein targeting and translocation systems.

REFERENCES

- Biochim. Biophys. Acta - Mol. Cell Res. **1803**: 1115–1130.
- Bölter, B., Mitterreiter, M.J., Schwenkert, S., Finkemeier, I., and Kunz, H.H.** (2020). The topology of plastid inner envelope potassium cation efflux antiporter KEA1 provides new insights into its regulatory features. *Photosynth. Res.* **145**: 43–54.
- Bölter, B., Soll, J., Hill, K., Hemmler, R., and Wagner, R.** (1999). A rectifying ATP-regulated solute channel in the chloroplastic outer envelope from pea. *EMBO J.* **18**: 5505–5516.
- Bonomi, F., Iametti, S., Morleo, A., Ta, D., and Vickery, L.E.** (2011). Facilitated transfer of IscU-[2Fe2S] clusters by chaperone-mediated ligand exchange. *Biochemistry* **50**: 9641–9650.
- Borgese, N.** (2020). Searching for remote homologs of CAML among eukaryotes. *Traffic*.
- Borgese, N., Coy-Vergara, J., Colombo, S.F., and Schwappach, B.** (2019). The Ways of Tails: the GET Pathway and more. *Protein J.* **38**: 289–305.
- Borgese, N. and Righi, M.** (2010). Remote origins of tail-anchored proteins. *Traffic* **11**: 877–885.
- Bourne, H.R.** (1995). GTPases: a family of molecular switches and clocks. *Philos. Trans. R. Soc. London. Ser. B, Biol. Sci.* **349**: 283–289.
- Boyes, D.C., Zayed, A.M., Ascenzi, R., McCaskill, A.J., Hoffman, N.E., Davis, K.R., and Görlach, J.** (2001). Growth stage-based phenotypic analysis of Arabidopsis: A model for high throughput functional genomics in plants. *Plant Cell* **13**: 1499–1510.
- Bozkurt, G., Stjepanovic, G., Vilardi, F., Amlacher, S., Wild, K., Bange, G., Favaloro, V., Rippe, K., Hurt, E., Dobberstein, B., and Sinning, I.** (2009). Structural insights into tail-anchored protein binding and membrane insertion by Get3. *Proc. Natl. Acad. Sci. U. S. A.* **106**: 21131–21136.
- Bradbury, M. and Baker, N.R.** (1981). Analysis of the slow phases of the in vivo chlorophyll fluorescence induction curve. Changes in the redox state of Photosystem II electron acceptors and fluorescence emission from Photosystems I and II. *BBA - Bioenerg.* **635**: 542–551.
- Bruce, B.D.** (2001). The paradox of plastid transit peptides: conservation of function despite divergence in primary structure. *Biochim. Biophys. Acta* **1541**: 2–21.
- Burnat, M., Schleiff, E., and Flores, E.** (2014). Cell envelope components influencing filament length in the heterocyst-forming cyanobacterium *Anabaena* sp. strain PCC 7120. *J. Bacteriol.* **196**: 4026–4035.
- Cabantous, S., Terwilliger, T.C., and Waldo, G.S.** (2005). Protein tagging and detection with engineered self-assembling fragments of green fluorescent protein. *Nat. Biotechnol.* **23**: 102–107.
- Camacho, C., Coulouris, G., Avagyan, V., Ma, N., Papadopoulos, J., Bealer, K., and Madden, T.L.** (2009). BLAST+: architecture and applications. *BMC Bioinformatics* **10**: 421.
- Carlsson, A.S., LaBrie, S.T., Kinney, A.J., Von Wettstein-Knowles, P., and Browse, J.** (2002). A KAS2 cDNA complements the phenotypes of the Arabidopsis *fab1* mutant that differs in a single residue

REFERENCES

- bordering the substrate binding pocket. *Plant J.* **29**: 761–770.
- Casson, J., McKenna, M., Haßdenteufel, S., Aviram, N., Zimmerman, R., and High, S. (2017). Multiple pathways facilitate the biogenesis of mammalian tail-anchored proteins. *J. Cell Sci.* **130**: 3851–3861.
- Chang, Y.W., Chuang, Y.C., Ho, Y.C., Cheng, M.Y., Sun, Y.J., Hsiao, C.D., and Wang, C. (2010). Crystal structure of Get4-Get5 complex and its interactions with Sgt2, Get3, and Ydj1. *J. Biol. Chem.* **285**: 9962–9970.
- Chartron, J.W., Suloway, C.J.M., Zaslaver, M., and Clemons, W.M. (2010). Structural characterization of the Get4/Get5 complex and its interaction with Get3. *Proc. Natl. Acad. Sci. U. S. A.* **107**: 12127–12132.
- Chartron, J.W., VanderVelde, D.G., Rao, M., and Clemons, W.M. (2012). Get5 carboxyl-terminal domain is a novel dimerization motif that tethers an extended Get4/Get5 complex. *J. Biol. Chem.* **287**: 8310–8317.
- Chen, Y.E., Yuan, S., Lezhneva, L., Meurer, J., Schwenkert, S., Mamedov, F., and Schröder, W.P. (2019). The low molecular mass photosystem II protein PsbTn is important for light acclimation. *Plant Physiol.* **179**: 1739–1753.
- Chen, Y.E., Zhang, C.M., Su, Y.Q., Ma, J., Zhang, Z.W., Yuan, M., Zhang, H.Y., and Yuan, S. (2017). Responses of photosystem II and antioxidative systems to high light and high temperature co-stress in wheat. *Environ. Exp. Bot.* **135**: 45–55.
- Chio, U.S., Chung, S.Y., Weiss, S., and Shan, S. (2019). A Chaperone Lid Ensures Efficient and Privileged Client Transfer during Tail-Anchored Protein Targeting. *Cell Rep.* **26**: 37-44.e7.
- Chio, U.S., Chung, S.Y., Weiss, S., and Shan, S. (2017). A protean clamp guides membrane targeting of tail-anchored proteins. *Proc. Natl. Acad. Sci. U. S. A.* **114**: E8585–E8594.
- Cho, H., Chio, U.S., and Shan, S. (2018). In vitro Assays for Targeting and Insertion of Tail-Anchored Proteins Into the ER Membrane. *Curr. Protoc. Cell Biol.* **81**: 1–16.
- Cho, H. and Shan, S. (2018). Substrate relay in an Hsp70-cochaperone cascade safeguards tail-anchored membrane protein targeting. *EMBO J.* **37**: 1–17.
- Choi, H.K. et al. (2004). A Sequence-Based Genetic Map of *Medicago truncatula* and Comparison of Marker Colinearity with *M. sativa*. *Genetics* **166**: 1463–1502.
- Clamp, M., Cuff, J., Searle, S.M., and Barton, G.J. (2004). The Jalview Java alignment editor. *Bioinformatics* **20**: 426–427.
- Cline, K., Henry, R., Li, C., and Yuan, J. (1993). Multiple pathways for protein transport into or across the thylakoid membrane. *EMBO J.* **12**: 4105–4114.
- Cline, K. and Mori, H. (2001). Thylakoid DeltapH-dependent precursor proteins bind to a cpTatC-Hcf106

REFERENCES

- complex before Tha4-dependent transport. *J. Cell Biol.* **154**: 719–729.
- Colombo, S.F., Cardani, S., Maroli, A., Vitiello, A., Soffientini, P., Crespi, A., Bram, R.F., Benfante, R., and Borgese, N.** (2016). Tail-anchored protein insertion in mammals function and reciprocal interactions of the two subunits of the trc40receptor. *J. Biol. Chem.* **291**: 15292–15306.
- Copic, A., Dorrington, M., Pagant, S., Barry, J., Lee, M.C.S., Singh, I., Hartman, J.L. 4th, and Miller, E.A.** (2009). Genomewide analysis reveals novel pathways affecting endoplasmic reticulum homeostasis, protein modification and quality control. *Genetics* **182**: 757–769.
- Cox, J. and Mann, M.** (2008). MaxQuant enables high peptide identification rates, individualized p.p.b.-range mass accuracies and proteome-wide protein quantification. *Nat. Biotechnol.* **26**: 1367–1372.
- Creighton, A.M., Hulford, A., Mant, A., Robinson, D., and Robinson, C.** (1995). A monomeric, tightly folded stromal intermediate on the Δ pH-dependent thylakoidal protein transport pathway. *J. Biol. Chem.* **270**: 1663–1669.
- Dabney-Smith, C. and Cline, K.** (2009). Clustering of C-terminal stromal domains of Tha4 homo-oligomers during translocation by the Tat protein transport system. *Mol. Biol. Cell* **20**: 2060–2069.
- Dabney-Smith, C., Mori, H., and Cline, K.** (2006). Oligomers of Tha4 organize at the thylakoid Tat translocase during protein transport. *J. Biol. Chem.* **281**: 5476–5483.
- DalCorso, G., Pesaresi, P., Masiero, S., Aseeva, E., Schünemann, D., Finazzi, G., Joliot, P., Barbato, R., and Leister, D.** (2008). A Complex Containing PGRL1 and PGR5 Is Involved in the Switch between Linear and Cyclic Electron Flow in Arabidopsis. *Cell* **132**: 273–285.
- Dekker, J.P. and Boekema, E.J.** (2005). Supramolecular organization of thylakoid membrane proteins in green plants. *Biochim. Biophys. Acta - Bioenerg.* **1706**: 12–39.
- Denic, V., Dötsch, V., and Sinning, I.** (2013). Endoplasmic reticulum targeting and insertion of tail-anchored membrane proteins by the GET pathway. *Cold Spring Harb. Perspect. Biol.* **5**: a013334.
- Dinkins, R.D., Bandaranayake, H., Green, B.R., and Griffiths, A.J.F.** (1994). A nuclear photosynthetic electron transport mutant of Arabidopsis thaliana with altered expression of the chloroplast petA gene. *Curr. Genet.* **25**: 282–288.
- Duncan, O., van der Merwe, M.J., Daley, D.O., and Whelan, J.** (2013). The outer mitochondrial membrane in higher plants. *Trends Plant Sci.* **18**: 207–217.
- Efremov, R.G., Baradaran, R., and Sazanov, L.A.** (2010). The architecture of respiratory complex I. *Nature* **465**: 441–445.
- Elofsson, A. and Von Heijne, G.** (2007). Membrane protein structure: Prediction versus reality. *Annu. Rev. Biochem.* **76**: 125–140.
- Emanuelsson, O., Nielsen, H., Brunak, S., and von Heijne, G.** (2000). Predicting subcellular localization of

REFERENCES

- proteins based on their N-terminal amino acid sequence. *J. Mol. Biol.* **300**: 1005–1016.
- Eubel, H., Jansch, L., and Braun, H.P. (2003). New insights into the respiratory chain of plant mitochondria. Supercomplexes and a unique composition of complex II. *Plant Physiol.* **133**: 274–286.
- Fagerlund, R.D., Forsman, J.A., Biswas, S., Vass, I., Davies, F.K., Summerfield, T.C., and Eaton-Rye, J.J. (2020). Stabilization of Photosystem II by the PsbT protein impacts photodamage, repair and biogenesis. *Biochim. Biophys. Acta - Bioenerg.* **1861**: 148234.
- Favaloro, V., Spasic, M., Schwappach, B., and Dobberstein, B. (2009). UKPMC Funders Group Author Manuscript Distinct targeting pathways for the membrane insertion of tail-. *Cell* **121**: 1832–1840.
- Fic, E., Kedracka-Krok, S., Jankowska, U., Pirog, A., and Dziejzicka-Wasylewska, M. (2010). Comparison of protein precipitation methods for various rat brain structures prior to proteomic analysis. *Electrophoresis* **31**: 3573–3579.
- Finn, R.D. et al. (2014). Pfam: the protein families database. *Nucleic Acids Res.* **42**: D222–30.
- Fleischer, T.C., Weaver, C.M., McAfee, K.J., Jennings, J.L., and Link, A.J. (2006). Systematic identification and functional screens of uncharacterized proteins associated with eukaryotic ribosomal complexes. *Genes Dev.* **20**: 1294–1307.
- Flores-Ortiz, C., Alvarez, L.M., Undurraga, A., Arias, D., Durán, F., Wegener, G., and Stange, C. (2020). Differential role of the two ζ -carotene desaturase paralogs in carrot (*Daucus carota*): ZDS1 is a functional gene essential for plant development and carotenoid synthesis. *Plant Sci.* **291**: 110327.
- Formighieri, C., Cazzaniga, S., Kuras, R., and Bassi, R. (2013). Biogenesis of photosynthetic complexes in the chloroplast of *Chlamydomonas reinhardtii* requires ARSA1, a homolog of prokaryotic arsenite transporter and eukaryotic TRC40 for guided entry of tail-anchored proteins. *Plant J.* **73**: 850–861.
- Franklin, A.E. and Hoffman, N.E. (1993). Characterization of a chloroplast homologue of the 54-kDa subunit of the signal recognition particle. *J. Biol. Chem.* **268**: 22175–22180.
- Fristedt, R., Hu, C., Wheatley, N., Roy, L.M., Wachter, R.M., Savage, L., Harbinson, J., Kramer, D.M., Merchant, S.S., Yeates, T., and Croce, R. (2018). RAF2 is a RuBisCO assembly factor in *Arabidopsis thaliana*. *Plant J.* **94**: 146–156.
- Frugoli, J.A., Zhong, H.H., Nuccio, M.L., McCourt, P., McPeck, M.A., Thomas, T.L., and McClung, C.R. (1996). Catalase Is Encoded by a Multigene Family in *Arabidopsis thaliana* (L.) Heynh. *Plant Physiol.* **112**: 327 LP – 336.
- Gao, H., Sage, T.L., and Osteryoung, K.W. (2006). FZL, an FZO-like protein in plants, is a determinant of thylakoid and chloroplast morphology. *Proc. Natl. Acad. Sci. U. S. A.* **103**: 6759–6764.
- García-Cerdán, J.G., Furst, A.L., McDonald, K.L., Schünemann, D., Francis, M.B., and Niyogi, K.K. (2019). A thylakoid membrane-bound and redox-active rubredoxin (RBD1) functions in de novo assembly

REFERENCES

- and repair of photosystem II. *Proc. Natl. Acad. Sci. U. S. A.* **116**: 16631–16640.
- García-Cerdán, J.G., Kovács, L., Tóth, T., Kereiche, S., Aseeva, E., Boekema, E.J., Mamedov, F., Funk, C., and Schröder, W.P.** (2011). The PsbW protein stabilizes the supramolecular organization of photosystem II in higher plants. *Plant J.* **65**: 368–381.
- Gasper, R., Meyer, S., Gotthardt, K., Sirajuddin, M., and Wittinghofer, A.** (2009). It Takes Two to Tango: Activation of Protein Kinase D by Dimerization. *Nat. Rev. Mol. Cell Biol.* **42**: 423–429.
- Gérard, F. and Cline, K.** (2006). Efficient twin arginine translocation (Tat) pathway transport of a precursor protein covalently anchored to its initial cpTatC binding site. *J. Biol. Chem.* **281**: 6130–6135.
- Gérard, F. and Cline, K.** (2007). The thylakoid proton gradient promotes an advanced stage of signal peptide binding deep within the Tat pathway receptor complex. *J. Biol. Chem.* **282**: 5263–5272.
- Gilmore, R., Walter, P., and Blobel, G.** (1982). Protein translocation across the endoplasmic reticulum. II. Isolation and characterization of the signal recognition particle receptor. *J. Cell Biol.* **95**: 470–477.
- Glynn, J.M., Froehlich, J.E., and Osteryoung, K.W.** (2008). Arabidopsis ARC6 coordinates the division machineries of the inner and outer chloroplast membranes through interaction with PDV2 in the intermembrane space. *Plant Cell* **20**: 2460–2470.
- Goetze, T.A., Patil, M., Jeshen, I., Bölter, B., Grahl, S., and Soll, J.** (2015). Oep23 forms an ion channel in the chloroplast outer envelope. *BMC Plant Biol.* **15**: 1–10.
- Gogala, M., Becker, T., Beatrix, B., Armache, J.P., Barrio-Garcia, C., Berninghausen, O., and Beckmann, R.** (2014). Structures of the Sec61 complex engaged in nascent peptide translocation or membrane insertion. *Nature* **506**: 107–110.
- Gohlke, U., Pullan, L., McDevitt, C.A., Porcelli, I., de Leeuw, E., Palmer, T., Saibil, H.R., and Berks, B.C.** (2005). The TatA component of the twin-arginine protein transport system forms channel complexes of variable diameter. *Proc. Natl. Acad. Sci. U. S. A.* **102**: 10482–10486.
- Görlich, D., Hartmann, E., Prehn, S., and Rapoport, T.A.** (1992). A protein of the endoplasmic reticulum involved early in polypeptide translocation. *Nature* **357**: 47–52.
- Goss, R. and Lepetit, B.** (2015). Biodiversity of NPQ. *J. Plant Physiol.* **172**: 13–32.
- Gristick, H.B., Rao, M., Chartron, J.W., Rome, M.E., Shan, S.O., and Clemons, W.M.** (2014). Crystal structure of ATP-bound Get3-Get4-Get5 complex reveals regulation of Get3 by Get4. *Nat. Struct. Mol. Biol.* **21**: 437–442.
- Hahn, A., Vonck, J., Mills, D.J., Meier, T., and Kühlbrandt, W.** (2018). Structure, mechanism, and regulation of the chloroplast ATP synthase. *Science* **360**.
- Halic, M., Becker, T., Pool, M.R., Spahn, C.M.T., Grassucci, R.A., Frank, J., and Beckmann, R.** (2004). Structure of the signal recognition particle interacting with the elongation-arrested ribosome.

REFERENCES

- Nature **427**: 808–814.
- Haßdenteufel, S., Sicking, M., Schorr, S., Aviram, N., Fecher-Trost, C., Schuldiner, M., Jung, M., Zimmermann, R., and Lang, S. (2017). hSnd2 protein represents an alternative targeting factor to the endoplasmic reticulum in human cells. *FEBS Lett.* **591**: 3211–3224.
- Hegde, R.S. and Bernstein, H.D. (2006). The surprising complexity of signal sequences. *Trends Biochem. Sci.* **31**: 563–571.
- Hegde, R.S. and Keenan, R.J. (2011). Tail-anchored membrane protein insertion into the endoplasmic reticulum. *Nat. Rev. Mol. Cell Biol.* **12**: 787–798.
- von Heijne, G., Steppuhn, J., and Herrmann, R.G. (1989). Domain structure of mitochondrial and chloroplast targeting peptides. *Eur. J. Biochem.* **180**: 535–545.
- Hicks, G.R. and Raikhel, N. V. (1995). Protein import into the nucleus: An Integrated View. *Annu. Rev. Cell Dev. Biol.* **11**: 155–188.
- High, S., Henry, R., Mould, R.M., Valent, Q., Meacock, S., Cline, K., Gray, J.C., and Luirink, J. (1997). Chloroplast SRP54 interacts with a specific subset of thylakoid precursor proteins. *J. Biol. Chem.* **272**: 11622–11628.
- High, S., Martoglio, B., Görlich, D., Andersen, S.S., Ashford, A.J., Giner, A., Hartmann, E., Prehn, S., Rapoport, T.A., and Dobberstein, B. (1993). Site-specific photocross-linking reveals that Sec61p and TRAM contact different regions of a membrane-inserted signal sequence. *J. Biol. Chem.* **268**: 26745–26751.
- Hilger, D., Masureel, M., and Kobilka, B.K. (2018). Structure and dynamics of GPCR signaling complexes. *Nat. Struct. Mol. Biol.* **25**: 4–12.
- Ho, Y. et al. (2002). Systematic identification of protein complexes in *Saccharomyces cerevisiae* by mass spectrometry. *Nature* **415**: 180–183.
- Hong, H.Y., Yoo, G.S., and Choi, J.K. (2000). Direct Blue 71 staining of proteins bound to blotting membranes. *Electrophoresis* **21**: 841–845.
- Hu, X., Kato, Y., Sumida, A., Tanaka, A., and Tanaka, R. (2017). The SUFBC2D complex is required for the biogenesis of all major classes of plastid Fe-S proteins. *Plant J.* **90**: 235–248.
- Huh, W.-K., Falvo, J. V, Gerke, L.C., Carroll, A.S., Howson, R.W., Weissman, J.S., and O’Shea, E.K. (2003). Global analysis of protein localization in budding yeast. *Nature* **425**: 686–691.
- Ihnatowicz, A., Pesaresi, P., and Leister, D. (2007). The E subunit of photosystem I is not essential for linear electron flow and photoautotrophic growth in *Arabidopsis thaliana*. *Planta* **226**: 889–895.
- Ihnatowicz, A., Pesaresi, P., Varotto, C., Richly, E., Schneider, A., Jahns, P., Salamini, F., and Leister, D. (2004). Mutants for photosystem I subunit D of *Arabidopsis thaliana*: Effects on photosynthesis, photosystem I stability and expression of nuclear genes for chloroplast functions. *Plant J.* **37**: 839–

852.

- Ilbert, M., Horst, J., Ahrens, S., Winter, J., Graf, P.C.F., Lilie, H., and Jakob, U. (2007). The redox-switch domain of Hsp33 functions as dual stress sensor. *Nat. Struct. Mol. Biol.* **14**: 556–563.
- Ishihara, S., Takabayashi, A., Ido, K., Endo, T., Ifuku, K., and Sato, F. (2007). Distinct Functions for the Two PsbP-Like Proteins PPL1 and PPL2 in the Chloroplast Thylakoid Lumen of Arabidopsis. *Plant Physiol.* **145**: 668 LP – 679.
- Itakura, E., Zavodszky, E., Shao, S., Wohlever, M.L., Keenan, R.J., Hegde, R.S., Itakura, E., Zavodszky, E., Shao, S., Wohlever, M.L., and Keenan, R.J. (2016). Ubiquilins Chaperone and Triage Mitochondrial Membrane Proteins for Degradation Article Ubiquilins Chaperone and Triage Mitochondrial Membrane Proteins for Degradation. *Mol. Cell* **63**: 21–33.
- Iwai, M., Takizawa, K., Tokutsu, R., Okamuro, A., Takahashi, Y., and Minagawa, J. (2010). Isolation of the elusive supercomplex that drives cyclic electron flow in photosynthesis. *Nature* **464**: 1210–1213.
- Jakob, U., Muse, W., Eser, M., and Bardwell, J.C.A. (1999). Chaperone activity with a redox switch. *Cell* **96**: 341–352.
- Järvi, S., Suorsa, M., and Aro, E.M. (2015). Photosystem II repair in plant chloroplasts - Regulation, assisting proteins and shared components with photosystem II biogenesis. *Biochim. Biophys. Acta - Bioenerg.* **1847**: 900–909.
- Jeong, I.S. et al. (2018). Purification and characterization of Arabidopsis thaliana oligosaccharyltransferase complexes from the native host: a protein super-expression system for structural studies. *Plant J.* **94**: 131–145.
- Jiang, X., Jiang, H., Shen, Z., and Wang, X. (2014). Activation of mitochondrial protease OMA1 by Bax and Bak promotes cytochrome c release during apoptosis. *Proc. Natl. Acad. Sci. U. S. A.* **111**: 14782–14787.
- Jin, H., Liu, B., Luo, L., Feng, D., Wang, P., Liu, J., Da, Q., He, Y., Qi, K., Wang, J., and Wang, H. Bin (2014). HYPERSENSITIVE TO HIGH LIGHT1 interacts with LOW QUANTUM YIELD OF PHOTOSYSTEM III1 and functions in protection of Photosystem II from Photodamage in Arabidopsis. *Plant Cell* **26**: 1213–1229.
- Jonikas, M.C., Collins, S.R., Denic, V., Oh, E., Quan, E.M., Schmid, V., Weibezahn, J., Schwappach, B., Walter, P., Weissman, J.S., and Schuldiner, M. (2009). Comprehensive characterization of genes required for protein folding in the endoplasmic reticulum. *Science (80-.)*. **323**: 1693–1697.
- Jores, T., Klinger, A., Groß, L.E., Kawano, S., Flinner, N., Duchardt-Ferner, E., Wöhnert, J., Kalbacher, H., Endo, T., Schleiff, E., and Rapaport, D. (2016). Characterization of the targeting signal in mitochondrial β -barrel proteins. *Nat. Commun.* **7**.
- Junne, T., Kocik, L., and Spiess, M. (2010). The hydrophobic core of the Sec61 translocon defines the

REFERENCES

- hydrophobicity threshold for membrane integration. *Mol. Biol. Cell* **21**: 1662–1670.
- Kadirjan-Kalbach, D.K., Yoder, D.W., Ruckle, M.E., Larkin, R.M., and Osteryoung, K.W. (2012). FtsHi1/ARC1 is an essential gene in Arabidopsis that links chloroplast biogenesis and division. *Plant J.* **72**: 856–867.
- Kaganovich, D., Kopito, R., and Frydman, J. (2008). Misfolded proteins partition between two distinct quality control compartments. *Nature* **454**: 1088–1095.
- Kalbfleisch, T., Cambon, A., and Wattenberg, B.W. (2007). A bioinformatics approach to identifying tail-anchored proteins in the human genome. *Traffic* **8**: 1687–1694.
- Karamoko, M., El-Kafafi, E.S., Mandaron, P., Lerbs-Mache, S., and Falconet, D. (2011). Multiple FtsZ2 isoforms involved in chloroplast division and biogenesis are developmentally associated with thylakoid membranes in Arabidopsis. *FEBS Lett.* **585**: 1203–1208.
- Kasmati, A.R., Töpel, M., Khan, N.Z., Patel, R., Ling, Q., Karim, S., Aronsson, H., and Jarvis, P. (2013). Evolutionary, Molecular and Genetic Analyses of Tic22 Homologues in Arabidopsis thaliana Chloroplasts. *PLoS One* **8**.
- Katoh, K., Misawa, K., Kuma, K., and Miyata, T. (2002). MAFFT: a novel method for rapid multiple sequence alignment based on fast Fourier transform. *Nucleic Acids Res.* **30**: 3059–3066.
- Kessler, F., Schnell, D., and Blobel, G. (1999). Identification of proteins associated with plastoglobules isolated from pea (*Pisum sativum* L.) chloroplasts. *Planta* **208**: 107–113.
- Khan, M.S., Haas, F.H., Samami, A.A., Gholami, A.M., Bauer, A., Fellenberg, K., Reichelt, M., Hänsch, R., Mendel, R.R., Meyer, A.J., Wirtz, M., and Hell, R. (2010). Sulfite reductase defines a newly discovered bottleneck for assimilatory sulfate reduction and is essential for growth and development in Arabidopsis thaliana. *Plant Cell* **22**: 1216–1231.
- Kikuchi, S. et al. (2018). A Ycf2-FtsHi heteromeric AAA-ATPase complex is required for chloroplast protein import. *Plant Cell* **30**: 2677–2703.
- Kikuchi, S., Bédard, J., Hirano, M., Hirabayashi, Y., Oishi, M., Imai, M., Takase, M., Ide, T., and Nakai, M. (2013). Uncovering the protein translocon at the chloroplast inner envelope membrane. *Science* (80-.). **339**: 571–574.
- Kikuchi, S., Oishi, M., Hirabayashi, Y., Lee, D.W., Hwang, I., and Nakai, M. (2009). A 1.1-Megadalton translocation complex containing tic20 and tic21 mediates chloroplast protein import at the inner envelope membrane. *Plant Cell* **21**: 1781–1797.
- Kim, D.H., Lee, J.E., Xu, Z.Y., Geem, K.R., Kwon, Y., Park, J.W., and Hwang, I. (2015). Cytosolic targeting factor AKR2A captures chloroplast outer membrane-localized client proteins at the ribosome during translation. *Nat. Commun.* **6**.
- Kim, S.J., Jansson, S., Hoffman, N.E., Robinson, C., and Mant, A. (1999). Distinct “ Assisted ” and “

REFERENCES

- Spontaneous " Mechanisms for the Insertion of Polytopic Chlorophyll-binding Proteins into the Thylakoid Membrane *. *J. Biol. Chem.* **274**: 4715–4721.
- Kim, S.J., Robinson, C., and Mant, A.** (1998). Sec/SRP-independent insertion of two thylakoid membrane proteins bearing cleavable signal peptides. *FEBS Lett.* **424**: 105–108.
- Klimmek, F., Sjödin, A., Noutsos, C., Leister, D., and Jansson, S.** (2006). Abundantly and Rarely Expressed Lhc Protein Genes Exhibit Distinct Regulation Patterns in Plants. *Plant Physiol.* **140**: 793–804.
- Klinger, A., Gosch, V., Bodensohn, U., Ladig, R., and Schleiff, E.** (2019). The signal distinguishing between targeting of outer membrane β -barrel protein to plastids and mitochondria in plants. *Biochim. Biophys. Acta - Mol. Cell Res.* **1866**.
- Klöggen, R.B., Brock, I.W., Herrmann, R.G., and Robinson, C.** (1992). Proton gradient-driven import of the 16 kDa oxygen-evolving complex protein as the full precursor protein by isolated thylakoids. *Plant Mol. Biol.* **18**: 1031–1034.
- Kogata, N., Nishio, K., Hirohashi, T., Kikuchi, S., and Nakai, M.** (1999). Involvement of a chloroplast homologue of the signal recognition particle receptor protein, FtsY, in protein targeting to thylakoids. *FEBS Lett.* **447**: 329–333.
- Kordes, E., Savelyeva, L., Schwab, M., Rommelaere, J., Jauniaux, J.C., and Cziepluch, C.** (1998). Isolation and characterization of human SGT and identification of homologues in *Saccharomyces cerevisiae* and *Caenorhabditis elegans*. *Genomics* **52**: 90–94.
- Kovacheva, S., Bédard, J., Wardle, A., Patel, R., and Jarvis, P.** (2007). Further in vivo studies on the role of the molecular chaperone, Hsp93, in plastid protein import. *Plant J.* **50**: 364–379.
- Kramer, D.M. and Evans, J.R.** (2011). The importance of energy balance in improving photosynthetic productivity. *Plant Physiol.* **155**: 70–78.
- Krieger-Liszkay, A., Shimakawa, G., and Sétif, P.** (2020). Role of the two PsaE isoforms on O₂ reduction at photosystem I in *Arabidopsis thaliana*. *Biochim. Biophys. Acta - Bioenerg.* **1861**: 148089.
- Krogh, A., Larsson, B., Von Heijne, G., and Sonnhammer, E.L.L.** (2001). Predicting transmembrane protein topology with a hidden Markov model: Application to complete genomes. *J. Mol. Biol.* **305**: 567–580.
- Kroll, D., Meierhoff, K., Bechtold, N., Kinoshita, M., Westphal, S., Vothknecht, U.C., Soll, J., and Westhoff, P.** (2001). VIPP1, a nuclear gene of *Arabidopsis thaliana* essential for thylakoid membrane formation. *Proc. Natl. Acad. Sci. U. S. A.* **98**: 4238–4242.
- Krueger, R.J. and Siegel, L.M.** (1982). Spinach Siroheme Enzymes: Isolation and Characterization of Ferredoxin-Sulfite Reductase and Comparison of Properties with Ferredoxin-Nitrite Reductase. *Biochemistry* **21**: 2892–2904.
- Krysan, P.J., Young, J.C., and Sussman, M.R.** (1999). T-DNA as an insertional mutagen in *Arabidopsis*. *Plant*

- Cell **11**: 2283–2290.
- Kurusu, G., Zhang, H., Smith, J.L., and Cramer, W.A.** (2003). Structure of the Cytochrome b6f Complex of Oxygenic Photosynthesis: Tuning the Cavity. *Science* (80-). **302**: 1009–1014.
- Kutay, U., Ahnert-Hilger, G., Hartmann, E., Wiedenmann, B., and Rapoport, T.A.** (1995). Transport route for synaptobrevin via a novel pathway of insertion into the endoplasmic reticulum membrane. *EMBO J.* **14**: 217–223.
- Kutay, U., Hartmann, E., and Rapoport, T.A.** (1993). A class of membrane proteins with a C-terminal anchor. *Trends Cell Biol.* **3**: 72–75.
- Laidler, V., Chaddock, A.M., Knott, T.G., Walker, D., and Robinson, C.** (1995). A SecY homolog in *Arabidopsis thaliana*: Sequence of a full-length cDNA clone and import of the precursor protein into chloroplasts. *J. Biol. Chem.* **270**: 17664–17667.
- Lakkaraju, A.K.K., Mary, C., Scherrer, A., Johnson, A.E., and Strub, K.** (2008). SRP Keeps Polypeptides Translocation-Competent by Slowing Translation to Match Limiting ER-Targeting Sites. *Cell* **133**: 440–451.
- Leake, M.C., Greene, N.P., Godun, R.M., Granjon, T., Buchanan, G., Chen, S., Berry, R.M., Palmer, T., and Berks, B.C.** (2008). Variable stoichiometry of the TatA component of the twin-arginine protein transport system observed by in vivo single-molecule imaging. *Proc. Natl. Acad. Sci. U. S. A.* **105**: 15376–15381.
- Leipe, D.D., Wolf, Y.I., Koonin, E. V., and Aravind, L.** (2002). Classification and evolution of P-loop GTPases and related ATPases. *J. Mol. Biol.* **317**: 41–72.
- Leitner-Dagan, Y., Ovadis, M., Shklarman, E., Elad, Y., David, D.R., and Vainstein, A.** (2006). Expression and functional analyses of the plastid lipid-associated protein CHRC suggest its role in chromoplastogenesis and stress. *Plant Physiol.* **142**: 233–244.
- Leliaert, F., Smith, D.R., Moreau, H., Herron, M.D., Verbruggen, H., Delwiche, C.F., and De Clerck, O.** (2012). Phylogeny and Molecular Evolution of the Green Algae. *CRC. Crit. Rev. Plant Sci.* **31**: 1–46.
- Lennartz, K., Plücken, H., Seidler, A., Westhoff, P., Bechtold, N., and Meierhoff, K.** (2001). HCF164 encodes a thioredoxin-like protein involved in the biogenesis of the cytochrome b6f complex in *Arabidopsis*. *Plant Cell* **13**: 2539–2551.
- León, I.R., Schwämmle, V., Jensen, O.N., and Sprenger, R.R.** (2013). Quantitative assessment of in-solution digestion efficiency identifies optimal protocols for unbiased protein analysis. *Mol. Cell. Proteomics* **12**: 2992–3005.
- Letierrier, M., Barroso, J.B., Valderrama, R., Begara-Morales, J.C., Sánchez-Calvo, B., Chaki, M., Luque, F., Viñegla, B., Palma, J.M., and Corpas, F.J.** (2016). Peroxisomal NADP-isocitrate dehydrogenase is required for *Arabidopsis* stomatal movement. *Protoplasma* **253**: 403–415.

REFERENCES

- Leznicki, P., Clancy, A., Schwappach, B., and High, S. (2010). Bat3 promotes the membrane integration of tail-anchored proteins. *J. Cell Sci.* **123**: 2170–2178.
- Leznicki, P. and High, S. (2012). SGTA antagonizes BAG6-mediated protein triage. *Proc. Natl. Acad. Sci. U. S. A.* **109**: 19214–19219.
- Leznicki, P. and High, S. (2020). SGTA associates with nascent membrane protein precursors.: 1–17.
- Leznicki, P., Warwicker, J., and High, S. (2011). A biochemical analysis of the constraints of tail-anchored protein biogenesis. *Biochem. J.* **436**: 719–727.
- Li, H.M., Theg, S.M., Bauerle, C.M., and Keegstra, K. (1990). Metal-ion-center assembly of ferredoxin and plastocyanin in isolated chloroplasts. *Proc. Natl. Acad. Sci. U. S. A.* **87**: 6748–6752.
- Li, X., Henry, R., Yuan, J., Cline, K., and Hoffman, N.E. (1995). A chloroplast homologue of the signal recognition particle subunit SRP54 is involved in the posttranslational integration of a protein into thylakoid membranes. *Proc. Natl. Acad. Sci. U. S. A.* **92**: 3789–3793.
- Liang, Z., Zhu, N., Mai, K.K., Liu, Z.Y., Tzeng, D., Osteryoung, K.W., Zhong, S., Staehelin, L.A., and Kang, B.H. (2018). Thylakoid-bound polysomes and a dynamin-related protein, FZL, mediate critical stages of the linear chloroplast biogenesis program in greening arabidopsis cotyledons. *Plant Cell* **30**: 1476–1495.
- Lim, H., Eng, J., Yates, J.R., Tollaksen, S.L., Giometti, C.S., Holden, J.F., Adams, M.W.W., Reich, C.I., Olsen, G.J., and Hays, L.G. (2003). Identification of 2D-gel proteins: A comparison of MALDI/TOF peptide mass mapping to μ LC-ESI tandem mass spectrometry. *J. Am. Soc. Mass Spectrom.* **14**: 957–970.
- Lin, T.W., Chen, C.C., Wu, S.M., Chang, Y.C., Li, Y.C., Su, Y.W., Hsiao, C.D., and Chang, H.Y. (2019). Structural analysis of chloroplast tail-anchored membrane protein recognition by ArsA1. *Plant J.* **99**: 128–143.
- Lintala, M., Allahverdiyeva, Y., Kangasjärvi, S., Lehtimäki, N., Keränen, M., Rintamäki, E., Aro, E.M., and Mulo, P. (2009). Comparative analysis of leaf-type ferredoxin-NADP⁺ oxidoreductase isoforms in *Arabidopsis thaliana*. *Plant J.* **57**: 1103–1115.
- Liou, S.T., Cheng, M.Y., and Wang, C. (2007). SGT2 and MDY2 interact with molecular chaperone YDJ1 in *Saccharomyces cerevisiae*. *Cell Stress Chaperones* **12**: 59–70.
- Lipp, J., Dobberstein, B., and Haeuptle, M.T. (1987). Signal recognition particle arrests elongation of nascent secretory and membrane proteins at multiple sites in a transient manner. *J. Biol. Chem.* **262**: 1680–1684.
- Liu, D., Gong, Q., Ma, Y., Li, P., Li, J., Yang, S., Yuan, L., Yu, Y., Pan, D., Xu, F., and Wang, N.N. (2010). CpSecA, a thylakoid protein translocase subunit, is essential for photosynthetic development in *Arabidopsis*. *J. Exp. Bot.* **61**: 1655–1669.
- Liu, Z., Yan, H., Wang, K., Kuang, T., Zhang, J., Gui, L., An, X., and Chang, W. (2004). Crystal structure of

REFERENCES

- spinach major light-harvesting complex at 2.72 Å resolution. *Nature* **428**: 287–292.
- Lorkovic, Z.J., Herrmann, R.G., and Oelmüller, R.** (1995). Molecular characterization of PsbW, a nuclear-encoded component of the photosystem II reaction center complex in spinach. *Plant Cell* **9**: 8930–8934.
- Luirink, J. and Sinning, I.** (2004). SRP-mediated protein targeting: Structure and function revisited. *Biochim. Biophys. Acta - Mol. Cell Res.* **1694**: 17–35.
- Luque, I. and Ochoa de Alda, J.A.G.** (2014). CURT1, CAAD-containing aaRSs, thylakoid curvature and gene translation. *Trends Plant Sci.* **19**: 63–66.
- Lyck, R., Harmening, U., Höhfeld, I., Treuter, E., Scharf, K.D., and Nover, L.** (1997). Intracellular distribution and identification of the nuclear localization signals of two plant heat-stress transcription factors. *Planta* **202**: 117–125.
- Ma, J., Peng, L., Guo, J., Lu, Q., Lu, C., and Zhang, L.** (2007). LPA2 is required for efficient assembly of photosystem II in *Arabidopsis thaliana*. *Plant Cell* **19**: 1980–1993.
- Maestre-Reyna, M., Wu, S.M., Chang, Y.C., Chen, C.C., Maestre-Reyna, A., Wang, A.H.J., and Chang, H.Y.** (2017). In search of tail-anchored protein machinery in plants: Reevaluating the role of arsenite transporters. *Sci. Rep.* **7**: 1–10.
- Mahler, H.-C., Friess, W., Grauschopf, U., and Kiese, S.** (2012). Molecular Nanomedicine Towards Cancer: J. Pharm. Sci. **101**: 2271–2280.
- Maio, N., Kim, K.S., Singh, A., and Rouault, T.A.** (2017). A Single Adaptable Cochaperone-Scaffold Complex Delivers Nascent Iron-Sulfur Clusters to Mammalian Respiratory Chain Complexes I–III. *Cell Metab.* **25**: 945-953.e6.
- Maio, N., Singh, A., Uhrigshardt, H., Saxena, N., Tong, W.H., and Rouault, T.A.** (2014). Cochaperone binding to LYR motifs confers specificity of iron sulfur cluster delivery. *Cell Metab.* **19**: 445–457.
- Malkin, L.I. and Rich, A.** (1967). Partial resistance of nascent polypeptide chains to proteolytic digestion due to ribosomal shielding. *J. Mol. Biol.* **26**: 329–346.
- Mant, A., Woolhead, C.A., Moore, M., Henry, R., and Robinson, C.** (2001). Insertion of PsbK into the Thylakoid Membrane in a “Horseshoe” Conformation Occurs in the Absence of Signal Recognition Particle, Nucleoside Triphosphates, or Functional Albino3*. *J. Biol. Chem.* **276**: 36200–36206.
- Mao, H., Chen, M., Su, Y., Wu, N., Yuan, M., Yuan, S., Brestic, M., Zivcak, M., Zhang, H., and Chen, Y.** (2018). Comparison on Photosynthesis and Antioxidant Defense Systems in Wheat with Different Ploidy Levels and Octoploid Triticale. *Int. J. Mol. Sci.* **19**.
- Mariappan, M., Li, X., Stefanovic, S., Sharma, A., Mateja, A., Keenan, R.J., and Hegde, R.S.** (2010). A ribosome-associating factor chaperones tail-anchored membrane proteins. *Nature* **466**: 1120–1124.
- Mariappan, M., Mateja, A., Dobosz, M., Bove, E., Hegde, R.S., and Keenan, R.J.** (2011). The mechanism of

REFERENCES

- membrane-associated steps in tail-anchored protein insertion. *Nature* **477**: 61–69.
- Marques, J.P., Schattat, M.H., Hause, G., Dudeck, I., and Klösgen, R.B.** (2004). In vivo transport of folded EGFP by the DeltapH/TAT-dependent pathway in chloroplasts of *Arabidopsis thaliana*. *J. Exp. Bot.* **55**: 1697–1706.
- Martoglio, B. and Dobberstein, B.** (1998). Signal sequences: More than just greasy peptides. *Trends Cell Biol.* **8**: 410–415.
- Masuda, T. et al.** (2003). Functional Analysis of Isoforms of NADPH:Protochlorophyllide Oxidoreductase (POR), PORB and PORC, in *Arabidopsis thaliana*. *Plant Cell Physiol.* **44**: 963–974.
- Mateja, A., Paduch, M., Chang, H.Y., Szydlowska, A., Kosiakoff, A.A., Hegde, R.S., and Keenan, R.J.** (2015). Structure of the Get3 targeting factor in complex with its membrane protein cargo. *Science* (80-.). **347**: 1152–1155.
- Mateja, A., Szlachcic, A., Downing, M.E., Dobosz, M., Mariappan, M., Hegde, R.S., and Keenan, R.J.** (2009). The structural basis of tail-anchored membrane protein recognition by Get3. *Nature* **461**: 361–366.
- McDowell, M.A. et al.** (2020). Structural Basis of Tail-Anchored Membrane Protein Biogenesis by the GET Insertase Complex. *Mol. Cell*: 1–15.
- McGilvray, P.T., Anghel, S.A., Sundaram, A., Zhong, F., Trnka, M.J., Fuller, J.R., Hu, H., Burlingame, A.L., and Keenan, R.J.** (2020). An ER translocon for multi-pass membrane protein biogenesis. *Elife* **9**: 1–43.
- Meyer, D.I., Krause, E., and Dobberstein, B.** (1982). Secretory protein translocation across membranes - The role of the “docking protein.” *Nature* **297**: 647–650.
- Michl, D., Robinson, C., Shackleton, J.B., Herrmann, R.G., and Klossgen, R.B.** (1994). Targeting of proteins to the thylakoids by bipartite presequences : CFoll is imported by a novel , third pathway. **13**: 1310–1317.
- Minami, R., Hayakawa, A., Kagawa, H., Yanagi, Y., Yokosawa, H., and Kawahara, H.** (2010). BAG-6 is essential for selective elimination of defective proteasomal substrates. *J. Cell Biol.* **190**: 637–650.
- Mishra, S.K., Tripp, J., Winkelhaus, S., Tschiersch, B., Theres, K., Nover, L., and Scharf, K.-D.** (2002). In the complex family of heat stress transcription factors, HsfA1 has a unique role as master regulator of thermotolerance in tomato. *Genes Dev.* **16**: 1555–1567.
- Mistry, J., Finn, R.D., Eddy, S.R., Bateman, A., and Punta, M.** (2013). Challenges in homology search: HMMER3 and convergent evolution of coiled-coil regions. *Nucleic Acids Res.* **41**: e121.
- Mock, J.Y., Chartron, J.W., Zaslaver, M., Xu, Y., Ye, Y., and Clemons, W.M.** (2015). Bag6 complex contains a minimal tail-anchor-targeting module and a mock BAG domain. *Proc. Natl. Acad. Sci. U. S. A.* **112**: 106–111.
- Moore, M., Goforth, R.L., Mori, H., and Henry, R.** (2003). Functional interaction of chloroplast SRP/FtsY

REFERENCES

- with the ALB3 translocase in thylakoids: Substrate not required. *J. Cell Biol.* **162**: 1245–1254.
- Moore, M., Harrison, M.S., Peterson, E.C., and Henry, R.** (2000). Chloroplast Oxa1p homolog albino3 is required for post-translational integration of the light harvesting chlorophyll-binding protein into thylakoid membranes. *J. Biol. Chem.* **275**: 1529–1532.
- Mori, H. and Cline, K.** (2001). Post-translational protein translocation into thylakoids by the Sec and Δ pH-dependent pathways. *Biochim. Biophys. Acta - Mol. Cell Res.* **1541**: 80–90.
- Mould, R.M. and Robinson, C.** (1991). A proton gradient is required for the transport of two luminal oxygen-evolving proteins across the thylakoid membrane. *J. Biol. Chem.* **266**: 12189–12193.
- Mühlhardt, C.** (2013). *Der Experimentator Molekularbiologie / Genomics.*
- Mukhopadhyay, R., Ho, Y.S., Swiatek, P.J., Rosen, B.P., and Bhattacharjee, H.** (2006). Targeted disruption of the mouse *Asna1* gene results in embryonic lethality. *FEBS Lett.* **580**: 3889–3894.
- Murashige, T. and Skoog, F.** (1962). A Revised Medium for Rapid Growth and Bio Assays with Tobacco Tissue Cultures. *Physiol. Plant.* **15**: 473–497.
- Nakai, M.** *New Perspectives on Chloroplast Protein Import.*
- Nakai, M., Goto, A., Nohara, T., Sugita, D., and Endo, T.** (1994). Identification of the SecA protein homolog in pea chloroplasts and its possible involvement in thylakoidal protein transport. *J. Biol. Chem.* **269**: 31338–31341.
- Nechushtai, R. et al.** (2012). Characterization of Arabidopsis NEET reveals an ancient role for NEET proteins in iron metabolism. *Plant Cell* **24**: 2139–2154.
- Nesterenko, M. V., Tilley, M., and Upton, S.J.** (1994). *Biochemical and Biophysical Methods*. *J. Biochem. Biophys. Methods* **28**: 239–242.
- Nguyen, L.-T., Schmidt, H.A., von Haeseler, A., and Minh, B.Q.** (2015). IQ-TREE: a fast and effective stochastic algorithm for estimating maximum-likelihood phylogenies. *Mol. Biol. Evol.* **32**: 268–274.
- Ni, D., Wang, Y., Yang, X., Zhou, H., Hou, X., Cao, B., Lu, Z., Zhao, X., Yang, K., and Huang, Y.** (2014). Structural and functional analysis of the β -barrel domain of BamA from *Escherichia coli*. *FASEB J.* **28**: 2677–2685.
- Nickelsen, J. and Rengstl, B.** (2013). Photosystem II assembly: From cyanobacteria to plants. *Annu. Rev. Plant Biol.* **64**: 609–635.
- Nielsen, V.S., Mant, A., Knoetzel, J., Møller, B.L., and Robinson, C.** (1994). Import of barley photosystem I subunit N into the thylakoid lumen is mediated by a bipartite presequence lacking an intermediate processing site. Role of the delta pH in translocation across the thylakoid membrane. *J. Biol. Chem.* **269**: 3762–3766.
- Nilsson, R. and van Wijk, K.J.** (2002). Transient interaction of cpSRP54 with elongating nascent chains of the chloroplast-encoded D1 protein; “cpSRP54 caught in the act.” *FEBS Lett.* **524**: 127–133.

REFERENCES

- Nixon, P.J., Michoux, F., Yu, J., Boehm, M., and Komenda, J. (2010). Recent advances in understanding the assembly and repair of photosystem II. *Ann. Bot.* **106**: 1–16.
- Okada, Y., Frey, A.B., Guenther, T.M., Oesch, F., Sabatini, D.D., and Kriebich, G. (1982). Studies on the biosynthesis of microsomal membrane proteins. Site of synthesis and mode of insertion of cytochrome b5, cytochrome b5 reductase, cytochrome P-450 reductase and epoxide hydrolase. *Eur. J. Biochem.* **122**: 393–402.
- Palade, G., Arch, A., Locke, M., Locke, E., and Palade, G. (1975). *Intracellular Aspects of the Process of Protein Synthesis* Published by : American Association for the Advancement of Science Stable. *Science (80-.)*. **189**: 347–358.
- Pan, X., Ma, J., Su, X., Cao, P., Chang, W., Liu, Z., Zhang, X., and Li, M. (2018). Structure of the maize photosystem I supercomplex with light-harvesting complexes I and II. *Science (80-.)*. **360**: 1109–1113.
- Parcerisa, I.L., Rosano, G.L., and Ceccarelli, E.A. (2020). Biochemical characterization of ClpB3, a chloroplastic disaggregase from *Arabidopsis thaliana*. *Plant Mol. Biol.* **104**: 451–465.
- Park, E. and Rapoport, T.A. (2012). Mechanisms of Sec61SecY-mediated protein translocation across membranes. *Annu. Rev. Biophys.* **41**: 21–40.
- Pattison, R.J. and Amtmann, A. (2009). N-glycan production in the endoplasmic reticulum of plants. *Trends Plant Sci.* **14**: 92–99.
- Paul, P., Simm, S., Blaumeiser, A., Scharf, K.-D., Fragkostefanakis, S., Mirus, O., and Schleiff, E. (2013). The protein translocation systems in plants - composition and variability on the example of *Solanum lycopersicum*. *BMC Genomics* **14**: 189.
- Payapilly, A. and High, S. (2014). BAG6 regulates the quality control of a polytopic ERAD substrate. *J. Cell Sci.* **127**: 2898–2909.
- Peng, L., Cai, W., and Shikanai, T. (2010). Chloroplast stromal proteins, CRR6 and CRR7, are required for assembly of the NAD(P)H dehydrogenase subcomplex A in *Arabidopsis*. *Plant J.* **63**: 203–211.
- Perez, D.M. (2005). From plants to man: The GPCR “tree of life.” *Mol. Pharmacol.* **67**: 1383–1384.
- PETIT, J.-M., BRIAT, J.-F., and LOBRÉAUX, S. (2001). Structure and differential expression of the four members of the *Arabidopsis thaliana* ferritin gene family. *Biochem. J.* **359**: 575–582.
- Pettersson, P., Patrick, J., Jakob, M., Jacobs, M., Klösgen, R.B., Wennmalm, S., and Mäler, L. (2021). Soluble TatA forms oligomers that interact with membranes: Structure and insertion studies of a versatile protein transporter. *Biochim. Biophys. Acta - Biomembr.* **1863**.
- Pfeffer, S., Burbaum, L., Unverdorben, P., Pech, M., Chen, Y., Zimmermann, R., Beckmann, R., and Förster, F. (2015). Structure of the native Sec61 protein-conducting channel. *Nat. Commun.* **6**: 8403.
- Picking, W.D., Picking, W.L., Odom, O.W., and Hardesty, B. (1992). Fluorescence characterization of the

REFERENCES

- environment encountered by nascent polyalanine and polyserine as they exit *Escherichia coli* ribosomes during translation. *Biochemistry* **31**: 2368–2375.
- Pilon, M., De Kruijff, B., and Weisbeek, P.J. (1992). New insights into the import mechanism of the ferredoxin precursor into chloroplasts. *J. Biol. Chem.* **267**: 2548–2556.
- Pleiner, T., Tomaleri, G.P., Januszyk, K., Inglis, A.J., Hazu, M., and Voorhees, R.M. (2020). Structural basis for membrane insertion by the human ER membrane protein complex. *Science* (80-.). **369**: 433–436.
- Pohlmeier, K., Soll, J., Grimm, R., Hill, K., and Wagner, R. (1998). A high-conductance solute channel in the chloroplastic outer envelope from Pea. *Plant Cell* **10**: 1207–1216.
- Popov, N., Schmitt, M., Schulzeck, S., and Matthies, H. (1975). [Reliable micromethod for determination of the protein content in tissue homogenates]. *Acta Biol. Med. Ger.* **34**: 1441–1446.
- Powers, T. and Walter, P. (1996). The nascent polypeptide-associated complex modulates interactions between the signal recognition particle and the ribosome. *Curr. Biol.* **6**: 331–338.
- Powis, K., Schrul, B., Tienson, H., Gostimskaya, I., Breker, M., High, S., Schuldiner, M., Jakob, U., and Schwappach, B. (2013). Get3 is a holdase chaperone and moves to deposition sites for aggregated proteins when membrane targeting is blocked. *J. Cell Sci.* **126**: 473–483.
- Pyhtila, B., Zheng, T., Lager, P.J., Keene, J.D., Reedy, M.C., and Nicchitta, C. V (2008). Signal sequence- and translation-independent mRNA localization to the endoplasmic reticulum. *RNA* **14**: 445–453.
- Rachubinski, R.A., Verma, D.P., and Bergeron, J.J. (1980). Synthesis of rat liver microsomal cytochrome b5 by free ribosomes. *J. Cell Biol.* **84**: 705–716.
- Rapoport, T.A. (1992). Transport of proteins across the endoplasmic reticulum membrane. *Science* (80-.). **258**: 931–936.
- Rappsilber, J., Mann, M., and Ishihama, Y. (2007). Protocol for micro-purification, enrichment, pre-fractionation and storage of peptides for proteomics using StageTips. *Nat. Protoc.* **2**: 1896–1906.
- Reinbothe, S., Quigley, F., Springer, A., Schemenewitz, A., and Reinbothe, C. (2004). The outer plastid envelope protein Oep16: Role as precursor translocase in import of protochlorophyllide oxidoreductase A. *Proc. Natl. Acad. Sci. U. S. A.* **101**: 2203–2208.
- Richter, S., Zhong, R., and Lamppa, G. (2005). Function of the stromal processing peptidase in the chloroplast import pathway. *Physiol. Plant.* **123**: 362–368.
- Rödiger, A., Baudisch, B., and Bernd Klösigen, R. (2010). Simultaneous isolation of intact mitochondria and chloroplasts from a single pulping of plant tissue. *J. Plant Physiol.* **167**: 620–624.
- Rodrigo-Brenni, M.C., Gutierrez, E., and Hegde, R.S. (2014). Cytosolic Quality Control of Mislocalized Proteins Requires RNF126 Recruitment to Bag6. *Mol. Cell* **55**: 227–237.
- Roesler, K.R., Shorrosh, B.S., and Ohlrogge, J.B. (1994). Structure and Expression of an Arabidopsis Acetyl-

REFERENCES

- Coenzyme A Carboxylase Gene. *Plant Physiol.* **105**: 611 LP – 617.
- Rome, M.E., Rao, M., Clemons, W.M., and Shan, S.O. (2013). Precise timing of ATPase activation drives targeting of tail-anchored proteins. *Proc. Natl. Acad. Sci. U. S. A.* **110**: 7666–7671.
- Roston, R.L., Gao, J., Murcha, M.W., Whelan, J., and Benning, C. (2012). TGD1, -2, and -3 proteins involved in lipid trafficking form ATP-binding cassette (ABC) transporter with multiple substrate-binding proteins. *J. Biol. Chem.* **287**: 21406–21415.
- Roy, L.M. and Barkan, A. (1998). A SecY homologue is required for the elaboration of the chloroplast thylakoid membrane and for normal chloroplast gene expression. *J. Cell Biol.* **141**: 385–395.
- Roychoudhury, A., Basu, S., and Sengupta, D.N. (2009). Analysis of comparative efficiencies of different transformation methods of *E. coli* using two common plasmid vectors. *Indian J. Biochem. Biophys.* **46**: 395–400.
- Rudhe, C., Chew, O., Whelan, J., and Glaser, E. (2002). A novel in vitro system for simultaneous import of precursor proteins into mitochondria and chloroplasts. *Plant J.* **30**: 213–220.
- Rudolf, M., MacHettira, A.B., Groß, L.E., Weber, K.L., Bolte, K., Bionda, T., Sommer, M.S., Maier, U.G., Weber, A.P.M., Schleiff, E., and Tripp, J. (2013). In vivo function of Tic22, a protein import component of the intermembrane space of chloroplasts. *Mol. Plant* **6**: 817–829.
- Rutz, C., Klein, W., and Schüle, R. (2015). N-terminal signal peptides of G protein-coupled receptors: Significance for receptor biosynthesis, trafficking, and signal transduction. *Prog. Mol. Biol. Transl. Sci.* **132**: 267–287.
- Sambrook, J. and Russel, D.W. (2001). *Molecular cloning - Sambrook and Russel*-Vol. 1, 2, 3.
- Saraste, M., Sibbald, P.R., and Wittinghofer, A. (1990). The P-loop--a common motif in ATP- and GTP-binding proteins. *Trends Biochem. Sci.* **15**: 430–434.
- Schägger, H. (2006). Tricine-SDS-PAGE. *Nat. Protoc.* **1**: 16–22.
- Schleiff, E. and Becker, T. (2011). Common ground for protein translocation: Access control for mitochondria and chloroplasts. *Nat. Rev. Mol. Cell Biol.* **12**: 48–59.
- Schleiff, E. and Soll, J. (2000). Travelling of proteins through membranes: translocation into chloroplasts. *Planta* **211**: 449–456.
- Schleiff, E., Soll, J., Küchler, M., Kühlbrandt, W., and Harrer, R. (2003). Characterization of the translocon of the outer envelope of chloroplasts. *J. Cell Biol.* **160**: 541–551.
- Schneiderei, J., Häusler, R.E., Fiene, G., Kaiser, W.M., and Weber, A.P.M. (2006). Antisense repression reveals a crucial role of the plastidic 2-oxoglutarate/malate translocator DiT1 at the interface between carbon and nitrogen metabolism. *Plant J.* **45**: 206–224.
- Schuenemann, D., Amin, P., Hartmann, E., and Hoffman, N.E. (1999). Chloroplast SecY is complexed to SecE and involved in the translocation of the 33-kDa but not the 23-kDa subunit of the oxygen-

- evolving complex. *J. Biol. Chem.* **274**: 12177–12182.
- Schuenemann, D., Gupta, S., Persello-Cartieaux, F., Klimyuk, V.I., Jones, J.D.G., Nussaume, L., and Hoffman, N.E. (1998). A novel signal recognition particle targets light-harvesting proteins to the thylakoid membranes. *Proc. Natl. Acad. Sci. U. S. A.* **95**: 10312–10316.
- Schuldiner, M., Collins, S.R., Thompson, N.J., Denic, V., Bhamidipati, A., Punna, T., Ihmels, J., Andrews, B., Boone, C., Greenblatt, J.F., Weissman, J.S., and Krogan, N.J. (2005). Exploration of the function and organization of the yeast early secretory pathway through an epistatic miniarray profile. *Cell* **123**: 507–519.
- Schuldiner, M., Metz, J., Schmid, V., Denic, V., Rakwalska, M., Schmitt, H.D., Schwappach, B., and Weissman, J.S. (2008). The GET Complex Mediates Insertion of Tail-Anchored Proteins into the ER Membrane. *Cell* **134**: 634–645.
- Schünemann, D. (2007). Mechanisms of protein import into thylakoids of chloroplasts. *Biol. Chem.* **388**: 907–915.
- Schwenker, S., Netz, D.J.A., Frazzon, J., Pierik, A.J., Bill, E., Gross, J., Lill, R., and Meurer, J. (2010). Chloroplast HCF101 is a scaffold protein for [4Fe-4S] cluster assembly. *Biochem. J.* **425**: 207–214.
- Schwenkert, S., Netz, D.J.A., Frazzon, J., Pierik, A.J., Bill, E., Gross, J., Lill, R., and Meurer, J. (2009). Chloroplast HCF101 is a scaffold protein for [4Fe-4S] cluster assembly. *Biochem. J.* **425**: 207–218.
- Serrano, M., Robatzek, S., Torres, M., Kombrink, E., Somssich, I.E., Robinson, M., and Schulze-Lefert, P. (2007). Chemical interference of pathogen-associated molecular pattern-triggered immune responses in Arabidopsis reveals a potential role for fatty-acid synthase type II complex-derived lipid signals. *J. Biol. Chem.* **282**: 6803–6811.
- Sétif, P., Fischer, N., Lagoutte, B., Bottin, H., and Rochaix, J.D. (2002). The ferredoxin docking site of photosystem I. *Biochim. Biophys. Acta - Bioenerg.* **1555**: 204–209.
- Shao, S., Rodrigo-Brenni, M.C., Kivlen, M.H., and Hegde, R.S. (2017). Mechanistic basis for a molecular triage reaction. *Science (80-.)*. **355**: 298–302.
- Shen, G., Kuppu, S., Venkataramani, S., Wang, J., Yan, J., Qiu, X., and Zhang, H. (2010). ANKYRIN REPEAT-CONTAINING PROTEIN 2A Is an essential molecular chaperone for peroxisomal membrane-bound ASCORBATE PEROXIDASE3 in Arabidopsis. *Plant Cell* **22**: 811–831.
- Shen, J., Hsu, C.-M., Kang, B.-K., Rosen, B.P., and Bhattacharjee, H. (2003). The *Saccharomyces cerevisiae* Arr4p is involved in metal and heat tolerance. *Biometals an Int. J. role Met. ions Biol. Biochem. Med.* **16**: 369–378.
- Shi, L.X. and Schröder, W.P. (2004). The low molecular mass subunits of the photosynthetic supracomplex, photosystem II. *Biochim. Biophys. Acta - Bioenerg.* **1608**: 75–96.
- Shikanai, T. (2016). Chloroplast NDH: A different enzyme with a structure similar to that of respiratory

REFERENCES

- NADH dehydrogenase. *Biochim. Biophys. Acta - Bioenerg.* **1857**: 1015–1022.
- Simm, S., Keller, M., Selymes, M., and Schleiff, E.** (2015). The composition of the global and feature specific cyanobacterial core-genomes. *Front. Microbiol.* **6**: 219.
- Simon, S.M. and Blobel, G.** (1991). A protein-conducting channel in the endoplasmic reticulum. *Cell* **65**: 371–380.
- Small, I., Peeters, N., Legeai, F., and Lurin, C.** (2004). Predotar: A tool for rapidly screening proteomes for N-terminal targeting sequences. *Proteomics* **4**: 1581–1590.
- Smeekens, S., Bauerle, C., Hageman, J., Keegstra, K., and Weisbeek, P.** (1986). The role of the transit peptide in the routing of precursors toward different chloroplast compartments. *Cell* **46**: 365–375.
- Sommer, M., Rudolf, M., Tillmann, B., Tripp, J., Sommer, M.S., and Schleiff, E.** (2013). Toc33 and Toc64-III cooperate in precursor protein import into the chloroplasts of *Arabidopsis thaliana*. *Plant, Cell Environ.* **36**: 970–983.
- Srivastava, R., Zalisko, B.E., Keenan, R.J., and Howell, S.H.** (2017). The GET system inserts the tail-anchored protein, SYP72, into Endoplasmic Reticulum Membranes. *Plant Physiol.* **173**: 1137–1145.
- Stefanovic, S. and Hegde, R.S.** (2007). Identification of a Targeting Factor for Posttranslational Membrane Protein Insertion into the ER. *Cell* **128**: 1147–1159.
- Stefer, S., Reitz, S., Wang, F., Wild, K., Pang, Y., Bomke, J., Hein, C., Löhr, F., and Bernhard, F.** (2013). NIH Public Access. **333**: 758–762.
- Stock, D., Gibbons, C., Arechaga, I., Leslie, A.G.W., and Walker, J.E.** (2000). The rotary mechanism of ATP synthase. *Curr. Opin. Struct. Biol.* **10**: 672–679.
- Strand, D.D., Fisher, N., and Kramer, D.M.** (2017). The higher plant plastid NAD(P)H dehydrogenase-like complex (NDH) is a high efficiency proton pump that increases ATP production by cyclic electron flow. *J. Biol. Chem.* **292**: 11850–11860.
- Stroebel, D., Choquet, Y., Popot, J.-L., and Picot, D.** (2003). An atypical haem in the cytochrome b(6)f complex. *Nature* **426**: 413–418.
- Suloway, C.J.M., Rome, M.E., and Clemons, W.M.** (2012). Tail-anchor targeting by a Get3 tetramer: The structure of an archaeal homologue. *EMBO J.* **31**: 707–719.
- Sun, F., Huo, X., Zhai, Y., Wang, A., Xu, J., Su, D., Bartlam, M., and Rao, Z.** (2005). Crystal structure of mitochondrial respiratory membrane protein complex II. *Cell* **121**: 1043–1057.
- Sun, Y., Yang, R., Li, L., and Huang, J.** (2017). The Magnesium Transporter MGT10 Is Essential for Chloroplast Development and Photosynthesis in *Arabidopsis thaliana*. *Mol. Plant* **10**: 1584–1587.
- Suorsa, M., Sirpiö, S., Paakkarinen, V., Kumari, N., Holmström, M., and Aro, E.-M.** (2010). Two Proteins Homologous to PsbQ are Novel Subunits of the Chloroplast NAD(P)H Dehydrogenase. *Plant Cell*

- Physiol. **51**: 877–883.
- Tan, F.-C., Cheng, Q., Saha, K., Heinemann, I.U., Jahn, M., Jahn, D., and Smith, A.G.** (2008). Identification and characterization of the Arabidopsis gene encoding the tetrapyrrole biosynthesis enzyme uroporphyrinogen III synthase. *Biochem. J.* **410**: 291–299.
- Thalhammer, A., Hundertmark, M., Popova, A. V., Seckler, R., and Hinch, D.K.** (2010). Interaction of two intrinsically disordered plant stress proteins (COR15A and COR15B) with lipid membranes in the dry state. *Biochim. Biophys. Acta - Biomembr.* **1798**: 1812–1820.
- Thompson, S.J., Kim, S.J., and Robinson, C.** (1998). Sec-independent Insertion of Thylakoid Membrane Proteins ANALYSIS OF INSERTION FORCES AND IDENTIFICATION OF A LOOP INTERMEDIATE INVOLVING THE. *J. Biol. Chem.* **273**: 18979–18983.
- Thompson, S.J., Robinson, C., and Mant, A.** (1999). Dual Signal Peptides Mediate the Signal Recognition Particle / Sec-independent Insertion of a Thylakoid Membrane Polyprotein , PsbY *. *J. Biol. Chem.* **274**: 4059–4066.
- Towbin, H., Staehelin, T., and Gordon, J.** (1992). Electrophoretic transfer of proteins from polyacrylamide gels to nitrocellulose sheets: procedure and some applications. 1979. *Biotechnology* **24**: 145–149.
- Trentmann, O., Mühlhaus, T., Zimmer, D., Sommer, F., Schroda, M., Haferkamp, I., Keller, I., Pommerrenig, B., and Neuhaus, H.E.** (2020). Identification of chloroplast envelope proteins with critical importance for cold acclimation. *Plant Physiol.* **182**: 1239–1255.
- Tsirigotaki, A., De Geyter, J., Šoštarić, N., Economou, A., and Karamanou, S.** (2017). Protein export through the bacterial Sec pathway. *Nat. Rev. Microbiol.* **15**: 21–36.
- Tu, C.J., Peterson, E.C., Henry, R., and Hoffman, N.E.** (2000). The L18 domain of light-harvesting chlorophyll proteins binds to chloroplast signal recognition particle 43. *J. Biol. Chem.* **275**: 13187–13190.
- Tung, J.Y., Li, Y.C., Lin, T.W., and Hsiao, C.D.** (2013). Structure of the Sgt2 dimerization domain complexed with the Get5 UBL domain involved in the targeting of tail-anchored membrane proteins to the endoplasmic reticulum. *Acta Crystallogr. Sect. D Biol. Crystallogr.* **69**: 2081–2090.
- Tyanova, S. and Cox, J.** (2018). Perseus: A Bioinformatics Platform for Integrative Analysis of Proteomics Data in Cancer Research. *Methods Mol. Biol.* **1711**: 133–148.
- Uhrigshardt, H., Singh, A., Kovtunovych, G., Ghosh, M., and Rouault, T.A.** (2010). Characterization of the human HSC20, an unusual DnaJ type III protein, involved in iron-sulfur cluster biogenesis. *Hum. Mol. Genet.* **19**: 3816–3834.
- Uniacke, J. and Zerges, W.** (2008). Stress induces the assembly of RNA granules in the chloroplast of *Chlamydomonas reinhardtii*. *J. Cell Biol.* **182**: 641–644.
- Uversky, V.N.** (2017). Protein intrinsic disorder-based liquid–liquid phase transitions in biological

- systems: Complex coacervates and membrane-less organelles. *Adv. Colloid Interface Sci.* **239**: 97–114.
- Vermeulen, M., Hubner, N.C., and Mann, M.** (2008). High confidence determination of specific protein-protein interactions using quantitative mass spectrometry. *Curr. Opin. Biotechnol.* **19**: 331–337.
- Vilardi, F., Lorenz, H., and Dobberstein, B.** (2011). WRB is the receptor for TRC40/Asna1-mediated insertion of tail-anchored proteins into the ER membrane. *J. Cell Sci.* **124**: 1301–1307.
- Vilardi, F., Stephan, M., Clancy, A., Janshoff, A., and Schwappach, B.** (2014). WRB and CAML are necessary and sufficient to mediate tail-anchored protein targeting to the ER membrane. *PLoS One* **9**.
- Vojta, L., Tomašić Paić, A., Horvat, L., Rac, A., Lepeduš, H., and Fulgosi, H.** (2019). Complex luminal immunophilin AtCYP38 influences thylakoid remodelling in *Arabidopsis thaliana*. *J. Plant Physiol.* **243**.
- Voss, N.R., Gerstein, M., Steitz, T.A., and Moore, P.B.** (2006). The geometry of the ribosomal polypeptide exit tunnel. *J. Mol. Biol.* **360**: 893–906.
- Voth, W., Schick, M., Gates, S., Li, S., Vilardi, F., Gostimskaya, I., Southworth, D.R., Schwappach, B., and Jakob, U.** (2014). The protein targeting factor Get3 functions as ATP-Independent chaperone under oxidative stress conditions. *Mol. Cell* **56**: 116–127.
- de Vries, J., Sousa, F.L., Bölter, B., Soll, J., and Goulda, S.B.** (2015). YCF1: A green TIC? *Plant Cell* **27**: 1827–1833.
- Wallin, E. and Von Heijne, G.** (1998). Genome-wide analysis of integral membrane proteins from eubacterial, archaean, and eukaryotic organisms. *Protein Sci.* **7**: 1029–1038.
- Walter, B., Hristou, A., Nowaczyk, M.M., and Schünemann, D.** (2015). In vitro reconstitution of co-translational D1 insertion reveals a role of the cpSec-Alb3 translocase and Vipp1 in Photosystem II biogenesis. *Biochem. J.* **468**: 315–324.
- Walter, P. and Blobel, G.** (1982). Signal recognition particle contains a 7S RNA essential for protein translocation across the endoplasmic reticulum. *Nature* **299**: 691–698.
- Walter, P., Ibrahimi, I., and Blobel, G.** (1981). Translocation of proteins across the endoplasmic reticulum. I. Signal recognition protein (SRP) binds to in-vitro-assembled polysomes synthesizing secretory protein. *J. Cell Biol.* **91**: 545–550.
- Walter, T. and Erdmann, R.** (2019). Current Advances in Protein Import into Peroxisomes. *Protein J.* **38**: 351–362.
- Wang, D.N. and Kühlbrandt, W.** (1991). High-resolution electron crystallography of light-harvesting chlorophyll a/b-protein complex in three different media. *J. Mol. Biol.* **217**: 691–699.
- Wang, F., Brown, E.C., Mak, G., Zhuang, J., and Denic, V.** (2010). A chaperone cascade sorts proteins for posttranslational membrane insertion into the endoplasmic reticulum. *Mol. Cell* **40**: 159–171.

- Wang, F., Chan, C., Weir, N.R., and Denic, V. (2014). The Get1/2 transmembrane complex is an endoplasmic-reticulum membrane protein insertase. *Nature* **512**: 441–444.
- Wang, F., Whynot, A., Tung, M., and Denic, V. (2013). *Membrane*. **43**: 738–750.
- Wang, M., Rui, L., Yan, H., Shi, H., Zhao, W., Lin, J.E., Zhang, K., Blakeslee, J.J., Mackey, D., Tang, D., Wei, Z., and Wang, G.L. (2018). The major leaf ferredoxin Fd2 regulates plant innate immunity in *Arabidopsis*. *Mol. Plant Pathol.* **19**: 1377–1390.
- Watson, H. (2015). Biological membranes. *Essays Biochem.* **59**: 43–70.
- Wei, X., Su, X., Cao, P., Liu, X., Chang, W., Li, M., Zhang, X., and Liu, Z. (2016). Structure of spinach photosystem II-LHCII supercomplex at 3.2 Å resolution. *Nature* **534**: 69–74.
- Weigel, M., Varotto, C., Pesaresi, P., Finazzi, G., Rappaport, F., Salamini, F., and Leister, D. (2003). Plastocyanin is indispensable for photosynthetic electron flow in *Arabidopsis thaliana*. *J. Biol. Chem.* **278**: 31286–31289.
- Whelan, J., Editors, M.W.M., and Walker, J.M. (2015). *Mitochondria IN Series Editor*.
- White, S.H. and Von Heijne, G. (2008). How translocons select transmembrane helices. *Annu. Rev. Biophys.* **37**: 23–42.
- White, T.J., Arnheim, N., and Erlich, H.A. (1989). The polymerase chain reaction. *Trends Genet.* **5**: 185–189.
- Whitney, S.M., Birch, R., Kelso, C., Beck, J.L., and Kapralov, M. V. (2015). Improving recombinant Rubisco biogenesis, plant photosynthesis and growth by coexpressing its ancillary RAF1 chaperone. *Proc. Natl. Acad. Sci. U. S. A.* **112**: 3564–3569.
- Wicke, S., Schneeweiss, G.M., dePamphilis, C.W., Müller, K.F., and Quandt, D. (2011). The evolution of the plastid chromosome in land plants: Gene content, gene order, gene function. *Plant Mol. Biol.* **76**: 273–297.
- Wiedemann, N. and Pfanner, N. (2017). Mitochondrial machineries for protein import and assembly. *Annu. Rev. Biochem.* **86**: 685–714.
- Wittig, I., Braun, H.P., and Schagger, H. (2006). Blue native PAGE. *Nat. Protoc.* **1**: 418–428.
- Wittinghofer, A. and Vetter, I.R. (2011). Structure-function relationships of the G domain, a canonical switch motif. *Annu. Rev. Biochem.* **80**: 943–971.
- Wu, G.-Z. and Xue, H.-W. (2010). *Arabidopsis*; β -Ketoacyl-[Acyl Carrier Protein] Synthase I Is Crucial for Fatty Acid Synthesis and Plays a Role in Chloroplast Division and Embryo Development. *Plant Cell* **22**: 3726 LP – 3744.
- Wunderley, L., Leznicki, P., Payapilly, A., and High, S. (2014). SGTA regulates the cytosolic quality control of hydrophobic substrates. *J. Cell Sci.* **127**: 4728–4739.

REFERENCES

- Xing, S., Mehlhorn, D.G., Wallmeroth, N., Asseck, L.Y., Kar, R., Voss, A., Denninger, P., Schmidt, V.A.F., Schwarzländer, M., Stierhof, Y.D., Grossmann, G., and Grefen, C. (2017). Loss of GET pathway orthologs in *Arabidopsis thaliana* causes root hair growth defects and affects SNARE abundance. *Proc. Natl. Acad. Sci. U. S. A.* **114**: E1544–E1553.
- Xu, X.M. and Møller, S.G. (2004). AtNAP7 is a plastidic SufC-like ATP-binding cassette/ATPase essential for *Arabidopsis* embryogenesis. *Proc. Natl. Acad. Sci. U. S. A.* **101**: 9143–9148.
- Xu, Y., Cai, M., Yang, Y., Huang, L., and Ye, Y. (2012). SGTA Recognizes a Noncanonical Ubiquitin-like Domain in the Bag6-Ubl4A-Trc35 Complex to Promote Endoplasmic Reticulum-Associated Degradation. *Cell Rep.* **2**: 1633–1644.
- Yabe, T., Morimoto, K., Kikuchi, S., Nishio, K., Terashima, I., and Nakai, M. (2004). The *Arabidopsis* chloroplastic NifU-like protein CnfU, which can act as an iron-sulfur cluster scaffold protein, is required for biogenesis of ferredoxin and photosystem I. *Plant Cell* **16**: 993–1007.
- Yamamoto, Y. and Sakisaka, T. (2012). Molecular Machinery for Insertion of Tail-Anchored Membrane Proteins into the Endoplasmic Reticulum Membrane in Mammalian Cells. *Mol. Cell* **48**: 387–397.
- Yamamoto, Y. and Sakisaka, T. (2015). The emerging role of calcium-modulating cyclophilin ligand in posttranslational insertion of tail-anchored proteins into the endoplasmic reticulum membrane. *J. Biochem.* **157**: 419–429.
- Yang, H., Li, P., Zhang, A., Wen, X., Zhang, L., and Lu, C. (2017). Tetratricopeptide repeat protein Pyg7 is essential for photosystem I assembly by interacting with PsaC in *Arabidopsis*. *Plant J.* **91**: 950–961.
- Ye, H., Garifullina, G.F., Abdel-Ghany, S.E., Zhang, L., Pilon-Smits, E.A.H., and Pilon, M. (2005). The chloroplast NifS-like protein of *Arabidopsis thaliana* is required for iron-sulfur cluster formation in ferredoxin. *Planta* **220**: 602–608.
- Ye, Y., Fulcher, Y.G., Sliman, D.J., Day, M.T., Schroeder, M.J., Koppiseti, R.K., Bates, P.D., Thelen, J.J., and van Doren, S.R. (2020). The BADC and BCCP subunits of chloroplast acetyl-CoA carboxylase sense the pH changes of the light-dark cycle. *J. Biol. Chem.* **295**: 9901–9916.
- Yeh, Y.-H., Lin, T.-W., Li, Y.-C., Tung, J.-Y., Lin, C.-Y., and Hsiao, C.-D. (2014). Structural and Functional Characterization of Ybr137wp Implicates Its Involvement in the Targeting of Tail-Anchored Proteins to Membranes. *Mol. Cell. Biol.* **34**: 4500–4512.
- Yuan, J., Henry, R., Mccaffery, M., and Cline, K. (1994). SecA homolog in protein transport within chloroplasts: Evidence for endosymbiont-derived sorting. *Science* (80-.). **266**: 796–798.
- Zandalinas, S.I., Song, L., Sengupta, S., McInturf, S.A., Grant, D.A.G., Marjault, H.B., Castro-Guerrero, N.A., Burks, D., Azad, R.K., Mendoza-Cozatl, D.G., Nechushtai, R., and Mittler, R. (2020). Expression of a dominant-negative AtNEET-H89C protein disrupts iron–sulfur metabolism and iron homeostasis in *Arabidopsis*. *Plant J.* **101**: 1152–1169.

REFERENCES

- Zhang, L. and Aro, E.M. (2002). Synthesis, membrane insertion and assembly of the chloroplast-encoded D1 protein into photosystem II. *FEBS Lett.* **512**: 13–18.
- Zhang, L., Duan, Z., Zhang, J., and Peng, L. (2016). Biogenesis factor required for ATP synthase 3 facilitates assembly of the chloroplast ATP synthase complex. *Plant Physiol.* **171**: 1291–1306.
- Zhang, L., Kato, Y., Otters, S., Vothknecht, U.C., and Sakamoto, W. (2012). Essential role of VIPP1 in chloroplast envelope maintenance in Arabidopsis. *Plant Cell* **24**: 3695–3707.
- Zhang, L., Pu, H., Duan, Z., Li, Y., Liu, B., Zhang, Q., Li, W., Rochaix, J.D., Liu, L., and Peng, L. (2018). Nucleus-encoded protein BFA1 promotes efficient assembly of the chloroplast ATP synthase coupling factor 1. *Plant Cell* **30**: 1770–1788.
- Zhao, Q. and Liu, C. (2018). Chloroplast chaperonin: An intricate protein folding machine for photosynthesis. *Front. Mol. Biosci.* **4**: 1–12.
- Zopf, D., Bernstein, H.D., Johnson, A.E., and Walter, P. (1990). The methionine-rich domain of the 54 kd protein subunit of the signal recognition particle contains an RNA binding site and can be crosslinked to a signal sequence. *EMBO J.* **9**: 4511–4517.
- Zygadlo, A., Robinson, C., Scheller, H.V., Mant, A., and Jensen, P.E. (2006). The Properties of the Positively Charged Loop Region in PSI-G Are Essential for Its “ Spontaneous ” Insertion into Thylakoids and Rapid Assembly into the Photosystem I Complex * □. *J. Biol. Chem.* **281**: 10548–10554.



Figure S1. Sequence alignment of representative Get3 plant protein sequences of different orthologous groups. Multiple sequence alignment (MSA) was performed using MUSCLE with default parameter settings. The three sequences of *A. thaliana* Get3 (AT1G01910, AT3G10350, AT5G60730) as well as the three sequences of *Sorghum bicolor* were used for the MSA. The sequences of *S. bicolor* were distributed to the “a” clade (Sobic.002G268800_g1), “bc” clade (Sobic.004G238200_g2) as well as the distinct Monocot clade (Sobic.006G106600_g4). Note, no sequence of *S. bicolor* is present in the orthologous group 3 (At5G60730, Supplementary Table S1). On top the secondary structure annotation is given. Amino acids unique for a sequences of an orthologous group are colored. Also note the conserved C-terminal tripeptide with physicochemical properties (bulky hydrophobic-invariant tryptophan-positive) preceding α13. Adapted from (Bodensohn et al., 2019).

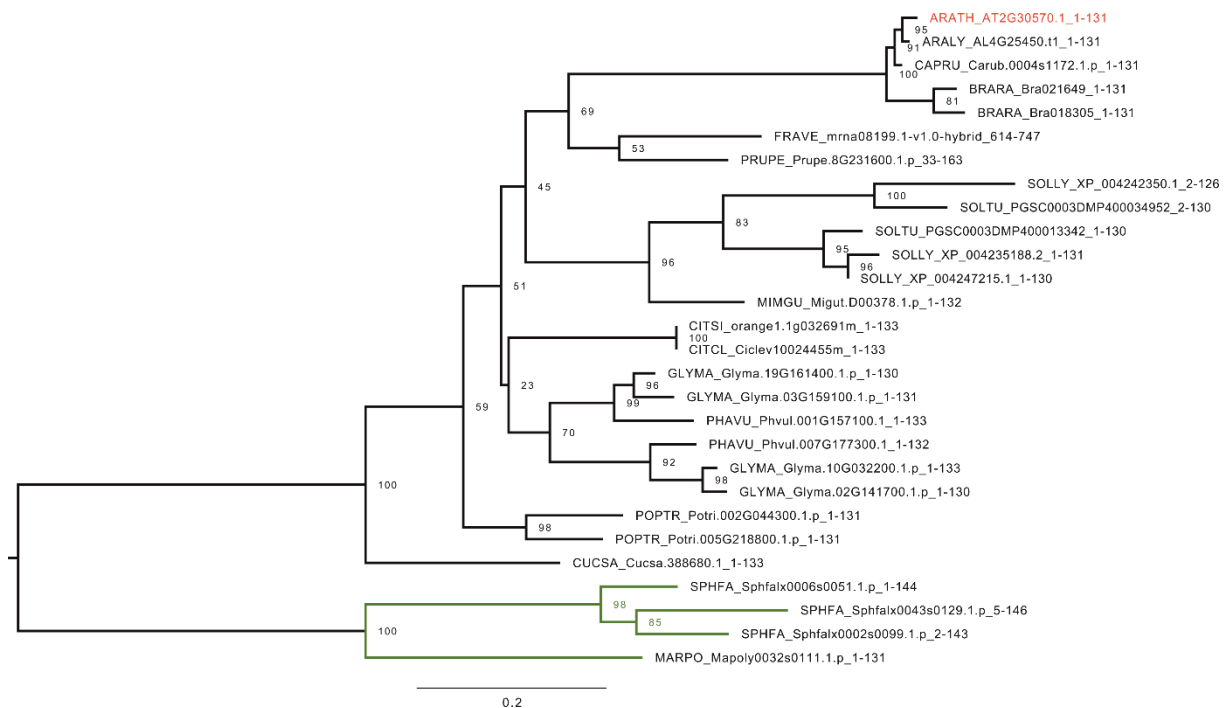


Figure S2. The Phylogenetic relation of PsbW in Viridiplantae. Maximum likelihood based phylogenetic tree of PsbW in the 52 examined Viridiplantae species. Tree branches belonging to Chlorophyta are green. The PsbW homologue of *A. thaliana* is shown in red. Note how PsbW does not occur in as many species as Get3 does (compare the branching of the proceeding trees).

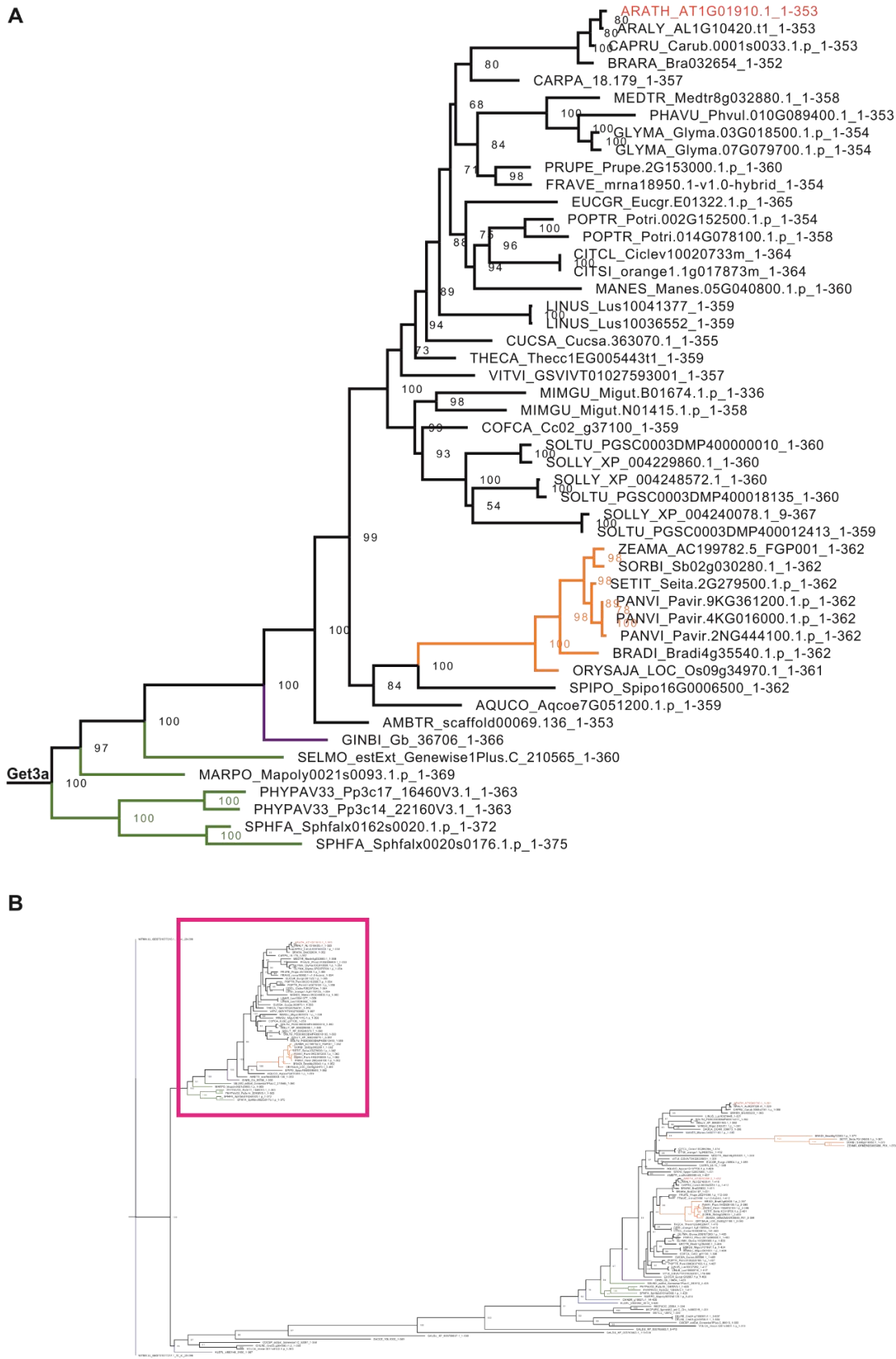


Figure S3. The Phylogenetic relation of GET3 domain in Viridiplantae.

Protein sequences of 52 Viridiplantae species were utilized to examine the phylogenetic relation of GET3 with *S. Cerevisiae* as out group. **A.** Enlargement of the area in the magenta rectangle in (B). Displaying the Get3a clade. **B.** Maximum likelihood based phylogenetic tree of GET3 in the 52 examined Viridiplantae species. Tree branches belonging to Chlorophyta are green, gymnosperms purple and species encompassing the $_{58}$ Get3 orthologues (see chapter 4.1) are orange. The Get3 orthologues of *A. thaliana* are illustrated in red. Clade names are shown in bold above their last common ancestor.



Figure S4. The Phylogenetic relation of GET3 domain in Viridiplantae.

Protein sequences of 52 Viridiplantae species were utilized to examine the phylogenetic relation of GET3 with *S. Cerevisiae* as out group. **A.** Resulting maximum likelihood based phylogenetic tree of GET3 in the 52 examined Viridiplantae species. **B.** Enlargement of the areas in the blue (top) and magenta (bottom) rectangles representing the Get3ab as well as Get3bc clades, respectively. Tree branches belonging to Chlorophyta are green, gymnosperms purple and species encompassing the _{SB}Get3 orthologues (see chapter 4.1) are orange. The Get3 orthologues of *A. thaliana* are illustrated in red. Clade names are shown in bold above their last common ancestor.



Figure S5. The Phylogenetic relation of GET3 domain in Viridiplantae.

Protein sequences of 52 Viridiplantae species were utilized to examine the phylogenetic relation of GET3 with *S. Cerevisiae* as out group. **A**. Enlargement of the area in the magenta rectangle in (B). Displaying the Get3b, Get3c _{sB}Get3 clade. **B**. Maximum likelihood based phylogenetic tree of GET3 in the 52 examined Viridiplantae species. Tree branches belonging to Chlorophyta are green, gymnosperms purple and species encompassing the _{sB}Get3 orthologues (see chapter 4.1) are orange. The Get3 orthologues of *A. thaliana* are illustrated in red. Asterisk in magenta denote the Get3b and Get3c clade members of *M. x varia* and the blue asterisk the Get3c clade member of *S. lycopersicum*. Clade names are shown in bold above their last common ancestor.

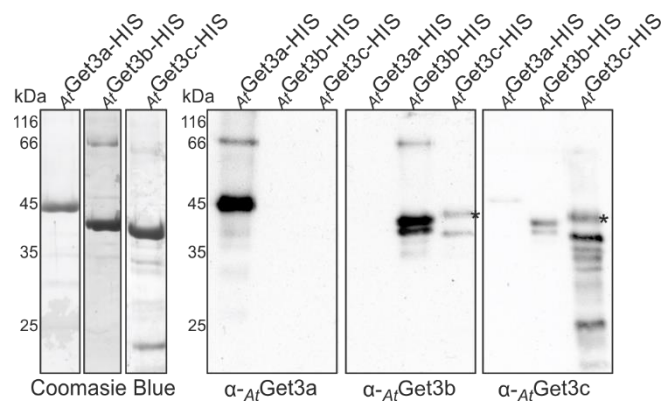


Figure S6. Get3 antibodies.

AtGet3a-His, *AtGet3b*-His and *AtGet3c*-His were expressed in *E. coli*. After cell lysis inclusion bodies were pelleted (6,000 xg, 15 min, 4°C), washed with (i) 50 mM Tris, 150mM NaCl, 1 mM EDTA, pH 8; (ii) 50 mM Tris, 2 M Urea, 10 mM MgSO₄, pH 8; and (iii) with 50 mM Tris, 0,5% Triton-X 100, 10 mM EDTA, pH 8. Inclusion bodies were solubilized in 50 mM Tris, 50 mM NaCl, 10 mM Imidazol, 8 M Urea, pH 8, centrifuged (25,000 xg, 10 min, 18°C) and the supernatant passed 3x over an Ni-NTA column (Qiagen, G). The column was washed with 10 column volumes (CV) (i) 50 mM Tris, 1 M NaCl, 15 mM Imidazol, 8 M Urea, pH 8; 10 CV (ii) 50 mM Tris, 15 mM NaCl, 15 mM Imidazol, 0,2% Triton-X 100, 8 M Urea, pH 8 and 10 CV (iii) 50 mM Tris, 50 mM NaCl, 10 mM Imidazol, 8 M Urea, pH 8. Protein was eluted in 5 CV 50 mM Tris, 50 mM NaCl, 400 mM Imidazol, 8 M Urea, pH 8. A fraction of the isolated protein (5 µg) was subjected to SDS-PAGE and stained with Coomassie Blue (left). 25 ng were subjected to SDS-PAGE, Western blotted and immunostained with indicated antibodies. The star indicates a cross-reaction with an *E. coli* protein. The antibody against the cytosolic *AtGet3a* did not recognize any of the other orthologues (α -*AtGet3a*), while the antibody against the putative chloroplast localized *AtGet3b* recognized *AtGet3c* (α -*AtGet3b*) to some extent. The antibody against the putative mitochondrial localized *AtGet3c* recognized *AtGet3a* and *AtGet3b* (α -*AtGet3c*).

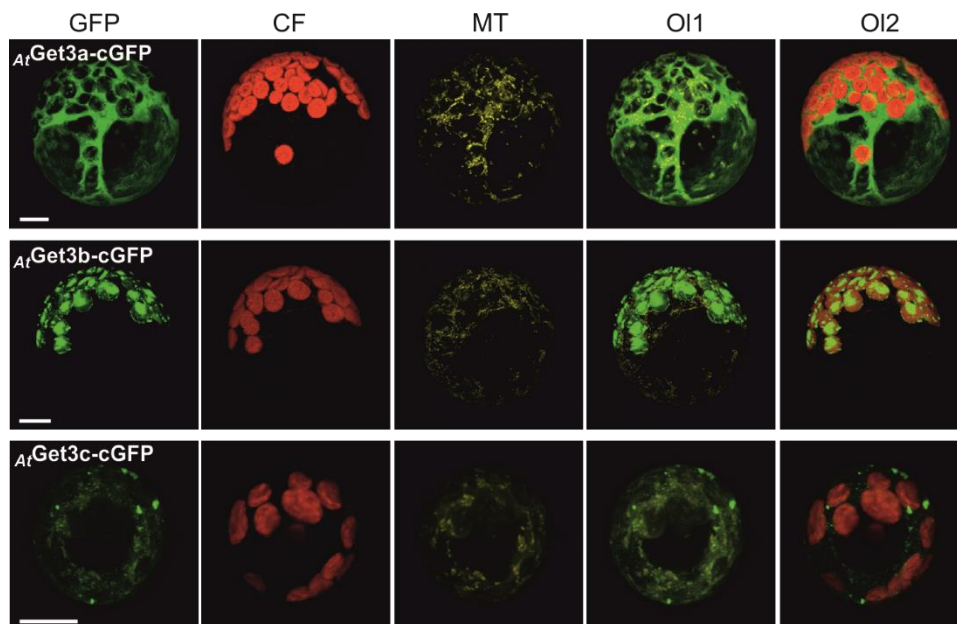


Figure S7. In vivo distribution of GFP tagged *AtGet3* proteins.

The *AtGet3* orthologues with C-terminal GFP-fusion were transfected into *A. thaliana* mesophyll protoplasts. After 16 h of expression, protoplasts were treated with MitoTracker Orange and subjected to confocal laser scanning microscopy (CLSM). GFP-fluorescence, chlorophyll-fluorescence (CF), MitoTracker signal (MT), overlays of GFP / MitoTracker signal (OI1), and of GFP / CF (OI2) are shown. The GFP-fluorescence after *AtGet3a*-cGFP expression indicated a cytosolic localization of the protein, as the signal was distinct from the chlorophyll-fluorescence and MitoTracker signal (upper panel). The GFP-fluorescence after *AtGet3b*-cGFP expression did not overlap with the MitoTracker signal (middle panel), but co-localized as patch-like structures with the chlorophyll-fluorescence indicative for stromal localization. The GFP-fluorescence of *AtGet3c*-cGFP was evenly distributed in the cytosol except for few punctuate structures partially co-localizing with the MitoTracker signal.

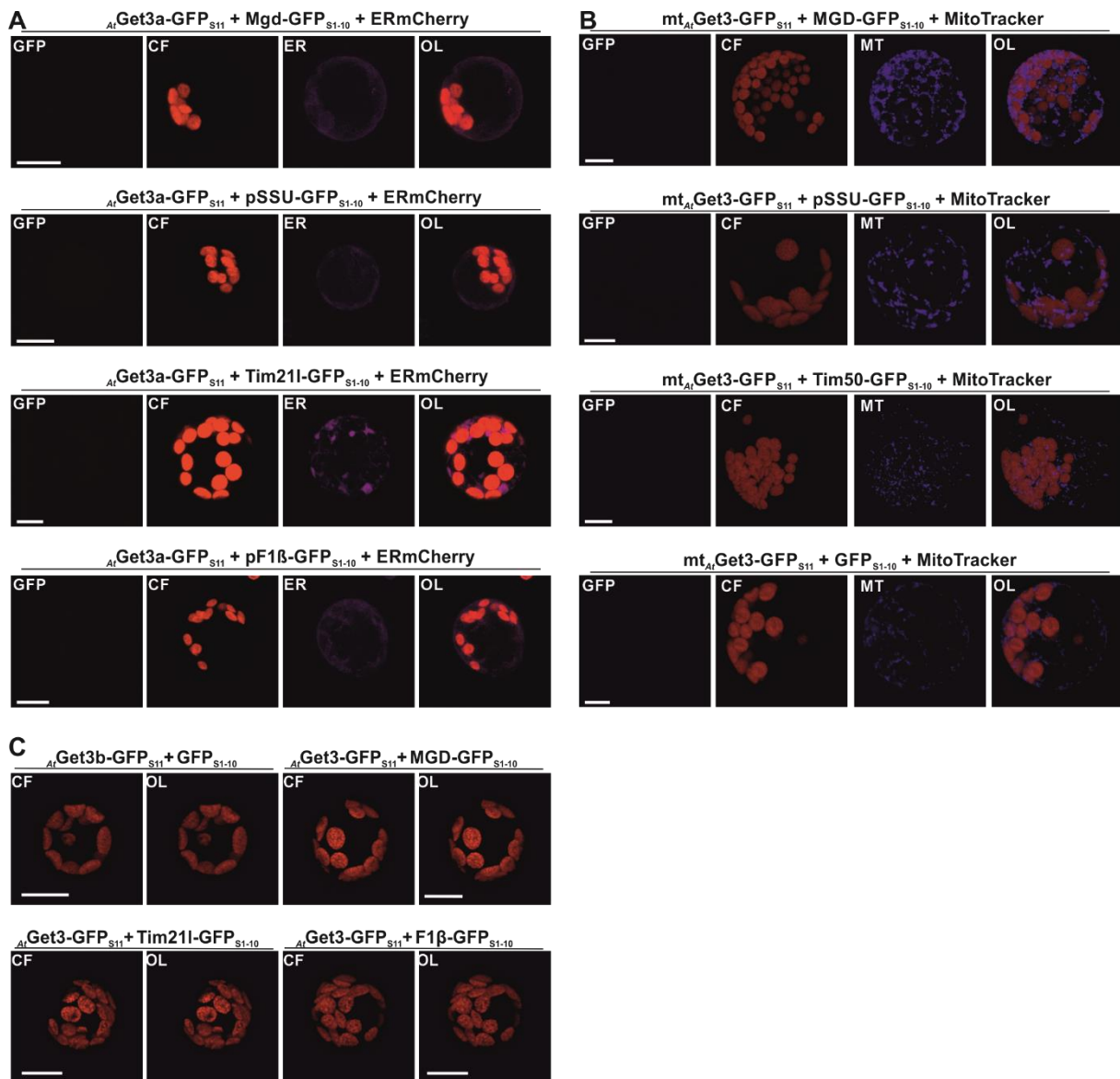


Figure S8. *AtGet3a* is specifically localized in the cytoplasm, *AtGet3b* in chloroplasts and *AtGet3c* in mitochondria. *A. thaliana* mesophyll protoplasts were co-transfected with **A.** *AtGet3a*-GFP_{S11} with Mgd-GFP_{S1-10} (top); pSSU-GFP_{S1-10} (second panel); Tim21-GFP_{S1-10} (third panel); pF1β-GFP_{S1-10} (fourth panel) and always ER-mCherry **B.** *AtGet3c*-GFP_{S1-10} with Mgd-GFP_{S1-10} (top); pSSU-GFP_{S1-10} (second panel); Tim50-GFP_{S1-10} (third panel); GFP_{S1-10} (fourth panel). **C.** *AtGet3b*-GFP_{S1-10} with GFP_{S1-10} (left half of top panel); Mgd-GFP_{S1-10} (right half of bottom panel); Tim21-GFP_{S1-10} (left half of bottom panel); pF1β-GFP_{S1-10} (right half of bottom panel). After 16 hours of 35-S promotor driven transient expression, protoplasts were subjected to confocal laser scanning microscopy (CLSM). In case of *AtGet3c*-GFP_{S11} protoplasts were incubated with MitoTracker. GFP-fluorescence (GFP), chlorophyll-fluorescence (CF), mCherry-fluorescence (A, ER), MitoTracker staining (B, MT) as well as overlays (OL) are shown. This figure is exemplarily for other control experiments.

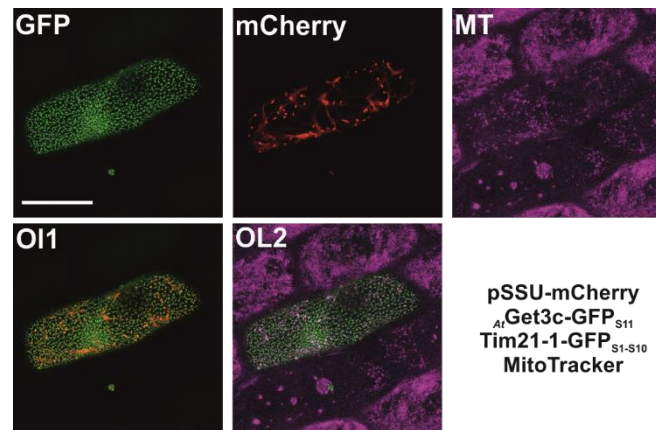


Figure S9. *At*Get3c is not localized in chloroplasts in *A. cepa* epidermal cells.

A. cepa cells were transfected with *At*Get3c-GFP_{S11}, pSSU-mCherry and Tim211-GFP_{S1-10} by biolistic transformation. Six hours after transfection cells were stained with MitoTracker. GFP-fluorescence (GFP), mCherry-fluorescence (mCherry), GFP- and mCherry-signal (OI1) as well as GFP-, mCherry- and Mitotracker-signal overlay (OI2) are shown.

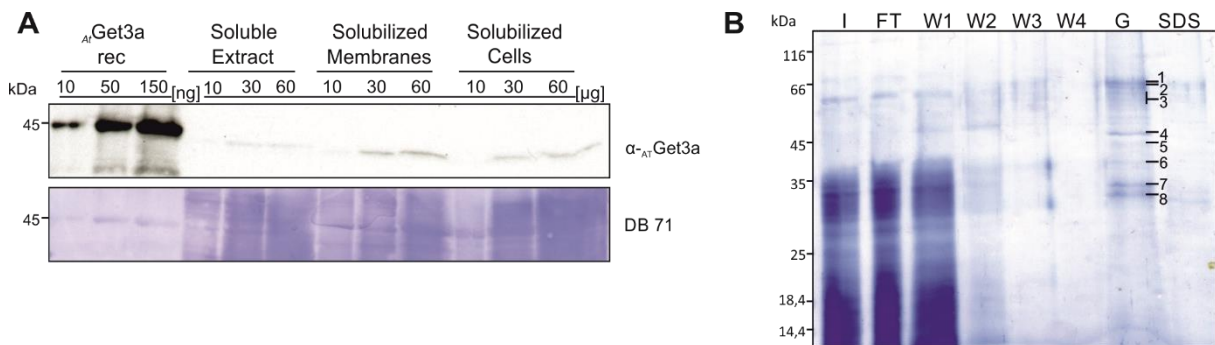


Figure S10. α -*At*Get3a co-precipitates candidates.

*A. At*Get3a protein abundance was approximated by comparing μ g amounts of differently recovered fractions (soluble cell extract without membranes, detergent solubilized total cell membranes, and total solubilized cells) to ng amounts of recombinant protein (*At*Get3a rec). **B.** Co-IP experiment from solubilized total cell extract with α -*At*Get3a antibodies. Shown are the proteins in input (I), flow through (FT), wash step 1 – 4 (W1-W4), the elution with glycine (G) and remaining on beads after elution (SDS). Eight bands of the glycine elution fraction were excised from the PAGE and utilized for mass spectrometry. Molecular weight marker in kDa on the left.

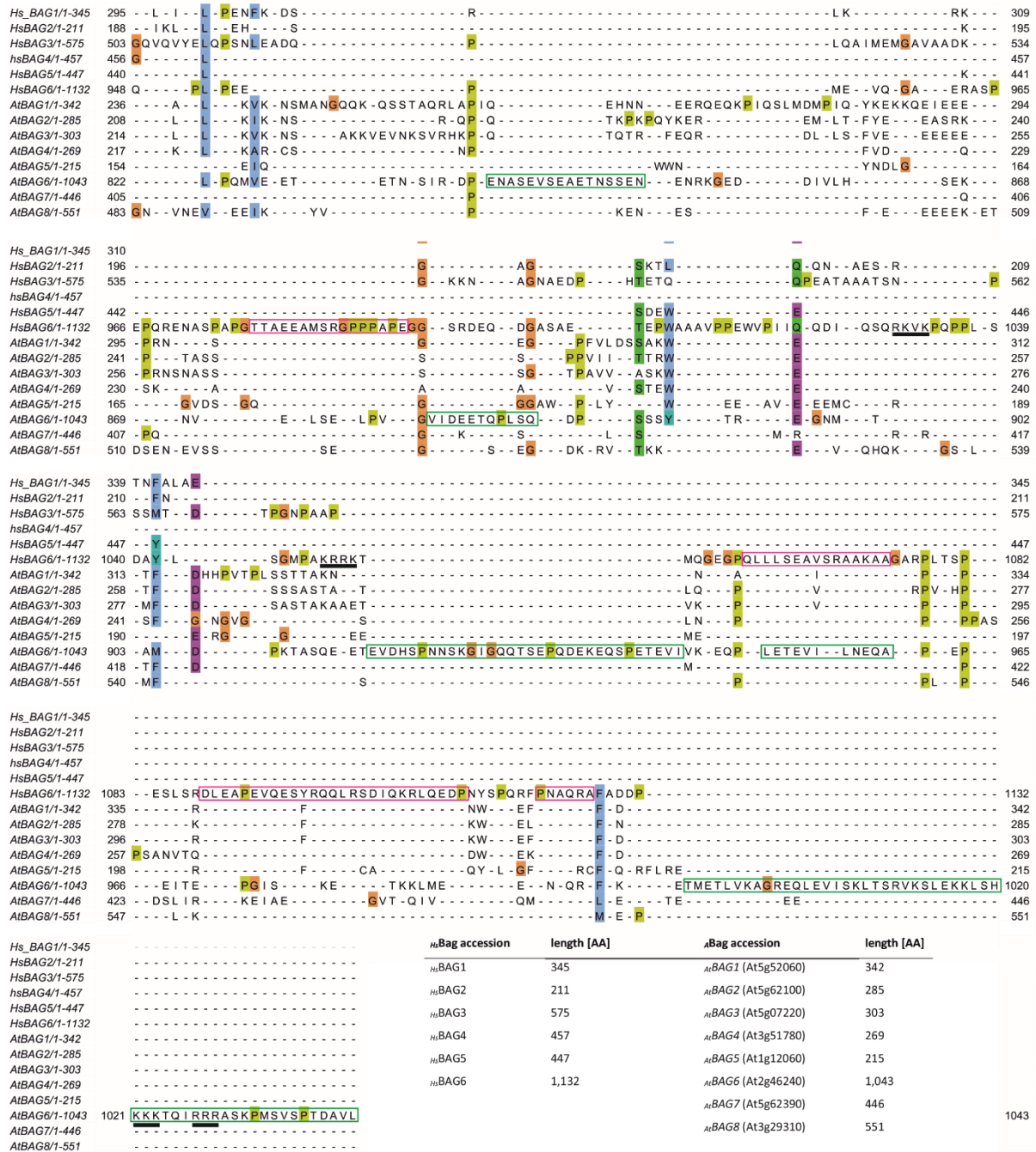


Figure S11. Sequence alignment of Bag6 homologues in *Homo sapiens* and *Arabidopsis thaliana*.

Multiple sequence alignment with MAFFT (Katoh et al., 2002) of the BAG domain of the indicated Bag protein orthologues. Insertions in the Bag6 proteins of *H. sapiens* and *A. thaliana* are highlighted in magenta and green boxes, respectively. Inlet displays the length in AAs of the individual Bag orthologues. Note how the *Hs*Bag6 and *At*Bag6 are both double the length than the biggest other orthologue of the respective group.

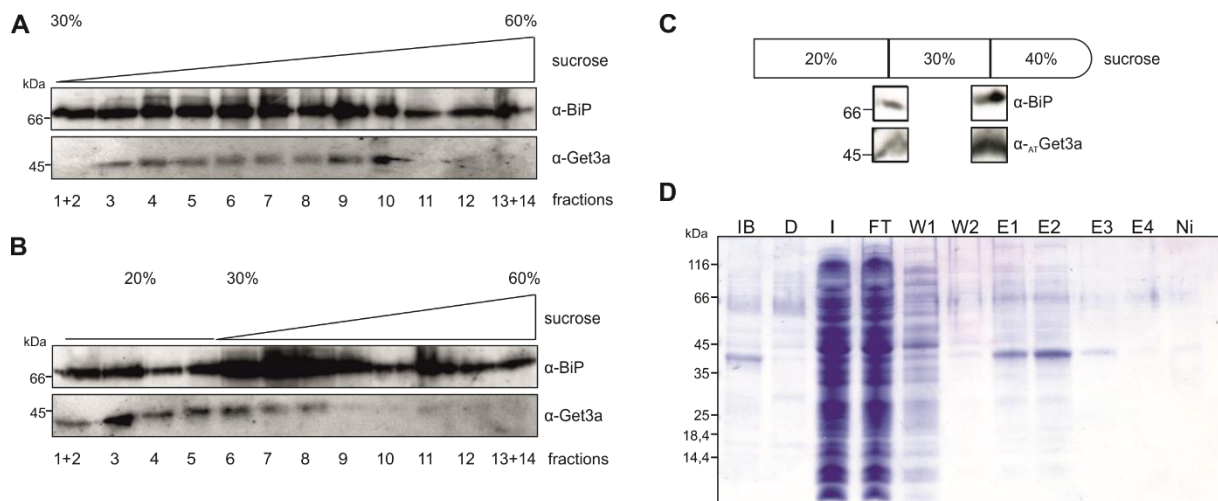


Figure S12. Optimizing microsomes isolation and recombinant *AtGet3* expression.

A. Linear sucrose gradient **B.** Linear sucrose gradient with cushion **C.** Discontinuous sucrose gradient. The illustrated fractions were immunologically examined for the concurrence of the indicated antibodies to isolate appropriate microsomes for TAT. Immunoblot signals are from the same gel **D.** Relocation of the hexahistidine tag from the C-terminus to the N-terminus leads to better solubility of recombinant expressed *AtGet3a*. Shown are inclusion body (IB), cellular debris (D), Ni-NTA input (I), wash (W1-2), soluble elution (E1-4) and eluted resin (Ni) fractions of the purification process. This figure is exemplary, relocation of the hexahistidine tag optimized the recombinant expression of all *AtGet3* orthologues.

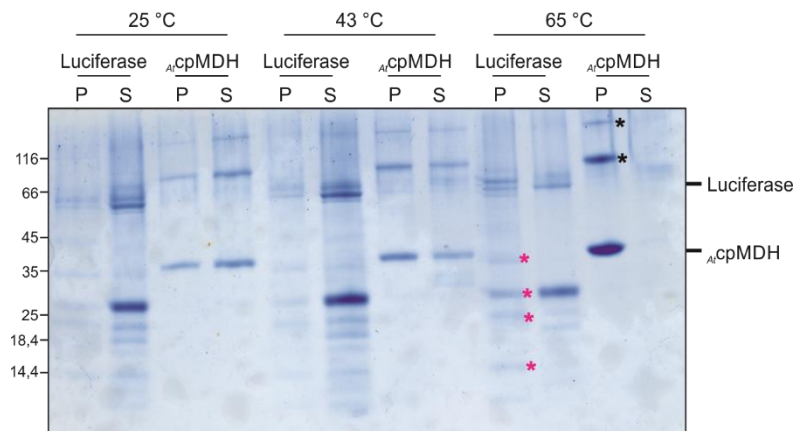


Figure S13. Examination of heat induced aggregation of model substrate chaperone

Luciferase and *AtcpMDH* were either kept at 25 °C, 43 °C or 65 °C for an hour and fractionated by centrifugation into insoluble (P) and soluble (S) portions. Samples were analyzed by SDS-PAGE followed by coomassie staining. The intact monomeric form of luciferase and *AtcpMDH* are labeled. The degradation forms of luciferase and oligomeric states of *AtcpMDH* are indicated by magenta and black asterisks, respectively.

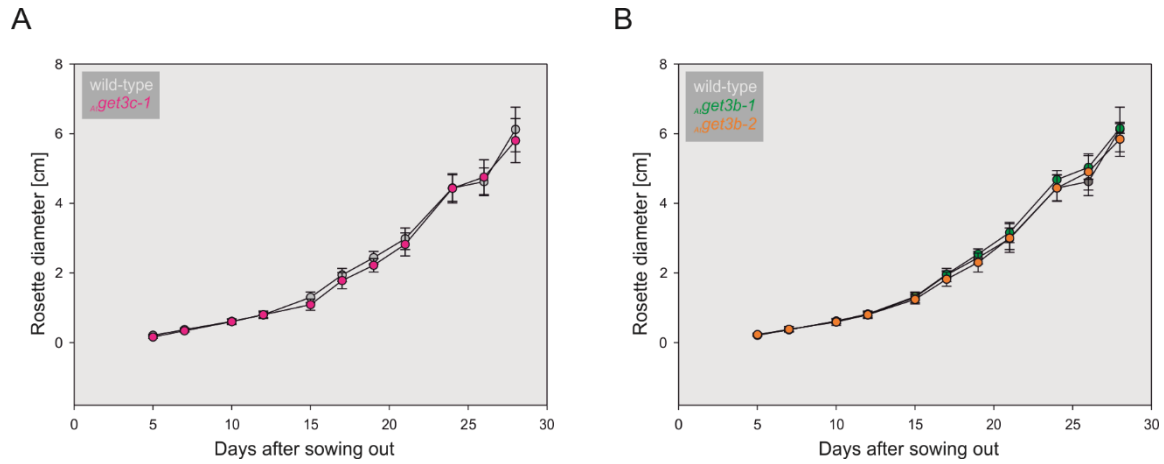


Figure S14. Growth analysis of *Atget3* mutants.

Rosette diameter of **A.** *AtGet3c-1* and **B.** *AtGet3b-1/2* mutant plants were analyzed according to (Boyes et al., 2001) and compared to co-cultivated wild-type plants.

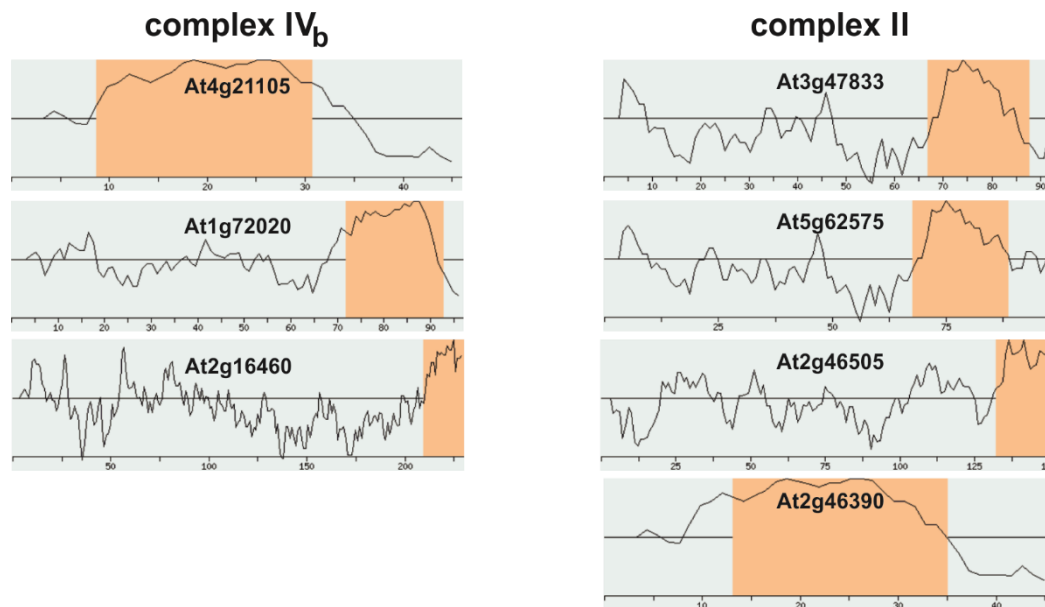


Figure S15. Topologies of the putative TA proteins in complex II and IV_b.

Representations of AAs and the occurrence of TMDs (orange) in these. The AGI numbers of the protein sequence is shown in bold. Images extracted from aramemnon.uni-koeln.de (TmPred)

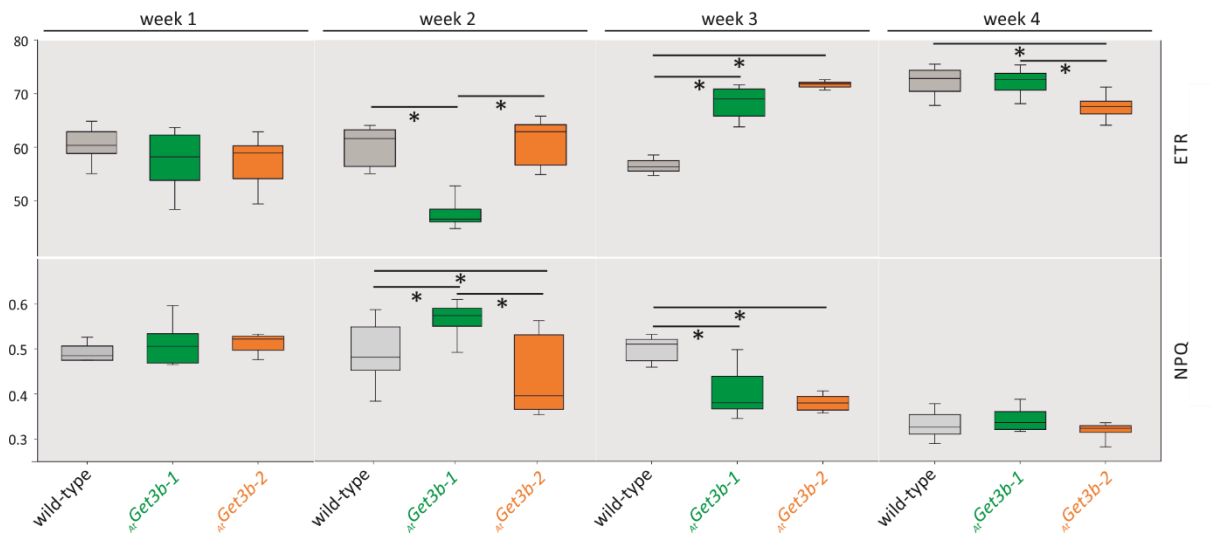


Figure S16. Photosynthetic parameters of the wild-type and mutant plants in the first month of development. The indicated plant lines were weekly subjected to pulse amplitude (PAM) measurements. Exemplary of these, aspects of electron transport (ETR; top) and non-photochemical quenching (NPQ; bottom) are depicted.

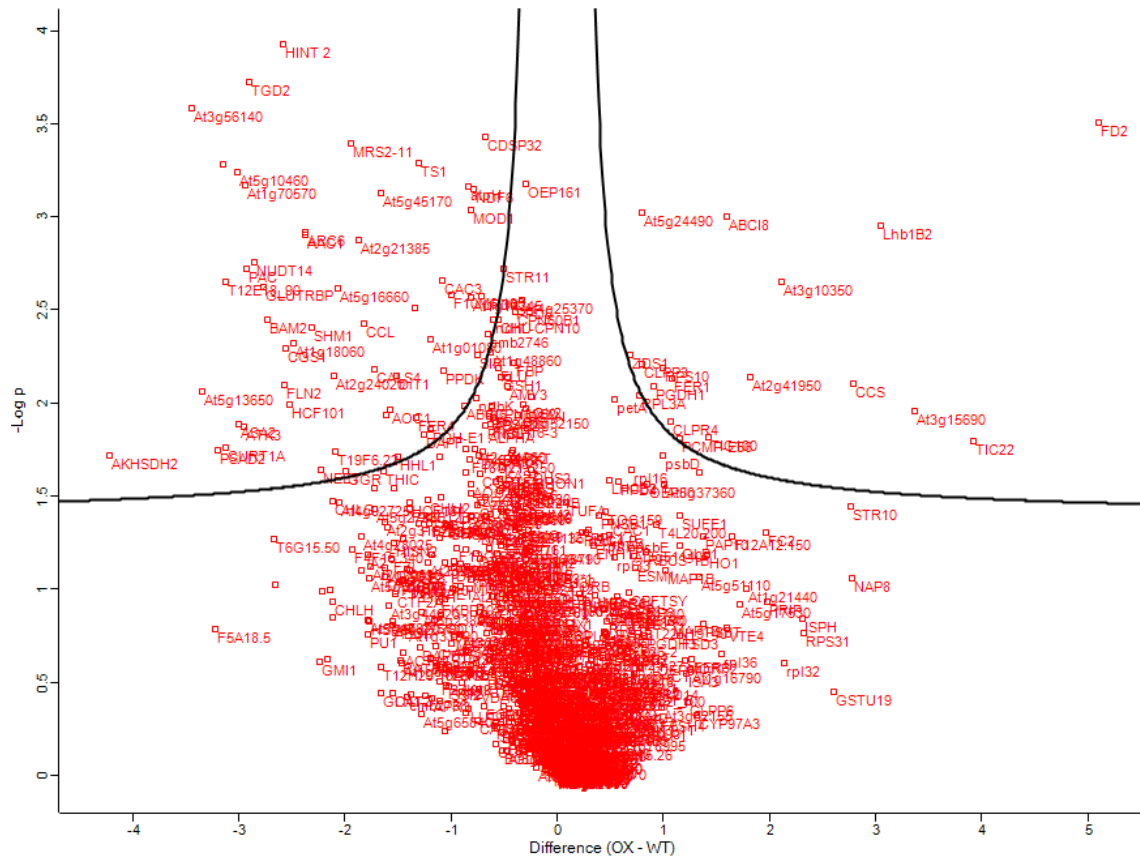


Figure S17. Volcano plot of t-test between the proteome wild-type vs *Atget3b-1* chloroplasts.

Chloroplasts were isolated from wild-type plants and *Atget3b-1* plants and subjected to LC-MS/MS. The retrieved data was analyzed in MaxQuant (Cox and Mann, 2008) in a label-free quantitative manner, further transformed and statistically evaluated in Perseus (Tyanova and Cox, 2018). Shown is a volcano plot of the t-test displaying the differences in fold change (x-axis) and p-values (y-axis). The black lines indicate the threshold for statistical significance. Uniprot (uniprot.org) identifiers are displayed.

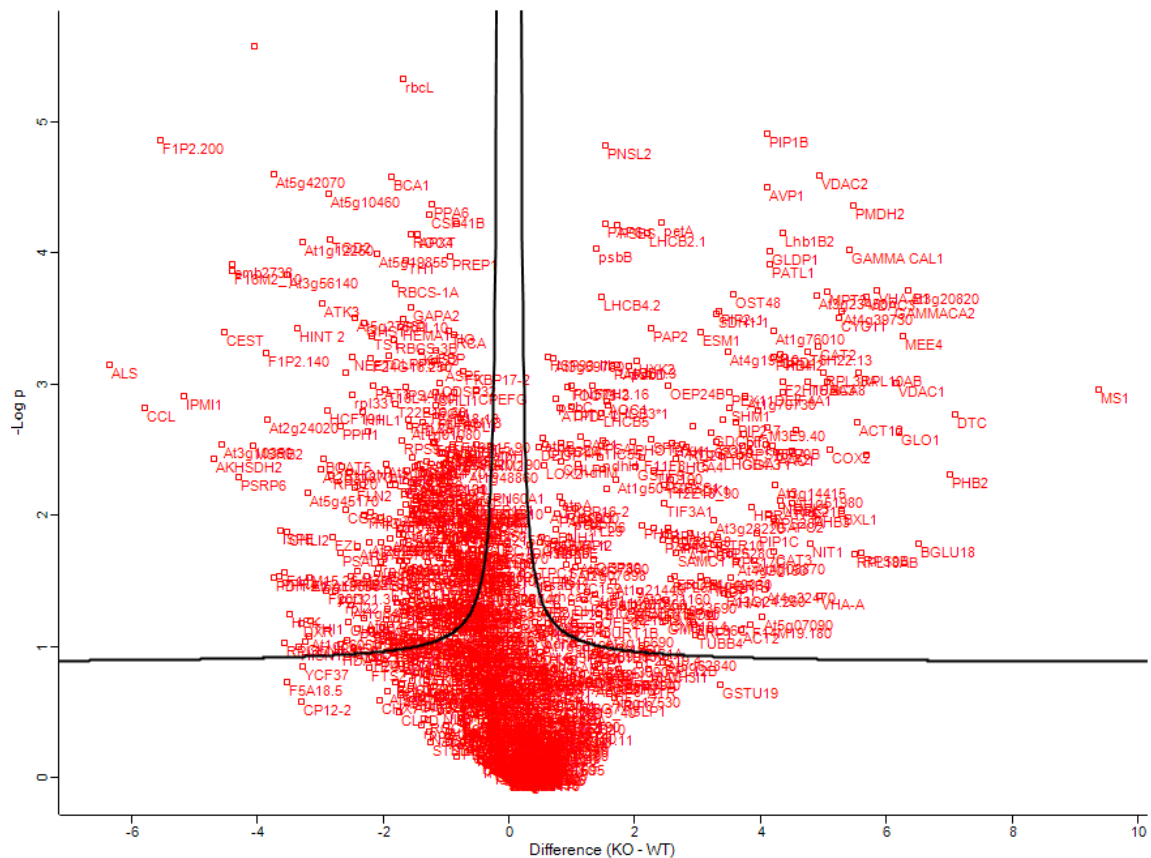


Figure S18. Volcano plot of t-test between the proteome of wild-type vs *Atget3b-2* chloroplasts. Chloroplasts were isolated from wild-type plants and *Atget3b-2* plants and subjected to LC-MS/MS. The retrieved data was analyzed in MaxQuant (Cox and Mann, 2008) in a label-free quantitative manner, further transformed and statistically evaluated in Perseus (Tyanova and Cox, 2018). Shown is a volcano plot of the t-test displaying the differences in fold change (x-axis) and p-values (y-axis). The black lines indicate the threshold for statistical significance. UniProt (uniprot.org) identifiers are displayed.

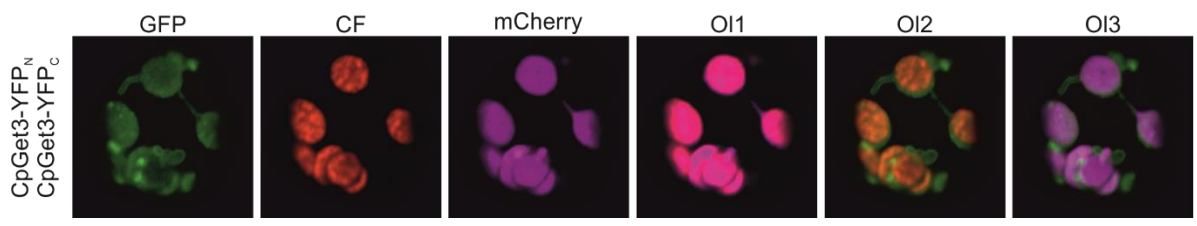


Figure S19. *AtGet3b* is associated with membranes in stromules and extrusions. Protoplasts isolated from *A. thaliana* were co-transformed with the indicated constructs. Shown are single channels of YFP, chlorophyll fluorescence (CF), mCherry as well as overlays of mCherry/CF (OI1), YFP/CF (OI2) and YFP/mCherry (OI3).

10.2 Supplemental tables

Table S1. Analyzed Get3 sequences. Get3 orthologues (columns 3-5) in plants, proteins with sequences similarity identified by BLAST in plant genomes forming an independent orthologous groups. The first column shows the species and the second the sequence identification number. The protein sequences of identified Get3 orthologues were used to predict the intracellular localization by Predotar (Simm et al., 2015), TargetP (Small et al., 2004), MultiLoc2 (Emanuelsson et al., 2000) and GTP / ATP2 (Blum et al., 2009). MultiLoc2 distinguishes between localization in the extracellular environment, nucleus, Golgi, ER, mitochondrion, plastid, plasma membrane, peroxisome, vacuole, cytosol and cytoskeleton. TargetP and Predotar distinguish between secretory pathway and targeting to chloroplast or mitochondria. GTP and ATP2 discriminate between dual targeted to mitochondria and chloroplast as well as take cytosol into account. The simple majority for one organelle consensus of all three programs was used to call for a putative localization. The predicted categories are cytosol: CYT; mitochondria: MIT; chloroplast: CHL; mitochondria and chloroplast: M/C. Adapted from (Bodensohn et al., 2019).

Species	Accession Number	Orthologous groups		
		AT1G01910	AT3G10350	AT5G60730
<i>Solanum tuberosum</i>	Stub PGSC0003DMP400018036			
<i>Solanum tuberosum</i>	Stub PGSC0003DMP400020866			
<i>Solanum lycopersium</i>	Slyc Solyc05g050480.1.1	CYT		
<i>Solanum tuberosum</i>	Stub PGSC0003DMP400057442	CYT		
<i>Brachypodium distachyon</i>	Bdis Bradi5g12380.1.p			
<i>Brachypodium stacei</i>	Bsta Brast09G105900.1.p			
<i>Panicum virgatum</i>	Pvir Pavir.Ga01458.1.p			
<i>Panicum virgatum</i>	Pvir Pavir.J13695.1.p			
<i>Panicum virgatum</i>	Pvir Pavir.J19670.1.p			
<i>Panicum virgatum</i>	Pvir Pavir.J20856.1.p			
<i>Panicum virgatum</i>	Pvir Pavir.J25173.1.p			
<i>Sorghum bicolor</i>	Sbic Sobic.006G106600.1.p			
<i>Setaria italica</i>	Sita Seita.7G124200.1.p			
<i>Setaria viridis</i>	Svir Sevir.7G132500.1.p			
<i>Zea mays</i>	Zmay GRMZM2G065480_P01			
<i>Zea mays</i>	Zmay GRMZM2G126887_P01			
<i>Zea mays</i>	Zmay GRMZM2G139472_P01			
<i>Zea mays</i>	Zmay GRMZM2G453581_P01			
<i>Chlamydomonas reinhardtii</i>	Crei Cre05.g245158.t1.1		CYT/MIT	
<i>Chlamydomonas reinhardtii</i>	Crei Cre24.g755097.t1.1/C.reinhardtii XP_001702275.1		CHL (dual)	
<i>Coccomyxa subellipsoidea C-169</i>	Csub 29034		CYT	
<i>Volvox carteri</i>	Vcar Vocar.0201s0001.1.p		CYT	
<i>Ostreococcus lucimarinus</i>	Oluc 12872		CYT	
<i>Micromonas pusilla</i>	Mpus 25594		CYT	
<i>Micromonas sp. RCC299</i>	MspR 98308		CYT	
<i>Manihot esculenta</i>	Mesc Manes.04G017100.1.p		MIT	
<i>Ricinus communis</i>	Rcom 29638.m000526		MIT	
<i>Medicago truncatula</i>	Mtru Medtr4g058005.1		MIT	
<i>Kalanchoe marnieriana</i>	Kmar Kalax.0032s0155.1.p		MIT	
<i>Kalanchoe marnieriana</i>	Kmar Kalax.0160s0019.1.p		MIT	
<i>Linum usitatissimum</i>	Lusi Lus10021449			
<i>Eucalyptus grandis</i>	Egra Eucgr.J00904.1.p		MIT (dual)	
<i>Arabidopsis thaliana</i>	Atha AT5G60730.1			MIT (dual)
<i>Arabidopsis lyrata</i>	Alyr 496221			MIT (dual)
<i>Brassica rapa FPsc</i>	Brap Brara.B01015.1.p			MIT
<i>Eutrema salsugineum</i>	Esal Thhalv10013776m			MIT (dual)
<i>Boechera stricta</i>	Bstr Bostr.26833s0166.1.p			MIT (dual)

SUPPLEMENTS

<i>Capsella grandiflora</i>	Cgra Cagra.2519s0043.1.p			MIT (dual)
<i>Capsella rubella</i>	Crub Carubv10026572m			MIT (dual)
<i>Erythranthe guttatus</i>	Mgut Migut.D02251.1.p			MIT (dual)
<i>Solanum lycopersicum</i>	Slyc Solyc11g069830.1.1			CHL (dual)
<i>Solanum tuberosum</i>	Stub PGSC0003DMP400014211			CHL (dual)
<i>Citrus clementina</i>	Ccle Ciclev10028528m			MIT (dual)
<i>Citrus sinensis</i>	Csin orange1.1g043873m			MIT (dual)
<i>Gossypium raimondii</i>	Grai Gorai.009G109800.1			MIT (dual)
<i>Aquilegia coerulea Goldsmith</i>	Acoe Aqua_030_00110.1			CHL (dual)
<i>Carica papaya</i>	Cpap evm.model.supercontig_65.13			CYT
<i>Vitis vinifera</i>	Vvin GSVIVT01025229001			CYT
<i>Amborella trichopoda</i>	Atri evm_27.model.AmTr_v1.0_scaffold00009.136			MIT (dual)
<i>Spirodela polyrhiza</i>	Spol Spipo1G0025000			MIT
<i>Picea abies</i>	Pabi MA_10436816g0010			CYT
<i>Physcomitrella patens</i>	Ppat Pp3c22_13860V3.1.p/XP_001764873.1			CHL
<i>Physcomitrella patens</i>	Ppat Pp3c19_12470V3.1.p/XP_001781368.1			CHL (dual)
<i>Selaginella moellendorffii</i>	Smoe 174109/XP_002974288.2			MIT/CHL
<i>Panicum virgatum</i>	Pvir Pavir.Ab02993.1.p			MIT
<i>Setaria italica</i>	Sita Seita.1G318700.1.p			MIT
<i>Sorghum bicolor</i>	Sbic Sobic.004G238200.1.p			MIT (dual)
<i>Setaria viridis</i>	Svir Sevir.1G324900.1.p			MIT
<i>Panicum virgatum</i>	Pvir Pavir.Aa00707.1.p			MIT
<i>Zea mays</i>	Zmay GRMZM2G105539_P01			MIT (dual)
<i>Zea mays</i>	Zmay GRMZM2G157437_P01			
<i>Brachypodium distachyon</i>	Bdis Bradi3g59400.1.p			MIT (dual)
<i>Brachypodium stacei</i>	Bsta Brast04G016500.1.p			MIT
<i>Oryza sativa</i>	Osat LOC_Os2g51100.1			MIT
<i>Kalanchoe marnieriana</i>	Kmar Kalax.0002s0063.1.p			CHL (dual)
<i>Kalanchoe marnieriana</i>	Kmar Kalax.0483s0003.1.p			CHL (dual)
<i>Kalanchoe marnieriana</i>	Kmar Kalax.0199s0035.1.p			CHL (
<i>Kalanchoe marnieriana</i>	Kmar Kalax.0139s0049.1.p			CYT
<i>Arabidopsis thaliana</i>	Atha AT3G10350.2			CHL (dual)
<i>Boechera stricta</i>	Bstr Bostr.22252s0029.1.p			CHL (dual)
<i>Arabidopsis lyrata</i>	Alyr 478365			CHL(dual)
<i>Brassica rapa FPsc</i>	Brap Brara.A03493.1.p			CHL (dual)
<i>Brassica rapa FPsc</i>	Brap Brara.E03022.1.p			CHL (dual)
<i>Eutrema salsugineum</i>	Esal Thhalv10020822m			CHL (dual)
<i>Capsella grandiflora</i>	Cgra Cagra.0834s0048.1.p			CHL (dual)
<i>Capsella rubella</i>	Crub Carubv10015946m			CHL (dual)
<i>Fragaria vesca</i>	Fves mra23188.1-v1.0-hybrid			CHL (dual)
<i>Prunus persica</i>	Pper Prupe.2G211000.1.p			MIT (dual)
<i>Malus domestica</i>	Mdom MDP0000259681			MIT (dual)
<i>Malus domestica</i>	Mdom MDP0000259922			CHL (dual)
<i>Cucumis sativus</i>	Csat Cucsa.308500.1			CHL (dual)
<i>Glycine max</i>	Gmax Glyma.10G209300.1.p			CHL (dual)
<i>Glycine max</i>	Gmax Glyma.20G181300.1.p			CHL (dual)
<i>Medicago truncatula</i>	Mtru Medtr1g094680.1			CHL (dual)
<i>Phaseolus vulgaris</i>	Pvul Phvul.007G096800.1			CHL (dual)
<i>Solanum lycopersicum</i>	Slyc Solyc04g025120.1.1			
<i>Manihot esculenta</i>	Mesc Manes.07G095700.1.p			
<i>Manihot esculenta</i>	Mesc Manes.07G096400.1.p			
<i>Manihot esculenta</i>	Mesc Manes.07G096700.1.p			
<i>Manihot esculenta</i>	Mesc Manes.07G096900.1.p			
<i>Citrus sinensis</i>	Csin orange1.1g015096m			CHL (dual)
<i>Citrus clementina</i>	Ccle Ciclev10030991m			CYT
<i>Carica papaya</i>	Cpap evm.model.supercontig_53.98			CHL
<i>Linum usitatissimum</i>	Lusi Lus10037982			CHL (dual)
<i>Linum usitatissimum</i>	Lusi Lus10038715			CHL (dual)
<i>Eucalyptus grandis</i>	Egra Eucgr.G02857.1.p			CHL
<i>Vitis vinifera</i>	Vvin GSVIVT01016242001			MIT (dual)

<i>Erythranthe guttatus</i>	Mgut Migut.D01651.1.p		CHL (dual)
<i>Erythranthe guttatus</i>	Mgut Migut.F01967.1.p		CHL (dual)
<i>Solanum lycopersicum</i>	Slyc Solyc04g025160.2.1		
<i>Manihot esculenta</i>	Mesc Manes.07G096000.1.p		
<i>Ricinus communis</i>	Rcom 29595.m000285		CHL (dual)
<i>Populus trichocarpa</i>	Ptri Potri.008G037100.1		CHL (dual)
<i>Salix purpurea</i>	Spur SapurV1A.0518s0270.1.p		CHL (dual)
<i>Populus trichocarpa</i>	Ptri Potri.010G225100.1		CHL (dual)
<i>Salix purpurea</i>	Spur SapurV1A.1694s0070.1.p		CHL (dual)
<i>Theobroma cacao</i>	Tcac Thecc1EG043187t1		
<i>Theobroma cacao</i>	Tcac Thecc1EG043200t1		
<i>Theobroma cacao</i>	Tcac Thecc1EG043204t1		CHL (dual)
<i>Gossypium raimondii</i>	Grai Gorai.009G312500.1		CHL (dual)
<i>Gossypium raimondii</i>	Grai Gorai.011G238300.1		CHL (dual)
<i>Chlamydomonas reinhardtii</i>	Crei Cre03.g204800.t1.2 (XP_001693332.1)	CYT	
<i>Volvox carteri</i>	Vcar Vocar.0011s0122.1.p	CYT (dual)	
<i>Coccomyxa subellipsoidea C-169</i>	Csub 22859	CYT (dual)	
<i>Physcomitrella patens</i>	Ppat Pp3c2_1504V3.1.p		
<i>Physcomitrella patens</i>	Ppat Pp3c14_22160V3.1.p	CYT	
<i>Physcomitrella patens</i>	Ppat Pp3c17_16460V3.1.p	CYT	
<i>Selaginella moellendorffii</i>	Smoe 173359	CYT	
<i>Picea abies</i>	Pabi MA_10431825g0010	CYT	
<i>Amborella trichopoda</i>	Atri evm_27.model.AmTr_v1.0_scaffold00069.43	CYT (dual)	
<i>Aquilegia coerulea Goldsmith</i>	Acoe Aqua_013_00455.1	CYT	
<i>Citrus clementina</i>	Ccle Ciclev10020733m	CYT	
<i>Citrus sinensis</i>	Csin orange1.1g017873m	CYT	
<i>Vitis vinifera</i>	Vvin GSVIVT01027593001	CYT (dual)	
<i>Populus trichocarpa</i>	Ptri Potri.002G152500.1	CYT (dual)	
<i>Salix purpurea</i>	Spur SapurV1A.1221s0030.1.p	CYT (dual)	
<i>Populus trichocarpa</i>	Ptri Potri.014G078100.1	CYT (dual)	
<i>Salix purpurea</i>	Spur SapurV1A.0024s0490.1.p	CYT (dual)	
<i>Medicago truncatula</i>	Mtru Medtr8g032880.1	CYT (dual)	
<i>Phaseolus vulgaris</i>	Pvul Phvul.010G089400.1	CYT (dual)	
<i>Glycine max</i>	Gmax Glyma.03G018500.1.p	CYT (dual)	
<i>Glycine max</i>	Gmax Glyma.07G079700.1.p	CYT (dual)	
<i>Gossypium raimondii</i>	Grai Gorai.004G155900.1	CYT (dual)	
<i>Theobroma cacao</i>	Tcac Thecc1EG005443t1	CYT	
<i>Gossypium raimondii</i>	Grai Gorai.001G172700.1	CYT	
<i>Gossypium raimondii</i>	Grai Gorai.008G115800.1	CYT (dual)	
<i>Erythranthe guttatus</i>	Mgut Migut.B01674.1.p	CYT	
<i>Erythranthe guttatus</i>	Mgut Migut.N01415.1.p	CYT	
<i>Cucumis sativus</i>	Csat Cucsa.363070.1	CYT (dual)	
<i>Solanum tuberosum</i>	Stub PGSC0003DMP400018135	CYT (dual)	
<i>Solanum lycopersicum</i>	Slyc Solyc10g017810.1.1	CYT (dual)	
<i>Solanum tuberosum</i>	Stub PGSC0003DMP400000010	CYT	
<i>Solanum lycopersicum</i>	Slyc Solyc01g091880.2.1	CYT	
<i>Solanum tuberosum</i>	Stub PGSC0003DMP400012413	CYT	
<i>Solanum lycopersicum</i>	Slyc Solyc05g050490.2.1	CYT	
<i>Fragaria vesca</i>	Fves mrna18950.1-v1.0-hybrid	CYT (dual)	
<i>Prunus persica</i>	Pper Prupe.2G153000.1.p	CYT (dual)	
<i>Malus domestica</i>	Mdom MDP0000222437	CYT	
<i>Malus domestica</i>	Mdom MDP0000431925		
<i>Malus domestica</i>	Mdom MDP0000812195	CYT	
<i>Vitis vinifera</i>	Vvin GSVIVT01020414001		
<i>Carica papaya</i>	Cpap evm.model.supercontig_18.179	CYT (dual)	
<i>Kalanchoe marnieriana</i>	Kmar Kalax.0017s0034.1.p	CYT (dual)	
<i>Kalanchoe marnieriana</i>	Kmar Kalax.0327s0009.1.p	CYT (dual)	
<i>Kalanchoe marnieriana</i>	Kmar Kalax.0032s0071.1.p	CYT (dual)	
<i>Kalanchoe marnieriana</i>	Kmar Kalax.0099s0070.1.p	CYT (dual)	
<i>Manihot esculenta</i>	Mesc Manes.05G040800.1.p	CYT (dual)	

<i>Eucalyptus grandis</i>	Egra Eucgr.E01322.1.p	CYT	
<i>Ricinus communis</i>	Rcom 30174.m008947	CYT (dual)	
<i>Manihot esculenta</i>	Mesc Manes.01G263000.1.p		
<i>Linum usitatissimum</i>	Lusi Lus10036552	CYT	
<i>Linum usitatissimum</i>	Lusi Lus10041377	CYT	
<i>Arabidopsis lyrata</i>	Alyr 470088	CYT (dual)	
<i>Arabidopsis thaliana</i>	Atha AT1G01910.1	CYT (dual)	
<i>Capsella grandiflora</i>	Cgra Cagra.1968s0127.1.p	CYT (dual)	
<i>Capsella rubella</i>	Crub Carubv10009581m	CYT (dual)	
<i>Boechera stricta</i>	Bstr Bostr.5325s0111.1.p	CYT (dual)	
<i>Eutrema salsugineum</i>	Esal Thhalv10008053m	CYT (dual)	
<i>Brassica rapa FPsc</i>	Brap Brara.I05625.1.p	CYT (dual)	
<i>Spirodela polyrhiza</i>	Spol Spipo16G0006500	CYT (dual)	
<i>Brachypodium stacei</i>	Bsta Brast05G186100.1.p	CYT	
<i>Brachypodium distachyon</i>	Bdis Bradi4g35540.1.p	CYT	
<i>Oryza sativa</i>	Osat LOC_Os09g34970.1	CYT	
<i>Zea mays</i>	Zmay AC199782.5_FGP001	CYT (dual)	
<i>Sorghum bicolor</i>	Sbic Sobic.002G268800.1.p	CYT	
<i>Zea mays</i>	Zmay GRMZM6G675851_P01		
<i>Setaria italica</i>	Sita Seita.2G279500.1.p	CYT	
<i>Setaria viridis</i>	Svir Sevir.2G289400.1.p	CYT	
<i>Panicum virgatum</i>	Pvir Pavir.J00630.1.p	CYT	
<i>Panicum virgatum</i>	Pvir Pavir.J15882.1.p	CYT	

Table S2. Accession numbers of the genes coding for the orthologues of Get1, in the plant species analyzed. Shown are the class (column 1), the name of the species (column 2), the accession number of orthologues identified for the orthologous groups of Get1 (column 3) in *A. thaliana* (Paul et al., 2013). Modified from (Bodensohn et al., 2019).

Taxon	Species	Get1 (At4g16444)
Chlorophyta	<i>Micromonas pusilla</i> <i>Micromonas sp. RCC299</i> <i>Ostreococcus lucimarinus</i> <i>Chlamydomonas reinhardtii</i> <i>Coccomyxa subellipsoidea C-169</i> <i>Volvox carteri</i>	Cre09.g387504.t1.1 52226 Vocar.0033s0111.1.p
Bryophyta	<i>Physcomitrella patens</i>	Pp3c7_8860V3.1.p
Lycopodiophyta	<i>Selaginella moellendorffii</i>	
Gymnosperms	<i>Picea abies</i>	MA_7581274g0010
basal Magnoliophyta	<i>Amborella trichopoda</i>	evm_27.model.AmTr_v1.0_scaffold00044.173
Monocots	<i>Brachypodium stacei</i> <i>Brachypodium distachyon</i> <i>Oryza sativa</i> <i>Panicum virgatum</i> <i>Setaria viridis</i> <i>Setaria italica</i> <i>Sorghum bicolor</i> <i>Spirodela polyrhiza</i> <i>Zea mays</i>	Brast07G065600.1.p Bradi1g46580.1.p LOC_Os06g09840.1 Pavir.Da01879.1.p; Pavir.Db01979.1.p; Pavir.J32354.1.p; Pavir.J14306.1.p Sevir.2G310100.1.p; Sevir.4G037100.1.p Seita.4G039200.1.p; Seita.2G299100.1.p Sobic.010G073900.1.p; Sobic.002G288200.1.p Spipo11G0046500 GRMZM2G053083_P01; GRMZM2G053083_P01; GRMZM2G127893_P01
Eudicots	<i>Aquilegia coerulea Goldsmith</i> <i>Arabidopsis lyrata</i> <i>Arabidopsis thaliana</i> <i>Boechera stricta</i> <i>Brassica rapa FPsc</i> <i>Capsella grandiflora</i>	Aquca_007_00894.1 493236 AT4G16444.1 Bostr.30275s0095.1.p Brara.C04498.1.p; Brara.H00861.1.p Cagra.12076s0014.1.p Carubv10005861m

	<p><i>Capsella rubella</i> <i>Carica papaya</i> <i>Citrus clementina</i> <i>Citrus sinensis</i> <i>Cucumis sativus</i> <i>Eucalyptus grandis</i> <i>Eutrema salsugineum</i> <i>Fragaria vesca</i> <i>Glycine max</i> <i>Gossypium raimondii</i> <i>Kalanchoe marnieriana</i> <i>Linum usitatissimum</i> <i>Malus domestica</i> <i>Manihot esculenta</i> <i>Medicago truncatula</i> <i>Erythranthe guttatus</i> <i>Phaseolus vulgaris</i> <i>Populus trichocarpa</i> <i>Prunus persica</i> <i>Ricinus communis</i> <i>Salix purpurea</i> <i>Solanum lycopersicum</i> <i>Solanum tuberosum</i> <i>Theobroma cacao</i> <i>Vitis vinifera</i></p>	<p>evm.TU.contig_27001.3 Ciclev10016602m orange1.1g033786m Cucsa.323110.1 Eucgr.I00568.1.p Thhalv10026376m mna13044.1-v1.0-hybrid Glyma.01G158900.1.p; Glyma.09G198400.1.p Gorai.010G212400.1 Kalax.0462s0003.1.p; Kalax.0462s0005.1.p Kalax.0326s0015.1.p; Kalax.0326s0017.1.p Lus10016696 MDP0000257001; MDP0000264158; MDP0000134902 Manes.S026700.1.p Medtr8g073600.1 Migut.K01195.1.p; Migut.M00637.1.p; Migut.N00197.1.p; Migut.G00971.1.p; Migut.C01149.1.p Phvul.009G210400.1; Phvul.003G269900.1 Potri.005G101300.1 Prupe.7G182100.1.p 29830.m001448 SapurV1A.0085s0040.1.p Solyc00g007080.2.1; Solyc02g082710.2.1 PGSC0003DMP400002738 Thecc1EG000069t1 GSVIVT01026644001</p>
--	---	---

Table S3. Accession numbers of the genes coding for the orthologues of Sgt2 in the plant species analyzed. Shown are the class (column 1), the name of the species (column 2), the accession number of orthologues identified for the orthologous groups of Sgt2 (column 3) in *A. thaliana* (Paul et al., 2013). Modified from (Bodensohn et al., 2019).

Taxon	Species	Sgt2 (At4g08320)
Chlorophyta	<p><i>Micromonas pusilla</i> <i>Micromonas sp. RCC299</i> <i>Ostreococcus lucimarinus</i> <i>Chlamydomonas reinhardtii</i> <i>Coccomyxa subellipsoidea C-169</i> <i>Volvox carteri</i></p>	
Bryophyta	<i>Physcomitrella patens</i>	
Lycopodiophyta	<i>Selaginella moellendorffii</i>	
Gymnosperms	<i>Picea abies</i>	MA_9891450g0010
basal Magnoliophyta	<i>Amborella trichopoda</i>	evm_27.model.AmTr_v1.0_scaffold00017.116
Monocots	<p><i>Brachypodium stacei</i> <i>Brachypodium distachyon</i> <i>Oryza sativa</i> <i>Panicum virgatum</i> <i>Setaria viridis</i> <i>Setaria italica</i> <i>Sorghum bicolor</i> <i>Spirodela polyrhiza</i> <i>Zea mays</i></p>	<p>Brast09G268000.1.p Bradi5g27367.2.p LOC_Os04g59394.1 Pavir.Ga00252.1.p; Pavir.Gb00176.1.p Sevir.3G004600.1.p Seita.3G003600.1.p Sobic.006G278700.1.p Spipo9G0041200 GRMZM5G827171_P03</p>
Eudicots	<p><i>Aquilegia coerulea Goldsmith</i> <i>Arabidopsis lyrata</i> <i>Arabidopsis thaliana</i> <i>Boechera stricta</i></p>	<p>Aquca_014_00212.1 AT4G08320.2 Bostr.3877s0030.1.p</p>

	<i>Brassica rapa</i> FPsc <i>Capsella grandiflora</i> <i>Capsella rubella</i> <i>Carica papaya</i> <i>Citrus clementina</i> <i>Citrus sinensis</i> <i>Cucumis sativus</i> <i>Eucalyptus grandis</i> <i>Eutrema salsugineum</i> <i>Fragaria vesca</i> <i>Glycine max</i> <i>Gossypium raimondii</i> <i>Kalanchoe marnieriana</i> <i>Linum usitatissimum</i> <i>Malus domestica</i> <i>Manihot esculenta</i> <i>Medicago truncatula</i> <i>Erythranthe guttatus</i> <i>Phaseolus vulgaris</i> <i>Populus trichocarpa</i> <i>Prunus persica</i> <i>Ricinus communis</i> <i>Salix purpurea</i> <i>Solanum lycopersicum</i> <i>Solanum tuberosum</i> <i>Theobroma cacao</i> <i>Vitis vinifera</i>	Brara.B02898.1.p Cagra.6321s0002.1.p Carubv10001000m evm.model.supercontig_64.83 Ciclev10001211m orange1.1g013948m Cucsa.125470.1 Eucgr.F03788.1.p Thhalv10028662m mrna11171.1-v1.0-hybrid Glyma.13G080100.1.p; Glyma.14G149300.1.p Gorai.009G245500.1; Gorai.010G050100.1 Kalax.0814s0011.1.p Lus10018179; Lus10025656 MDP0000183096; MDP0000456232 Manes.18G076800.1.p Medtr1g030300.1 Migut.C01133.1.p Phvul.008G163200.1 Potri.005G177400.1 Prupe.1G499100.1.p 29908.m006184 SapurV1A.0105s0290.1.p Solyc11g012900.1.1 Thecc1EG035111t1
--	--	---

Table S4. Accession numbers of the genes coding for the orthologues of Get4 in the plant species analyzed. Shown are the class (column 1), the name of the species (column 2), the accession number of orthologues identified for the orthologous groups of Get4, (column 3), in *A. thaliana* (Paul et al., 2013). Adapted from (Bodensohn et al., 2019).

Taxon	Species	Get4 (At5g63220)
Chlorophyta	<i>Micromonas pusilla</i> <i>Micromonas sp. RCC299</i> <i>Ostreococcus lucimarinus</i> <i>Chlamydomonas reinhardtii</i> <i>Coccomyxa subellipsoidea C-169</i> <i>Volvox carteri</i>	Cre06.g282950.t1.2 65140 Vocar.0002s0040.1.p
Bryophyta	<i>Physcomitrella patens</i>	Pp3c11_21230V3.1.p; Pp3c7_7450V3.1.p
Lycopodiophyta	<i>Selaginella moellendorffii</i>	92949
Gymnosperms	<i>Picea abies</i>	MA_90021g0010
basal Magnoliophyta	<i>Amborella trichopoda</i>	evm_27.model.AmTr_v1.0_scaffold00001.168
Monocots	<i>Brachypodium stacei</i> <i>Brachypodium distachyon</i> <i>Oryza sativa</i> <i>Panicum virgatum</i> <i>Setaria viridis</i> <i>Setaria italica</i> <i>Sorghum bicolor</i> <i>Spirodela polyrhiza</i> <i>Zea mays</i>	Bradi2g03980.1.p LOC_Os01g07100.1 Pavir.Ea00431.1.p Sevir.5G111600.1.p Seita.5G114800.1.p Sobic.003G058500.1.p Spipo23G0040900 GRMZM2G048804_P02
Eudicots	<i>Aquilegia coerulea</i> Goldsmith <i>Arabidopsis lyrata</i>	Aquca_004_00443.1 496506

	<i>Arabidopsis thaliana</i>	AT5G63220.1
	<i>Boechera stricta</i>	Bostr.0568s0484.1.p
	<i>Brassica rapa FPsc</i>	Brara.F02220.1.p; Brara.I00734.1.p
	<i>Capsella grandiflora</i>	Cagra.0248s0005.1.p
	<i>Capsella rubella</i>	Carubv10027604m
	<i>Carica papaya</i>	evm.model.supercontig_53.21
	<i>Citrus clementina</i>	Ciclev10032131m
	<i>Citrus sinensis</i>	orange1.1g020832m
	<i>Cucumis sativus</i>	Cucsa.120720.1
	<i>Eucalyptus grandis</i>	Eucgr.G02801.1.p
	<i>Eutrema salsugineum</i>	Thhalv10004594m
	<i>Fragaria vesca</i>	mrna23229.1-v1.0-hybrid
	<i>Glycine max</i>	Glyma.10G214100.1.p; Glyma.20G177500.1.p
	<i>Gossypium raimondii</i>	Gorai.012G093600.1; Gorai.013G025000.1
	<i>Kalanchoe marnieriana</i>	Kalax.0183s0033.1.p; Kalax.0738s0020.1.p
	<i>Linum usitatissimum</i>	Lus10023490; Lus10040371; Lus10036505
	<i>Malus domestica</i>	MDP0000222362; MDP0000316147
	<i>Manihot esculenta</i>	Manes.07G102100.1.p
	<i>Medicago truncatula</i>	Medtr1g095910.1
	<i>Erythranthe guttatus</i>	Migut.M00004.1.p
	<i>Phaseolus vulgaris</i>	Phvul.007G091600.1
	<i>Populus trichocarpa</i>	Potri.008G044100.1 Potri.010G217400.1
	<i>Prunus persica</i>	Prupe.2G218300.1.p
	<i>Ricinus communis</i>	29923.m000803
	<i>Salix purpurea</i>	SapurV1A.0023s0460.1.p; SapurV1A.0038s0120.1.p
	<i>Solanum lycopersicum</i>	Solyc08g015990.2.1; Solyc12g017820.1.1
	<i>Solanum tuberosum</i>	PGSC0003DMP400004002; PGSC0003DMP400013542
	<i>Theobroma cacao</i>	Thecc1EG043075t
	<i>Vitis vinifera</i>	GSVIVT01016338001

Table S5. Distribution of orthologues of Sgt2, Get1, Get3 and Get4 in the plant species analyzed. Shown are the class (column 1), the name of the species (column 2), the number of orthologues identified in the orthologous groups of Sgt2 (column 3), Get1 (column 4), Get3 (column 5-7) and Get4 (column 8) found in *A. thaliana* (Paul et al., 2013). Modified form (Bodensohn et al., 2019).

Taxon	Species	Sgt2	Get1	Get3			Get4
				AtGet3a	AtGet3b	AtGet3c	
Chlorophyta	<i>Micromonas pusilla</i>	0	0	0	1	0	0
	<i>Micromonas sp. RCC299</i>	0	0	0	1	0	0
	<i>Ostreococcus lucimarinus</i>	0	0	0	1	0	0
	<i>Chlamydomonas reinhardtii</i>	0	1	1	2	0	1
	<i>Coccomyxa subellipsoidea C-169</i>	0	1	1	1	0	1
	<i>Volvox carteri</i>	0	1	1	1	0	1
Bryophyta	<i>Physcomitrella patens</i>	0	1	2	2	0	2
Lycopodiophyta	<i>Selaginella moellendorffii</i>	0	0	1	1	0	1
Gymnosperms	<i>Picea abies</i>	1	1	1	1	0	1
basal Magnoliophyta	<i>Amborella trichopoda</i>	1	1	1	1	0	1
Monocots	<i>Brachypodium stacei</i>	1	1	1	1	0	0
	<i>Brachypodium distachyon</i>	1	1	1	1	0	1
	<i>Oryza sativa</i>	1	1	1	1	0	1
	<i>Panicum virgatum</i>	2	4	2	2	0	1
	<i>Setaria viridis</i>	1	2	1	1	0	1
	<i>Setaria italica</i>	1	2	1	1	0	1
	<i>Sorghum bicolor</i>	1	2	1	1	0	1
	<i>Spirodela polyrhiza</i>	1	1	1	1	0	1

	<i>Zea mays</i>	1	2	1	1	0	1
	<i>Aquilegia coerulea</i> Goldsmith	1	1	1	1	0	1
	<i>Arabidopsis lyrata</i>	0	1	1	1	1	1
	<i>Arabidopsis thaliana</i>	1	1	1	1	1	1
	<i>Boechera stricta</i>	1	1	1	1	1	1
	<i>Brassica rapa</i> FPsc	1	2	1	2	1	2
	<i>Capsella grandiflora</i>	1	1	1	1	1	1
	<i>Capsella rubella</i>	1	1	1	1	1	1
	<i>Carica papaya</i>	1	1	1	2	0	1
	<i>Citrus clementina</i>	1	1	1	2	0	1
	<i>Citrus sinensis</i>	1	1	1	2	0	1
	<i>Cucumis sativus</i>	1	1	1	1	0	1
	<i>Eucalyptus grandis</i>	1	1	1	2	0	1
	<i>Eutrema salsugineum</i>	1	1	1	1	1	1
	<i>Fragaria vesca</i>	1	1	1	1	0	1
	<i>Glycine max</i>	2	2	2	2	0	1
	<i>Gossypium raimondii</i>	2	1	3	3	0	1
	<i>Kalanchoe marnieriana</i>	1	4	4	6	0	1
	<i>Linum usitatissimum</i>	2	1	2	2	0	3
	<i>Malus domestica</i>	2	3	2	2	0	2
	<i>Manihot esculenta</i>	1	1	1	1	0	1
	<i>Medicago truncatula</i>	1	1	1	2	0	1
	<i>Erythranthe guttatus</i>	1	5	2	3	0	1
	<i>Phaseolus vulgaris</i>	1	2	1	1	0	1
	<i>Populus trichocarpa</i>	1	1	2	2	0	2
	<i>Prunus persica</i>	1	1	1	1	0	1
	<i>Ricinus communis</i>	1	1	1	2	0	1
	<i>Salix purpurea</i>	1	1	2	2	0	2
	<i>Solanum lycopersicum</i>	1	2	4	1	0	2
	<i>Solanum tuberosum</i>	0	1	4	1	0	2
	<i>Theobroma cacao</i>	1	1	1	1	0	1
	<i>Vitis vinifera</i>	0	1	1	2	0	1

Eudicots

Table S6. Positioning of domain architecture *Hs*Ubl4A and *At*Ub-RPL40B. The domain architecture and its positioning of Ubl4A of *Homo sapiens* and Ub-RPL40B of *Arabidopsis thaliana*. Performed with PFAM (Finn et al., 2014).

Accession	Length [AA]	UBL domain [AA]
<i>Hs</i> Ubl4A	157	3 – 74
<i>At</i> Ub-RPL40B (At3g52590)	128	3 – 74

ACKNOWLEDGEMENTS

First of all, I would like to thank Prof. Dr. Enrico Schleiff for having me in his laboratories for the past decade. Moving on from my B.Sc. and M.Sc. to my PhD under your supervision was actually exactly how I envisioned my scientific maturation. I cannot express how I profited from your seemingly unlimited knowledge and your capability of staying in a good mood irrespective of the obstacles that the day had in stall for you.

I would also like to express my gratitude for Prof. Dr. Claudia Büchel for being my second reviewer for the second time during my scientific development. If Enrico would not exist, I would be working in your lab.

I would like to thank Maik Sommer and Roman Ladig for the secondary supervision in the lab. Further, I would like to thank Gisela English, Daniela Bublak and Maike Ruprecht for excellent technical assistance.

Christian Ehmann, Lucia Evita Groß, Oliver Mirus, Stefan Simm, Anna Gepp, Christoph Ruland, Bodo Tillmann, Sascha Röth, Mara Stevanovic, Mareike Rudolf, Hasret Altan-Martin, Deniz Streit, Mario Keller, Theresa Ernst, Nicole Spiess, Bo Zhang, Phillip Gebhart, Niklas Fester, Remus Rosenkranz, Hannah Schätzle, Anida Mesihovic, Giang Ngo, Leonard Fresenborg, Thiru Shanmugam, Sarah Ullrich, Special K, "R"io, Triple K and all the other affiliates that I forgot, thanks for making my time here worthwhile. We discussed, laughed our asses off, cheered each other up and most importantly we tried to science the shit out of this.

I have to thank Holger Schranz for the excellent greenhouse work and keeping *A. thaliana* in good mood for further downstream applications.

Aki thank you very much for being the social glue that keeps this department adherent and working together, your priceless advice, the correction of the thesis and the countless laughs we had.

Last but not least, I would like to thank my family, especially my beloved girlfriend Giannina for always being there for me and giving me eternal support.

PUBLICATIONS

Parts of chapter 5.1 and 5.2 were published in the following publication the individual contributions of each author is indicated:

Bodensohn US, Simm S, Fischer K, Jäschke M, Gross LE, Kramer K, Ehmann C, Ladig R, Schleiff E. (2019) The intracellular distribution of components of the GET system in vascular plants. *Biochim. Biophys. Acta - Mol. Cell Res.*

Bodensohn US: Molecular cloning, Recombinant protein expression, antibody purification, organelle isolation plants (chloroplast, mitochondria, microsome, cytosol), organelle isolation protoplast (microsome, cytosol), *in vivo* localization studies in *A. thaliana*, *P. patens*, manuscript preparation.

Simm S: Bioinformatic analyses of orthology as well as localization predictions

Fischer K: *In vivo* localization studies in *M. x varia*.

Jäschke M: *In vivo* localization studies in *S. lycopersicum*

Gross LE: *In vitro* dual import assay

Kramer K: Bioinformatic analysis of orthology

Ehmann C: *In vivo* analysis in *A. cepa*

Ladig R: Experimental support and manuscript revision

Schleiff E: Supervision and manuscript preparation

Further publications from side projects or method establishment

Bodensohn US, Ruland C, Ladig R, Schleiff E. (2020) Membrane extracts from plant tissue. *Methods in Molecular Biology*.

Klinger A, Gosch V, Bodensohn U, Ladig R, Schleiff E. (2019) The signal distinguishing between targeting of outer membrane β -barrel protein to plastids and mitochondria in plants. *Biochim. Biophys. Acta - Mol. Cell Res.*

Gross LE, Klinger A, Spies N, Ernst T, Flinnner N, Simm S, Ladig R, Bodensohn U, Schleiff E. (2021) Insertion of plastidic β -barrel proteins into the outer envelopes of plastids involves an intermembrane space intermediate. *Plant Cell*.

CURRICULUM VITAE

Persönliche Daten

Name Uwe Sakamuzi Bodensohn
 E-Mail uwebodensohn@hotmail.de

Ausbildung

- 12/14 - heute Wissenschaftlicher Mitarbeiter im Rahmen einer Dissertation bei Prof. Dr. Enrico Schleiff, Goethe-Universität Frankfurt am Main
 Forschungsthema: „Get3 in Arabidopsis“
 Betreuer: Prof. Dr. Enrico Schleiff (JWGU Frankfurt)
 Abgabe der Dissertation 02/21
- 03/14 - 09/14 Masterthesis bei Prof. Dr. Enrico Schleiff
 Forschungsthema: „Get in the picture“
 Betreuer: Prof. Dr. Enrico Schleiff (JWGU Frankfurt), Prof. Dr. Claudia Büchel (JWGU Frankfurt)
- 10/11 - 09/14 Studium *cell physiology and biology*, M.Sc., JWGU Frankfurt, Note: 1,3
- 10/08 - 09/11 Studium Biowissenschaften, B.Sc., JWGU Frankfurt, Note 2,2
- 10/01 - 10/07 Studium Informatik, Vordiplom, TU Darmstadt
- 07/01 International Baccalaureate, International school Kuala Lumpur, Malaysia, Note 2,8

Vorträge und Posterpräsentationen

- 09/16 EMBO meeting, Mannheim; Poster
- 02/18 31. Tagung Molekularbiologie der Pflanzen, Dabringhausen; Poster
- 02/19 32. Tagung Molekularbiologie der Pflanzen, Dabringhausen; Vortrag
- 03/19 EMBO workshop, Sant Feliu de Guixols, Spanien; Poster

ERKLÄRUNG

Ich erkläre hiermit, dass ich mich bisher keiner Doktorprüfung unterzogen habe.

Frankfurt am Main, den

EIDESSTATLICHE VERSICHERUNG

Ich erkläre hiermit an Eides statt, die vorgelegte Dissertation über

„Get3 in Arabidopsis“

selbständig angefertigt und mich anderer Hilfsmittel als der in ihr angegebenen nicht bedient habe, insbesondere, dass alle Entlehnungen aus anderen Schriften mit Angaben der betreffenden Schrift gekennzeichnet sind.

Ich versichere die Grundsätze der guten wissenschaftlichen Praxis beachtet, und nicht die Hilfe einer kommerziellen Promotionsvermittlung in Anspruch genommen zu haben.

Frankfurt am Main, den



Publiziert unter der Creative Commons-Lizenz Namensnennung (CC BY) 4.0 International.

Published under a Creative Commons Attribution (CC BY) 4.0 International License.

<https://creativecommons.org/licenses/by/4.0/>